HPC-EUROPA3 SECOND RESEARCH PROJECTS DIRECTORY

October 2018 - March 2020

HPC-Europa3 aims to maintain a persistent and high-quality service offering Transnational Access to the most advanced HPC infrastructures in Europe which are currently available to the scientific research community. This third HPC-Europa programme builds on the success of previous Transnational Access programmes, which operated in Europe for almost two decades.

As would be expected from a Transnational Access programme, HPC-Europa3 offers collaborative visits to research groups in a different country from the one in which the participant currently works Researchers collaborate with a scientific host in their own area of research, while also receiving mentoring from one of the partner HPC centres, to help them make the best use of the HPC facilities for their research.

HPC-Europa3 therefore represents a powerful mechanism to support researchers to become proficient in the use of HPC and numerical simulation.

HPC-Europa3 is a truly multi-disciplinary programme attracting applications from all computational disciplines. From its beginning in 2017, more than 250 applications were made to the programme.

The present Second Research Projects Directory presents the results of 127 projects that have been completed in the between October 2018 and March 2020 in wide range of scientific disciplines. The Projects Directory series will continue in the next year with a similar report to document scientific projects that will be accomplished during the HPC-Europa3 life time.

Reading the contributions presented in this report, the importance of the scientific results can be seen. This is also evidenced by the number of publications produced, confirming the significant contribution of the HPC-Europa programme to support European researchers in computational science.

Summary

STRUCTURAL ANALYSIS OF WATER-IONIC LIQUID MIXTURES: LARGE-SCALE MOLECULAR DYNAMICS SIMULATIONS

K. Aidas[1], *D. Lengvinaitė*[1], *A. Laaksonen*[2]

[1]*Institute of Chemical Physics, Vilnius University, Lithuania;* [2]*Department of Materials and Environmental Chemistry, Stockholm University, Sweden*

Introduction

Ionic liquids, IL, are substances composed of solely organic cations and mostly inorganic anions. Provided the cations possess a degree of asymmetry, ionic liquids, unlike ordinary molten salts, remain liquid well below 100 °C and therefore they are often termed room-temperature ionic liquids, RTIL [1]. The imidazolium-based IL are among the most widely studied RTIL. The NMR spectra of IL based on 1-butyl-3methyl-imidazolium, C4Mim, and different anions such as halides, Cl-/Br-/I-, tetrafluoroborate, BF_4-, and nitrate, NO_3-, were considered by the NMR spectroscopy group of Vilnius University, Lithuania. Interestingly, the H-1 NMR chemical shift of water was found to evolve non-monotonically with the changing concentration of the binary solution of IL and water. These experimental findings reflect the structural changes of the samples with changing concentration of IL and water. In this presentation, we briefly discuss structural results of our large-scale molecular dynamics simulations of [C4Mim][Cl] and [C4Mim][BF_4] mixtures with water. These results are of importance for the interpretation of the NMR spectra to be modelled using combined QM/MM approaches.

Methods

Classical molecular dynamics (MD) simulations were performed for [C4Mim][Cl] and [C4Mim][BF_4] ionic liquids represented by 1000 ionic pairs with varying concentration of water (χ_w=0.05 and χ_w=0.5, respectively) using OPLS-AA force field for the ionic liquids [2,3]. The standard TIP4Pew potential was utilized for water. All simulations were performed using AMBER program [4]. We have performed extensive equilibration of all molecular systems at the NPT ensemble by heating them gradually to 500 K and then cooling to the desired temperature of 298 K. The final equilibration at ambient conditions of around 16 ns was necessary to get the density converged. We finally switched to NVT ensemble in order to record 10 ns long trajectories for further analysis.

Results

The primary aim of the results of MD simulations is the identification of water binding modes within the ionic liquid with special interest on the formation of aggregates of water known as water pockets. We have initialized our systems by placing a water droplet of appropriate size for a given molar fraction of water within the ionic liquid. At low molar concentration of water, χ_w=0.05, we have observed a rapid disintegration of the water droplet, so that well-separated water molecules are found within the simulation box. In the case of the [C4Mim][Cl] IL, pronounced hydrogen bonding between water molecules and the chloride anions was observed with the formation of the Cl-...HOH...Cl- aggregates. In addition, the formation of the hydrogen bonding between the oxygen atom of water and the acidic C-H bond at the 2nd position of the imidazolium ring was seen for both ILs. This in fact was anticipated due to the analysis of the experimental 1H NMR spectra of corresponding IL/water mixtures.

At high water concentration, χ_w=0.5, rather different behaviour of water molecules was observed in their mixtures with the [C4Mim][Cl] and [C4Mim][BF4] ionic liquids. In the [C4Mim][Cl] IL, water molecules were found to persistently form hydrogen bonding with the chloride anions. Interesting chloride sharing water aggregates as shown in Figure 1 were found to be rather ubiquitous. However, no water pocket-like aggregates were seen to be formed in the [C4Mim][Cl] IL. On the other hand, small water aggregates as shown in Figure 1 could be identified in the [C4Mim][BF_4] ionic liquid. This could be expected due to the known hydrophobicity of the BF_4- anions.

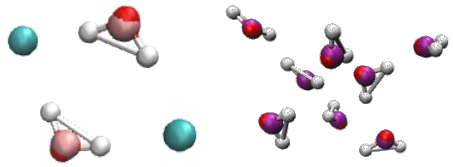

Figure 1 – The associates of water molecules in the ionic liquids: [C4Mim][Cl] (on the left) and [C4Mim][BF4] (on the right).

Conclusions

Molecular trajectories recorded during present MD simulations will be used in the QM/MM calculations of NMR spectra. The results will hopefully allow for the explanation of non-monotonic behaviour of the NMR chemical shift of water with the changing concentration in the [C4Mim][Cl] and [C4Mim][BF_4] ionic liquids.

References

[1] Welton T., Chem. Rev., 99(8):2071, 1999. [2] Lopes J. N.C. et al., J. Phys. Chem. B, 108(6):2038, 2004. [3] Andrade J. et al., J. Phys. Chem. B, 106(51):13344, 2002. [4] Case D. A. et al., Amber 2012, University of California, San Francisco, 2012.

Acknowledgements

The work has been performed under the Project HPC-EUROPA3 (INFRAIA-2016-1-730897), with the support of the EC Research Innovation Action under the H2020 Programme; in particular, the authors gratefully acknowledge the support of Prof. Aatto Laaksonen of the Department of Materials and Environmental Chemistry, Stockholm University, and the computer resources and technical support provided by PDC centre for high performance computing at Royal Institute of Technology.

DEVELOPMENT OF THE FFLUX FORCE FIELD FOR HALOGEN BONDED COMPLEXES

I. Alkorta

Instituto de Química Médica (CSIC), Madrid, Spain

Introduction

Covalently-bonded halogens are negatively charged, but curiously they form favourable interactions with nucleophiles (see Scheme 1) [1,2]. This proves that there is a compelling need to describe a halogen beyond the use of a simple point charge. In addition, electrophiles can simultaneously form favourable interactions. However, these occur at 90°–120° relative to the covalent R-X bond. Again, point charges cannot explain this strong directionality. However, multipole moments (charge, dipole, quadrupole, etc.) do predict this behaviour correctly. Finally, halogens are highly polarisable, which calls for a multipolar polarisable force field. This is exactly what Prof Popelier and his research group are developing for peptides, under the force field name FFLUX.

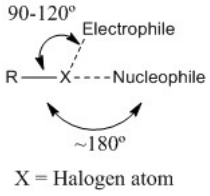

Scheme 1

Methods

The FFLUX force field is based on four cornerstones: (i) the quantum topological partitioning of a system's energy into atomic and inter-atomic contributions, (ii) multipole moments for medium- and long-range electrostatic interactions, (iii) the non-electrostatic terms (i.e. bonding, steric repulsion, dispersion) are modelled by the QCT method IQA[3], which provides delocalisation energy Vxc and intra-atomic energies, and (iv) machine-learning (kriging) to capture (and then predict) how these atomic quantities change in response to a change in nuclear positions. Both the precise constellation of these three methods and their intrinsic (and individual) advantages lead to a very powerful approach called FFLUX [4].

The dissociation profile of the $FCl{:}NH_3$ binary complex has been calculated at the MP4(sdq)/6-31+G(2d,2p) computational level with the Gaussian-16 program. The AIMAll program has been used to analyse the Hartree-Fock electron density and MORPHY for the correlation part. The analysis of the IQA terms has been carried out with the ANANKE program.

Results

The energetic profile at MP4, HF levels and correlation contribution are shown in Figure 1.

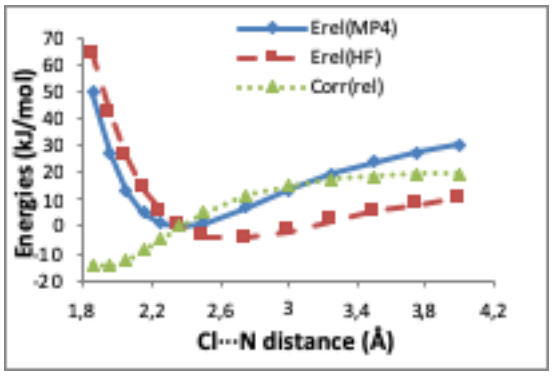

Figure 1 – Relative MP4, HF and correlation contributions along the $FCl{:}NH_3$ dissociation path.

The ANANKE program divides the dissociation profile in two segments. The first one corresponds to those distances equal and shorter than the equilibrium distance while the second segment is associated with distances equal and longer than the equilibrium one. The most important terms favouring the barrier in segment 1 are the self-energy of the nitrogen atom and the Vx (F-Cl) contribution while the interatomic Vx and Vcl of Cl-N work against this barrier. The opposite happens for the second segment barrier, where the interatomic terms of the Cl-N pair are favourable while the self-energy of the nitrogen atom is unfavourable. Interestingly, the importance of the correlation terms in explaining the dissociation profile is minimal.

Conclusions

The theoretical analysis of the dissociation profile at MP4 level with the IQA method shows that the most important energetic terms along the $FCl{:}NH_3$ dissociation path are the Vx (F-Cl) contribution, and the Vx and Vc of the Cl-N pair. The contribution of electron correlation is not important to explain the profile.

References

[1] Metrangolo, Resnati, in Halogen Bonding, Springer, 2008. [2] Politzer, et al. Phys Chem Chem Phys, 15:11178, 2013. [3] Blanco, et al. J.Chem.Theor.Comput., 1: 1096, 2005. [4] Popelier, Int. J. Quantum Chem.,115:1005, 2015.

Acknowledgements

The work has been performed under the Project HPC-EUROPA3 (INFRAIA-2016-1-730897), with the support of the EC Research Innovation Action under the H2020 Programme; in particular, the author gratefully acknowledges the support of Prof Paul Popelier (MIB, University of Manchester) and the computer resources and technical support provided by ARCHER.

DESIGN OF NEW DRUGS FOR THE D-ALA:D:ALA LIGASE

M. Badaoui[1], T. Kronenberger[2], E. Rosta[1], A. Poso[3]

[1]King's College University, United Kingdom; [2]University Hospital of Tübingen, Germany; [3]University of Eastern Finland, Finland

Introduction

In developing countries, Tuberculosis (TB) remains a major cause of mortality, particularly, childhood morbidity and mortality worldwide. As for many bacterial pathogens, the cell wall of TB is an interesting and essential component of the organism, and, interfering with it can lead to the disruption and death of the TB cells [1]. D-Alanine:D-Alanine Ligase (Ddl) catalyses the ATP-driven reaction of ligation between two D-Alanine molecules to form the D-Alanine: D-Alanine dipeptide. This dipeptide is an essential building block of peptidoglycan that is the scaffold of the lipid-rich bacterial cell wall. As the blockage of the biosynthesis of cell wall will result in extensively weaker cell walls and cell death, Ddl is an attractive target for the developing new antibiotics. We focused our interest in the reaction mechanism of the *Mycobacterium Tuberculosis* Ddl (MtDdl), understanding the catalytic reaction mechanism using QM/MM calculations [2]. Building on accurate QM/MM structures obtained in my current group led by Dr. Rosta, the next step of this project is to discover new specific inhibitors against this enzyme. Our aim is to find inhibitors that bind selectively and strongly to this protein, avoiding side effect, as caused for example by cycloserine, an already existing drug in therapy for the treatment of tuberculosis.

Methods

As a reference structure, we used the PDB structure 3LWB, while for the missing portion we use 2ZDQ structure as template.3 The ATP and ions coordinates were retrieved from the PDB: 1EHI. Using the entire Molport library3 we did a virtual screening using 3D docking with different precision levels in an integrated pipeline (Glide, with HTVS, SP and XP precision). We finally obtained 1,627 compounds, which we clustered and analysed using in-house developed procedures in the host laboratory of Prof. Poso, where both ligand-target geometries and interactions (including solvent effects) are classified. The docking poses were then validated by the means of molecular dynamics simulation (MD), to evaluate the ligand stability within the pockets. Using the Protein Preparation tool in Schrodinger we prepare the systems for running long MD simulations. MD simulations were carried out using Desmond with the OPLS3e force-field. This force-field has a better performance representing ligand properties and therefore is suitable to deal with the chemical diversity derived from the virtual screenings. Simulations have been analysed using the obtained trajectories, assessing both the ligand stability and the overall changes in the protein conformation, along the time. From this analysis, we chose 32 representative molecules which are expected to have high affinity and different type of interactions in the binding site. In collaboration with Carvalho group at the Crick Institute, we will be soon able to test enzymatically these 32 compounds and see the inhibition activity to MtDdl.

Results

We tested the 32 interesting molecules experimentally, using a known spectrophotometer technique. 11 of these molecules has shown inhibition activity to Ddl. Out of these 11 molecules, 2 of them presented inhibition activities (IC50) with similar order of magnitude to a known Ddl inhibitor (D-cycloserine).

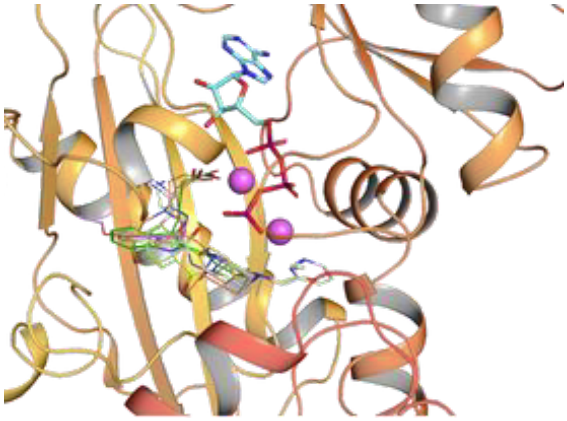

Figure 1 – Cartoon representation of the DDL structure including ATP as stick, the Mg^{2+} ions as spheres and some the selected representative molecules in lines.

Conclusions

In this work we provide an excellent example of how using a combination of computational and experimental technique, we are able to identify interesting hit candidates that demonstrate inhibition activities to an important pharmacological target against MtDdl. Starting from a library of ~7 M molecules, and using a well-established docking technique and molecular dynamics simulation we choose 32 representative molecules that show high affinity to the binding site. From 32 of these representative molecules, 2 of these molecules show "in vitro" activity similar to D-cycloserine.

References

[1] G. L. Moraes, et al., Tuberculosis, 2015(95): 95-111. [2] G. A. Prosser et al., FEBS Journal, 2013(280): 1150-1166. [3] www.molport.com [4] Schrödinger Release 2019:Schrödinger, LLC, New York, 2019.

Acknowledgements

The work has been performed under the Project HPC-EUROPA3 (INFRAIA-2016-1-730897), with the support of the EC Research Innovation Action under the H2020 Programme; in particular, the author gratefully acknowledges the support of Prof Antti Poso from the University of Eastern Finland and the computer resources and technical support provided by Taito (CSC).

DIRAC-KOHN-SHAM CALCULATIONS FOR ELASTIC X-RAY SCATTERING SIMULATIONS IN MOLECULES CONTAINING HEAVY ELEMENTS

L. Belpassi

Istituto CNR di Scienze e Tecnologie Chimiche c/o Università di Perugia, Italy

Introduction

The development of accurate theoretical and computational methods, based on first principles, for the characterization of electronic excited states and electron dynamics under external (weak and strong) electromagnetic fields in molecular systems containing heavy atoms is now one of the most important challenges of theoretical chemistry and computational science. Furthermore, the emergence of new Free Electron Lasers (FEL) and attosecond methodologies opened an area of research in which experiments can now probe electron dynamics and chemical reactions in real-time (bond breaking/forming) and the movement of electrons in molecules may be controlled. We mention the case of the Au(I)-Au(I) chemical bond formation in the electronic excited states of a gold dimer and trimer complex, followed in real time with femtosecond time-resolved X-ray scattering experiments [1].

A promising approach to tract electron correlation and relativistic effects is offered by the Dirac-Kohn-Sham (DKS) method. Obviously full four-component DKS calculations have an intrinsically larger computational cost, mainly because of the four-component structure in the representation of the DKS equation, and the complex matrix representation that usually arises as a consequence. The aim of this research project was to enable the DKS calculations, as implemented in the relativistic code BERTHA [2], to simulate the X-ray scattering spectra in molecular systems containing heavy elements, and, thus, open the possibility to investigate the effect of relativity on this interesting topic.

Methods & Results

The very first step of this research program was to improve the actual parallelization strategy already implemented in BERTHA and port and optimize the code on the multi-core processors architectures, available at EPCC. By using a relatively simple approach based on the use of OpenMP, we were able to distribute the computational burden, during the various time-consuming steps of the DKS calculation in a very efficient way. Concerning the linear algebra operations, we can easily take advantage of the multithreaded version of the BLAS and LAPACK routines, so that we do not need to modify the code with respect to the serial version, but just link the appropriate library. Using this parallel implementation, we were able to evaluate, with an unprecedented manner the X-ray scattering profile, and thus to investigate, for the first time, the effect of relativity in X-Ray scattering profile (see for instance Figure 1.

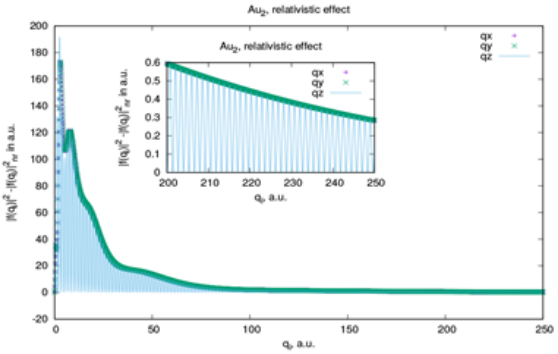

Figure 1 – Effect of relativity on the scattering form factor in gold dimer. The non-relativistic limit has been obtained increasing the speed of light in DKS simulation (from its actual value of about 137 a.u.) of one order of magnitude.

Conclusions

The method and the computational efficiency achieved in this research program for the DKS calculations represents a fundamental advance toward the wider diffusion of full relativistic methodologies in molecular science. In particular, it has been demonstrated that the proper inclusion of relativity represents a fundamental ingredient to gain accurate X-ray simulations in molecular systems containing heavy elements. Furthermore, the tool described here may contribute to extract meaningful chemical information from the new time-resolved X-ray scattering experiments in schedule at new FEL facilities.

References

[1] Kim K. H. et al., Nature, 518:385, 2015. [2] Belpassi L.et al., Phy. Chem. Chem. Phys., 13:12368, 2011.

Acknowledgements

The work has been performed under the Project HPC-EUROPA3 (INFRAIA-2016-1-730897), with the support of the EC Research Innovation Action under the H2020 Programme; in particular, the author gratefully acknowledges the support of Dr. Adam Kirrander of the School of Chemistry (University of Edinburgh) and the computer resources and technical support provided by EPCC.

SPIN-ORBIT COUPLING, JAHN-TELLER EFFECT AND PARAMAGNETIC RESPONSE

R.J.F. Berger

Chemistry and Physics of Materials, University of Salzburg, Jakob-Haringer-Str. 2a, 5020 Salzburg, Austria

Introduction

The main goal of the project was to identify molecular systems that show as large as possible contributions from spin-orbit coupling (SOC) to the magnetic response. We focussed hereby on formal closed shell singlet cases. The main idea was to investigate systems where there is a known spin-orbit coupling quenching of a Jahn-Teller (JT) distortion. Examples include $[Tl_6]^{-6}$, Pb_6, Pb_4 and $[Tl_3]^-$.[1] We have focussed on the possibly simplest examples of Pb_4 and $[Tl_3]^-$ for the initial calculations, however it turned out that quite often SCF convergence issues where occurring inthe four-component relativistic DFT calculations. For that reason we have decided to first study the general electronic structure of Jahn-Teller systems and magnetic response properties in the non-relativistic domain.

Methods

Geometry optimizations of were performed with the GAMESS-US programme package (version 5 DEC 2014 (R1))[2] and in the spirit of an early work from Voter and Goddard at the generalized valence bond-perfect pairing (GVB(PP)) level of theory and using the Karlsruhe def-TZVPP basis sets.[3] Starting orbitals and geometry were used from restricted Hartree-Fock (RHF) calculations. The main reason for choosing GVB(PP) instead of CAS was to be able to extract orbital energies from a "multi-configurational" wave function.

Magnetically induced currents were calculated for the using the program ReSpect (version 4.0.0) from Repisky and Komorovsky. To stay consistent we have also used for the magnetic response the HF level of theory and the Dyalls (relativistic) triple-ζ basis sets for C and H.For the density calculation the GVB(PP) structure has been used a point nucleus model, the "mdhf" method (multicomponent Dirac-HF hamiltonian) but quasi-non relativistic settings "cscale=20.0" and "soscale=0.0" and "grid: large". The magnetic response calculation was done using the London orbital approach (GIAO) and the ' 'dft-kernel: xalda" option and the magnetic field was set perpendicular to the molecular plane.

Results

Hereby we have found some intimate relation between the occurrence of a Jahn-Teller effect and paramagnetic response in point groups that are not iso- metric (the isometric point groups are: T, T_d, T_h, O, O_h, I and I_h). We could find a general prove of this relation and verify it on some of the most well-known examples for antiaromaticity. The result can be stated as a theorem:

First order and primoid second order JT distorted molecules out of non-isometric point groups are prone to paramagnetic current susceptibility parallel to the main axis of symmetry.

Moreover we suggest that this shall be considered as the basic principle of antiaormaticity.

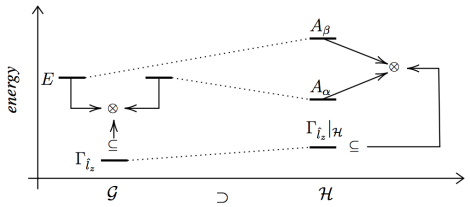

Figure 1 – Diagrammatic representation of a JT-distortion and the angular momentum representation in symmetry labelled energy levels in a non-isometric point group G.

Conclusions

We have shown by symmetry considerations how Jahn-Teller distortion and paramagnetic response are intimately related in the family of points groups comprised of C_n, C_{nv}, C_{nh}, D_n, D_{nh}, for $n > 2$ and S_{2n} and D_{nd} for $n > 1$. We suggest that this connection is the underlying symmetry principle of antiaromaticity, since the latter is defined by the central properties of a small HOMO-LUMO gap, proneness to structural distortion or instability and magnetically induced paramagnetic ring currents. The sparsity of examples may not only go back to the fact that antiaromaticity is related to low energetic stability but also due the paradox between distortion and paramagneticity that is hidden under its definition and that we have revealed in this work.

In the next step we will try to extend these considerations to the relativistic domain and hope to obtain the originally desired "record breaking SOC" effects in the magnetic response as a byproduct.

References

[1] Pyykkö P, Ann. Rev. Phys. Chem., 63(1):45-64, 2012. [2] Schmidt MW, et al., J. Comp. Chem. 14:1347–1363, 1993. [3] Schäfer A, Horn H, Ahlrichs R, J. Chem. Phys. 97:2571–2577, 1992.

Acknowledgements

The work has been performed under the Project HPC-EUROPA3 (INFRAIA-2016-1-730897), with the support of the EC Research Innovation Action under the H2020 Programme; in particular, the author gratefully acknowledges the support of Prof. Dage Sundholm and the computer resources and technical support provided by the CSC Helsinki.

THERMOELECTRIC PROPERTIES OF TiMSn (M = Ni, Pd, Pt) HALF-HEUSLER ALLOYS USING LOCALIZED GAUSSIANS AND HYBRID DENSITY FUNCTIONAL THEORY

A. Dasmahapatra[1], L.E. Daga[1], S. Casassa[1], A.J. Karttunen[3] and L. Maschio[1,2]

[1]Dipartimento di Chimica, Università di Torino, Italy; [2]NIS (Nanostructured Interfaces and Surfaces) Centre, Torino, Italy; [3]Department of Chemistry and Materials Science, Aalto University, Finland

Introduction

Half-Heusler (HH) alloys, intermetallic compounds of the composition ABX, are presently actively investigated for their thermoelectric (TE) performance.

These compounds have tunable band gaps which allow the possibility of tailoring TE efficiency and have potential applications in spintronics, solar cells, and data storage [1]. The primary focus, however, is doping the parent material to maximize the thermoelectrics. In this work, we investigate three thermoelectric compounds: TiNiSn, TiPdSn and TiPtSn using hybrid density functional theory and localized Gaussian type orbitals (GTO). We use the CRYSTAL code for all computations [2].

Methods

The CRYSTAL program is based on Gaussian type functions allowing for an easy and relatively cheap use of hybrid functionals. In this study we adopt a comprehensive screening in the choice of: 1) Basis-sets and 2) DFT functionals. In a previous work, we developed the BDIIS technique for the optimization of Gaussian-type basis set exponents and contraction coefficients, that is based on the Direct Inversion of the Iterative Subspace (DIIS) technique.3 We utilize this algorithm, primarily, for a system-specific optimization of the exponents, and we arrive at a new set of basis sets that behave optimally in describing the electronic structure of the considered compounds. We further explore three different DFT functionals to describe the electron exchange and correlation in these systems. The functionals considered are: 1) pure PBE (0% exchange), 2) PBE10 – hybrid functional with 10% exchange, and 3) PBE0 with 25% exchange. For computation of thermoelectric properties, we also use CRYSTAL where is available the implementation of a new algorithm based on the semi-classical Boltzmann theory and frozen band approximation.

Results

The three alloys considered exhibit an indirect bandgap of 0.69, 0.73 and 1.20 eV (Ti(Ni/Pt/Pd)Sn respectively) between the Γ and X point. Our computations suggest that p-type doping results in higher thermoelectric efficiency in TiNiSn as visible in the higher value of PF obtained when considering ptype carriers in contrast to n-type (Figure 1). The most reported value of S (Seebeck) for TiNiSn found through computational and experimental studies in literature is ~ -250 µV/K, which we achieve at a n (carrier concentration) of ~10^{19} cm^{-3}. For TiPdSn (p-type behaviour), S at 300 K is half of the value suggested in literature that arises from different lifetime. With change in temperature, TiPtSn, shows an increasing trend in S for p-type and a decreasing trend in S for ntype carrier, irrespective of the carrier concentration. We attempt to introduce defects (Ni from its original HH site to a new Full-H site) in the pure TiNiSn to replicate the lower experimentally measured band-gap and the value achieved in this work is 0.23 eV. Moreover, the defect model prefers n-type carriers and exhibits a higher power factor.

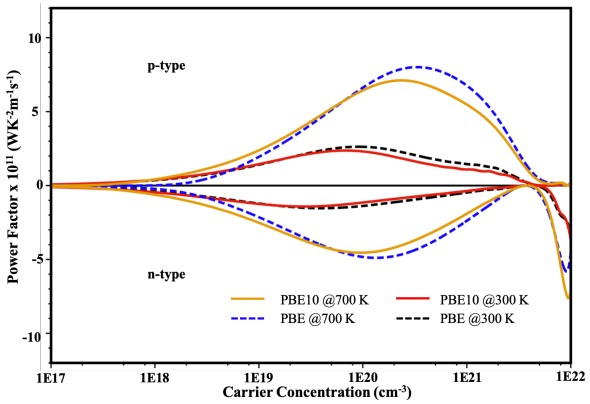

Figure 1 – Power-factor with respect to relaxation time, for ptype and n-type doping at T= 300 K (dotted line, black: PBE and solid line, red: PBE10) and T = 700 K (dotted line, blue: PBE and solid line, orange: PBE10).

Conclusions

We have used the CRYSTAL code to perform a thorough investigation of the geometry, electronic band structure and thermoelectrics of three half-Heusler alloys: TiNiSn, TiPdSn and TiPtSn. We described each of these compounds using optimized basis sets and PBE10 hybrid functional. As regards thermoelectric properties TiNiSn showed a preference for p-type behaviour, as often noticed in computational studies.

For TiPdSn and TiPtSn, we predicted both alloys to favor p-type transport and have high room temperature values of power factor. Lastly, we presented a defect TiNiSn model which is a better description of the real material. We were able to achieve a smaller value of band-gap and better thermoelectric properties.

References

[1] Gautier R. et al., Nat. Chem., 7(4):308, 2015. [2] Dovesi R. et al., Wiley Int. Rev., 8:e1360, 2018. [3] Maschio L., Theor. Chem. Acc. 137(4):60, 2018.

Acknowledgements

The work has been performed under the Project HPC-EUROPA3 (INFRAIA-2016-1-730897), with the support of the EC Research Innovation Action under the H2020 Programme; in particular, the author gratefully acknowledges the support of Antti J. Karttunen of the Aalto University (Finland) and the computer resources and technical support provided by CSC.

NITROSYL···NITROSYL INTERACTIONS IN METAL COMPLEXES

J. Echeverría[1] and C. Fonseca Guerra[2]

[1]Inorganic Chemistry Department & IQTC-UB, Universitat de Barcelona, Spain; [2]Department of Theoretical Chemistry and Amsterdam Center for Multiscale Modeling, Amsterdam, The Netherlands

Introduction

Noncovalent interactions are key in numerous chemical and biological processes. A particular type of weak interaction, called the n->π* interaction, has attracted much interest in recent years due to its unambiguous contribution to protein structure, but also because it dictates the conformation of a plethora of organic molecules. One of the most common n->π* interactions is that involving two carbonyl groups with a C=O···C=O distance shorter than the sum of the corresponding van der Waals radii (3.27 Å). Such carbonyl–carbonyl interaction has the origin in the overlap of an oxygen lone pair (n) and a carbonyl empty antibonding orbital (π*) that involves some degree of electron delocalization of the first into the second [1]. The energy release resulting from this orbital mixing (approximately 0.27 kcal/mol) makes the interaction attractive [2]. In the present work, we try to elucidate whether nitrosyl ligands, which are isoelectronic with carbonyl, are able to engage in n->π* interactions.

Methods

Structural searches were performed in the Cambridge Structural Database (CSD version 5.39 (November 2017) + 1 update). Only structures with their 3D coordinates determined, non-disordered, without errors, not polymeric and with R < 0.1 were allowed in searches. We used the van der Waals proposed by Alvarez [3]. Electronic structure calculations were carried out using ADF suite of programs at the ZORABLYP-D3(BJ)/TZ2P level of theory. Energy decomposition analysis (EDA) was carried out with ADF. The EDA decomposes the total interaction energy (ΔE_{int}) into different contributions that are chemically meaningful, i.e. Pauli orbital repulsion (ΔE_{Pauli}), electrostatic interaction (ΔE_{elstat}), interaction due to dispersion forces (ΔE_{disp}) and orbital interactions (ΔE_{oi}) that emerge from charge transfer and polarization.

Results

There are in the structural databases many examples of both intra- and intermolecular short contacts involving two nitrosyl groups. The contacts are directional and approach to an attack angle of 90 degrees. The interaction must be shorter than the sum of the vdW radii (3.27 Å) and can be as short as 2.7 Å. For the dimer in Figure 1, we decomposed the interaction energy for several interaction distances. The results are summarized in Table 1. The study of the interaction energy as a function of the Fe-N-O angle shows that the interaction energy is maximum for 90 degrees (ΔE_{int} = -1.32 kcal/mol), weakening as the angle increases or decreases (ΔE_{int} for 70 and 110 degrees are -0.46 and -0.80 kcal/mol, respectively).

Table 1. EDA results for Fe complex dimer (kcal/mol).

N-O (Å)	ΔE_{Pauli}	ΔE_{Elect}	ΔE_{Disp}	ΔE_{Oi}	ΔE_{INT}
2.0	78.48	-33.02	-4.10	-15.30	26.06
2.5	16.90	-7.99	-3.16	-3.26	2.49
3.0	4.12	-2.10	-2.24	-0.95	-1.17
3.5	1.28	-0.68	-1.46	-0.36	-1.22
4.0	0.81	-0.31	-0.88	-0.17	-0.82

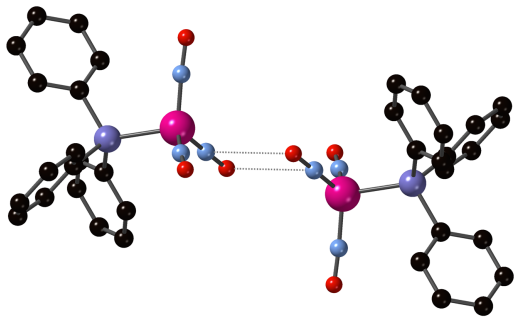

Figure 1 – Iron complex dimer used as a model for the study of nitrosyl···nitrosyl interactions.

Conclusions

The results from our theoretical calculations evidence, for the first time, that nitrosyl ligands are able to engage in n->π* interactions similarly to those found for carbonyl groups. These interactions are directional and arise from electrostatics and some degree of orbital overlap. Future work must be directed to a deeper understanding of their features.

References

[1] Echeverría, J., Chem. Commun., 2018, 54, 3061-3064. [2] Newberry, R. W. et al., Acc. Chem. Res., 2017, 50, 1838-1846. [3] Alvarez, S., Dalton Trans., 2013, 42, 8617-8636.

Acknowledgements

The work has been performed under the Project HPC-EUROPA3 (INFRAIA-2016-1-730897), with the support of the EC Research Innovation Action under the H2020 Programme; in particular, the author gratefully acknowledges the support of Celia Fonseca Guerra (VU Amsterdam) and the computer resources and technical support provided by SURFsara.

EFFECTS OF STRAIN AND ALLOYING ON LINEAR SCALING RELATIONSHIPS IN METAL CATALYSTS

E. Fako[1], N. Lopez[1], N. Skorodumova[2]

[1]Institute of Chemical Research of Catalonia (ICIQ), The Barcelona Institute of Science and Technology, Tarragona, Spain; [2]Department of Materials Science and Engineering, School of Industrial Engineering and Management, KTH–Royal Institute of Technology, Stockholm, Sweden

Introduction

Catalysis is a key tool for tailoring a sustainable future of our society. In particular, nano and subnano heterogeneous catalysts (nanoparticles, NPs), provide superior price to performance ratio and gives rise to behaviours intrinsically present on the nano/subnano scale. Alloying has proven to be a viable strategy for tuning NPs properties and bimetal systems became popular for their tunability [1.] The activity of pure metal surfaces is dictated by linear scaling relationships (LSR) where an activity descriptor is represented as a function of a parameter describing the interaction between the substrate and surface (adsorption energy of a reactant or reaction intermediate, d-band centre, etc.) [2]. One common trait of LSR is that they have the shape of a volcano with a peak in the peak of activity corresponding to the optimal affinity descriptor [3], implying that there is a fundamental maximum to the catalysts activity. In order to break this paradigm of heterogeneous catalysis, many strategies have been employed, most notably alloying (intrinsically followed by strain [4]). The vast configuration space of multicomponent metal surfaces provides a playground for finding means of overcoming these apparent limitations.

Methods

Density functional theory (DFT) calculations were performed using the Vienna Ab initio Simulation Package (VASP) code. The functional of choice was Perdew-Becke-Ernzerhof (PBE) with dispersion contributions introduced through the D3 approach. While non-valent electrons were described by projector augmented-waves (PAW) the valence monoelectronic states were expanded as plane waves with maximal kinetic energy of 450 eV. The metallic (111) and (001) surfaces were with 3x3 and 4x4 expanded supercells, respectively with a thickness of 4 atoms. For all systems the top two layers of the slab were allowed to relax and the slabs were separated by 8 Å of vacuum. The k-points sampling was a Γ–cantered 3×3×1 grid (~0.3 Å−1). Epitaxial strain was introduced by stretching/compressing the supercell in the x-y plane, and the zero strain reference state was chosen as the unperturbed solvent metal. Vacancies/single atom sites were formed by removing/replacing one atom in the top layer. A dipole correction was employed along the z-direction normal to the slab faces. The molecules were placed in a cubic box of 15 Å sides. In all cases the optimization thresholds were 10^{-6} and 10^{-4} eV for electronic and ionic relaxations, respectively.

Results

From a set of d-block metals (Ag, Au, Cu, Ir, Pd, Pt, Rh) all pristine, vacancy, and single atom (SA, all perturbations of the set of metals, Figure 1a) species have been computed both without and with epitaxial strain applied (-6, -3, 0, 3, 6 %). Dissolution energies were computed as a stability descriptor and the projected density of states (DOS) was employed to evaluate the effect of strain on the catalytic electronic states. In Ag/Cu (and other), free-atom-like states have been noticed. Strain was found to have no detrimental effect on the sharp DOS profiles, and allowed for tuning with respect to the Fermi level (Figure 1b), while not compromising stability (Figure 1c).

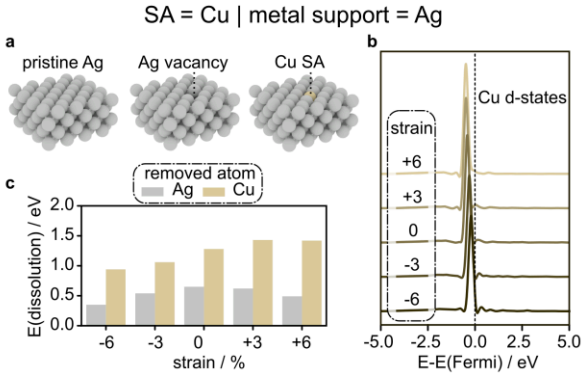

Figure 1 – sample Structure of the Ag/Cu (001) system (a); dissolution energies with respect to strain (b); Cu d-band profiles for the Cu SAs in Ag (c)

Conclusions

The response of SA alloys to strain was investigated, and it was concluded that the traits of different SA systems can be linearly combined to accurately represent more complex systems. The implications of these findings could be of interest in the field of catalysis and beyond.

References

[1] Studt F et al., Science, 320: 1320-1322, 2008. [2] Hammer B et al., Surf. Sci. 343: 211–220, 1995. [3] Stamenkovic V et al., Nat. Mater., 6: 241–247, 2007. [4] Fako E et al., PCCP, 20: 1524-1530, 2018.

Acknowledgements

The work has been performed under the Project HPC-EUROPA3 (INFRAIA-2016-1-730897), with the support of the EC Research Innovation Action under the H2020 Programme; in particular, the author gratefully acknowledges the support of Department of Materials Science and Engineering and the computer resources and technical support provided by PDC at KTH.

MIXING THERMODYNAMICS AND ELECTRONIC STRUCTURE OF HETEROMETALLIC ZEOLITIC IMIDAZOLATE FRAMEWORKS

R. Grau-Crespo[1], N.C. Hernandez[2], A.R. Ruiz-Salvador[3], S. Hamad[3], D. Tiana[4]

[1]University of Reading, United Kingdom; [2]University of Seville, Spain; [3]U. Pablo de Olavide, Spain; [4]University College Cork, Ireland

Introduction

Metal-organic frameworks (MOFs) are porous crystalline materials, consisting of metal (or metal-based cluster) nodes joined by organic linkers. Thanks to their porous structures, they have applications in gas adsorption and separation and in catalysis. More recently, they have been investigated for photochemical applications, including photocatalysis and solar cells, for which the electronic structure must be tuned to achieve specific target properties. In order to realize these properties, it is often necessary to combine different metals or different linkers within a MOF structure [1,2].

We have investigated the mixing thermodynamics and electronic properties of a family of MOF: zeolitic imidazolate frameworks (ZIFs), which are known to be flexible to accommodate different metals and linkers. We have investigated the mixing of Zn-Cd, Zn-Co, Zn-Cu and Zn-Ni in MIm_2 (M = metal, Im=imidazolate) ZIFs with sodalite topology, as well as the optical properties of these structures as a function of the nature of the metal centre.

Methods

Density functional theory (DFT) simulations were performed with the VASP code. All the symmetrically inequivalent configurations of the cations within a cubic sodalite unit cell were generated using the SOD method [3] and fully relaxed to minimize the DFT energy. We developed a method to reduce the computational cost of performing DFT calculations for the whole configurational space (see Results section). Finally, we performed time-dependent DFT (TDDFT) simulations using the CP2K code, in order to understand the optical properties of ZIFs as a function of the metal centre.

Results

One important outcome from this project was the development of a methodology to accelerate the evaluation of energies in the configurational space. The methodology is based on a site- and pair-based expansion (SPBE) of the energies when the number *n* of substitutions is greater than 2. Explicit (DFT-based in this case) calculations only need to be performed for *n*=0, 1 and 2, and the expansion is used to extrapolate for *n*>2. An initial formulation of this method was given in [4], but we have developed a rescaling algorithm that improves significantly the agreement with the DFT reference, at very little extra cost. Figure 1 shows the good correspondence between DFT and SPBE energies, particularly after rescaling. The methodology was implemented within the SOD code and released for public use in the GitHub repository [5].

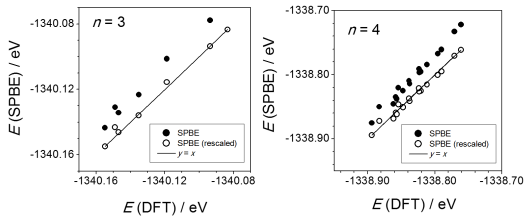

Figure 1 – Comparison of inexpensive SPBE and expensive DFT energies for n=3 or 4 Cd/Zn substitutions in the ZnIm2 cubic unit cell.

After validating this approach for the (Cd, Zn)Im_2 mixed ZIF, we obtained the thermodynamic enthalpies, entropies and free energies of mixing for all the different compositions. Interestingly, we found that the mixing of cations was nearly ideal, in the sense of having very small enthalpies of mixing at all compositions. We therefore expect heterometallic ZIFs to be almost ideally disordered.

We also calculated the electronic and optical properties as a function of the metals substituted in the nodes using TDFT simulations. Contrasting with the standard Zn(Im)2 ZIF, transition-metal-based ZIFs have a richer photochemistry, with contributions from the metal orbitals to the excited states.

Conclusions

Our DFT simulations have offered insights into the thermodynamic, electronic and optical properties of mixed ZIFs, which will inform future efforts to design photochemical applications for this class of material.

References

[1] Grau-Crespo R et al., Angewandte Chem., 128: 16246-16250, 2016. [2] Aziz A et al. J. Mater. Chem. A., 5: 11894-11904, 2017. [3] Grau-Crespo R et al., J. Phys. Condens. Matter 19: 256201, 2007. [4] Arce-Molina J et al., Phys. Chem. Chem. Phys., 20:18047-18055, 2018. [5] github.com/gcmt-group/sod/releases/tag/Sod-v0.46

Acknowledgements

The work has been performed under the Project HPC-EUROPA3 (INFRAIA-2016-1-730897), with the support of the EC Research Innovation Action under the H2020 Programme; in particular, the authors gratefully acknowledges the support of the Department of Chemistry of University College Cork, Ireland, and the computer resources and technical support provided by the Irish Centre for High-End Computing.

FRUSTRATED LEWIS PAIRS FOR SUSTAINABLE FUTURE

M. Heshmat, B. Ensing

Stockholm University, University of Amsterdam

Introduction

The advent of the metal-free Frustrated Lewis Pair (FLP) concept for activation of small molecules, such as H2, and FLP-catalysed hydrogenations has attracted increasing interest ever since Stephan et al. reported their pioneering metal-free reversible H2 activation in 2006 [1]. The field of heterogeneous (solid-state) FLPs, s-FLP in short, has very recently (in 2016) been proposed and examined and is now a developing research field [2]. The goal of the current HPC project is development of new, cheap and sustainable s-FLP catalysts in order to improve the efficiency of chemical transformations. Implementation of such metal-free catalysts solves the concerns of homogeneous catalysts: stability, recyclability, and catalyst-product separation. It is for this reason that the notion of heterogeneous or solid FLP catalysts is an attractive one. To this end, we aim to predict the structure and dynamics of s-FLP molecular systems and unravel the mechanistic details of the complex small molecule activation in s-FLP catalysts, by taking advantage of combining molecular dynamics (MD) simulations and electronic structure analysis. By computing the free energy landscape, we can obtain the reaction rates and interpret the experimental observation of synthetic s-FLPs.

Methods

We have used CP2K program to perform ab initio molecular dynamics (AIMD) simulations with DFT in combination with Gaussian and plane-wave (GPW) method. PBE exchange correlation functional plus D3BJ dispersion correction and DZVP-MOLOPT in combination with GTH and GPW basis sets have been used. Density Functional Theory is the most widely used approach in the field of condensed matter electronic structure calculations, which provides predictions of specific properties of bulk materials and surfaces. Plumed plug-in program was used to analyse features of the dynamics on-the-fly and to calculate free energy surface. Using PLUMED plug-in, the metadynamics and path-metadynamics and steered molecular dynamics simulations may be carried out in combination with CP2K.

Results

We have started the project with a reaction that have been reported in the literature for Lewis pair-functionalized UiO-66 primitive structure [3] and calculated the entire energy profile of the hydrogenation of CO2 to obtain HCOOH. Figure 1 shows the results of our calculations (numbers in black) in comparison with literature (blue numbers in parentheses). We have considered both H2 and CO2 reaction paths that are depicted in Figure 1. Simulation of the dynamics of this system is our ongoing plan, which we could obtain part of the reaction mechanism using metadynamics simulations within 50 ps run.

Considering that this is a rather complicated system, due to the presence of both MOF structure and functional LP (Lewis pair) group, dynamics simulations are not so straightforward and take more computation time.

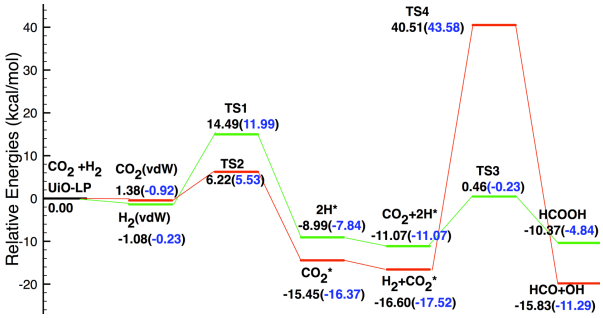

Figure 1 – Computed energy profile of CO2 hydrogenation inside the LP-functionalized UiO-66 considering two pathways. The H2 and CO2 pathways have been calculated and numbers in parentheses have been taken from [3].

As can be seen in Figure 1, our and literature results are in good agreement [3]. Computation of the entire energy profile for similar reactions with other LP-functionalized MOFs and getting insights into the reaction mechanism of small molecule activation inside the MOFs are still in progress.

Conclusions

During the past few years many efforts have been performed to develop heterogeneous FLP catalysts. Recently in 2018 there was an experimental report that combines FLPs and MOFs for heterogeneous catalysis [4]. We have calculated the energy profile for CO2 hydrogenation inside the LP-functionalized UiO-66, which is in good agreement with previous results. Dynamics and metadynamics simulations of the intermediates and calculating the free energy surface along the reaction paths for both reactions are our ongoing studies.

References

[1] Stephan D. W. et al., Science, 314(5802): 1124-1126, 2006. [2] Erker G et al., Chem. Sci, 9(21): 4859-4865, 2018. [3] Johnson J. K. et al, ACS Catal., 5(5): 2921-2928, 2015. [4] Ma S. et al., Chem 4(11): 1–13, 2018.

Acknowledgements

The work has been performed under the Project HPC-EUROPA3 (INFRAIA-2016-1-730897), with the support of the EC Research Innovation Action under the H2020 Programme; in particular, the author gratefully acknowledges the support of Prof. Bernd Ensing and computational chemistry department of University of Amsterdam and the computer resources and technical support provided by SURFSARA.

IDENTIFYING BONDS IN EXTENDED MOLECULAR SYSTEMS

G. La Penna[1], *D. Tiana*[2]

[1]*National research council of Italy, Institute for chemistry of organometallic compounds, Italy;* [2]*University college Cork, School of chemistry, Ireland*

Introduction

The calculation of the ground state electron density in extended atomic system is important to understand and guide the design of properties and functions of materials and molecular assemblies. One of the best performing method, as a compromise between computational cost and accuracy of results, is density-functional theory (DFT), with electron density represented in terms of effective one-electron states (Kohn-Sham states, KS), the latter expanded in plane-waves. Atoms are represented by means of the respective frozen atomic cores (pseudo-potentials) acting on a completely delocalized representation of valence electrons. This representation is typical of solid state, but, thanks to HPC, extended to liquid and disordered samples. With these approximations, calculation of ground state electron density achieved a good performance for systems composed by more than 1000 atoms, a super-cell size of about 2 nm and statistics of reasonable length/size. One of the major limitations of these models is that chemical bonds cannot be easily identified. With the project, we aimed at providing a post-processing tool for calculating delocalization indices (DIs) for all atomic pairs in an extended system, thus measuring the number of electrons shared via covalent bonds between any pair of atoms directly from the ground state wave function represented on the basis of plane-waves. Though similar tools exist, they are limited to a few tens of atoms [1,2].

Methods

The equation for DIs is well known and it involves the integral over all the atomic basins of the overlap between all pairs of different KS states [3]. We designed an extended system as a test for applying the DI equation. We built models of a CO-isolated Pt nano-wire, composed by a number of $Pt_3(CO)_6$ clusters stacked in the direction of the Pt3 plane of each cluster. Experimental studies of oligomers of these clusters have been reported and the infinite nano-wire has been isolated in a crystal [4]. The energy of the series of compounds $[Pt_3(CO)_6]_n^{2-}$ with n=1,2,4,8 has been minimized in a routinely used DFT model, starting with a super-cell of 2 nmx2 nmx2.56 nm, with variable L_z in the latter case. The n=1,2,4 cases represent isolated oligomers, while the n=8 case represents the infinite nano-wire. We computed the DIs for all atom pairs in the series. Systems are of 15, 30, 60, and 120 atoms with, respectively, 46, 91, 181, and 363 filled KS states. The number of points in the real-space representation of density and KS states is 192x192x243. We performed all the calculations with the extensively parallel code Quantum-Espresso (QE) in the 6.4.1 version (released in Apr. 2019).

Results

We added to QE one post-processing code, DI. Also, a little modification of the main post-processing tool, PP, was done in order to rapidly build an all-electron estimate of electron density in real space. The latter function is required for a correct definition of atomic basins [3]. The calculation of DIs requires a large amount of memory, since the real-space representation of all the KS states representing the valence electron density must be kept in memory for the calculation of overlap integrals in the different atomic basins. The final DI code contains most of the parallel algorithms of the QE distribution. In particular, the band parallelization allows to perform a bunch of MPI tasks (with multi-threading via OpenMP), over bands of KS states handled in parallel.

This memory requirement limits all of the existing tools to 10-20 atoms [1,2]. We could perform the calculation of DIs for 120 atoms, without storing the KS states on disk, a strong limitation of our previous PP code [3].

pair/n	1	2	4	8
Pt1-Ct	1.5	1.4	1.3	1.3
Pt1-Ot	0.25	0.24	0.23	0.22
Pt1-Cb	0.88	0.85	0.81	0.78
Pt1-Ob	0.16	0.16	0.15	0.14
Pt1-Pt1	0.55	0.48	0.47	0.46
Pt1-Pt2		0.35	0.34	0.28
Ct-Ot	1.6	1.6	1.6	1.6
Cb-Ob	1.5	1.5	1.5	1.6

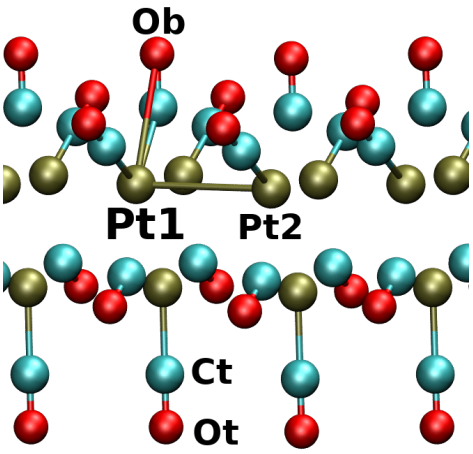

Figure 1 – Atomic positions and labels.

Conclusions

The goal of the project was fulfilled up to systems of 120 atoms. We are still working to make the DI code faster to achieve systems of 1000 atoms.

References

[1] Golub P et al., J. Chem. Phys., 145(15):154107, 2016. [2] Otero-de-la-Roza, A et al., J. Chem. Theory Comput., 14(9): 4699, 2018. [3] La Penna G et al., Theor. Chem. Acc., 130:27, 2011. [4] Femoni C et al., Angew. Chemie Int. Ed., Journal, 45(13):2560, 2006.

Acknowledgements

The work has been performed under the Project HPC-EUROPA3 (INFRAIA-2016-1-730897), with the support of the EC Research Innovation Action under the H2020 Programme; in particular, the author gratefully acknowledges the support of University College Cork, School of chemistry and the computer resources and technical support provided by ICHEC.

WHEN ADDITIVE MOLECULAR DYNAMICS FAILS: QUANTUM EFFECTS IN CALCIUM-DEPENDENT LECTIN/CARBOHYDRATE COMPLEX

M. Lepsik[1], M. Lelimousin[1], E. Paci[2], A. Imberty[1]

[1]Centre de recherches sur les macromolécules végétales (CERMAV), CNRS, Grenoble, France; [2]Astbury Centre and School of Molecular and Cellular Biology, University of Leeds, United Kingdom

Introduction

The developments of additive carbohydrate force fields [1] increased the reliability of molecular dynamics simulations (MD) of protein-carbohydrate complexes. The presence of bridging Ca^{2+} ions can, however, pose problems for structural and energetic description due to quantum effects, such as polarization [2-4].

Methods

MD was run in AMBER14 with ff14SB force field[5] for the protein, GLYCAM06-j[6] for the carbohydrate and TIP3P[7] as explicit water model. For Ca^{2+} we used parameters with effective electronic polarisation which we had developed previously.[4] The production phase was 100 ns long.

For quantum mechanical/molecular mechanical (QM/MM) calculations we used DFT-D in the QM part (binding site, around 300 atoms) and AMBER in the MM part. Natural Population Analysis[8] was used to obtain the partial charges.

Results

A calcium-dependent lectin/carbohydrate complex was subjected to MD to explain the ligand binding mode. However, despite the improved description of the binding site structure (Ca^{2+}…Ca^{2+} distance matching that of the crystal structure), the pattern of protein/carbohydrate interactions and the location of specific bridging water molecules were not maintained.

We have therefore invoked QM/MM optimizations followed by charge calculations. As can be seen from Table 1, polarization phenomena are present for the active-site aspartates induced by the Ca^{2+} ions. Specifically, Asp99 and Asp104 experience a large asymmetry (difference of 0.1 e^-) in the partial charges of the OD1/OD2 carboxylic oxygens. These effects cannot be described by a non-additive force field and are thus the cause of inaccurate description of this protein/carbohydrate system.

Atom name	AMBER	NBO isol	NBO complex			
	Asp	Asp	D96	**D99**	D101	**D104**
OD1	-0.80	-0.85	-0.79	-0.85	-0.87	-0.91
OD2	-0.80	-0.84	-0.80	-0.77	-0.84	-0.80

Table 1 – Partial charges on carboxylate atoms calculated with different methods.

Conclusions

We utilized classical additive MD with new Ca^{2+} parameters to study a lectin/carbohydrate complex. Although the structural features of the binding site were improved due to the use of the new Ca^{2+} parameters, the details of the binding mode were not retained. QM/MM calculations revealed that the underlying reason were polarisation phenomena present in the binding site.

References

[1] Fadda E and Woods RJ, Drug Discov Today, 15: 596-609, 2010. [2] Mitchell EP et al., Proteins: Struct Funct Bioinf 58: 735–746, 2005. [3] Lepsik M and Field MJ, J. Phys. Chem. B, 111 : 10012-10022, 2007. [4] Kohagen et al. J. Phys. Chem. Lett. 5 : 3964−3969, 2014. [5] Maier JA et al., J. Chem. Theory Comput., 11: 3696–3713, 2015. [6] Kirschner KN et al., J. Comput. Chem., 29: 622–655, 2008. [7] Jorgensen, W.L. et al. J. Chem. Phys., 79: 926–935, 1983. [8] Reed, A. E. et al., Chem. Rev. 88: 899-926, 1988.

Acknowledgements

The work has been performed under the Project HPC-EUROPA3 (INFRAIA-2016-1-730897), with the support of the EC Research Innovation Action under the H2020 Programme; in particular, the author gratefully acknowledges the computer resources and technical support provided by EPCC. This project has received funding from the European Union's Horizon 2020 research and innovation programme under the Marie Sklodowska-Curie grant agreement No 795605".

THE IMPACT OF THE SUBSTITUENT EFFECT ON INTERMOLECULAR INTERACTIONS OF ADENINE

P.H. Marek[1,2], H. Szatylowicz[1], O. Stasyuk[3], M. Sola[3]

[1]Warsaw University of Technology, Faculty of Chemistry, Warsaw, Poland; [2]University of Warsaw, Faculty of Chemistry, Warsaw, Poland; [3]Institut de Quimica Computacional i Catalisi (IQCC) and Departament de Quimica, Universitat de Girona, Girona, Spain

Introduction

Adenine (A) molecules can form three different quartets of close to flat conformations (Figure 1) [1]. Their geometries depend on the mutual orientation of the molecules and variant hydrogen bond acceptors involved in the interactions. The goal of this project was to study the effects of different substituents on the stabilisation of adenine quartets and on their interaction energies. In every case, adenine molecules were substituted symmetrically at C8, N9 or C2 positions by functional groups with different electronic properties (namely, Cl, F, NO_2, NH_2 and Me). As a result 33 different systems were analysed.

Methods

All systems were optimized using Density Functional Theory (DFT) at BLYP-D3/TZ2P level of theory with ADF package [2]. To ensure if resulting geometries are the minima on potential energy surface, vibrational frequencies analyses were performed. Analysis of the interaction energy values showed A-A interactions to be weak, yet dependency on the substituent could be observed. In order to determine the nature of the observed energy changes, energy decomposition analysis (EDA) was performed on the quarters optimised with C_{4h} symmetry constraints. The major contributions were determined to be connected to electrostatic and orbital interactions energy terms. For deeper analysis, investigation of VDD charges was performed. Calculations necessary to determine if the synergy effect is present in the systems were carried out.

Results

Due to both small values of E_{int} and long distances between adenine molecules in the quartets, synergy effect was not pronounced. Meticulous analysis of all of the data allowed to conclude that depending on the geometry of the quartet, substituents can significantly influence the interaction energy in the system. Furthermore, depending on the mutual distance of the substitution and the H-bond acceptor or donor, the interaction energy can increase or decrease with intensification of electron-donating properties of the substituent. What is more, this effect can be connected with changes in aromaticity of the adenine 6- and 5-membered rings.

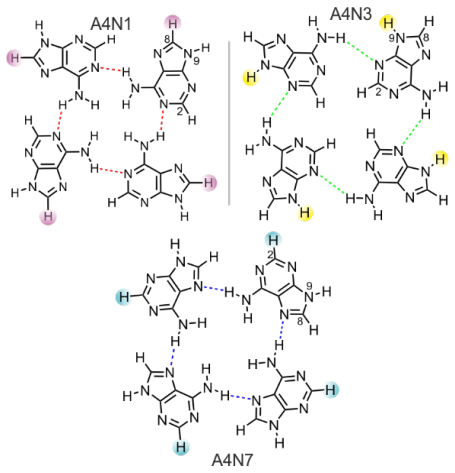

Figure 1 – Analysed tetramers, with substitution places marked.

Conclusions

To conclude, for A4N1 system small change in E_{int} after introduction of a substituent could be explained by long distance between substituent and donor/acceptor, and therefore weakened interaction between substituent and engaged in H-bonds groups. In N9-substituted A4N7 system stabilization of the quartet is observed when electron donating group such as NH2 is introduced, while for C2-substitution electron withdrawing groups are preferable. Analysis of VDD charges on the hydrogen bonds along with HOMA and cCAR parameters allowed to connect this tendency to the mutual location of the substituent and acceptor or donor, respectively. Close distance is allowing better polarization of the bonds, and in a result, more pronounced substituent effect. Withdrawing groups are depleting in elections H-bond donors, while electron donating groups are providing more electron density in the H-bond acceptor region, in both cases leading to stronger hydrogen bonds.

References

[1] Guerra FC et al., Theoret. Chem. Acc. 125, 245-252, 2010. [2] Baerends EJ et al., ADF2008.01, SCM, Vrije Universiteit, Amsterdam, The Netherlands.

Acknowledgements

The work has been performed under the Project HPC-EUROPA3 (INFRAIA-2016-1-730897), with the support of the EC Research Innovation Action under the H2020 Programme; in particular, the author gratefully acknowledges the support of Miquel Sola and Olga Stasyuk from Universitat de Girona and the computer resources and technical support provided by BSC Barcelona Supercomputing Center.

BOOSTING HYDROGEN ATOM TRANSFER TO MODEL THE ANTIOXIDANT PROPERTIES OF NEUROPSYCHIATRIC DRUGS

L. Orian

Dipartimento di Scienze Chimiche Università degli Studi di Padova, Italy

Introduction

In the brain, a high quantity of oxygen is consumed; this evidence, combined with the very lipid-rich environment, makes the brain vulnerable to oxidative stress. Gingrich [1] defined oxidative stress as the 'new stress', which is related to a serious unbalance of prooxidants (in excess) and antioxidants in the cell, a condition in which high concentrations of reactive oxygen species (ROS) provoke irreversible damage to the tissues. Thus, it is not surprising that several mental disorders, including schizophrenia, bipolar disorder, major depression disorder and anxiety, are accompanied by oxidative stress. Despite the sole antioxidant treatments have not been able to cure any illness, clinical, pre-clinical and epidemiological studies suggest that antioxidant therapy could enhance neuroprotection.

The most important mechanism for ROS quenching is hydrogen atom transfer (HAT), which consists in the transfer of H radical from an organic antioxidant molecule to a radical (typically an alkoxyl or peroxyl radical), leading to the formation of a larger and less reactive radical and a neutral product. HAT may occur from different molecular sites with different thermodynamics and kinetics. Numerous natural substances act as antioxidants against radicals via HAT, like polyphenols, carotenoids, Trolox, curcumin, gallic acid. Recently, it has been reported that the effects of some psychotropic drugs may be associated with antioxidant activity and it has been demonstrated for selected compounds among hypnotics (zolpidem) and SSRI (fluoxetine) that indeed HAT is operative [2-3]. Phenothiazine based molecules are another important class of antipsychotic drugs. In this Project, we have analysed the radical scavenging properties of the parent compound, considering also the selenium and tellurium derivatives, employing the hydroxyl radical.

Methods

Calculations were carried out at ZORA-MO6-2X/TZ2P ae level of theory as implemented in the Amsterdam Density Functional software [4].

Results

The thermodynamically favoured HAT occurs from the amino site. The process resulted slightly less exergonic when going from S to Se and Te; in all cases the energy was larger (in absolute value) than 50 kcal mol^{-1}. Another mechanism was considered for the C sites of the rings, i.e. Radical Adduct Formation (RAF), which consists in the addition of the electrophilic radical and the formation of a bigger and less reactive radical species. For this process, the reaction energies were larger (in absolute value) than 30 kcal mol^{-1} and the same trend with the chalcogens emerged.

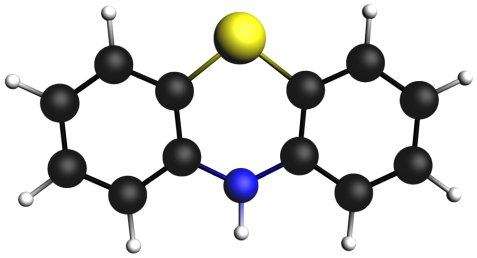

Figure 1 – Phenothiazine.

Conclusions

Based on these results, there is evidence of antioxidant activity of phenothiazine and its Se and Te derivatives. The replacement of the chalcogen (originally S) does not bring any enhancement to the feasibility of the investigated processes, i.e. HAT and RAF. The results are likely transferrable to the substituted phenothiazines which are the real antipsychotic drugs. These results have potential great impact, since any strategy to ameliorate oxidative stress is valuable and they may help to better interpret clinical evidence during therapy.

References

[1] Gingrich J.A., Nat Med, 11:1281–2, 2005. [2] Bortoli M. et al., Comp. Struct. Biotech. J., 17:311-318, 2019. [3] Muraro C. et al., Appl. Sc., 9:6231, 2019. [4] Baerends E. J. et al., ADF2018, SCM, Theoretical Chemistry, Vrije Universiteit, Amsterdam, The Netherlands, http://www.scm.com.

Acknowledgements

The work has been performed under the Project HPC-EUROPA3 (INFRAIA-2016-1-730897), with the support of the EC Research Innovation Action under the H2020 Programme; in particular, the author gratefully acknowledges the support of Prof. Dr. F. M. Bickelhaupt (Theoretical Chemistry, VU Amsterdam) and the computer resources and technical support provided by SURFsara (The Netherlands).

OLEFIN METATHESIS CATALYSED BY RUTENIUM HOVEYADA-GRUBBS COMPLEXES

G. Pareras[1], D. Tiana[1], S. Simon[2], A. Poater[2]

[1]School of Chemistry, University College Cork, Ireland; [2]Institut de Química Computacional i Catàlisi and Departament de Química, Universitat de Girona, Spain

Introduction

Olefins metathesis (OM) catalysis is a soft but powerful synthetic method that allows the formation of carbon-carbon links. OM shows undeniable advantages, but it also presents some disadvantages due to it consists in a homogeneous catalysis process. For example, product contamination by catalyst waste which may cause some unwanted secondary reactions. Therefore, several methodologies of heterogenization of OM catalysts have been developed. Metal-Organic Frameworks (MOFs) are perfect candidates in order to perform this heterogenization of the homogeneous catalysts. Their crystalline, highly porous and easily tuneable structures offer unique environments for the immobilization of active catalytic species. In this work we propose to study computationally the mechanism of OM with possible candidates that could covalently bond within the MOFs (Al)MIL-101-NH2 and (Cr)MIL-101-SO3H.

Methods

DFT static calculations were performed at B3LYP[1] level with the Gaussian16 package. The electronic configuration of the system was described with the triple-ζ basis set cc-pVTZ[2] for O, N, C and H atoms together with the Grimme D3 correction term. For Ru atoms we used the small-core, quasi relativistic Stuttgart/Dresden effective core potential, with the associated triple valence basis set (SDD ECP keyword implemented in Gaussian16). The transition states were located using the synchronous transit-guided quasi-Newton (QST3) approach and the extrema have been checked by analytical frequency calculations.

Results

OM mechanism catalysed by Hoveyada-Grubbs type complexes[3] has been studied. Here we propose two different mechanisms (see Figure 1) for the alkene coordination to the Ru metal centre. Dissociative mechanism consisting first with an activation of the metal due to a dissociation of the Ru-O bond, and consequently the coordination of the alkene. Concerted mechanism where the Ru-O become dissociated due to the direct coordination of the alkene specie. The Hoveyada-Grubbs catalysts of chosen is the SIMes type (see Figure 1). Previous experimental data showed that SIMes are the most reactive and versatile towards different alkenes. Base on experimental data also the solvent of choice it was Dimethyl carbonate (DMC). Finally, the mechanism has been studied in two different temperatures (298.15K and 323.15K).

Dissociative mechanism involves two transition states, first dissociation of the Ru-O bond (TS_Open) and subsequent alkene coordination (TS_Cl1). Energy barrier required for TS_Open is 20.5 Kcal/mol and TS_Cl1 is 22.3 Kcal/mol). While the Concerted mechanism only involves a transition state (TS_Con), energy required to reach this state is 30.6 Kcal/mol. The main difference in between both reaction pathways is the rate determining step (RDS). For the concerted mechanism the direct coordination of the alkene specie becomes the RDS. The two steps coordination in the activated mechanism is substantially lower in energy, becoming the releasing of the final alkene product (TS_I14e) the RDS. Both reaction paths lead to the formation of the intermediate Cl1. From the intermediate Cl1 and the final releasing of the alkene product the reaction pathway presents energy barriers no larger than 12 Kcal/mol. The solvent analysis showed, as expected, a slight stabilization of the different transition states involved in the reaction. Calculations at 323.15 Kcal/mol increased the energy required for all the process.

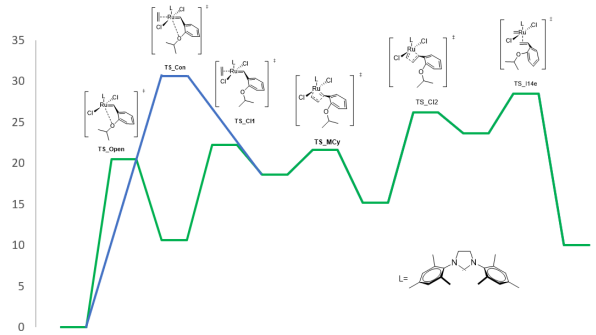

Figure 1 – Gibbs energy profile in Kcal/mol at 298.15K. Green dissociative mechanism. Blue concerted mechanism.

Conclusions

We performed an exhaustive analysis of the metathesis reaction mechanism with Ru Hoveyada-Grubbs catalysts considering two different reaction pathways. The dissociative reaction mechanism, involving two different transition states, showed being the lowest path in energy. The concerted mechanism only including one transition state, is considerably higher in energy. A previous activation of the catalysts facilitates the alkene coordination. Solvent analysis with DMC showed a stabilization of the transition states however, working at higher temperatures than 289.15K could lead a destabilization of the principal transition structures.

References

[1] Stephens, P. et al., J. Phys. Chem., 98, 11623–11627, 1994. [2] Kendall, R. et al., J. Chem. Phys., 96, 6796–6806, 1992. [3] Solodenko, W., et al., J. Chem., 66, 183−191, 2013.

Acknowledgements

The work has been performed under the Project HPC-EUROPA3 (HPC17O1XXP), with the support of the EC Research Innovation Action under the H2020 Programme; in particular, the author gratefully acknowledges the support of Dr. Albert Poater (University of Girona) and the computer resources and technical support provided by BSC.

SIMULATION OF MASS SPECTRA OF MOLYBDENUM OXIDE CLUSTERS BY MOLECULAR DYNAMICS

M. Patzschke[1], M. Steppert[2]

[1]Helmholtz-Zentrum Dresden Rossendorf, Department of Resource Ecology (HZDR), Germany; [2]Leibnitz Universität Hannover, Institut für Radioökologie und Strahlenschutz (IRS), Germany

Introduction

Generation IV nuclear reactors currently under research will use new fuel and will include reprocessing options of nuclear waste. One matrix material for the new fuel types is molybdenum oxide. In the reprocessing step, this will be dissolved in nitric acid. The possible formation of precipitates in all stages of fuel production and reprocessing needs to be understood. Very detailed experimental studies employing mass spectroscopy have been performed at the IRS Hannover [1]. Interesting differences in the stability of certain clusters emerged from this study.

Computational chemistry in the form of molecular dynamics calculations is a powerful tool to simulate mass spectra [2]. We therefore decided to gain better understanding in the stability and structure of molybdenum oxide clusters using molecular dynamics with GFN-xTB [3] combined with higher level of theory calculation for electron attachment and ionisation energies.

Methods

Different crystal structures for molybdenum oxide are known, furthermore two different hydrates known as molybdic acid exist. These crystal structures were obtained from databases. From the structures, fragments with the desired number of molybdenum atoms were cut. The dangling oxygen atoms in the generated structures were capped with hydrogen atoms to ensure neutral species.

The program package Turbomole [4] was then used to optimise the fragments. This was done using the BP86 functional and an SVP basis set an effective core potential was used for Mo. Then the program package QCEIMS [2] was used to perform the actual mass spectrum simulation. This program uses the GFN-xTB approach which is a tight binding method. First an equilibrating run is performed, from this the program generates starting structures (up to 2000 for Mo_{12} clusters). For all these structures MD runs are started and the resulting fragments stored. Once all runs are finished, the number of incidents for a certain fragment is used to calculate its relative intensity in the mass spectrum.

Results

From the mass spectrum the mass of the molecular ion and its fragments are known and due to the excellent resolution of the available mass spectra sum formulas can be generated. But nothing is known about the structures. To ensure that all structural possibilities were included we generated 64 different starting structures with cluster sizes from 4 to 12 molybdenum atoms. The pre-optimised structures showed the very high flexibility of molybdenum oxide clusters. Comparison of the energies of the pre-optimised clusters showed, that all of them are accessible at room temperature. As an example, the simulated mass spectrum for a Mo_{12} cluster can be seen in Figure 1. The cluster selection and pre-optimisation proved rather time consuming. To finalise the project the MD runs will have to be performed after the visit was concluded.

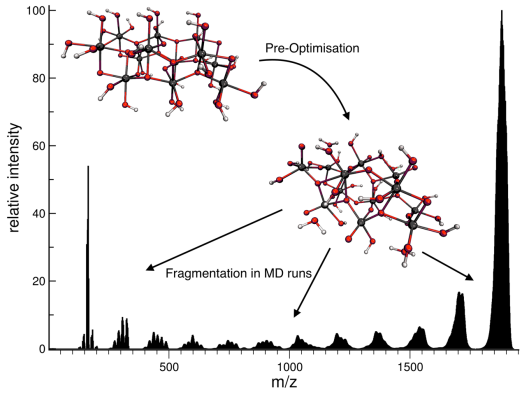

Figure 1 – Simulated mass spectrum of a Mo12 fragment. Also shown is the starting structure capped with hydrogen and the resulting pre-optimised structure which was used to start the MD runs.

Conclusions

The obtained results are very encouraging. However, some features of the measured mass spectra differ from the simulated ones in order to understand this, more MD simulations are necessary and the obtained fragments have to be analysed further. This includes the calculation of ionisation and electron attachment energies.

References

[1] Schulte, V, Masters Thesis, University of Hannover, 2017. [2] Grimme S, Angewandte Chemie, 52(24):6306,2013. [3] Grimme S at al., J.Chem.Theory Comput., 13:1989,2017. [4] Turbomole V7.1 (20405) 2016 available from http://www.turbomole.com

Acknowledgements

The work has been performed under the Project HPC-EUROPA3 (INFRAIA-2016-1-730897), with the support of the EC Research Innovation Action under the H2020 Programme; in particular, the author gratefully acknowledges the support of Mikael Johansson at the Chemistry department of the university of Helsinki and the computer resources and technical support provided by the CSC – IT center for Science Ltd., Espoo Finland.

COMBINED ORBITAL-SPACE/REAL-SPACE ANALYSIS OF ELECTRON-CHARGE REDISTRIBUTIONS ON PARALLEL ARCHITECTURES

S. Rampino

SMART Laboratory, Scuola Normale Superiore, Pisa, Italy

Introduction

Chemical processes such as bond formation or electron excitation are often interpreted in terms of the changes that the electron density of a system undergoes in going from a reference (unbound or ground) state to the final (bound or excited) one. A static picture of such electron-charge redistribution is conveniently obtained by computing the electron-density difference $\Delta\rho(x, y, z)$ between the final and the reference state, thus obtaining a three-dimensional function such as that one depicted in Figure 1, featuring negative values in regions of electron depletion (red lobes) and positive values in regions of electron accumulation (blue lobes) [1].

WAVERLEY is a modern-Fortran program for a combined orbital-space/real-space analysis of charge redistributions allowing for a quantitative resolution of concurrent, chemically meaningful charge flows [2,3]. WAVERLEY has proved most powerful in singling out σ-donation and π-backdonation in coordination complexes [4], however its applicability is hampered by the performance limits of its serial implementation.

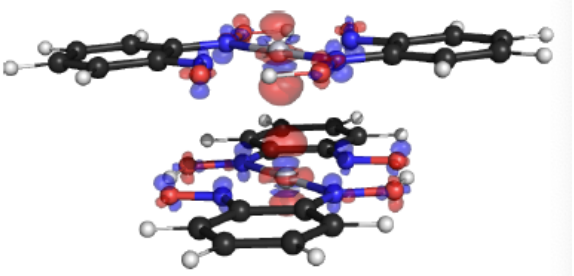

Figure 1 – Charge redistribution upon dimerization of bis(1,2-benzoquinonedioximato)-platinum(II), $Pt(bqd)_2$.

Combined orbital-space/real-space analysis

Once a suitably formulated $\Delta\rho(x, y, z)$ has been computed, WAVERLEY performs a decomposition in terms of additive contributions coupling pairs of so-called natural orbitals for chemical valence $\phi_k(x, y, z)$ through a weight factor v_k:

$$\Delta\rho = \sum_k v_k(|\varphi_k|^2 - |\varphi_{-k}|^2) = \sum_k v_k \Delta\rho_k$$

In other words, the total electron charge redistribution results from additive charge flows of v_k electrons flowing from orbital ϕ_{-k} to orbital ϕ_k, with k ranging from one to the number of occupied molecular orbitals of the adduct. Quantitative charge-flow profiles for each of these components can then be extracted by a suitable partial integration in physical space of the associated $v_k\Delta\rho_k$.

Parallel implementation

A profiling of the serial version of WAVERLEY shows that most of the execution time is spent in evaluating the orbitals as linear combinations of known basis functions in nested loops over the orbital index and a grid of x, y, and z values. An efficient approach is therefore to target such loops within a shared-memory parallel-programming paradigm with OpenMP. Test calculations on a relatively small system of 12 atoms, 66 electrons and 544 primitive basis functions, involving the evaluation of 66 orbitals on 90 x 69 x 95 grids, shows almost linear speed-up up to 8 threads (Figure 2). Additional preliminary tests show that linear speed-up up to 16 and 32 can be reached for larger systems and larger basis sets.

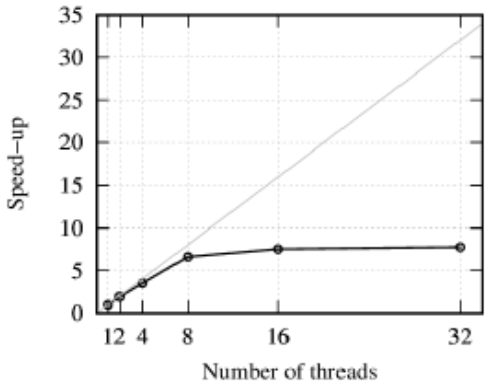

Figure 2 – Speed-up as a function of the number of threads.

Conclusions

A parallel version of WAVERLEY has been developed which overcomes the barrier associated with large computing resources in order to reach more complex systems of interest in catalysis, material science and biology within a high-accuracy framework.

References

[1] Bader RFW et al., The Journal of Chemical Physics, 46:3341-3363, 1967. [2] Bistoni G et al., The Journal of Chemical Physics, 142:084112, 2015. [3] Salvadori A et al., Journal of Computational Chemistry, 39:2607-2617, 2018. [6] Fusè M et al., Chemical Communications, 54:2397-2400, 2018.

Acknowledgements

The work has been performed under the Project HPC-EUROPA3 (INFRAIA-2016-1-730897), with the support of the EC Research Innovation Action under the H2020 Programme; in particular, the author gratefully acknowledges the support of Prof. Carole Morrison of the School of Chemistry of the University of Edinburgh and the computer resources and technical support provided by EPCC.

PATH SAMPLING FOR ATMOSPHERIC REACTIONS: FORMIC ACID CATALYSED CONVERSION OF SO$_3$ + H$_2$O TO H$_2$SO$_4$

E. Riccardi[1], *C. Daub*[2]

[1]*Department of Chemistry, University of Helsinki, Helsinki, Finland;* [2]*Department of Chemistry, Norwegian University of Science and Technology, Trondheim, Norway*

Introduction

SO_3 dispersed in the atmosphere reacts with water, generating H_2SO_4 which is one of the main contributors to acidic rain. It also contributes to nucleation processes in the upper atmosphere.

Static quantum chemical calculations of the initial and final states show that the reaction becomes nearly barrier-less, and hence that HCOOH is a very effective catalyst. It seems likely that the formic acid catalysed hydration of SO_3 is a significant contributor to sulphuric acid concentrations in the atmosphere.

To study the dynamics of the process, path sampling approach appears to be a suitable. It can sample accurately the reaction process respective the system natural dynamics. The path sampling approach here chosen to study the reaction is the replica exchange transition interface sampling (RETIS). It permits the investigation of the path space, and thus the determination of a reaction rate, orders of magnitude faster than conventional simulations.

The RETIS methodology has been combined with molecular dynamics (AIMD) simulations to predict the reaction rate of the unimolecular SO_3 hydration reaction with formic acid, considering different density functional theory (DFT) functionals and basis sets. The results produced y the path sampling approach will then be compared with data available in the literature produced by more approximate methods (e.g. TST).

Methods

We perform DFT-based Born-Oppenheimer molecular dynamics (BOMD) simulations using the QUICKSTEP module in CP2K. Hybrid functionals such as B3LYP or PBE0 which include some of the Hartree-Fock exchange correlation are necessary to obtain DFT based results which are in good agreement with fully ab initio methods. However, using hybrid functionals in BOMD simulations would be prohibitively expensive, especially for an exploratory study such as this one. In the end, in our BOMD simulations, we have decided to compare two Generalized Gradient Approximation (GGA) DFT methods, with three different basis sets. First, we use the BLYP functional with the DZVPMOLOPT-GTH basis functions, which we have previously used to investigate formic acid in bulk water [1]. Although the BLYP results are not very accurate in terms of the comparative energies of the initial and final states, it was a fairly inexpensive methodology to use for initial investigation.

After this, we also set up simulations with the PBE functional and both the TZVP-MOLOPT-GTH and TZV2P-MOLOPT-GTH basis sets. Path Sampling simulation, with the RETIS [2] method, has been performed with the PyRETIS python library [3]. The approach computed the rate from the reactant to the product state by the estimation a reaction flux and a transition probability. The relative molecular configurations are depicted in Figure 1.

Results

Our most accurate estimate has been obtained via PBE calculations with the TZV2P basis set, k = 3.5×10−4 fs−1, with a statistical error of ∼ 50%. Overall, our predicted rate constant is in reasonable agreement with previous estimates in the literature, despite the fact that we significantly underestimate the energy difference between the reactant and product states. We might reasonably expect that a RETIS calculation using a hybrid functional such as PBE0 with a more accurate energy difference would result in a somewhat higher rate constant. Unfortunately, at the present time the computational load for such calculations leaves the use of hybrid functionals in path sampling calculations beyond our reach. Comparison of results using the same basis set and level of theory (BLYP, DZVP) at two different temperatures (300~Kand 250K) shows that the RETIS simulations predict a significantly lower rate constant at lower temperature. While this may make intuitive sense, it disagrees with the TST results, which predict an increase in the unimolecular rate constant as temperature lowers.

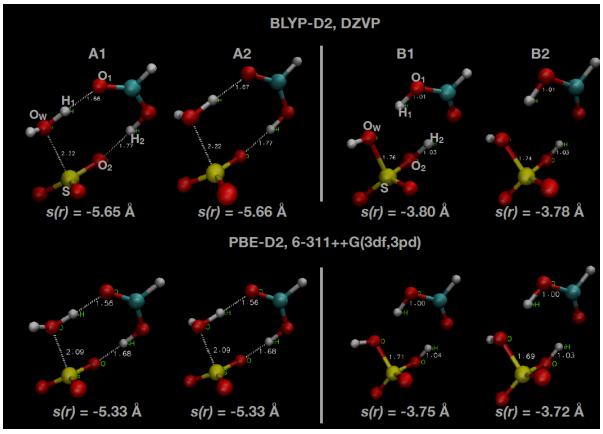

Conclusions

We have made use of path sampling AIMD simulations to study the hydrolysis of SO_3 when catalysed by formic acid. We discuss in detail the reaction pathway(s) that can describe the conversion from $SO_3 + H_2O$ to H_2SO_4. The mechanism has been highlighted and the overall rate computed with different levels of theory.

References

[1] Daub, C. et all J. Phys. Chem. B, 123:6823–6829. [2] van Erp, T. S. Phys. Rev. Lett., 98:268301. [3] Lervik, A., et al J. Comput. Chem., 38:2439–2451.

Acknowledgements

The work has been performed under the Project HPC-EUROPA3 (INFRAIA-2016-1-730897), with the support of the EC Research Innovation Action under the H2020 Programme; in particular, the author gratefully acknowledges the support of Christopher Daub at the Department of Chemistry, University of Helsinki, Helsinki, Finland and the computer resources and technical support provided by CSC - IT Center for Science Ltd.

THEORETICAL INSIGHTS ON LIGHT-DRIVEN ROTARY MOLECULAR MOTORS

F. Romeo Gella[1], *S. Faraji*[2]

[1]*Departamento de Química, Universidad Autónoma de Madrid, Spain;* [2]*Theoretical Chemistry Group, Zernike Institute for Advanced Materials, University of Groningen, The Netherlands*

Introduction

Exerting control over biological processes is a great challenge which could revolutionize the fields of nanotechnology or biotechnology. Light is perhaps one of the most convenient external agents as it allows fine control, both in a temporal and a spatial manner, avoiding contamination and invasiveness of the tissue. Introducing molecular switches into nucleic acids has been used as an efficient tool for reversibility, initiating or avoiding hybridization of nucleic acids [1]. A new twist in the field of photoregulation of biomolecules has been recently proposed by the group of Ben Feringa [2], which is based on the replacement of standard photoswitches by light-driven rotary molecular motors. The proposed xylene-based rotor maximizes structural change in the hybrid DNA hairpin and several photophysical and dynamical parameters were experimentally determined. The aim of this work is to investigate from a theoretical perspective the excited-state participation in the *cis-trans* isomerization occurring on the proposed rotor.

Methods

DFT and TDDFT calculations have been performed in the Q-Chem 5.2 code. Geometry optimizations for the ground state of the *cis* and *trans* isomers and their respective vertical excitation calculations were performed at the ωB97X-D/cc-pVDZ level of theory. This level of theory was also used for scanning, within a relaxed scheme, the dihedral coordinate driving from the *trans* to the *cis* isomer and vice versa. All calculations have been performed in gas phase.

Spin-Flip TDDFT calculations were also performed at the B5050LYP/cc-pVDZ level of theory, as the method requires a large fraction of Hartree-Fock exchange to give accurate results [3].

Results

Vertical excitations were calculated for the minimum energy geometries of the ground state of both *trans* and *cis* isomers. Both isomeric forms show an electronic transition of character ππ* corresponding to the first excited state (S_1) and also the bright state. Vertical excitation energies are 4.28 eV (290 nm) for the *trans* isomer and 4.11 eV (302 nm) for the *cis*. A blue-shift of excitation energies is observed in comparison with the absorption spectra experiments for the stable *trans* form (no data was published for the *cis*) of around 0.3 eV, which may arise from not taking into account solvent effects in our simulations.

Scan of the ground state along the dihedral $C_2C_8C_{15}C_{19}$ separating both symmetric subunits reveals several remarks: (1) an energy barrier of around 70 kcal/mol, which is, in principle, unsurpassable at room temperature, (2) occurrence of a region of degeneracy in the in-between region of both stable isomeric forms, (3) unstable *cis* or *trans* forms were not found along the scan coordinate.

Same approach was used with Spin-Flip TDDFT and, despite a slightly clearer description of the near-degeneracy region, no unstable intermediates were found. The energy barrier was reported to be slightly smaller, although being still significant (around 55 kcal/mol).

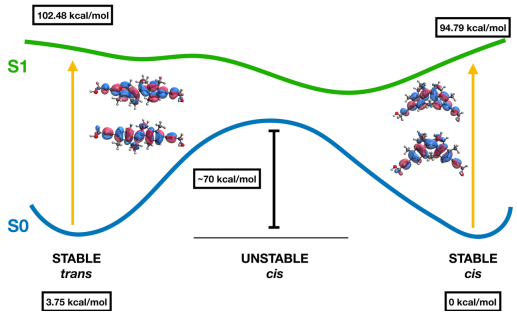

Figure 1 – Potential Energy Surface of the system. Relevant molecular orbitals are plotted and energies are in kcal/mol with respect to the minimum of cis.

Conclusions

We managed to describe the ground and the excited states of our system at the (TD)DFT level of theory and also using the Spin-Flip approach [3]. The isomerization process seems unfeasible to happen directly through the ground state of the system, requiring an initiating photoactivation event which excites the molecule to a ππ* state. Although unable to describe the whole isomerization process, further research on the topic is planned. In particular, exploring a new reaction coordinate to try to locate the unstable intermediates on both directions of the reaction and study the possible influence of the triplet manifold on the photoswithing event.

References

[1] Letsinger R. L. et al., JACS, 117(28): 7323-7328, 1995. [2] Lubbe A. S. et al., JACS, 140(15): 5069-5076, 2018. [3] Shao Y. et al. J. Chem. Phys., 118(11):4807-4818,2003.

Acknowledgements

The work has been performed under the Project HPC-EUROPA3 (INFRAIA-2016-1-730897), with the support of the EC Research Innovation Action under the H2020 Programme; in particular, the author gratefully acknowledges the support of Shirin Faraji and the Theoretical Chemistry Group (Zernike Institute of Advanced Materials at the University of Groningen) and the computer resources and technical support provided by SurfSARA.

AB INITIO SIMULATION OF CHARGED AND POLAR INTERFACES IN CONTACT WITH THE LIQUID PHASE

T. Sayer[1], *C. Zhang*[2]

[1]*Cambridge University, United Kingdom;* [2]*Uppsala University, Sweden*

Introduction

Supercomputer time was requested from KTH to perform density functional theory molecular dynamics (DFTMD) simulations. These were split between an ongoing project and a new project to be agreed upon at the start of the residency. The visit took place at Uppsala University from the 1st August to the 18th of September.

Besides the treatment of the electronic degrees of freedom, to use DFTMD is to use a reactive forcefield. This is of particular interest because of the reported dissociation of water on magnesium oxide (MgO). MgO has an analogous structure to the first project's NaCl system, but with additional complexity owing to its more covalent bonding, partial charges, and surface stability. It is believed that the MgO(001) non-polar surface dissociates water [1], and it is has further been believed for some time that this surface is ultimately unstable with respect to the compensated, polar termination [2]. We therefore set out to answer several questions: can the stabilities of these two surfaces be reproduced and/or rationalized from their differing pKa values, and can this quantity be straightforwardly separated from capacitive charging in a simulation? Does the presence of an electrolyte significantly affect behaviour, specifically the dissociation of water near the interface – indeed will we observe such dissociation in a pure water system to begin with?

Methods

Use of the supercomputing facilities comprises the final, straightforward part of the project workflow. Firstly, classical simulations are run locally to ascertain the correct boundary conditions and then obtain locally equilibrated starting configurations for DFTMD. These configurations were then subject to a standard geometry optimization, before being propagated under Born-Oppenheimer DFTMD using the CP2K open-source software package. To optimize, test calculations were run to determine the charge density cutoff of the plane-wave expansion, which was found to be sufficiently accurate at 320 Ry and a relative cutoff of 40 Ry. With these parameters, the computing time (per-step-per-node) plateaued at 8 nodes (with 32 tasks per node, on the Beskow system. 110 kcoreh were allocated, of which 69.6 were used within the time limit. Just over 1 ps could be computed in 12 real hours, which is around 3 kcoreh of budget. These systems contained between 500 and 600 atoms (O,H,Na,Cl).

Results

A small amount of the budget was used to extend existing DFTMD trajectories for a polar-electrolyte interface, NaCl(111)|$NaCl_{(aq)}$. These data form the basis for a paper soon to be published in JCP [3]. Further to those ideas already matured before the visit, significant analysis and discussion of these data occurred between the author and the host during the residency. This would not have been possible to nearly the same extent without the support of the HPC-Europa3 scheme.

Our data for MgO is preliminary. We found that the polar system prompts the immediate dissociation of interfacial waters upon DFTMD restarts of classically equilibrated structures: in sharp contrast to the NaCl system reported in [3]. This raises several challenges in terms of equilibration that we are addressing. In contrast, with the non-polar system we *did not* see the expected 1/3 dissociation of interfacial waters we expected [1], on the 10 ps timescale. Moreover, in the presence of electrolyte, pre-dissociated (by hand) structures readily recombined (see Figure 1).

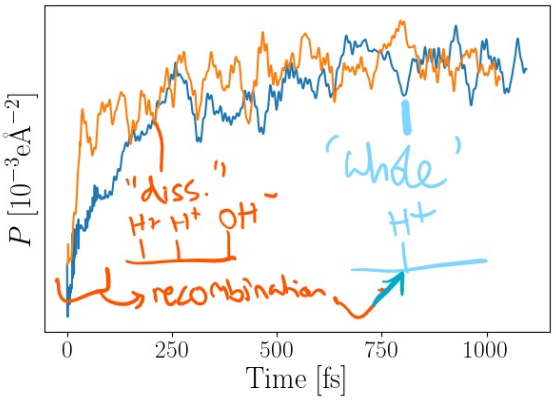

Figure 1 – MgO(001)|$NaCl_{(aq)}$ with dissociated (orange) and whole (blue) interfacial waters re-equilibrated to the same polarization state with recombination of the water ions (orange) on the femtosecond timescale.

Conclusions

Significant further study will be needed to reconcile these data. Nevertheless, *via* both the importance of the electronics [3] and the unexpectedly variable reactivity (chemoadsorption) displayed by apparently similar interfacial systems (Figure 1), DFTMD readily demonstrates the inadequacy of classical forcefields and by extension, the desirability of high-performance computing.

References

[1] Laporte, S et al., Phys. Chem. Chem. Phys., 2015, 17, 20382. [2] Refson, K et al., Phys. Rev. B, 1995, 52, 10823. [3] Sayer, T et al., arXiv:1908.00892 (accepted, JCP).

Acknowledgements

The work has been performed under the Project HPC-EUROPA3 (INFRAIA-2016-1-730897), with the support of the EC Research Innovation Action under the H2020 Programme; in particular, the author gratefully acknowledges the support of Chao Zhang, Lilit Axner and the computer resources and technical support provided by KTH. TS kindly thanks Professor Hermansson and her group for their hospitality.

ADSORPTION OF ORGANIC SEMICONDUCTORS ON THE RECONSTRUCTED GOLD SURFACE

L.K. Scarbath-Evers[1], M. Todorović[2], D. Golze[2] and P. Rinke[2]

[1]Institute of Chemistry, Martin-Luther University Halle-Wittenberg, Germany; [2]Department of Applied Physics, Aalto University School of Science, Finland

Introduction

This short report highlights a few of the results obtained during the visit. We investigate the adsorption of the organic semiconductor α-sexithiophene (α-6T) on the reconstructed Au(100) surface using density functional theory (DFT) calculations. Due to its complex reconstruction the Au(100) surface offers various adsorption sites that can be classified into on-ridge and in-valley of the reconstruction rows, with the latter one being energetically preferred. Previous calculations revealed that when placed on the ill-preferred on-ridge position, the molecule prefers to alter the surface reconstruction and create itself a valley-like environment instead of migrating into the valley during the structural optimization [1].

Methods

Calculations were carried out with the electronic structure code FHI-AIMS [2] using the tier1-tight numerical basis sets, the Perdew-Burke-Ernzerhof (PBE) exchange-correlation functional [3] the Tkatchenko-Scheffler van der Waals correction (TS-vsW) [4] and vdWsurfcorrection [5], respectively, and the atomic zeroth-order regular approximation (ZORA) [6,7]. For the reconstructed Au(100) surface, we used the (20x5) DFT model from Havu et al. [8].

Results

We investigated the adsorption of a single molecule in more detail by comparing the effect of two different dispersion corrections, the DFT+vdW method developed by Tkatchenko et al. [3] and the the vdWsurf dispersion correction [4]. The latter one employs the Lifshitz-Zaremba-Kohn (LZK) theory [9,10] to account for non-local screening effects. A comparison of the adsorption structures after on-ridge adsorption with the TS-vdW and the vdWsurf method respectively is presented in Figure 1 a. In both cases, when placed on the ill-favoured on-ridge position, the molecule alters the surface reconstruction and creates itself a valley-like environment. This created valley position is further denoted as r-to-v. The altered surface looks similar for both dispersion corrections. Moreover, the molecule adsorbs completely flat and with the Cα atoms (see Figure 1 b) directly above the reconstruction valley, albeit the adsorption distance is slightly smaller in case of the vdWsurf dispersion correction, see also Table 1. Furthermore, employing the vdWsurf dispersion correction leads to reduced adsorption energies as shown in Table 1.

System	E_{ads} [eV]	d_{ads} C_α-Au [Å]
v (TS-vdW)	-4.34	3.34
v (vsW^{surf})	-3.77	3.19
r-to-v (TS-vdW)	-4.31	3.22
r-to-v (vsW^{surf})	-3.78	3.15

Table 1 – Adsorption energy (E_{ads}) and distances (d_{ads}) after *on-ridge* (r-to-v) and *in valley* (v) adsorption

Conclusions

We investigated adsorption of α-6T on the reconstructed Au(100) surface by electronic structure calculations. We compared two different dispersion corrections and find that both give similar qualitative results. Quantitatively, the vdWsurf dispersion correction yields smaller adsorption heights and lower adsorption energies. These results are in agreement with results obtained for PTCDA on Ag(111) [5].

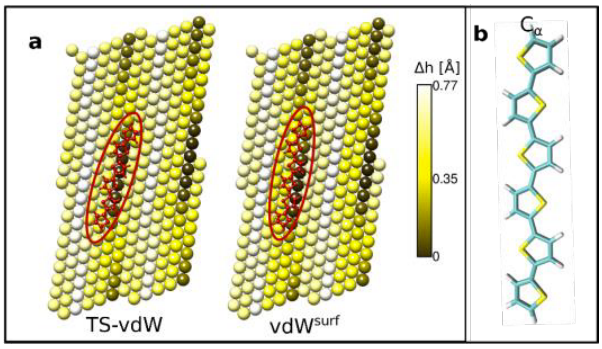

Figure 1 – a: Color coded height image of the Au(100) surface after on-ridge adsorption when using the TS-vdW and the vdWsurf dispersion correction, respectively. b: the investigated molecule α-6T.

References

[1] Laura Scarbath-Evers et al., PRM, 3, 011601(R),2019. [2] V. Blum, et al. Comput. Phys. Commun., 180, 2175 ,2009. [3] J. P. Perdew, et al. PRL, 77, 3865, 1996. [4] A. Tkatchenko et al., PRL., 102, 073005, 2009. [5] V. G. Ruiz, et al., PRL., 108, 146103, 2012. [6] C. van Wüllen, J. Chem. Phys., 109, 392, 1999. [7] J. van Lenthe, et al., Chem. Phys. Lett., 328, 107 – 112, 2000. [8] P. Havu et al., Phys. Rev. B, 82, 161418, 2010. [9] E. Zaremba et al, Phys. Rev. B, 13, 2270, 1976. [10] E. M. Lifshitz, Sov. Phys. JETP, 2, 73, 1956.

Acknowledgements

The work has been performed under the Project HPC-EUROPA3 (INFRAIA-2016-1-730897), with the support of the EC Research Innovation Action under the H2020 Programme; in particular, the author gratefully acknowledges the support of Prof. Patrick Rinke, Department of Applied Physics, Aalto University and the computer resources and technical support provided by the CSC-IT Center for Science.

MODELLING URANYL CHEMISTRY IN LIQUID AMMONIA

N. Sieffert[1], *M. Bühl*[2]

[1]*Univ. Grenoble Alpes & CNRS. Grenoble. France;* [2]*University of St Andrews, School of Chemistry, St Andrews, United Kingdom*

Introduction

Uranium (generally found as uranyl UO_2^{2+} cation) is of key importance in the framework of radioactive waste management. In order to efficiently recycle UO_2^{2+}, a detailed knowledge of its complexation properties is essential. The latter are significantly influenced by the nature of the solvent, so that the rationalisation of solvation effects is intimately linked to the study of complexation equilibriums. Herein, we explored uranyl chemistry considering liquid ammonia as solvent. The latter is widely used in inorganic chemistry, however, it is still little employed as far as uranyl is concerned, so that structural, thermodynamic and kinetic information is scarce in the literature [1]. Herein, we developed a cost-effective computational protocol, allowing for the computation of complexation free energies "in solution", focusing on the reactions shown in Scheme 1.

Methods

Car-Parrinello Molecular Dynamics (CPMD) simulations have been performed on a system composed of 1 UO_2^{2+} cation and 37 NH_3 molecules, in a periodic cubic box of cell-length 13.22 Å, corresponding to a liquid density of 0.71. The Pointwise Thermodynamic Integration (PTI) technique has been employed to compute the free energy profile of complexation of NH_3 to uranyl. "Static" Density Functional Theory (DFT) calculations have been performed using the (small core) SDD Effective Core Potential (and its corresponding basis set) to describe U, and aug-ccpVTZ basis sets for other elements. Several Continuum Solvation Models (CSMs) have been investigated, and standard corrections for thermochemistry (obtained from harmonic frequencies) have been applied. See reference [2] for full information, including full citations of each methods.

Results

Our "static" DFT protocol is based on the following equation: $\Delta G_{liq} = \Delta E_{gas} + \delta E_{BSSE} + \delta E_{solv} + \delta E_G$ (eq. 1), where ΔE_{gas} stands for reaction energies in the gas phase, whereas δE_{BSSE}, δE_{solv} and δE_G are correcting terms for the basis set superposition error (BSSE), solvation effects and thermochemistry, respectively. We first benchmarked 17 density functionals for the calculations of ΔE_{gas} for the two processes described by eq. 2 and 3 (see Scheme 1). The five most accurate of them are: ωB97X (0.6) < PBE0-D3(bj) (0.8) < PBE0 (1.0) < B3PW91-D3(bj) (1.0) < B3LYP-D3(bj) (1.1), where the number in parenthesis is the mean absolute error (in kcal/mol) against our CCSD(T) reference. Next, we evaluated the performance of 5 CSMs to reproduce solvation free energies (in eq. 2 and 3) obtained from reference PTI/CPMD calculations. The COSMO model is found to be the most accurate, followed by the SMD model. IEFPCM, CPCM and IPCM showed larger errors.

Using our protocol, we found that the reaction free energies of eq. 2 and 3 are 14.4 and 6.1 kcal/mol, respectively. Finally, the applicability of our protocol has been evaluated considering the following reaction:

$$[UO_2(NH_3)_5]^{2+} ... 2X^- \rightarrow [UO_2X_2(NH_3)_3] ... 2NH_3 \text{ (eq. 4)}$$

The corresponding reaction energies are: -23.4, -2.9 and +2.7 kcal/mol, with X = F-, Cl- and Br-, respectively.

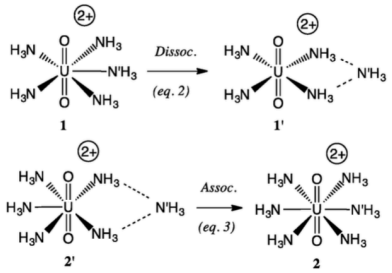

Scheme 1 Reactions and labelling of the complexes considered for the development of the computational protocol.

Conclusions

We developed a cost-effective "static" DFT model allowing for the computation of complexation free energies "in ammonia". The latter involve the computation of gas phase reaction energies at the PBE0-D3(bj) level (including BSSE correction) and correction for solvation effects using the COSMO model. The latter have been carefully validated against high-level CCSD(T) reference calculations and PTI/CPMD simulations (involving explicit solvation), respectively. Using our protocol, we found that the 5-fold coordinated complex $[UO_2(NH_3)_5]^{2+}$ is the most stable in "neat" ammonia (compared to tetra- and hexa- coordinated analogues). In presence of halide (X^-), the formation of $[UO_2(X)_2(NH_3)_3]^{2+}$ from $[UO_2(NH_3)_5]^{2+}$ is significantly exergonic with X = F^-, slightly exergonic with Cl- and clearly endergonic with Br^-. All these results [2] are in qualitative agreement with the experiments [1].

References

[1] S. S. Rudel, S. A. Baer, P. Woidy, T. G. Müller, H.-L. Deubner, B. Scheibe and F. Kraus, Z. Kristallogr. Cryst. Mater 2018, in press. DOI: 10.1515/zkri-2018-2066. [2] N. Sieffert, A. Thakkar and M. Bühl, Chem. Commun. 2018, 54, 10431-10434.

Acknowledgements

The work has been performed under the Project HPC-EUROPA3 (INFRAIA-2016-1-730897), with the support of the EC Research Innovation Action under the H2020 Programme; in particular, the author gratefully acknowledges the support of EastCHEM and the computer resources and technical support provided by EPCC.

EVALUATION OF ONE-ELECTRON SCATTERING MATRIX ELEMENTS OF MOLECULES

M. Simmermacher[1], A.M. Carrascosa[2] and A. Kirrander[2]

[1]Department of Chemistry, Technical University of Denmark, Denmark; [2]EaStCHEM, School of Chemistry, University of Edinburgh, United Kingdom

Introduction

The advent of x-ray free-electron laser facilities (XFELs) that provide ultrashort, highly intense, and coherent pulses of x-rays permit the experimental investigation of chemical reactions or photophysical relaxation processes in real-time. They enable chemists and physicists to obtain unprecedented insights into the dynamical behaviour of matter. One of the experimental techniques that becomes possible at XFELs is ultrafast non-resonant x-ray scattering. Here, a target molecule is first excited by a laser pulse and subsequently probed by an x-ray pulse that is scattered onto a detector. By variation of the time delay between the two pulses and by analysis of the recorded scattering patterns, detailed information about the time evolution of the excited molecule is gathered.

In order to exploit the vast potential of this new technique and to interpret existing or future experiments, extensive *in silico* simulations based on quantum electrodynamics are required. These simulations necessitate new computer codes that allow the evaluation of scattering matrix elements (SMEs) from highly accurate *ab initio* electronic wave functions calculated with available quantum chemical software. SMEs describe the amplitude and probability of scattering an x-ray photon by an atom or a molecule into a certain direction in space. Many of such matrix elements for various molecular geometries and several electronic states are involved in a reliable simulation and each element is evaluated on a two-dimensional grid that covers the detector. Such a task is computationally very demanding but can be carried out in parallel. It is thus a case for the use of high-performance computing (HPC).

We report the development, parallelization, and extensive testing of a code that evaluates one-electron SMEs from multiconfigurational wave functions on ARCHER. SMEs of the hydrogen molecule H_2 in its nine energetically lowest-lying electronic singlet states for different H–H bond lengths are computed. The results serve as a basis for the first complete simulation of the two-dimensional ultrafast scattering signal of an excited molecule within a fully quantised framework [1, 2].

Methods

A one-electron SMEs can be expressed as a Fourier transform of the electron density. The electron density, in turn, is given by the absolute square of the electronic wave function where all coordinates apart from one are integrated out. Considering that most quantum chemical programmes optimise the *ab initio* wave function in terms of Gaussian functions, known as Gaussian-type orbitals (GTOs), one can construct an algorithm that computes SMEs efficiently from *ab initio* data. For that we made use of the Gaussian product theorem as well as of the fact that the Fourier transform of any Gaussian function has an analytical solution.[3,4] We have furthermore parallelised our code to make use of HPC facilities such as ARCHER. Since the evaluation of an SME on a given grid point of the detector is independent of all other grid points, the computation on the entire grid is embarrassingly parallel. Moreover, we have split the operations performed on the GTOs evenly across the available nodes by means of an MPI reduction.

We have tested the code extensively with *ab initio* data for the nine energetically lowest-lying singlet states of the hydrogen molecule H_2. The wave functions were optimised using State-Averaged Complete Active Space Self-Consistent Field theory (SA-CASSCF) and the d-aug-cc-pVQZ basis set in the quantum chemical programme package MOLPRO. Once our code consistently provided results that visually and numerically matched our theoretical expectations, the SMEs were interpolated to a finer grid and used in a simulation of ultrafast time-resolved x-ray scattering.

Results

The results of the simulations are reported and discussed in detail in References 1 and 2.

Conclusions

We have developed, parallelised, and tested a code that efficiently evaluates accurate one-electron SMEs from *ab initio* electronic wave functions. These matrix elements are urgently required for the simulation of ultrafast time-resolved x-ray scattering experiments that become possible at XFELs. Their evaluation is computationally very demanding but can be significantly accelerated by making use of HPC. The feasibility and reliability of such calculations were demonstrated for the hydrogen molecule H_2. The results are published in renowned physics journals.

References

[1] Simmermacher M et al., Phys. Rev. Lett., 122(7):073003, 2019. [2] Simmermacher M et al., J. Chem. Phys., 151(17):174302, 2019. [3] Northey T et al., J. Chem. Theory Comput., 10(11):4911–4920, 2014. [4] Carrascosa A M et al., Phys. Chem. Chem. Phys., 19(30):19545–19553, 2017.

Acknowledgements

The work has been performed under the Project HPC-EUROPA3 (INFRAIA-2016-1-730897), with the support of the EC Research Innovation Action under the H2020 Programme; in particular, the author gratefully acknowledges the support of Dr Adam Kirrander at the University of Edinburgh and the computer resources and technical support provided by the EPCC.

REACTIVITY OF FE(IV)-OXO COMPLEXES WITH TRIPEPTIDE IN OXIDATION REACTION OF C-H BOND

O.A. Stasyuk[1], M. Swart[2]

[1]Institute of Organic Chemistry and Biochemistry, Prague, Czech Republic; [2]Institute of Computational Chemistry and Catalysis of the University of Girona, Spain

Introduction

Very recently different peptides have been tested in combination with iron complex in the asymmetric epoxidation of α-methylstyrene derivatives [1,2]. Synthetic iron(IV)-oxo complexes are also employed in C-H bond activation process. Previous studies showed that reactivity of such complexes depends on supporting ligands and spin state of iron. Usually reactivity of synthetic complexes is characterized as "two-state reactivity" because of small gap between triplet (S=1) ground state and quintet (S=2) excited state. As a result, the spin state of the system changes when approaching the transition state and reaction proceeds via quintet surface with remarkably lower activation barrier [3]. However, last year nonclassical single-state reactivity of iron(IV)-oxo complex has been reported [4].

The main goal of this project is to study reactivity of Fe(IV)O-GGHa complex in oxidation reactions of C-H bond in cyclohexane and cyclohexadiene depending on a spin state of iron and solvent.

Methods

Structure of Gly-Gly-His-N-methyl amide (GGHa) fragment was taken from the crystal structure of Cu(II)–glycylglycyl-L-histidine-N-methyl amide monoaquo complex. Structures of Fe(IV)O-GGHa complex in different spin states were optimized using ADF program with three functionals: BP86-D3, S12g and B3LYP; including ZORA scalar relativistic corrections and COSMO solvation model (water and acetonitrile). Search of stationary points and calculation of their Gibbs energies have been performed at the BP86-D3/TDZP level of theory. The nature of the found transition states was investigated using MO analysis.

Results

According to the results, the ground state of Fe(IV)-oxo complex both in water and acetonitrile is triplet state as for other biomimetic iron complexes. The value of quintet-triplet energy gap varies from 16 to 24 kcal/mol depending on the DFT functional used.

The first hydrogen abstraction step can pass through different trajectories (σ and π). However, our calculations for triplet and quintet spin states always converged to one type of TS – bent structure with σ(CH)- $\pi^*_{xz/yz}$ interaction. An investigation of the molecular orbitals involved in the reaction shows that unoccupied π-orbitals of the complex are located slightly lower than σ-orbitals and thus interact with occupied σ(CH) orbital of cyclohexane or cyclohexadiene.

In the second step, there is a competition between radical rebound to form the alcohol product and desaturation process. This step proceeds with significantly smaller energy barrier for cyclohexane than for cyclohexadiene. It means that cyclohexadiene probably undergoes desaturation to give benzene rather than forms the alcohol product.

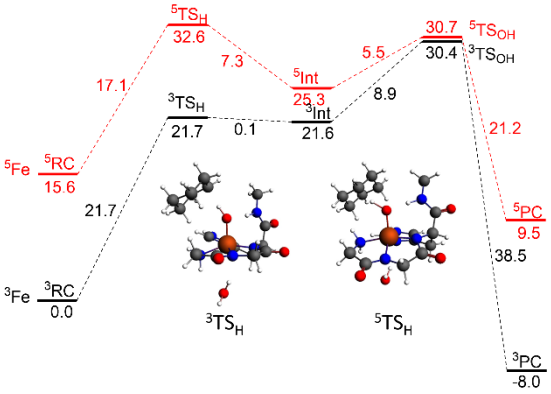

Figure 1 - Gibbs energy profiles (in kcal/mol) for cyclo-hexane oxidation. RC - reactant complex, TS - transition state, Int – intermediate.

Conclusions

Based on the value of quintet-triplet energy gap for the Fe(IV)O-GGHa complex, it can be concluded that the quintet state is thermally unreachable and the oxidation reaction will proceed only on the triplet surface in both water and acetonitrile. The energy barrier for the first hydrogen abstraction step is higher for the reaction with cyclohexane than with cyclohexadiene. In the second step, the formation of the alcohol product is more likely for cyclohexane rather than for cyclohexadiene, where the process of desaturation with the formation of benzene prevails.

References

[1] Cussó O et al., Chem. Sci. 8:3660-3667, 2017. [2] Vicens L et al., Dalton Trans. 47:1755-1763, 2018. [3] Hirao H et al., J. Am. Chem. Soc. 128:8590-8606, 2006. [4] Kupper C. et al., J. Am. Chem. Soc. 139:8939-8949, 2017.

Acknowledgements

The work has been performed under the Project HPC-EUROPA3 (INFRAIA-2016-1-730897), with the support of the EC Research Innovation Action under the H2020 Programme; in particular, the author gratefully acknowledges the support of the Institute of Computational Chemistry and Catalysis of the University of Girona and the computer resources and technical support provided by BSC.

INVESTIGATION OF A HYBRID RESTRICTED ACTIVE SPACE CONFIGURATION INTERACTION-DENSITY FUNCTIONAL THEORY METHOD FOR ELECTRONIC PROPERTIES IN SINGLET FISSION CHROMOPHORES

M. Wibowo

Theoretical Chemistry, Zernike Institute for Advanced Materials, University of Groningen, The Netherlands; Dipartimento di Chimica e Chimica Industriale, Università di Pisa, Italy

Introduction

The research presented here is aimed to benchmark the performance of a hybrid restricted active space configuration interaction-short range density functional method (RASCI-srDFT or RAS-srDFT for simplicity) [1]. The RASCI method provides a good description of the electronic ground and excited states and of the near degeneracy cases, but one limitation of this method is the lack of dynamical correlation. The DFT method, on the other hand, is known to be very efficient in recovering dynamical correlation energy. The idea of the RAS-srDFT method is to combine the best of both methods. It is based on the range separation of the electron-electron Coulomb interaction. The short-range electron interactions are treated at the DFT level, while the long-range part is evaluated using RASCI. To do so, the RAS-srDFT method is used to investigate the electronic properties of singlet fission (SF) chromophores. SF can occur in pairs of certain molecules in which the molecular S_1 energy is equal or higher than twice the T_1 energy so that it is an exoergic process. This process can be used to overcome the theoretical limit of a single junction solar cell [2].

Methods

The quality of the RAS-srDFT method might depend on the basis set, range separation (μ), short-range density functionals, a number of states computed for the state average approximation and active space. Besides, the inclusion of dynamical correlation might change the electronic nature of low-lying singlet excited states, allowing the state mixing. These dependencies were tested using ethylene molecule and its dimer model with different intermolecular distances as model tests. Moreover, the wave function decomposition analyses were performed to investigate the electronic nature of the low-lying singlet excited states of the dimer system. Then, the vertical excitation energies of SF chromophores, i.e. tetracene, pentacene, the bis(inner salt) of 2,5-dihydroxy-1,4-dimethyl-pyrazinium (DHDMPY), 2,5-bis(fluorene-9-ylidene)-2,5-dihydrothiophene (ThBF), and orthobis(5-ethynyltetracenyl)-benzene (BET-B), presented in Figure 1, were computed using the RAS-srDFT method. For the pairs of these chromophores, the wave function decomposition analyses were also performed. All the calculations were performed using the Q-Chem software [3].

Results

The results of the ethylene molecule show that the basis set and active space dependence has a marginal effect on the computed excitation energies with a maximum standard deviation of 0.1 eV. Additionally, the number of states computed for the state average approximation in the RAS-srDFT method does not change the excitation energies significantly, and the optimal μ- parameter value was found to be equal to 0.4 a.u. As expected, the short-range GGA functional (sr-PBE) does provide a more accurate result in comparison with the LDA functionals (sr-VWN5 and sr-PW92). This trend has also been observed in the ethylene dimer. Further, the inclusion of dynamical electron correlation for the calculations of dimer systems not only shifts the excitation energies but also slightly changes the electronic nature of the low-lying singlet excited states. For the ethylene dimer at the small intermolecular distance, the electronic nature of the low-lying singlet excited states is mixed between the local excitation on one molecule and the charge resonance. This state mixing is less pronounced at large intermolecular distance for which the electronic nature of the low-lying singlet excited states is local excitation on one molecule.

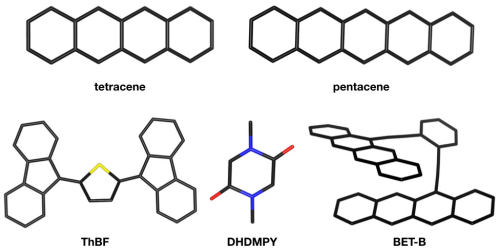

Figure 1 - Chemical structures of singlet fission chromophores.

The results of the tetracene, pentacene, DHDMPY, ThBF, and BET-B molecules show the same tendency as ethylene in which the basis set, active space, and a number of computed states do not change the computed excitation energies significantly. Moreover, the optimal μ-parameter value lies in between 0.4 and 0.5 a.u. The GGA functional provides more accurate results. However, the results of the BET-B molecule, which represents the covalently linked dimer, show larger effects of the state mixing in the low-lying singlet excited states.

Conclusions

In this paper, I have investigated the vertical excitation energies and electronic nature of the low-lying excited states for a benchmark set of five SF chromophores using the RAS-srDFT method. The aim was to test the quality and the dependency of the RAS-srDFT method. The basis set, μ-parameter, active space, and number of computed state dependencies were found to show a relatively small variation on the computed excitation energies. The sr-PBE functional gives more accurate results. In the dimer system, the inclusion of the dynamical correlation changes the electronic nature of the low-lying singlet excited states, allowing the state mixing.

References

[1] Casanova, D., J. Chem. Phys., 148:124118, 2018. [2] Smith, M.B., et al., Chem. Rev., 110:6891-6936, 2010. [3] Shao Y., et al., Mol. Phys., 113:184-215, 2015.

Acknowledgements

The work has been performed under the Project HPC-Europa3 (INFRAIA-2016-1-730897), with the support of the EC Research Innovation Action under the H2020 Programme; in particular, M.W. gratefully acknowledges the support of Dr. David Casanova and Dr. Abel Carreras Conil from the Donostia International Physics Center (DIPC), Donostia-San Sebastián, Spain, and the computer resources and technical support provided by the Barcelona Supercomputing Center (BSC).

A GIS-BASED APPROACH TO DEFINE AN UPDATED BIOCLIMATIC MAP OF EUROPE FOR LANDSCAPE CLASSIFICATION AND PLANNING

G. Bazan[1], R. Fealy[2]

[1]Department of Biological, Chemical and Pharmaceutical Sciences and Technologies, University of Palermo, Italy; [2]Department of Geography, University Maynooth, Ireland

Introduction

Bioclimatic maps are an important tool for land-use planning/management and for biodiversity conservation purposes. Such maps show the distribution of some important bioclimatic indicators, obtained through a rigorous classification process. These indicators aim to link climatic elements to the distribution of biological entities at different levels (individuals, populations, ecosystems, biomes). Interest in this topic dates back to the XIX century, with the proposal of different bioclimatic classifications [1, 2]. However, it was only in the last decades that such classifications became of practical use even on a local scale [3]. This was made possible thanks to the development of new technologies of geostatistical calculation and by the availability of new and increasingly accurate climatic data. Nowadays, the Rivas-Martinez's Worldwide bioclimatic classification system (WBCS) [4] is the most accepted method used in vegetation science.

In this paper, we present the applications of WBSC for the elaborations of a new European bioclimatic map at a high spatial resolution (approximately 1 km2), performed using the most accurate climatic dataset available [5].

Methods

We have performed GIS analysis to define bioclimatic indicators and build Bioclimatic maps. The analyses – focused on the Rivas-Martínez bioclimatic classification (WBSC) [4] and based on the CHELSA dataset [5] – were carried out using GRASS GIS 7.6, an open source and native Linux application. The migration of analyses to a Linux based software and the re-building of procedures (planned for ESRI ArGis) was done in order to make the method compatible with HPC. Analytical and Dichotomous Keys for the definition of Bioclimatic and Macro Bioclimatic classes performed by the WBCS was translated in GRASS GIS scripts for the bioclimatic parameters and indices computation. The script was compiled on GRASS GIS for MacOsX.

Results

GIS analysis was carried out for global land areas and the following datasets were produces: the Macrobioclimatic map, that encompassed five macrobioclimates (Tropical, Mediterranean, Temperate, Boreal and Polar); the Bioclimatic map (subdivided into 27 Bioclimates); the Thermotypes map (31 Thermotypes); the Ombrotypes map (36 Ombrotypes). Furthermore, all the map of bioclimatic indices (Io, Itc, Ic, etc.) were needed to build the above maps. The maps obtained are different with respect to the Rivas-Martinez's map due to more accurate datasets being used. The subset of European Bioclimatic data is the first step in defining the correspondence and correlation between plant communities distribution and the bioclimatic units.

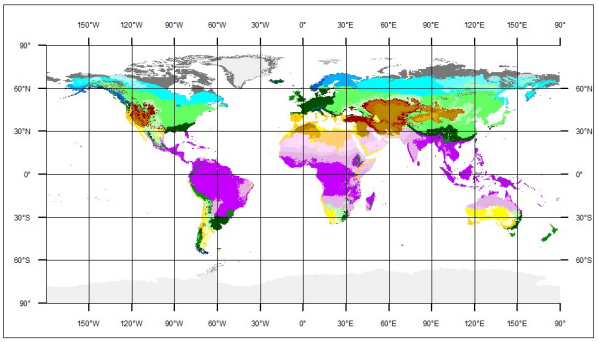

Figure 1 – World Bioclimates dataset performed in GIS.

Conclusions

The results of the calculations provide high quality-resolution bioclimatic data that will be essential not only to understand the geographical distribution of vegetation, but also to define predictive models for the distribution of habitats, biotopes and ecosystems, and to describe the dynamic relationships between communities within the vegetation series as well. Such bioclimatic data are the base for ecologic classifications like the Land Classification Maps and the Ecoregional Maps [e.g. 6, 7], which serve as reference framework for environmental investigations, evaluation of resources, environmental monitoring programs and landscape management. Understanding the relationship between climate and vegetation is crucial to predict the impact of Climate Change on organisms, to find threatened ecosystems and to implement biodiversity conservation strategies.

References

[1] Köppen W, Geographische Zeitschrift 6:593-611, 1900. [2] Thornthwaite CW, Geographical Review, 38:55-94, 1948. [3] Metzger M.J et al., Global Ecology and Biogeography 22:630-638, 2013. [4] Rivas-Martinez S et al., Global Geobotany 1:1-638, 2011. [5] Karger DN et al., Scientific data 4:170122, 2017. [6] EEA, European Environment Agency, Copenhagen, 2017. [7] Blasi C et al., Plant Biosystems, 148(6): 1255-1345, 2014.

Acknowledgements

The work has been performed under the Project HPC-EUROPA3 (INFRAIA-2016-1-730897), with the support of the EC Research Innovation Action under the H2020 Programme; in particular, the author gratefully acknowledges the support of Dr. Rowan Fealy of Maynooth University (Ireland) and the computer resources and technical support provided by Irish Centre for High-End Computing – ICHEC.

THE SPATIAL CONSISTENCY OF SPECIES ROLES IN HOST-HELMINTH NETWORKS

T.A. Dallas[1,2], P. Jordano[3] and O. Ovaskainena[4]

[1]Organismal and Evolutionary Biology Research Programme, University of Helsinki, Finland; [2]Department of Biological Science, Louisiana State University, Baton Rouge, USA; [3]Integrative Ecology Group, Estación Biológica de Doñana Isla de La Cartuja, Sevilla, Spain; [4]Centre for Biodiversity Dynamics, Norwegian University of Science and Technology, Trondheim, Norway

Introduction

A species role in an interaction network can be defined in a number of ways (reviewed with respect to food webs by [1]). Species role estimation has previously been applied to plant-pollinator systems in order to identify the most important plant and pollinator species to network structure [2, 3], and in host-parasite systems to examine species roles in relation to species life history and phylogeny [6, 7]. Demonstrating spatial variation in species roles is the first step towards understanding how spatial and environmental gradients influence the composition and relative importance of species across networks.

Apart from spatial or environmental structuring of species roles, the estimation of species roles allows the estimation of the consistency of species roles for a given species. That is, how spatially variable are species roles?

Methods

We examine the conservation of species roles in host-helminth networks using a global dataset on host-helminth interactions from the London Natural History Museum [13]. We define species roles by first grouping species into modules using the short random walk method. After this, we defined species roles by comparing the number of interactions a species has within its own module relative to the interactions outside its module, conditional upon the local network (i.e., measures are standardized relative to other species in the local network). This creates a two-dimensional space where we can define species roles as the minimum convex polygon area encompassed for a given species, as species appearing in multiple networks will have multiple estimates of species roles. We then test if this area is different from a null model, which randomly selects species role measures for either host or helminth species and calculates the species role area.

Results

We failed to detect any indication that species served similar roles across their ranges. Given the variability in parasite specialization and host permissiveness to infection by parasite species, it was expected that some subset of host and helminth parasites would serve a consistent role. For instance, specialist parasites should consistently parasitize few host species across networks, which should result in a smaller cz area than expected under the null model, and a consistently peripheral role for that species.

Conclusions

Our failure to detect significant conservation of species roles for hosts and helminth parasites suggests the paramount importance of the local network relative to constraints on the number of interactions (number of parasites infecting a host species or number of host species a parasite infects). That is, predicting parasite burdens on host species cannot be achieved solely with global estimates of host permissiveness to infection. Information on the composition of the local community will inform the relative parasite burden of host species found in the local network, or the host range of parasite species. Taken together, our findings suggest that species roles in host-parasite networks may not be conserved, making characterizations of species roles at the global scale unrepresentative of local networks.

References

[1] A. R. Cirtwill, et al., Food Webs 16, e00093 (2018). [2] J. M. Olesen, J. Bascompte, Y. L. Dupont, P. Jordano, Proceedings of the National Academy of Sciences 104, 19891 (2007). [3] A. Nielsen, Ø. Totland, Oikos 123, 323 (2014). [4] S. Kortsch, R. Primicerio, M. Fossheim, A. V. Dolgov, M. Aschan, Proceedings of the Royal Society B: Biological Sciences 282, 20151546 (2015). [5] M. Albrecht, B. Padrón, I. Bartomeus, A. Traveset, Proceedings of the Royal Society B: Biological Sciences 281, 20140773 (2014). [6] S. Bellay, et al., PloS one 8, e75710 (2013). [7] R. Poulin, B. R. Krasnov, S. Pilosof, D. W. Thieltges, Journal of Animal Ecology 82, 1265 (2013). [8] K. Trøjelsgaard, J. M. Olesen, Functional Ecology 30, 1926 (2016). [9] E. L. Rezende, J. E. Lavabre, P. R. Guimarães, P. Jordano, J. Bascompte, Nature 448, 925 (2007). [10] P. Jordano, J. Bascompte, J. M. Olesen, Ecology letters 6, 69 (2003). [11] N. J. Baker, R. Kaartinen, T. Roslin, D. B. Stouffer, Ecography 38, 130 (2015). [12] C. Emer, J. Memmott, I. P. Vaughan, D. Montoya, J. M. Tylianakis, Diversity and Distributions 22, 841 (2016). [13] D. Gibson, R. Bray, E. Harris (2005).

GLOBAL MONITORING OF METHANE AND NITROUS OXIDE FROM METOP/IASI

O. García[1], M. Schneider[2], B. Ertl[2], E. Sepúlveda[1], C. Borger[2], C. Diekmann[2], A. Wiegele[2], F. Hase[2], T. Blumenstock[2]

[1]Izaña Atmospheric Research Centre (IARC), Meteorological State Agency of Spain, Spain; [2]Institute for Meteorology and Climate Research (IMK-ASF), Karlsruhe Institute of Technology, Germany

Introduction

Multiple evidences in our environment indicate climate change is happening. Scientific consensus recognises that the main driver of this climate change is being the increase in the atmospheric concentration of the well-mixed greenhouse gases (GHGs). Identifying and quantifying the global GHGs sources/sinks and an improved understanding of the complex climate feedback processes are, thus, major challenges of current climate research.

One of the major limitations for addressing these challenges is the lack of accurate observations of the atmospheric composition on all spatial and temporal scales. In this context, space-based data of high and well documented quality are an essential element of current observational strategies for monitoring the Earth-atmosphere system. The development of new and more powerful retrieval strategies for space-based observations, together with the continuous documentation of their accuracy and precision, are, therefore, crucial tasks for improving our understanding of the Earth's climate system.

In this context, this work, supported by the HPC-Europa3 Transnational Access programme, aims at assessing the potential of the space-based IASI (Infrared Atmospheric Sounding Interferometer) mission for surveying the atmospheric concentrations in the troposphere of two of most important GHGs: methane (CH4) and nitrous oxide (N2O). But, this is not a trivial task due to the huge amount of space-based information to be treated and, thus, high performance computer (HPC) resources are mandatory.

Methods

IASI sensor is a nadir-viewing Fourier Transform spectrometers on-board the EUMETSAT Metop satellites, which operate in a polar, sun synchronous, low Earth orbit since 2006. Since 2012 there are two IASI sensors in orbit on MetOp-A and MetOp-B operating in a co-planar orbit. Jointly both IASI sensors measure about 2.5 Millions spectra per day. Thereby, the usage of high performance computing resources is crucial.

The IASI spectra have been analysed with the processor developed during the project MUSICA (MUlti-platform remote Sensing of Isotopologues for investigating the Cycle of Atmospheric water) [1]. The MUSICA IASI processor and the retrievals strategies described by [2] were implemented at the CINECA-HPC resources to retrieve IASI CH4 and N2O global distributions in selected periods representative for the most important seasonal variations of these gases on the global scale.

Results and Conclusions

The MUSICA IASI data capture signals that are larger than 1-2%, like the latitudinal gradients, the long-term increase and the seasonal cycles. The obtained CH4 and N2O global distributions show the well-known latitudinal gradient with a tendency to higher concentrations in low latitudes than in high latitudes. Regarding seasonal variations, the concentrations are higher in summer than in winter. This seasonal cycle is more pronounced for CH4 than for N2O and in the northern hemisphere than in the southern hemisphere due to the location of the stronger emission sources, confirming the main results pointed out by literature. Highest CH4 concentrations are found in the northern hemispheric summer. As an example, Figure 1 shows the tropospheric CH4 global distribution in a selected period of winter.

In summary, IASI has proven to be a very useful tool in the context of GHGs monitoring, among other essential climate variables, showing a great potential for climate research.

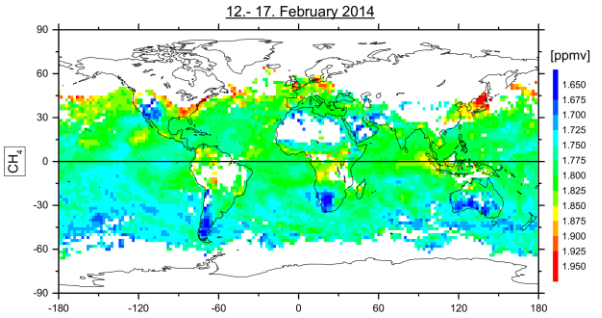

Figure 1 – Example of tropospheric CH4 global distribution (4.2 km a.s.l.) retrieved from IASI sensor.

References

[1] Schneider, M., et al., Atmos. Meas. Tech., 9:2845–2875, 2016. [2] García, O. E., et al., Atmos. Meas. Tech., 11:4171-4215, 2018.

Acknowledgements

The work has been performed under the Project HPC-EUROPA3 (INFRAIA-2016-1-730897), with the support of the EC Research Innovation Action under the H2020 Programme; in particular, the author gratefully acknowledges the support of Dr. Debora Testi (SuperComputing Applications and Innovation, SCAI) and the computer resources and technical support provided by CINECA.

PARALLEL LAGRANGIAN PARTICLE SIMULATIONS

T. Nordam

SINTEF Ocean, Trondheim, Norway
Department of Physics, NTNU, Trondheim, Norway

Introduction

For studies in Lagrangian oceanography, a common tool is the modelling of particle trajectories through a velocity field defined by the ocean currents [1]. This is equivalent to solving an Ordinary Differential Equation (ODE) given by

$$\dot{x} = v(x,t)$$

where v_{is} the velocity field. In many applications, individual particle trajectories are independent, which means that the problem of calculating a large number of trajectories is trivially parallelisable. However, the ocean current data can in some cases be relatively large. Therefore, it is of interest to divide the problem in such a way that each process does not have to store the entire dataset in memory. If each process can have only one or more smaller subsets of the entire dataset, and be responsible for transporting only those particles that reside within those areas, this can be achieved.

Methods

The chosen approach to dividing the domain is to use a chequerboard approach, as illustrated in Figure 1. The rationale is to allow the domain to be divided into a large number of subsets, while at the same time maintaining reasonable load balancing in those cases where the particles are not uniformly distributed.

Figure 1 – Dividing particles among processes with a chequerboard scheme.

For numerical integration of the particle trajectories, any ODE integration scheme can be used. In particular, variable timestep integrators of the Runge-Kutta family, such as Dormand-Prince 5(4) [2], are found to be quite efficient for these types of problems. However, a high-order Runge-Kutta scheme also requires high-order interpolation to give smooth and continuous partial derivatives of the velocity field. Hence, an interpolation scheme such as cubic splines should be used.

Results

Results so far indicate that the chosen scheme has good parallel performance up to several hundreds of cores. At the moment, only linear interpolation has been tested. The next steps include the use of cubic spline interpolation, globally on each subset of the domain, with a suitable halo of cells to ensure smooth derivatives when transferring from one subdomain to another.

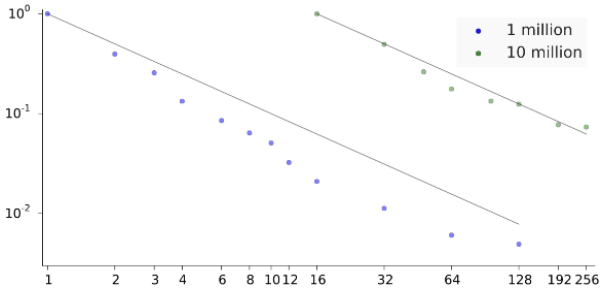

Figure 2 – Relative walltime, as a function of number of cores, for 1 million and 10 million particles.

Conclusions

The chequerboard parallelisation scheme has been tested, and found to give satisfactory performance and good scaling. This scheme should thus be a good candidate for applications where large numbers of independent particle trajectories are calculated, such as calculation of Lagrangian Coherent Structures [3], or simulation of diffuse pollutants, such as microplastics.

References

[1] van Sebille, E. et al, Ocean Modelling 121:49-75, 2018. [2] Dormand, J., Prince, P., Journal of Computational and Applied Mathematics 6:19–26, 1980. [3] Farazmand, M., Haller, G., Chaos 22(1), 2012.

Acknowledgements

The work has been performed under the Project HPC-EUROPA3 (INFRAIA-2016-1-730897), with the support of the EC Research Innovation Action under the H2020 Programme; in particular, the author gratefully acknowledges the support of Dr. Colin Cotter at the Department of Mathematics, Imperial College, and the computer resources and technical support provided by the EPCC.

THE CURRENT FEEDBACK IN COUPLED OCEAN-ATMOSPHERE MODEL

L. Renault[1], T. Arsouze[2]

[1]LEGOS, Université de Toulouse, IRD, CNRS, CNES, UPS, Toulouse, France; [2]Barcelona SuperComputing Center, Barcelona, Spain

Introduction

The Current FeedBack (CFB) to the atmosphere simply represents the influence of the surface oceanic currents on near-surface wind and surface stress. The CFB largely controls the oceanic circulation, it is therefore crucial to implement it properly in a coupled Ocean-Atmosphere model. However, so far, the BSC was running a high-resolution coupled simulation without CFB. In this 13-weeks visit, L. Renault (visitor) and T. Arsouze (host) aim to assess to consequences of the lack of current feedback in the BSC coupled simulations, to implement and test it in the BSC coupled model, to prepare a new coupled simulation that includes the CFB, and to test and validate a parameterization of the current feedback in a forced ocean model.

Methods

We first used existing outputs from the BSC coupled simulation to assess the realism of the Western Boundary Currents (strongly affected by the CFB, see (1) and (2)). We furthermore implement in IFS (atmospheric model used in the BSC) the current feedback in the bulk formula and in the Planet Boundary Layer parameterization and run new simulations. Finally, parameterizations of the CFB in a forced ocean model (NEMO) have been implemented and tested.

Results

Four main tasks have been done as detailed in the following:

- Analyse outputs from a global coupled model from a western boundary current perspective. Because of the absence of current feedback (not yet implemented), the WBCs are too strong in the simulation.
- Implement, test, and run CFB in the BSC coupled model. In the implementation, two steps are needed: a) modify the bulk formula, b) modify the Planet Boundary Layer Scheme. Short-term coupled simulations have been carried out to test our implementation. A study on how to implement the current feedback in a coupled model has been written and will be submitted to Ocean Modelling (3)
- The implementation of the CFB in a bulk formula when forcing an ocean model is like trying to square the circle. A larger relative stress will slow down surface winds that are therefore not independent from the surface currents. This wind response induces a partial re-energization of the ocean at both large-scale and mesoscale, and, thus, should be taken into account in a forced ocean model. Wind products based on observations have "seen" real currents that will inevitably not correspond to model currents (at least at the mesoscale), whereas reanalyses products often neglect surface currents or use surface currents that, again, will differ from the surface currents of the model we want to force. Additional errors are made when using 10 winds derived from scatterometers (e.g., QuikSCAT) as they represent the relative wind to the surface currents. In this other study, a set of quasi-global ocean simulations, coupled or not with the atmosphere is used to (i) quantify the error one does with the different existing strategies of forcing an ocean model and (ii) to test parameterizations of the wind response to the CFB in a forced ocean model and propose the better method to force an ocean model. We show a parameterization of the CFB based on the coupling coefficient between the surface current vorticity and the stress curl allows to reproduce the main characteristics of a coupled model in term of mean circulation, sink of energy, and mesoscale activity. This study will be submitted to JAMES (4).

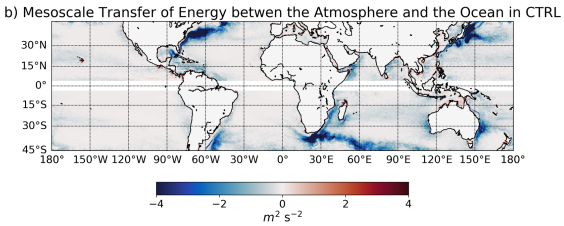

Figure 1 – Snapshot of the mesoscale surface stress curl induced by the current feedback (CFB) in IFS as estimated from (a) a simulation with a partial and (b) with a full CFB parameterization. As expected, the CFB induces mesoscale surface stress curl anomalies collocated over the eddies and the Gulf Stream. In a simulation that ignores the CFB modifications in the PBL scheme (i.e., CRT10), the mesoscale stress induces anomalies are largely underestimated.

Conclusions

To conclude, this visit has been fruitful as the initial objectives have been reached. The BSC is currently running a new coupled simulation with CFB that will be analysed in the future. L. Renault developed his network with new collaborations at the BSC and also his knowledge on supercomputers. L. Renault and T. Arsouze plan to pursue their collaboration analysing the new coupled simulations and improving the representation of the air-sea interactions.

References

(1) Renault, L. et al. (2017), JPO, 47(8), 2077-2100. (2) Renault L. et al., JPO, 46(11), 3439-3453 (3) Renault L., Lemarié F., Arsouze T., Masson S, to be submitted. (4) Renault L., Masson S., Arszoue T., et al., to be submitted.

Acknowledgements

The work has been performed under the Project HPC-EUROPA3 (INFRAIA-2016-1-730897), with the support of the EC Research Innovation Action under the H2020 Programme; in particular, the author gratefully acknowledges the support of T. Arsouze from BSC and the computer resources and technical support provided by BSC.

IMPACT OF BASAL HYDROLOGY ON DYNAMICS OF OUTLET GLACIERS IN SOUTHEAST GREENLAND

S.H. Svendsen

DTU-Space, Technical University of Denmark

Climate change driven by anthropogenic forcings are changing conditions in the Arctic, placing the Greenland ice sheet under significant stress, and changes in ice melt, discharge and dynamics are evident [2]. A firm understanding of the drivers of ice sheet dynamics and how the ice sheet interacts with the surrounding environment is crucial in order to produce reliable estimates of future changes of the Greenland ice sheet.

The dynamics of the Greenland ice sheet is shaped by the complex interplay between the intricate geometry of the bedrock in the fjord and outlet systems and climate drivers such as temperature, surface mass balance and ocean temperature. Observations indicate seasonal patterns in velocities of a number of Greenland glaciers, most likely caused by seasonal transitions in the subglacial drainage systems while others display sensitivity to glacier front position [8]. Similar links between melt water and ice dynamics have been observed in Svalbard and Alaska as well [4, 9]. These observations indicate that besides overall drivers of the Greenland Ice Sheet mass loss such as temperature and surface mass balance, basal conditions of the outlet glaciers are important for flow dynamics.

The flow of an ice sheet may be modelled as a highly viscous Stokes flow and when con- sidering extended bodies of ice such as the Greenland ice sheet, the low thickness to width ratio justifies the use of approximations to the full Stokes equations such as the shallow ice approximation (SIA) [6]. Ice sheet models based on the shallow ice approximation are a useful tool when evaluating the overall flow patterns of the entire Greenland ice sheet, see e.g. [3, 1]. However, the dynamics of the outlet glaciers of the Greenland ice sheet are important for the overall ice flow since the ice flow through these outlets controls the dynamic mass loss of the entire ice sheet. Given the spatial scales and complex bedrock topography of the outlet systems, ice sheet models based on the shallow ice approximation alone are insufficient to resolve the flow dynamics properly. For such detailed studies of individual outlet glaciers and basins, ice flow models of a higher complexity capable of dealing with the full Stokes flow problem are required.

Finite element models (FEM) are a type of models capable of solving the full Stokes flow and are hence a most suitable tool for examining the ice flow in the narrow and complex outlet glacier systems [7, 5]. The current project aims at utilising a finite element model to examine various drivers and regulators of ice dynamics of a select number of outlet glaciers in southeast Greenland, evaluating the model results against observations in an effort to pinpoint dominating mechanisms of the flow.

References

[1] G Adalgeirsdottir, A. Aschwanden, C. Khroulev, F. Boberg, R. Mottram, P. Lucas- Picher, and J. H. Christensen. Role of model initialization for porjections of 21st-century Greenland ice sheet mass loss. Journal of Glaciology, 60(222):782–794, 2014. [2] AMAP. Snow, water, ice and permafrost in the arctic (swipa): Climate change and the cryosphere. Technical report, Arctic Monitoring and Assessment Programme (AMAP), 2017. [3] A. Aschwanden, M. A. Fahnestock, and M. Truffer. Complex greenland outlet glacier flow captured. Nature Communications, 7(10524), 2016. [4] T. Dunse, T. Schellenberger, J. O. Hagen, A. K ̈a ̈ab, T. V. Schuler, and C. H. Reijmer. Glacier-surge mechanisms promoted by a hydro-thermodynamic feedback to summer melt. The Cryosphere, 9:197–215, DOI: 10.5194/tc–9–197–2015, 2015. [5] O. Gagliardini, T. Zwinger, F. Gillet-Chaulet, G. Durand, L. Favier, B. de Fleurian, R. Greve, M. Malinen, C. Mart ́ın, P. R ̊aback, J. Ruokolainen, M. Sacchettini, M. Sch ̈afer, H. Seddik, and J. Thies. Capabilities and performance of elmer/ice, a new-generation ice sheet model. Geoscientific Model Development, 6(4):1299–1318, 2013. [6] Ralf Greve and Heinz Blatter. Dynamics of Ice Sheets and Glaciers. Advances in Geophysical and Environmental Mechanics and Mathematics. Springer, 2009. [7] Emmanuel Le Meur, Olivier Gagliardini, Thomas Zwinger, and Juha Ruokolainen. Glacier flow modelling: a comparison of the Shallow Ice Approximation and the full- Stokes solution. Comptes Rendus Physique, 5:709–722, 2004. [8] Twila Moon, Ian Joughin, Ben Smith, Michiel van den Broeke, Willem Jan van de Berg, Brice No ̈el, and MIka Usher. Distinct patterns of seasonal greenland glacier velocity. Geophysical Research Letters, 41:7209–7216, DOI: 10.1002/2014GL061836, 2014. [9] Saurabh Vijay and Matthias Braun. Seasonal and interannual variability of columbia glacier, alaska (2011-2016): Ice velocity, mass flux, surface elevation and front position. Remote Sensing, 9:635–652, DOI: 10.3390/rs9060635, 2017.

Acknowledgements

The work has been performed under the Project HPC-EUROPA3 (INFRAIA-2016-1-730897), with the support of the EC Research Innovation Action under the H2020 Programme; in particular, the author gratefully acknowledges the support of Thomas Zwinger, Dept. of High Performance Computing Support, CSC and the computer resources and technical support provided by CSC – IT centre for science Ltd.

MODELING FRACTURE INITIATION AT BOWDOIN GLACIER

E. van Dongen[1], J. Åström[2]

[1]ETH Zurich, Switzerland; [2]CSC IT Centre for Science, Finland

Introduction

Warming in recent decades has caused glaciers and ice sheets to shrink substantially, and thus to contribute to the observed global sea-level rise. Iceberg calving – the breaking off of icebergs at the edge of glaciers into the sea – is responsible for approximately half of the ice mass loss of the Greenland ice sheet. However, calving mechanisms are still not entirely understood.

The main purpose of my visit at CSC in Finland was to apply the Helsinki Discrete Element Model (HiDEM) to model the initiation of crevasses – fractures in the ice – and iceberg calving at Bowdoin Glacier, a glacier for which we have very detailed field data. These data give a unique opportunity to validate the model output and improve our understanding of calving mechanisms.

Several physical processes that are known to affect iceberg calving are poorly constrained by observations, which reflects the need for sensitivity experiments. For example, submarine melting can act to promote calving, by progressively undercutting the glacier front. At Bowdoin Glacier, a so-called plume is observed, which consists of meltwater, produced either at the glacier surface or the bed. This meltwater flows through the subglacial hydrological system to calving front, where it rises rapidly through the denser seawater. By turbulent mixing, the plume entrains warm seawater such that it becomes capable of melting the glacier front below the waterline. At other glaciers, observations have shown that a plume may cause a significantly undercutted glacier front. Such observations are not available for Bowdoin Glacier, but the possible influence of an undercutted front on calving can be assessed with HiDEM.

Methods

For Bowdoin Glacier, we use a highly detailed, 1m resolution, Digital Surface Model obtained by unmanned aerial vehicle (UAV) photogrammetry (unpublished data). The modelled glacier geometry is shown in Figure 1. We apply a simple friction distribution, based on observed satellite velocity. A shear line is identified where the highest velocity gradients are observed and two different friction values are applied on each side of the shear line in order to reproduce the observed velocity gradient. We test the influence of the size of the discrete elements in HiDEM, and whether or not the front geometry is undercut by submarine melting.

Results

We find that a small particle size on the order of 2 meters is necessary to reproduce the observed crevasse pattern on Bowdoin Glacier. When applying such small particle size, the observed crevasse orientation and location is well reproduced.

If a distributed overhanging terminus geometry is introduced, HiDEM predicts rapid collapse of the entire front. However, local undercuts seem to have a limited effect on initiated fractures.

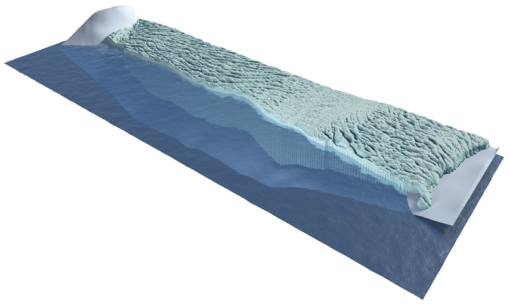

Figure 1 – HiDEM model set-up.

Conclusions

HiDEM is a first-principles fracture model that is capable of reproducing the observed crevasse pattern from only observed glacier geometry and some knowledge about velocity (high vs low friction area). The influence of particle size on modelled crevasses has not been analysed extensively in previous studies, and turns out to be a critical model parameter. Our results demonstrate that calving at Bowdoin is to a high degree controlled by the detailed shape of the submarine ice-clif such as under-cuts and over-hangs. There has not been any detailed in-situ measurement of the shape of the submarine ice-cliff, hence this is still lacking as input for the numerical model. Consequently, at the moment we have to use, more or less, educated guesses to what the submarine ice-cliff looks like based on submarine observations on other glaciers and surface observations at Bowdoin Glacier. Such particular shapes are simulated to test to what extent it can reproduce observed calving. This approach is, however, computationally extremely demanding. Further observations and simulations are necessary to assess the impact of submarine melt-undercutting on the calving behaviour of Bowdoin Glacier.

Acknowledgements

The work has been performed under the Project HPC-EUROPA3 (INFRAIA-2016-1-730897), with the support of the EC Research Innovation Action under the H2020 Programme; in particular, the author gratefully acknowledges the support of Jan Åström and the computer resources and technical support provided by CSC.

CAPTURING THE FLOW PHYSICS OF FLOATING OFFSHORE WIND TURBINE UNSTEADY AERODYNAMICS WITH HIGH-FIDELITY COMPUTATIONAL FLUID DYNAMICS AND ASSESSING THE RELIABILITY OF PRESENT ENGINEERING CODES FOR THEIR DESIGN

M.S. Campobasso[1], *A. Ortolani*[2], *G. Persico*[2]

[1]*Engineering Department, Lancaster University, United Kingdom,* [2]*Department of Energy, Politecnico di Milano, Italy*

Introduction

Floating offshore wind turbines (FOWTs) can tap into more abundant and higher-quality wind available further away from coasts, where the cost of building foundations in deep sea waters makes fixed-bottom turbines prohibitive. Due to whole-system interactions with waves and currents, FOWT unsteady aerodynamics is still not fully understood, and affects in a complex manner turbine stability and survivability, fatigue loads, and power output. Large uncertainty affects the widespread low-fidelity aerodynamic codes used in industry and academia for FOWT development. This may either yield excessive design conservatism, hindering cost reductions, or jeopardize the system durability, which also adversely impacts on wind energy costs and further growth. This project uses high-fidelity Navier-Stokes (NS) Computational Fluid Dynamics (CFD) to investigate FOWT aerodynamics and provide knowledge to improve the reliability of computationally faster low-fidelity aerodynamic codes.

Methods

High-fidelity simulations of the unsteady aerodynamics of a 5MW FOWT animated by prescribed tower pitching are performed using the COSA NS CFD structured multi-block finite volume code [1], previously used for unsteady aerodynamics of fixed-bottom horizontal and vertical axis wind turbines, and thoroughly validated against the National Renewable Energy Laboratory (NREL) flow measurements of the 11m-diameter Phase VI turbine. COSA has a high parallel scalability of both its computing and IO sections. Mesh sensitivity of the solutions is accomplished by computing selected regimes with a 64M cell-grid and a coarser grid with 8M cells. Further verification and validation is also accomplished by comparing selected COSA solutions to those of the ANSYS FLUENT commercial NS CFD code [2].

The comparative assessment of high- and low-fidelity FOWT computational aerodynamics is accomplished by computing the FOWT regimes analysed with COSA also with the state-of-the-art NREL aero-hydro-servo-elastic wind turbine code FAST, which features the low-fidelity blade element momentum theory (BEMT) model of the NREL AERODYN code for rotor aerodynamics. The analysed FOWT regimes correspond to periodic tower pitching and differ for the values of pitching amplitude and frequency; regimes with wind and wave misalignment are also considered [3].

Results

The COSA CFD simulations allowed adequately resolving the aerodynamic FOWT rotor/wake interactions, key to understanding, assessing and controlling turbine loads and power. These interactions are highly intermittent in FOWTs. The tangential vorticity contour plots of Fig. 1 show more marked tangential vorticity contours in the leeward stroke (middle) than in the windward stroke (right), as in former case the rotor moves axially towards the wake, and in latter one moves away from it, resulting in large periodic variations of loads and power. The study preliminary findings show that, unlike what often claimed, the largest discrepancies of low- and high-fidelity predictions are not seen when rotor/wake interactions are strongest (leeward stroke), but when FOWT entrainment speeds are highest (windward stroke). The research also highlighted notable levels of dynamic stall occurring in severe metocean regimes.

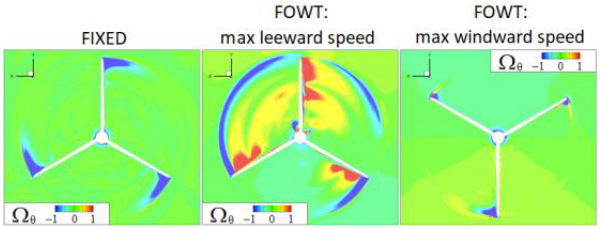

Figure 1 - Tangential vorticity (Ω_θ) contours in rotor plane for fixed tower (left), and FOWT with maximum leeward and windward speed.

Conclusions

The study's findings open new research avenues. Since the largest discrepancies between FOWT power and load predictions of high- and low-fidelity methods do not occur where rotor/wake interactions are strongest, faster and widespread low-fidelity methods may be improved more easily than commonly believed. The quantified highly intermittent nature of rotor/wake interactions and wake generation, made more complex by possible wave/wind misalignment, may result in FOWT farm aerodynamics and control being more challenging than for farms of fixed-bottom turbines.

References

[1] Drofelnik J, Da Ronch A, Campobasso M, Wind Energy, 21(7): 515-530, 2018. [2] Ortolani A, Persico G, Campobasso M, ASME paper GT2020-15552, ASME Turbo Expo Technical Congress, London, 2020. [3] Ortolani A, Persico G, Campobasso M, Torque paper 2020-89, TORQUE Conference, Delft, 2020.

Acknowledgements

The work has been performed under the Project HPC-EUROPA3 (INFRAIA-2016-1-730897), with the support of the EC Research Innovation Action under the H2020 Programme; Prof. Campobasso gratefully acknowledges the support of Prof. Persico and the Department of Energy at the Politecnico di Milano and the computer resources and technical support provided by CINECA.

COARSE-GRAIN MOLECULAR DYNAMICS SOLVENT EVAPORATION SIMULATIONS OF ORGANIC SOLAR CELL LAYERS

A.S. Gertsen

Technical University of Denmark, Department of Energy Conversion and Storage, Lyngby, Denmark

Introduction

Organic photovoltaics (OPVs) are presently used for niche applications due to their semi-transparency, flexibility, low weight, and possibilities of custom designs in terms of colours and shapes, but low efficiencies of large-scale fabricated modules have hampered grid implementations [1]. Important properties that directly affect the performance of OPVs such as charge carrier mobility and optical absorption are crucially dependent on the morphology of the active layer. Here, we present coarse-grained molecular dynamics solvent evaporation simulations of blends of donor polymers and small-molecule, non-fullerene acceptors. From these, we can follow the morphology evolution during post-deposition drying and get information of the effects of different processing conditions such as solvents on the active layers' structure-property relationships.

Methods

We have used the newly developed MARTINI 3.0 force field [2,3] to build coarse-grained models for the donor polymer PffBT4T-2OD, the non-fullerene acceptor O-IDTBR as well as the two green solvents o-methylanisole and p-cymene. Additionally, refined models for the donor polymer P3HT and the solvents chlorobenzene, o-dichlorobenzene, and o-xylene have been used in connection with this work [4]. These models were then used to simulate the drying of solution deposited organic solar cell active layers using our solvent evaporation script in the framework of the molecular dynamics package GROMACS 2019 [5]. For this, 1.25 % of the remaining solvent molecules were removed randomly from throughout the simulation box each step, amounting to a total of 264 steps. After each removal step, the box was equilibrated for 0.5 ns in an NVT ensemble and 4.0 ns in an NPT ensemble with semi-isotropic pressure coupling, allowing the box to contract only in the vertical direction, before doing a production run of 3.0 ns. This adds up to a total simulation time of 2 µs for all 264 steps. The morphologies of the dry thin-films were then subject to analysis.

Results

Here, we will focus on the results obtained from simulations of P3HT:O-IDTBR blends in five different solvents: chlorobenzene, o-dichlorobenzene, o-xylene, o-methylanisole, and p-cymene. From scattering simulations of the polymer (P3HT) phase in the dry thin-films, a π-stacking distance of 3.8 Å was found, whereas lamellar stacking distances were determined to be around 17 Å. These are in excellent correspondence with experiments [6]. In order to follow the morphology evolution during drying and its dependence on the solvent, we have calculated the number of close contacts in the different components as a function of simulation time and plotted them in Fig. 1. As seen, the P3HT chains quickly aggregate, and the P3HT ↔ O-IDTBR contacts plateau due to this. In contrast, the number of O-IDTBR ↔ O-IDTBR contacts increases sharply in the last 0.25 µs of drying. Interestingly, the trend of a more aggregated O-IDTBR phase during the drying corresponds to a trend of higher efficiencies in devices (o-methylanisole > p-cymene > o-xylene > chlorobenzene) [7]. This indicates that a high number of contacts, i.e. a high structural order, in the acceptor phase could be key to improve the efficiencies of devices.

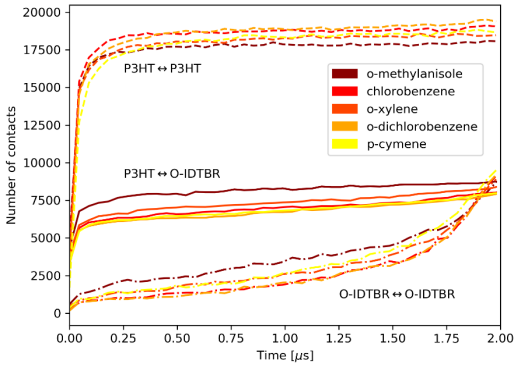

Figure 1 - The number of close contacts (< 6 Å) as a function of time for P3HT ↔ P3HT, O-IDTBR ↔ O-IDTBR, and P3HT ↔ O-IDTBR for the five solvents. Solvents are ordered as more hydrophobic downwards in the legend.

Conclusions

The coarse-grain models developed for a range of polymers and molecules relevant for organic solar cells have, in concert with our script for solvent evaporation simulations, allowed us to follow the morphology evolution of solution deposited donor: acceptor blends during post-deposition drying. Next step is to correlate these simulations to in situ X-ray scattering measurements.

References

[1] B. Azzopardi et al., Energy Environ. Sci., 4:3741-3753, 2011. [2] S.-J. Marrink et al., J. Phys. Chem. B 111:7812–7824, 2007. [3] P. C. T. Souza et al., Martini 3.0 open-beta release, http://cgmartini.nl/index.php/martini3beta [4] R. Alessandri et al., in preparation, 2020. [5] M.J Abraham et al., SoftwareX 1:19-25, 2015. [6] M. Brinkmann et al., Adv. Mater. 18:860-863, 2006. [7] S. Strohm et al., Energy Environ. Sci. 11:2225-2234, 2018.

Acknowledgements

The work has been performed under the Project HPC-EUROPA3 (INFRAIA-2016-1-730897), with the support of the EC Research Innovation Action under the H2020 Programme; in particular, the author gratefully acknowledges the support of Dr. R. Alessandri and Prof. S.-J. Marrink, Zernike Institute for Advanced Material, University of Groningen and the computer resources and technical support provided by SURFsara.

NUMERICAL INVESTIGATION OF INFLUENCE OF ACOUSTIC OSCILLATIONS ON TURBULENT AXISYMMETRIC IMPINGING JET HEAT TRANSFER USING OPEN SOURCE CFD CODE OPENFOAM

R. Jovanović, D. Cvetinović

University of Belgrade, "Vinča" Institute of nuclear sciences, Laboratory for Thermal Engineering and Energy, Belgrade, Serbia

Introduction

The main subject of this research is numerical modelling of submerged, round, unconfined, turbulent axisymmetric jet, impinging on the flat heated plate using open source CFD code OpenFOAM. Jet is issued from the convergent nozzle and impinges to the plate which is positioned normally to the jet axis. Primary vortices which roll-up in the jet shear layer induce an unsteady flow separation at the wall, prohibiting the heat transfer between the wall and the fluid jet. Thus, controlling of the vortex structures in a turbulent jet consequently leads to the control of the heat transfer from the jet to the wall surface.

The main aim of the investigation is to describe the vortex structure of the free and impinging jet and to examine the possibility of its control by low-amplitude modulation of the nozzle exit velocity. It is expected that performed numerical simulations will describe: a) behaviour of the vortex structures in the impinging jet flow with and without sound modulations, b) jet vortex structures influence on the jet temperature field and the heat transfer, c) possibility to control these structures by artificial disturbances, e.g. by small modulation of the nozzle exit velocity, and d) possibilities to control the heat transfer in this way, especially to increase it.

Methods

The performed work was divided in the two main phases: a) model development and model validation and b) numerical simulation of influence of small amplitude sound oscillations on the impinging jet vortex structure and heat transfer. The developed model is based on the free open source CFD code OpenFOAM 2.3.1. OpenFOAM solver RhoPimpleFoam, for compressible, turbulent flows with heat transfer, was adopted for all numerical simulations in this work. It is important to note that, since nozzle velocity profile changes both in temporal dimension (in time) and in spatial dimension (in space) it was necessary to implement custom boundary condition. This was done using swak4Foam library.

Totally six different computational cases were calculated in the first phase in order to verify suggested numerical model. Simulations were performed for two different axial distances of heated plate from the nozzle outlet and for the two different Re number values. Two different classes of turbulent models were used: standard k – ε model and LES (Large Eddy Simulation) one equation eddy-viscosity model. Numerical simulations of influence of acoustic oscillations on vortex structures and consequently on the heat transfer of impinging jet were performed in the next phase of the presented work. Totally four simulations were conducted: 1) undisturbed jet, 2) jet modified with acoustic oscillations with frequency defined by Strouhal number (St) value 0.3, 3) jet modified with acoustic oscillations with at St value 0.6, and 4) jet modified with acoustic oscillations at St number value 2.0. The same solver, rhoPimpleFoam, used in the previous investigation phase was also utilized in this phase. Turbulence was modelled using LES turbulence model. One equation eddy viscosity model was used to model subgrid scale turbulent eddies. Jet Reynolds number was 10000 in all four cases, and heated plate was positioned at axial distance of two nozzle diameters from the nozzle outlet. Unsteady simulations were performed with adaptive time step varying between 5e-05 s and 1.2 e-04 s. Total simulation time was 0.5 s, and each simulation lasted for about 48 hours using 100 HPC computing cores.

Results

Model verification was performed by the comparison between calculated results and experimental values taken from ERCOFTAC Classic Database (Wall Jets – 1. – C25, Baughn el al). Nusselt number distribution showed that standard k – ε model cannot be successfully used even for qualitative predictions. Calculated results based on LES turbulence model showed much closer agreement with experiments. Numerically calculated velocity magnitude distribution in the second phase of this investigation was compared with experimental measurements. It can be concluded that satisfying accuracy, compared with experimental measurements (Dejan Cvetinović et al), Institute of Chemical Process Fundamentals, Academy of Sciences of the Czech Republic, was achieved.

Conclusions

The obtained results showed that strong rotation caused by the vortices formed near stagnation zone causes separation. Sound oscillations at Strouhal number value 2.0 enabled generation of stronger shear stresses in vortex zone, which prevents separation. Heat transfer for Strouhal number value 2.0 is significantly enhanced compared with undisturbed case.

Acknowledgements

The work has been performed under the Project HPC-EUROPA3 (INFRAIA-2016-1-730897), with the support of the EC Research Innovation Action under the H2020 Programme; in particular, the author gratefully acknowledges the support of Parallel CFD & Optimization Unit, Lab. of Thermal Turbomachines, School of Mechanical Engineering, National Technical University of Athens and the computer resources and technical support provided by The Greek Research and Technology Network – GRNET.

BROWNIAN DYNAMICS SIMULATION OF ION TRANSPORT THROUGH A RECTIFYING BIPOLAR NANOPORE

D. Boda[1], *S. Furini*[2]

[1]*Department of Physical Chemistry, University of Pannonia, Hungary;* [2]*Department of Medical Biotechnologies, University of Siena, Italy*

Introduction

In order to understand the mechanism behind device behaviour of nanopore devices, we need a multiscale modeling approach where different parts of the device are modeled with different resolutions. In Refs. [1,2], we computed ionic current through a rectifying nanopore as a case study with different methods that are based on models of different resolutions.

Methods

The molecular dynamics (MD) simulation method is used to simulate all-atom models, where all degrees of freedom, including water molecules (explicit water model) are handled explicitly. MD solves Newton's equations of motion to compute trajectories. If we reduce our model and replace explicit water with an implicit water, the basic simulation method is the Brownian dynamics (BD) simulation that solves Langevin equations of motion that are the extension of the Newtonian system by adding frictional and random forces. The friction coefficient, γ_i can be related to the diffusion constant, D_i, in bulk and dilute electrolytes with the Einstein relation:

$$D_i = \frac{kT}{m_i \gamma_i},$$

where k is Boltzmann's constant and T is temperature. Whether this equation is valid in confined systems and in concentrated electrolytes is a major question of our research.

Implicit water electrolyte systems can also by studied by calculating the ionic flux with the Nernst-Planck (NP) transport equation. We can couple it to the Local Equilibrium Monte Carlo (LEMC) method that is a grand canonical MC simulation adapted to a non-equilibrium situation [3]. A systematic comparison between MD and LEMC was given in Ref. [1], while a systematic comparison between NP+LEMC and Poisson-Nernst-Planck was given in Ref. [2]. Here, we report some preliminary results for comparison between MD, NP+LEMC, and BD.

Results

The bipolar nanopore model is described in our previous paper [2]. Basically, there are surface charges on the wall of the cylindrical nanopore (see Fig. 1), σ on the left hand side and $-\sigma$ on the right hand side. This bipolar charge pattern results in rectification. Rectification is defined by the ratio of currents at 200 mV (ON state) and -200 mV (OFF state) voltages. The values of the diffusion coefficient in the baths are experimental values, while values in the pore are fitted the NP+LEMC calculations to MD current results for σ = 1 e/nm2 in the ON state. In BD, the γ values in the pore were obtained from the Einstein relation (Eq. 1) using the fitted NP+LEMC diffusion coefficient values.

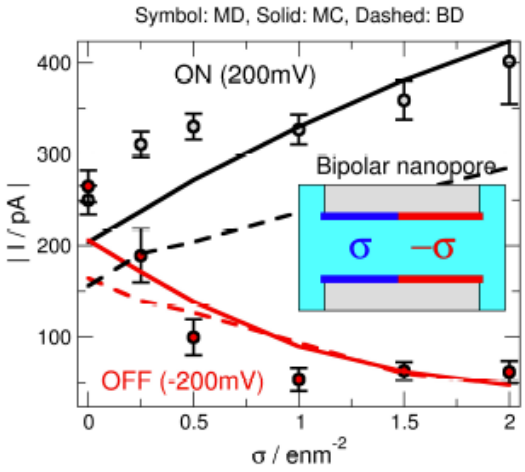

Figure 1 – The currents as functions of surface charge density as obtained from MD simulations for the all-atom explicit-water model (symbols), NP+LEMC simulations for the reduced implicit-water model (solid curves), and BD simulations for the same reduced model (dashed curves). Black and red colours refer to the ON and OFF states of the diode, respectively.

The results are shown in Figure 1. The MD and NP+LEMC data are those published in Ref. [1], while the BD results are new calculations performed using the BD code written by Claudio Berti [4]. As surface charge is increased, the polarity of the pore increases, and, thus, the currents in the ON and OFF states are increasingly different. This means that rectification increases.

While MD and NP+LEMC data agree well due to the fitting, the BD data are smaller than the NP+LEMC data. We hypothesize that this is due to the fact that the diffusion coefficient has a different meaning in BD and in NP+LEMC.

Conclusions

The cooperation between the authors continues in order to figure out the details about the different nature of the diffusion coefficient in NP+LEMC and in BD, and also the applicability of the Einstein relation in concentrated confined systems.

References

[1] Ható Z. et al., Phys. Chem. Chem. Phys., 19(27):17816-17826, 2017. [2] Matejczyk B et al., J. Chem. Phys., 146(12):124125, 2017. [3] Boda D. et al., J. Chem. Theory Comput., 8(3):824-829, 2012. [4] Berti C. et al., J. Chem. Theory Comput., 10(8):2911-2926, 2014.

Acknowledgements

The work has been performed under the Project HPC-EUROPA3 (HPC17RJ8MP), with the support of the EC Research Innovation Action under the H2020 Programme; in particular, the author gratefully acknowledges the support of Department of Medical Biotechnologies, University of Siena and the computer resources and technical support provided by CINECA.

FLUID-STRUCTURE INTERACTION SIMULATIONS USING A COUPLING BETWEEN CODE SATURNE AND ALYA

R. Borrell[1], *C. Moulinec*[2]

[1]*Barcelona Supercomputing Center (BSC), Barcelona, Spain;* [2]*STFC Daresbury Laboratory, Sci-Tech Daresbury, United Kingdom*

Abstract

Advances on multi-physics simulations at extream scale can be realized by summing up the best features of leading-edge software, that can be coupled together to produce a new capability. Aligned with this vision, this project focuses on enabling the coupled execution of Alya [1] and Code Saturne [2], aiming to foster as well the collaboration between the respective communities of users. Both codes are included at the Unified European Applications Benchmark Suite [3] of PRACE, complying thus with the highest standards in HPC. Alya relies on the Finite Element method to solve the equations of mechanics, and Code Saturne on the Finite Volume method to solve the Navier Stokes equations. This coupling between codes has been implemented through the open source Parallel Location and Exchange (PLE) library [4].

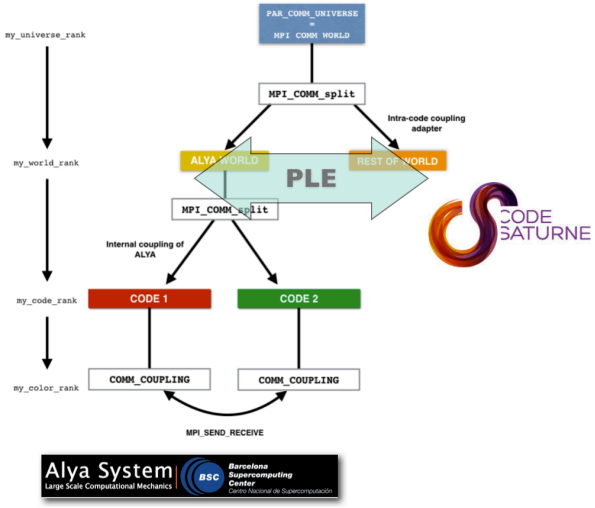

Figure 1 – Hierarchy of communicators for multi-code executions in Alya

Progress report

This project has brought the opportunity of sitting together the developers of Code Saturne and PLE (STFC) on the one hand, and Alya (BSC) on the other, to design and implement the coupled execution of the respective codes. Furthermore, the developments were attested on the ARCHER supercomputer hosted by EPCC at the University of Edinburg, with the collaboration of their support team. Putting all these ingredients together for three weeks was highly productive to settle the basis for a robust and scalable solution.

PLE is already a satellite library of Code Saturne. Therefore, most of the implementations were required from the Alya side, where we included PLE at the highest level of the hierarchy of communicators used for multi-code executions, see Figure 1. The PLE library deals with all the issues related with the coupling setup, namely the parallel location of matching interfaces and the generation of communicators for data exchange.

A strong requirement for this project has been to avoid any bottleneck on the parallel implementation since both codes target cutting edge HPC systems.

Concluding remarks

By the end of the stay, PLE has been fully integrated within Alya. We validated the development by coupling different instances of the code but using PLE instead of the internal coupling modules of Alya. We resolved a flow in the ascending aorta that is an FSI problem previously studied by the author [5]. The refactoring introduced in Alya required more effort than expected, for this reason, we could not achieve the last part of the workplan during the stay, consisting of performing a coupled simulation using both codes. However, the collaboration between the development teams of Alya and Code Saturne has been established and, being now PLE available in both codes, the next step will be to plug them for the solution of FSI problems.

References

[1] V´azquez, M., Houzeaux, G., Koric, S., Artigues, A., Aguado-Sierra, J., Aris, R., Mira, D., Calmet, H., Cucchietti, F., Owen, H., Taha, A., Derin Burness E., Cela, J.M. and Valero, M. Alya: Multiphysics Engineerin Simulation toward Exascale. Journal of Computational Science 201 14:15–27. [2] Fournier, Y., Bonelle, J., Moulinec, C., Shang, Z., Sunderland, A. an Uribe, J. Optimizing Code Saturne Computations on Petascale Systems Computers & Fluids (2011) 45:103–108. [3] http://www.prace-ri.eu/ueabs [4] https://www.code-saturne.org/cms/sites/default/files/docs/ple/doxygen/index.html [5] Cajas, J.C., Houzeaux, G., V´azquez, M., Garc´ıa, M., Casoni, E., Calmet, H., Artigues, A., Borrell, R., Lehmkuhl, O., Pastrana, D., Ynez, D.J., Pons, R. and Martorell, J. Fluid-Structure Interaction Based on HPC Multicode Coupling. SIAM Journal on Scientific Computing (2018) 40(6):C677–C703.

Acknowledgements

The work has been performed under the Project HPC-EUROPA3 (INFRAIA-2016-1-730897), with the support of the EC Research Innovation Action under the H2020 Programme; in particular, the author gratefully acknowledges the support of Scientific Computing Department of STFC and the computer resources and technical support provided by EPCC. In particular, we would like to acknowledge Gavin Pringle and Catherine Inglis from EPCC, for their support throughout the project.

EFFICIENT FE2 MULTI-SCALE IMPLEMENTATION APPLIED TO COMPOSITE DEFORMATION

G. Giuntoli[1], G. Houzeaux[1], M. Vázquez[1], J. Grasset[2], C. Moulinec[2] and S. Longshaw[2]

[1]Barcelona Supercomputing Center, Spain; [2]STFC, Daresbury Laboratory, United Kingdom

Introduction

The FE2 multi-scale has started to be considered for solving engineering composite material problems thanks to the computational advances of the last decades. The method is primarily used for solving structural composite material problems, i.e., for predicting the damage caused by hailstones on aircraft carbon-fiber wings. The advantage of it is that it allows solving accurately composite problems without requiring phenomenological laws for modeling the micro-scale, these lasts are generally complicated to be obtained. The main complication of the FE2 method resides in the large computational cost to solve the nested system of equations between the macro- and micro-scale.

This work, funded by the HPC-Europa3 programme and performed as a collaboration between the Barcelona Supercomputing Center and the STFC, Daresbury Laboratory, has the purpose of testing and benchmarking an implementation of the FE2 multi-scale technique developed during the last two years by both research centers. This application differentiates from others due to the use of a hybrid CPU/GPU scheme for accelerating the computations.

The final objective of the project, within one year, is to solve problems with a mesh discretization of at least 1 million elements in both scales (macro- and microscales). This last is equivalent to solve a problem of about 10^12 - 10^13 degrees of freedom, i.e., for simulating an entire wind turbine blade or an aircraft wing.

Methods

The FE2 application developed in this project consists of a coupling between two codes, as shown in Figure 1. The first is Alya, an MPI-based multi-physics code used for calculating the macro-scale, the other is Micropp, a hybrid CPU/GPU implementation used to model the micro-scale.

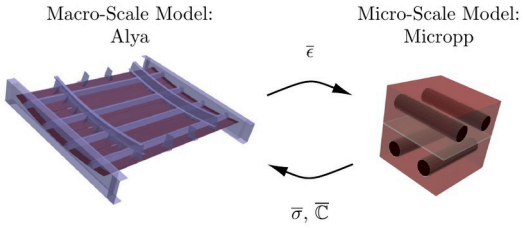

Figure 1 – Coupling between Alya and Micropp to solve the FE2 multi-scale problem.

Most of the work was focused on the development and GPU offloading of the micro-scale code. This is the most computationally intensive part of the coupled algorithm representing more than 99% of the calculation time. For the GPU offloading OpenACC and CUDA were used.

Results

The coupled application with Alya and Micropp was tested in three different machines provided by the HPC-Europa3 program: Wilkes-2, POWER9 (CTE-POWER), and Cirrus. All of them consist of hybrid CPU/GPU architectures.

The micro-scale code was benchmarked in a standalone way on the three machines using the OpenACC offloading. Speedups of about x9, x14, and x9 were measured using the CPU/GPU execution (respect to CPU-only) in Wilkes-2, POWER9, and Cirrus, respectively, as outlined in Fig. 2. On the other hand, the coupled algorithm with Alya and Micropp has achieved speedups of x8.4, x2.9, and x4 in Wilkes-2, POWER9, and Cirrus, respectively.

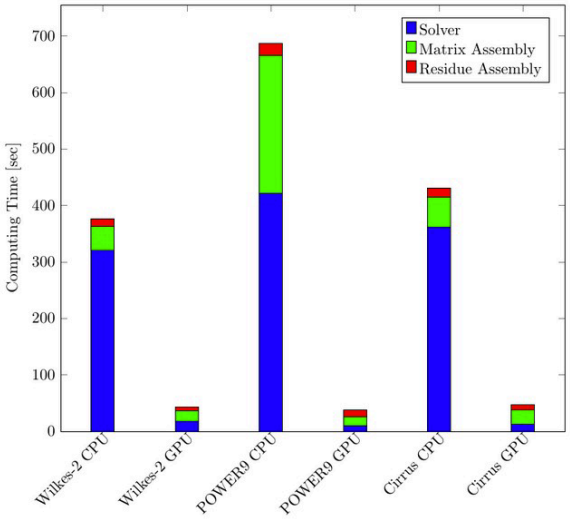

Figure 2 – Comparison of CPU-only and CPU/GPU execution on different machines for the micro-scale.

The results with CUDA in POWER9 machine, using a representative benchmark, have shown that OpenACC can give a speedup of about x20 while CUDA can at least provide a speedup of about x30.

Conclusions

The results obtained during this visit are going to be used to write a scientific paper focusing on the hybrid CPU/GPU execution of the FE2 multi-scale implementation developed. Currently this application has solved the largest problem in literature using the FE2 multi-scale method: 10 K elements for the macro-scale and 1 M element for the micro-scale (POWER9 – 40 computing nodes with 4 GPUs NVIDIA V100 per node).

Acknowledgements

The work has been performed under the HPC-EUROPA3 programme, with the support of the EC Research Innovation Action under the H2020 Programme; in particular, the author gratefully acknowledges the support of Charles Moulinec and the computer resources and technical support provided by the Edinburg University.

EMBEDDED FLAME HEAT FLUX METHOD FOR SIMULATION OF QUASI-STEADY STATE VERTICAL FLAME SPREAD

K. Li[1], S. Hostikka[2]

[1]School of Resources and Environmental Engineering, Wuhan University of Technology, China; [2]Department of Civil Engineering, School of Engineering, Aalto University, Finland

Introduction

Flame spread leads to fire growth and enlargement. Accurate predictive flame spread models for combustible materials in different configurations have been sought for long [1] and many computational studies have been conducted for various materials with different in-house [2] and open-source codes [3]. Although a better understanding on the flame spread dynamics has been gained in the last few decades, accurate modelling a bench-scale experiment is still challenging because of the multi-physics and multi-scale nature of the problem.

In this work, we want to investigate if the flame heat flux profiles can be extracted from quasi-steady state flame spread solutions, and expressed as similarity solutions using a non-dimensional spatial position, which can be applied for different grid resolutions.

Methods

In the paper, the flame spread experiments are firstly modelled using a fine mesh which is capable of leading to the steady state flame spread. Then, the model results are compared to the experimental measurements to make sure reasonable flame heat flux fields can be extracted meanwhile the effects of flame heat flux on steady state flame spread are presented by comparing the spread rates of different flame heat fluxes. Finally, the flame heat fluxes extracted from the fine mesh simulations are embedded in the coarse mesh simulations with different simplification levels to reveal the possibility of modelling flame spread with an engineering grid size by fixing the near wall heat flux.

Results

When the flame spreads up, a pyrolysis zone forms from the flame root to the edge of preheating area. The pyrolysis zone moves up with the flame and generates gases to sustain the flame during spread. Figure 1 shows the typical experimental and modelling turbulent flow fields of rod flame.

Three different alternatives for transferring the fine-mesh heat flux profile were studied. If the heat flux profiles were fixed in terms of magnitude and absolute vertical profile, the coarse-mesh simulations accurately reproduce the fine-mesh results. This, however, means breaking the coupling between the gas-and solid phase phenomena. If the heat flux magnitude was retained and the profile normalized by the pyrolysis length, i.e. simulation outcome, the steady state flame spread was accurate only if the initial length of the pyrolysis region was initialized (enforced) to a correct value. Finally, a compromise solution was proposed where the heat flux within the pyrolysis region is prescribed using the normalized coordinates, thus making it coupled to the simulation outcome, but the preheating zone heat flux profile is prescribed using the physical coordinates. Embedding this type of heat flux to the coarse mesh computation was shown to reproduce the fine mesh flame spread rate and pyrolysis length with a factor of ten increase of gas phase cell size.

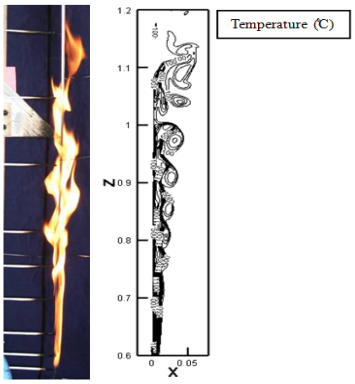

Figure 1 – Typical experimental and modelling turbulent flow fields of rod flame

Conclusions

The current study proposes a new numerical strategy of modelling vertical flame spread with CFD simulations. The strategy makes use of the heat flux fields obtained from well-resolved mesh to overcome the difficulties of modelling near-field heat fluxes with different mesh resolutions. The numerical predictions with 1 mm gas phase mesh were found to be comparable to the experimental results. To improve the flame spread in coarse meshes, the incident heat fluxes from 1 mm mesh are used as virtual heat flux boundary condition, normalized by the pyrolysis zone length. The modelling results indicate that accurate coarse-mesh predictions are possible when the total heat flux is enforced to follow the prediction of the fine-mesh simulation.

References

[1] Jiang L et al., Proc. Combust. Inst., 36: 2987-2994, 2017. [2] Di Blasi C, Combust. Flame., 97: 225-239, 1994. [3] Kwon J et al., Fire Technol., 43: 255–284,2007.

Acknowledgements

The work has been performed under the Project HPC-EUROPA3 (INFRAIA-2016-1-730897), with the support of the EC Research Innovation Action under the H2020 Programme; in particular, the author gratefully acknowledges the support of Aalto University and the computer resources and technical support provided by CSC – IT Center for Science, Finland.

VORTEX FORMATION FROM AN OSCILLATING CYLINDER

T. Parra

University of Valladolid - ITAP, Spain

Introduction

Actual society has a commitment with renewable energies as a result of climate change and strict regulation on CO2 emissions. However, some technologies are more developed than others. Hydrokinetic conversion systems are suitable for harvesting energy from flowing river streams, tidal currents or other artificial water channels.

The final aim of this research line is numerical study of self-excited vibrations in a body due to fluid-elastic instability, commonly known as Vortex Induced Vibrations (VIV), that is one technology in process of development. The principle of operation is the vibrations from vortices forming and shedding vortex formed downstream from the bluff body in a current. This method operates at lower heads and offers a wider range of flow rates than the turbines.

A sequence of steps is to be carry out in order to accomplish the numerical modelling of the Fluid-Structure Interaction (FSI) of a cylinder in the Vortex Induced Vibration (VIV) regime and gain some insight of this kind of energy generation water current devices. The first step is the validation of forced oscillating cylinders. The second step is to be the challenging free oscillating cylinders. Finally, the study of an array of cylinders should be carried out.

The HPC Europa3 grant was used to stablish the seeds to achieve in the future the VIV modelling. The host group from Helmut-Schmidt-University, has experience in the modelling of the FSI. They even have reference test cases to validate numerical codes [1-2]. The period granted was devoted to training on the study of forced oscillating cylinders. The granted access to the High-Performance Computing Center Stuttgart (HLRS) using the Cray XC40 Hazel Hen was devoted to numerical study of an oscillating cylinder in a laminar regime.

Methods

The model was implemented using the standard OpenFOAM v. 5.0, [3]. Independence of results to the spatial and temporal resolution was tested. The computational domain has dimensions 27.5D x 10D with D the diameter of the cylinder being the final mesh around 360 thousand cells.

Results

The first task was the numerical study of an oscillating cylinder in laminar regime using the benchmark provided by [4]. The cylinder is forced to oscillate with an amplitude of 20% D and an excitation frequency, fe, that varies between the frequency of shedding of the vortices for steady cylinder, fo, and other that is 20% higher. The behaviour of the instantaneous drag and lift coefficients, as well as the Strouhal number were investigated, see figure 1.

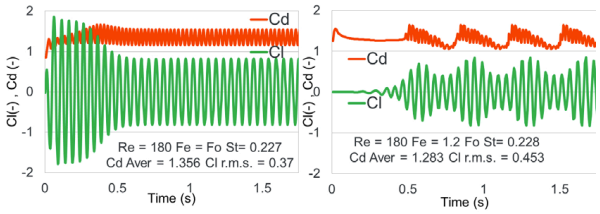

Figure 1 – Lift and drag coefficient versus time for Re = 180. Left fe = fo. Right fe = 1.2 fo.

As for the vortex shedding, figure 2 shows the influence of increasing the excitation frequency for Re = 180. The location of the cylinder is at the extreme upper, at null and at the extreme bottom positions.

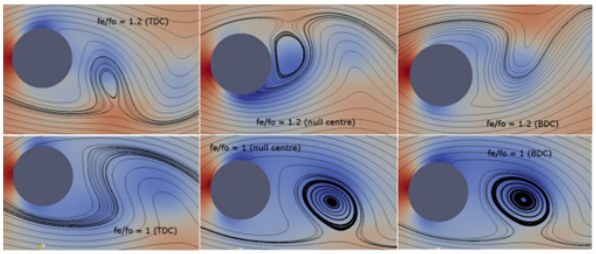

Figure 1 – Streamlines over pressure contours for Reynolds = 180. Upper line fe = 1.2 fo. Lower lines fe = fo. Left row at top dead centre, middle at null position of the centre, right row at bottom dead centre. The alternative vortex detachment from one side of the cylinder to the other is the precursor of the wake downstream from the cylinder. The vortices are nearer each other when the excitation frequency increases.

Conclusions

Future works will be the study of a free cylinder in a turbulent flow with two degrees of freedom (in streamwise and vertical direction). It is elastically mounted and vibrates as a result of drag and lift forces. The equations of classical rigid body motion involve structural damping c, structural stiffness k, the mass of the cylinder as well as the corresponding aerodynamic forces.

References

[1] Breuer M., et al., Journal of Fluids and Structures, 29:107-130, 2012. [2] De Nayer G. et al., International Journal of Heat and Fluid Flow, 50:300–315, 2014. [3] OpenFOAM. User Guid version 5, 2018. [4] Guilmineau E. et al., Journal of Fluids and Structures, 16(6):773-794, 2002.

Acknowledgements

The work has been performed under the Project HPC-EUROPA3 (INFRAIA-2016-1-730897), with the support of the EC Research Innovation Action under the H2020 Programme; in particular, the author gratefully acknowledges the support of Michael Breuer and Guillaume De Nayer from Strömungsmechanik - Universität der Bundeswehr Hamburg and the computer resources and technical support provided by HLRS.

UPGRADING AND OPTIMIZATION OF MONTE CARLO SIMULATOR FOR ADVANCED MODELLING OF 2D MATERIALS AND DEVICES

E. Pascual

Department of Applied Physics, University of Salamanca, Spain

Introduction

The Monte Carlo (MC) method for electron transport is based on computational algorithms that approximates complex mathematical expressions (particularly, those derived from the Boltzmann Transport Equation and the probabilities of scattering in solids) relying on repeated random sampling. The parallelization of MC based simulation codes seems a very appealing way to optimize computational resources.

Our main interest was the parallelization of our ensemble MC simulator for two dimensional (2D) materials such as Graphene, Silicene or metal dichalcogenides as the Molybdenum disulfide (MoS2) [1, 2], developed with a purely sequential philosophy. The parallelization of MC simulators is not a trivial task due to the fact that the motion of the set of particles, following Boltzmann Transport Equation (with classical free flights interrupted by scattering mechanisms determined by quantum-mechanical probabilities) depends on their prior motion and cannot be performed independently [3].

Methods

The Message Passage Interface (MPI) was considered for the parallelization of our in-house simulator (written in Fortran programming language), so in the first instance, the implemented physical model and the feature of the simulator needed to be analysed in depth.

We focused first on parallelizing the material simulation module instead of the device simulation module, therefore assuming a constant field. The particle motion (this is, the core of the MC method -Figure 1-) was identified as the most critical stage of the simulation, and thus, the most interesting to be parallelized. Inside the loop, parallelization between different MPI processes, implies that each one must read and write from different arrays of data structures: The Band Structure, where all the distribution functions of the reciprocal space are, and the queue of the particles to be simulated, being both updated inside the loop of motion of particles.

Results

The exhaustive analysis of our code and the work and tests carried out have evidenced the strong inherent serial nature of the simulator. The most significant problem is the update of the distribution function of the particles in the reciprocal space (k-space) and the particle queue, which takes place after every particle flight (Figure 1). These data structures would need for every MPI process to be readily accessible for writing and reading purpose, since they are indispensable for the Pauli Exclusion Principle and the generation-recombination mechanisms.

An alternative solution –currently in progress– is to update the distribution function at the end of each time step, pass it to all MPI tasks and consider it to be constant during the next time step so that particles could then be distributed between the different MPI processes. The changes produced in each MPI task would then be gathered and the distribution function updated for the next time step. This way, the simulation time would be considerably reduced. However, it also entails losing accuracy since this approach is incompatible with some critical aspects like carrier-carrier interactions and interband phenomena and therefore, simulations possibilities will be restricted with the parallelized code.

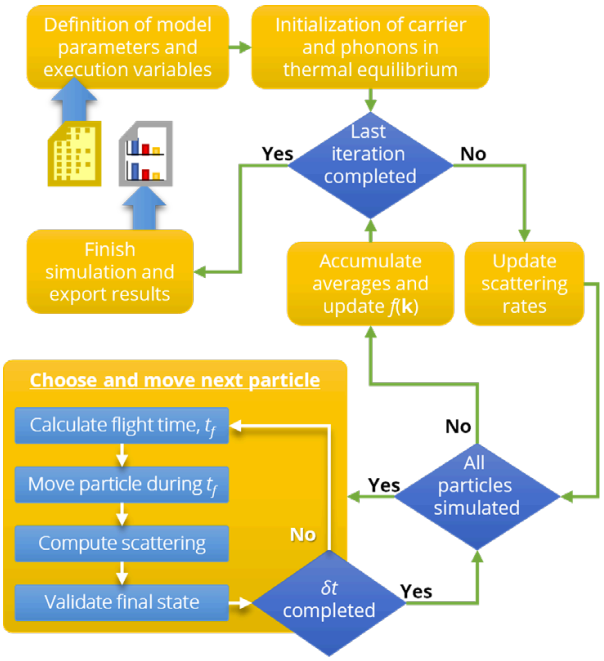

Figure 1 – Operation flow diagram of our MC simulator.

Conclusions

The work carried out has allowed us to determine that it is not possible to develop a parallelization of the complete code, although an alternative partial solution has been designed in order to distribute the particles in different MPI processes, at the expense of some restrictions in the kind of simulations to be performed.

References

[1] Rengel R et al., Journal of App. Phys., 114: 143702, 2013. [2] Rengel R et al., Semic. Sci. and Tech., 33: 065011, 2018. [3] Anderson J A et al., Journal of Comp. Phys., 254:27-38, 2013.

Acknowledgements

The work has been performed under the Project HPC-EUROPA3 (INFRAIA-2016-1-730897), with the support of the EC Research Innovation Action under the H2020 Programme; in particular, the author gratefully acknowledges the support of Prof. K. Kalna from Nanoelectronic Devices Computational Group at College of Engineering, Swansea University, and the computer resources and technical support provided by EPCC.

EVALUATION OF CONDUCTANCE-BASED NEURAL MODEL ON A MULTINODE INTEL XEON PHI KNL DEPLOYMENT

G. Chatzikonstantis[1], H. Sidiropoulos[1], C. Strydis[2], M. Negrello[2], G. Smaragdos[2], C.I. De Zeeuw[2], D.J. Soudris[1]

[1]School of Electrical and Computer Engineering, NTUA, Athens, Greece; [2]Erasmus MC, Neuroscience Department, Rotterdam, Germany

Introduction

One of the most biochemically realistic but also compute-intensive neural models for simulating the brain is the Hodgkin-Huxley (HH) model. We present a new simulator implemented on Intel Xeon Phi Knights Landing (KNL) manycore processors employing a mix of OpenMP and MPI. The simulator performance is evaluated when calculating neuronal networks of varying sizes, density and network connectivity maps. Evaluation investigates the optimal processor count per neural-network problem size and is scalable to populations of millions of neurons.

Methods

Simulator code has been written in a mix of MPI and OpenMP. Design-wise, we have organized neurons in a 3-dimensional grid [1]. For exploring the impact of network topology, we explored two different (and naturally occurring) distributions: a uniform distribution of synapses in the network; and a Gaussian distribution of synapses where neurons in proximate positions on the 3D grid are significantly more likely to form a bond. As will be shown, synapse distribution affects performance in a definitive manner. Neural-networks of various sizes are tested.

Results

Selected results are presented concisely, next:

1) *Optimal Allocation of Resources*: One of the focal points in this work is the concept of matching hardware utilization to the workload that requires calculating. The suggested amount of hardware to deploy for each network simulation varies according to network size and its corresponding connectivity map. In this work, up to 8 KNL processor nodes have been employed due to availability, Figure 1 depicts a general guideline for allocating the minimal KNL instances necessary for achieving the best possible performance for workload instance. Various interesting observations are made.

- Uniformly-distributed connectivity maps force the simulator to become completely communication-bound, due to model complexity.
- Because neighboring neurons are more likely to form bonds in Gaussian distributions, significantly more scalable network configurations are possible.
- Connectivity maps based on the Gaussian distribution expose data locality better and support utilizing multiple KNL nodes.
- Network density directly correlates with employing multinode allocations.
- When network sizes are large while network synaptic count is low, the neuromodeling problem becomes an embarrassingly parallel use case and utilizing a high number of processors is recommended. Even a small number of synapses per neuron can impose a non-trivial communication overhead.
- Small, dense networks benefit from single-node allocations, otherwise computational resources are effectively wasted and performance suffers.

2) *Simulator Sensitivity to Workload Parameters*: Even in the strictly-defined parameter space of this work, the simulator behaviour, as shown in Figure 1, clearly shows that even small changes to its parameters can have a large impact on performance, confirming prior results [2]. Inversely seen, the resources can be scaled to match problem size in a cost-efficient manner.

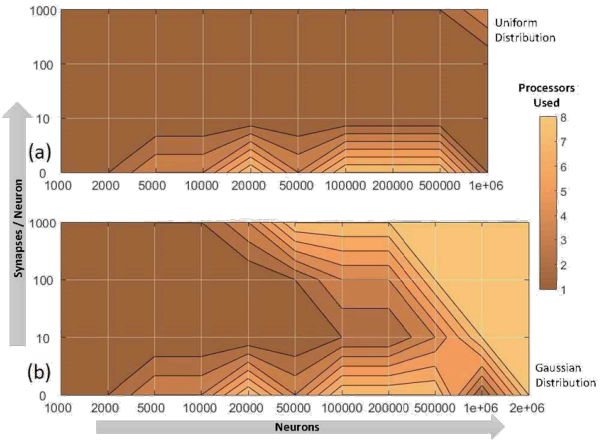

Figure 1 – Colourmaps depicting the number of processors providing the best simulation speed for networks of uniform and Gaussian synaptic patterns. Single-node implementations dominate networks with uniform synaptic distributions due to poor scalability.

Conclusions

This work has briefly discussed the performance and scalability of a computationally complex and biologically accurate neuron simulator on Intel Xeon Phi KNL processors. The simulator has been designed with a broader manycore architecture in mind, since the KNL hardware assets are found on most x86-based manycore processors and the simulator was written using traditional parallelization techniques of OpenMP and MPI. The work proves that efficient usage of a small cluster of manycore processors is able to achieve high performance, even when facing a very demanding computational neuron model featuring millions of neurons and billions of synapses, respectively.

References

[1] G. Chatzikonstantis, D. Rodopoulos, et al., First Impressions from Detailed Brain Model Simulations on a Xeon-Xeon Phi Node, ACM CF 2016, May 16 - 18, Como, Italy, pp. 361-364. [2] G. Smaragdos, G. Chatzikostantis, et al., Performance Analysis of Accelerated Biophysically-Meaningful Neuron Simulations, IEEE ISPASS 2016, April 17-19, Uppsala, Sweden, pp. 1-11 – Ranked 1st (Best-Paper Nominee).

Acknowledgements

The work has been performed under the Project HPC-EUROPA3 (INFRAIA-2016-1-730897), with the support of the EC Research Innovation Action under the H2020 Programme; in particular, the author gratefully acknowledges the support of Prof. Dimitrios Soudris (ICCS, NTUA), and the computer resources and technical support provided by GRNET.

STENCIL SELECTION ALGORITHMS FOR WENO SCHEMES ON UNSTRUCTURED MESHES

P. Tsoutsanis

Cranfield University, United Kingdom

Introduction

In this paper, a family of stencil selection algorithms is presented for WENO schemes on unstructured meshes. The associated freedom of stencil selection for unstructured meshes, in the context of WENO schemes present a plethora of various stencil selection algorithms. The particular focus of this paper is to assess the performance of various stencil selection algorithm, investigate the parameters that dictate their robustness, accuracy and computational efficiency. Ultimately, efficient and robust stencils are pursued that can provide significant savings in computational performance, while retaining the non-oscillatory character of WENO schemes. This is achieved when making the stencil selection algorithms adaptive, based on the quality of the cells for unstructured meshes, that can in turn reduce the computational cost of WENO schemes. For assessing the performance of the developed algorithms well established test problems are employed. These include the least square approximation of polynomial functions, linear advection equation of smooth functions and solid body rotation test problem. Euler and Navier-Stokes equations test problems are also pursued such as the Shu-Osher test problem, the Double Mach Reflection, the supersonic Forward Facing step, the Kelvin-Helmholtz instability, the Taylor- Green Vortex, and the flow past a transonic circular cylinder.

Methods

WENO methods have been used in the finite-volume framework, following the work of Tsoutsanis et al. [1]. The reconstruction was carried out in characteristics variables, and an HLLC Riemann solver was used with a 4th-order explicit Runge-Kutta time stepping scheme.

Results

The results obtained highlight that significant savings in computational performance can be obtained using the adaptive stencil based compact algorithm in conjunction with the Type 3 directional stencil. The results also demonstrate that simulations using higher-order spatial discretisations are now more affordable due to the enhanced and more compact stencils employed.

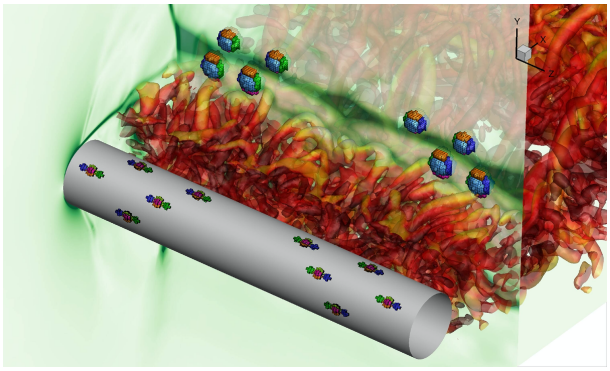

Figure 1 – Plot of stencils at various regions of the computational domain, for the transonic flow past an infinite cylinder at Re=3900 and Mach number of 0.8.

Conclusions

This paper investigates various stencil selection algorithms for WENO schemes for smooth and discontinuous flow problems. The algorithms are differentiated with respect to the central stencil and directional stencils since different parameters need to be considered for each one of them. From the various central stencil algorithms presented the SBC algorithm in its present implementation is the most robust, for good and bad quality meshes, and it is therefore the selected algorithm for the present WENO schemes. Regarding the directional stencils, the situation is more complicated, in the sense that a fine balance between computational cost and non-oscillatory properties of the WENO schemes are pursued. The Type 3 directional stencil algorithm provides significant computational savings and a satisfactory level of robustness for all the test-problems investigated and remains the algorithm of choice for the present implementation.

References

[1] Tsoutsanis et al., Journal of Computational Physics, volume 320 (4):1585-1601, 2011.

Acknowledgements

The work has been performed under the Project HPC-EUROPA3 (INFRAIA-2016-1-730897), with the support of the EC Research Innovation Action under the H2020 Programme; in particular, the author gratefully acknowledges the support of Professor M. Dumbser at University of Trento and the computer resources and technical support provided by CINECA (Bologna – IT).

AERODYNAMIC ANALYSIS OF J-29 WINGS BY CFD

S. Yang

Key Laboratory of Pattern Recognition and Intelligent Systems of Guizhou Province, Guizhou Minzu University, China

Introduction

This project was about the calculation of aerodynamic characteristics of wings in RANS flow field. Three wing types of Saab J29 (traditional wing type wing A, chord extension wing F, chord extension wing F with fence) were selected as research models. Simulations using Computational fluid dynamics (CFD) was carried out by the high-performance computing resources Beskow at KTH-PDC. The aerodynamic characteristics of different wing models were studied and discussed with aerodynamics experts of Airinnova to analyse the differences and learnt the motivations of different designs.

Methods

The CAD models of three wing models are built in SUMO[1] software from 3-view drawings. There are, a clean wing A, chord-extension wing F (denoted as wingFwoF), and chord-extension wing F with fence (denoted as wingFwF) respectively. CFD calculation is performed by Open Source CFD tool SU2 [2] on Beskow [3] for a series Mach numbers from subsonic to transonic up to Mach 0.92, with a range of angles of attack. The calculations were performed for both Euler and RANS.

Results

The RANS results show that, wing FwF and wing FwoF reduce the shock at the outer wing, which significantly reduces the drag coefficient, or increases L/D, see Figure 1. By comparing the pressure distribution of wing FwF and wing FwoF, it can be found that the pressure at the tip of the chord extending out is dispersed due to the existence of the fence, making the drag coefficient of wing FwF slightly smaller than that of wing FwoF. Moreover, the vortex fence tends to reduce the vorticities shedding behind the wing, this would release the outer part of the wing and make the aileron more efficient. In conclusion, wing FwF performs best in terms of aerodynamic characteristics.

Conclusions

The whole process from CAD modelling, grids generation, and to CFD calculation is mainly conducted by open source software. This leads to a more flexible and integrated framework for analysis and design. The calculated results also support the contribution of the fence regarding to the aerodynamic characteristics of wing. The future work will focus on aerodynamic dataset generation for J-29 by high fidelity CFD for flight simulation.

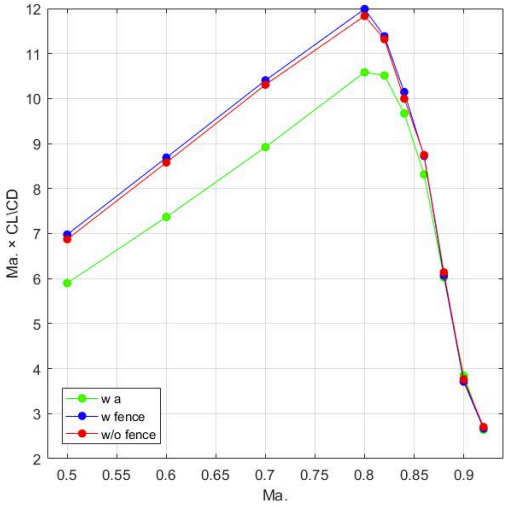

Figure 1 – M*L/D for three wing models, RANS simulation at aoa = 3 deg.

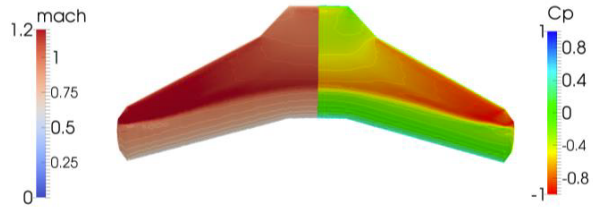

Figure 2 – Mach and Cp contours for wing A, RANS simulation at Mach = 0.82, aoa = 3 deg.

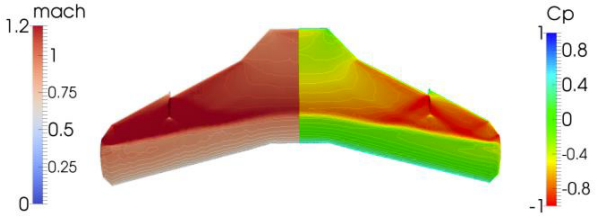

Figure 3 – Mach and Cp contours for wing FwF, RANS simulation at Mach = 0.82, aoa = 3 deg.

References

[1] SUMO: the SUrface Modeler, https://www.larosterna.com/products/open-source, accessed date 2019-07-30; [2] SU2, https://su2code.github.io/; [3] Beskow, https://www.pdc.kth.se/hpc-services/computing-systems/beskow-1.737436

Acknowledgements

The work has been performed under the Project HPC-EUROPA3 (INFRAIA-2016-1-730897), with the support of the EC Research Innovation Action under the H2020 Programme; in particular, the author gratefully acknowledges the support of Dr. Mengmeng Zhang from Airinnova AB and the computer resources and technical support provided by KTH-PDC.

LARGE SCALE MUTATION TESTING

P.C. Cañizares[1], A. Núñez[1], R. Filgueira[2], D. Henty[2]

[1]Complutense University of Madrid, Spain; [2]University of Edinburgh, United Kingdom

Introduction

Large-scale systems have been widely adopted due to its cost-effectiveness and the evolution of networks. In general, large scale systems can be used to reduce the long execution time of applications that require a vast amount of computational resources and, especially, techniques that are usually deployed in centralized environments - like testing - can be deployed in these systems. Currently, one of the main challenges in testing is to obtain an appropriate test suite. In essence, the main difficulty lies in the elevated number of potential test cases. Mutation testing is a valuable technique to measure the quality of test suites that can be used to overcome this difficulty. However, one of the main drawbacks of mutation testing is the high computational cost associated with this process [1]. In this work, we propose two improvements based on our previous approach, called OUTRIDER [2,3], a set of strategies to optimize the mutation testing process in distributed systems. Although OUTRIDER efficiently exploits the computational resources in distributed systems, several bottlenecks have been detected while applying these strategies using large-scale systems. For this reason, this proposal is three folded: i) Providing a hybrid algorithm designed to reduce the communications between the master and the worker processes while maintaining a high level of resources usage, ii) Improving the compilation phase, iii) Comparing the proposal with other distribution solutions, such as Spark or Cloud systems.

Methods

This work focuses on evaluating the scalability the different optimizations for parallelizing the mutation testing process using large scale systems. For this, we have identified the existing bottlenecks and drawbacks that hamper the performance of the mutation testing process. Specifically, we have identified drawbacks related with the high level of communication and network traffic between master and workers processes and the elevated compilation time. Therefore, we have implemented two solutions: i) the compilation phase has been parallelised in order to reduce the overall time, ii) the distribution algorithm has been improved including an adaptive mechanism that changes the size of the execution grain depending on the remaining workload. This algorithm reduces the total number of exchanged messages between master and workers up to 90%.

Results

In order to check the scalability and performance of the proposed framework we have carried out a thorough performance evaluation. In this phase, the mutant set used in these experiments has been created using the MuToMVo mutation testing framework to seed faults in three different applications. The first one is an image an image filtering application consisting of 3 algorithms to filter BMP images. The second one is the open source compression application BZIP2. The third one is an open source FFT library. These experiments have been performed in a cluster with 280 nodes, which are interconnected through an Infiniband fabric network. Each node contains two 18-core Intel(R) Xeon CPU@ 2.1 Ghz with hyper-threading, 256 GB of RAM and 406TB Lustre file system. In general, the results show that the improvements proposed in this work outperform OUTRIDER up to 15%.

Conclusions

In this paper we have presented an HPC-based optimization for the MT process in Large Scale Systems. This optimization consists of a set of strategies aimed at improving the resource usage efficiency, which uses OUTRIDER as basis. Also, an experimental phase has been carried out to evaluate the effectiveness and scalability of this work. The experiments show that the improvements proposed in this work outperforms previous proposals to improve performance of the MT process.

References

[1] B. Choi et al. High-performance mutation testing. Journal of Systems and Software, 20(2):13-152, 1993. [2] P. C. Cañizares et al. OUTRIDER. In ICCS'17, volume 108, pages 505-514. Elsevier. [3] P. C. Cañiizares et al. EMINENT: Embarrassingly parallel mutation testing. In ICCS'16, volume 80, pages 63 -73. Elsevier.

Acknowledgements

The work has been performed under the Project HPC-EUROPA3 (INFRAIA-2016-1-730897), with the support of the EC Research Innovation Action under the H2020 Programme; in particular, the author gratefully acknowledges the support of David Henty of EPCC at University of Edinburgh and the computer resources and technical support provided by EPCC.

IMPROVING THE PERFORMANCE OF THE SPMV PRODUCT ON MULTI/MANY-CORE PROCESSORS USING AVX-512 INSTRUCTIONS AND CUDA

E. Coronado-Barrientos

CiTIUS, Universidad de Santiago de Compostela, Santiago de Compostela, Spain

Introduction

The Sparse Matrix-Vector (SpMV) product is an essential building block for numerous scientific applications that depend on Krylov iterative solvers for the resolution of sparse linear systems. Improving its performance on modern processors is not a trivial task because, generally, the sparse matrices generated by real applications exhibit irregular patterns that do not spawn regular computations, which are necessary to harness the maximum computing power on modern processors. Thus, this work retakes the AXC format, a sparse matrix storage scheme previously introduced in [1] for the Intel Xeon Phi architecture, and proposes a new format referred as NFT that expands its use to NVIDIA Graphics Processing Units (GPUs).

Methods

In order to evaluate the performance of our proposal, we measured the time required to perform 100 iterations of the SpMV product and used the average time per iteration to calculate the performance achieved by each format. Our proposal was implemented using AVX-512 instructions and CUDA for testing on the Intel Xeon Gold 6148 processor with Skylake architecture and NVIDIA Tesla V100 GPU with Volta architecture respectively. In order to validate the results, we compared the performance of our proposal against the performance of the SpMV functions based on the Compressed Sparse Row (CSR) format from the MKL and cuSPARSE libraries. In this report, we include the results for five matrices presented in Table 1. It is worth to remark that these matrices exhibit an arrow-head sparsity pattern.

MATRIX	*NAME*	*NNZ*
M1	e001	159119
M2	e002	1615118
M3	e003	3922721
M4	e004	9160735
M5	e005	27367235

Tabe 1 – NNZ is the number of non zero elements of each matrix.

Results

The numerical results from Figure 1 show that the NFT format performs faster a 41.0 % and 12.2 % on average than the CSR format on the Intel and NVIDIA devices respectively; the corresponding percentages of improvement of the NFT format when compared against the AXC format are 4.0 % and 40.3 %.

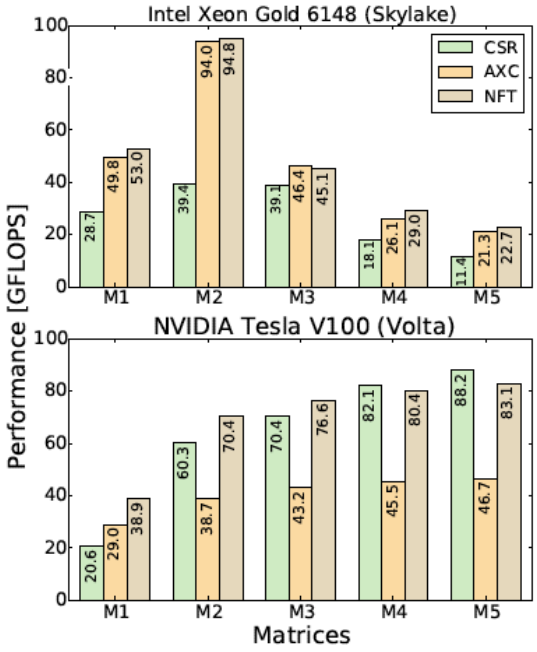

Figure 1 – Comparison of the SpMV performance from the CSR, AXC and NFT formats on two architectures.

Conclusions

Clearly, the AXC format and, consequently, the NFT format are well suited for the Intel Xeon architecture due to the fact that both formats outperform the CSR format in a roughly 40 % on this platform. The most interesting results are obtained on the NVIDIA platform where the NFT managed to outperform the CSR format by a 12.2 % while the AXC was bested by the latter in a 51.8 %.

References

[1] E. Coronado-Barrientos, G. Indalecio, and A. Garca-Loureiro. Improving Performance of Iterative Solvers with the AXC Format Using the Intel Xeon Phi. J. Supercomput., 74(6):2823{2840, June 2018.

Acknowledgements

The work has been performed under the Project HPC-EUROPA3 (INFRAIA-2016-1-730897), with the support of the EC Research Innovation Action under the H2020 Programme; in particular, the author gratefully acknowledges the support of Adrian Jackson EPCC, Mario Antonioletti EPCC, Catherine Inglis EPCC and the computer resources and technical support provided by the Edinburgh Parallel Computing Centre (EPCC) and the Irish Centre for High-End Computing (ICHEC).

OMPSS-2 RUNTIME LINTER: SPOTTING DATA RACES IN OMPSS-2 APPLICATIONS

S. Economo[1], *V. Beltran*[2]

[1]*Sapienza Università di Roma, Italy;* [2]*Barcellona Supercomputing Center, Spain*

Introduction

Programming models for task-based parallelization such as OmpSs-2 are very effective at uncovering the parallelism available in scientific applications. However, the nonnegligible cost of annotating complex applications for task based parallelization still hinders the adoption of these models. We targeted the OmpSs-2 programming model and developed a runtime tool to spot parallelization errors coming from wrong annotations. Our linter verifies the correctness of applications by ensuring that all the tasks are properly annotated and synchronized for a given set of inputs. Programmers can use the hints provided by this tool to make sure that nothing was left behind during the annotation process and that the application will be exempt from data races.

Methods

The main focus of the tool is that of data dependencies expressed via the in, out and inout clauses. A wrong specification of dependencies via these clauses may severely hamper the performance and the correctness of the program, thus forcing developers to debug their programs in conventional (and typically less effective) ways. Compared to other debugging and verification tools, the proposed one interprets data dependencies and compare them with concrete memory accesses issued by tasks at runtime to detect potential problems and propose solutions. For example, if one of the tasks is writing a global variable that has not been properly annotated (e.g., with the out clause) the tool will identify the lack of a data dependency and will also suggest annotating the identified variable accordingly (i.e., with the out clause).

When an OmpSs-2 application is run through our linter, memory accesses issued by tasks are recorded and temporarily stored to disk. For each task, the recorded memory accesses are later processed at task completion time and compared with the declared data dependencies to see if (a.) the task reads(writes) data but has no in(out) dependency, or (b.) the task has an in(out) dependency but it doesn't read(write) from it. For each of such mismatches a warning is generated to report to the user about the problem. The report comes with additional contextual information such as: address and size of the mismatching memory access (if any) along with its access mode (i.e., read or write); name of the involved dependency (if any) with the expected directionality (in, out, inout); variable name (if found); task invocation point in the source code (i.e., line in the respective file).

Figure 1 shows the conceptual organization of our linter and its interaction with external software. The target program is composed of the actual OmpSs-2 application and, if available, debug meta-data. The target program interacts with the runtime library (RTL) on which BSC's OmpSs-2 implementation is based, called Nanos 6, to invoke task based primitives and parallelize the application on the available cores. The linter is composed of an instrumentation tool and the actual memory tracer, divided into a traces producer and a traces consumer. The former generates memory traces and subscribes to task transition events provided by Nanos6 to enable/disable tracing. The latter processes memory traces and uses debug meta-data in the application, if any, to provide the user with further contextual information when the report is generated. The instrumentation logic is provided by Intel Pin, while the tracing logic is provided by a custom Pin-tool. Traces are placed inside a secondary storage area for later processing.

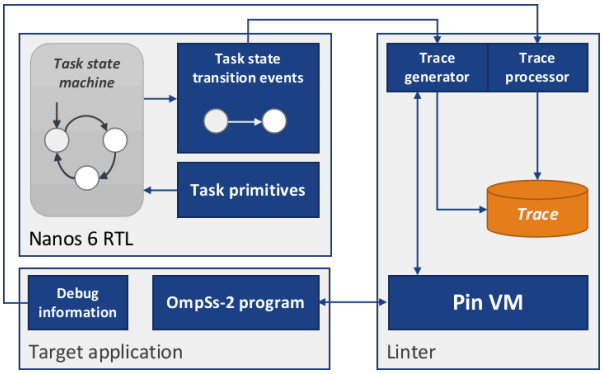

Figure 1 – Interaction between our Linter and other Ompss-2 software.

Results

To date, the tool is already able to run on and report about potential correctness issues in some simple OmpSs-2 implementations of matrix multiplication, merge sort, multisaxpy, and nqueens. As of date, the tool also supports: concurrent and commutative dependencies; the detection of accesses outside of the specified array section bounds of a dependency; the detection of unexpected accesses to release or weak regions.

Conclusions

We have presented a tool to spot data races in OmpSs-2 applications, developed at BSC under the HPC-EUROPA3 grant. Collaboration with BSC has continued beyond the scope of the grant, with the purpose of detecting additional classes of data races coming from: (1) the lack of taskwait directives to synchronize accesses between a task and its children; (2) the lack of weak dependencies in the parent task to synchronize child tasks in different dependency domains. Future work will entail reducing the tracing overhead of the tool, as well as further improving the quality of reports.

Acknowledgements

The work has been performed under the Project HPC-EUROPA3 (INFRAIA-2016-1-730897), with the support of the EC Research Innovation Action under the H2020 Programme; in particular, the author gratefully acknowledges the support of the Programming Models group and the computer resources and technical support provided by BSC.

ENHANCING DATA-STREAM PROGRAMMING PLATFORMS: A CASE FOR DISPEL4PY AND GRPPI COMPARISON

J. Fernández Muñoz

Computer Science and Engineering Department, University Carlos III of Madrid, Spain

Introduction

To address the issues surrounding on-line big data management, data stream processing (DaSP) paradigm is a suitable approach. Several programming frameworks have been proposed for DASP applications. The dispel4py system [1] is a parallel python-based stream-oriented dataflow framework that acts as a bridge to existing distributed programming frameworks like: MPI, Storm and Python multiprocessing. On the other hand, GrPPI [2] is a C++ generic high-level library that acts as a layer between developers and shared-memory parallel programming frameworks, such as C++ threads, OpenMP and Intel TBB.

Use case and methodology

Earthquakes and volcanic eruptions are often preceded or accompanied by changes in the geophysical properties of the Earth, such as seismic wave velocities or event rates. Reliable risk assessment methods for these hazards require real-time analysis of seismic data. However, potential techniques require a large number of waveform cross-correlations, which is computationally intensive, and is particularly challenging in real time. In this work, we employ a use case implemented as a pipelined workflow. The pipeline is divided in two phases: on the first phase, each continuous time series (or trace) obtained from a given seismic station is pre-processed independently. Later, on the second phase, every single trace is cross-correlated with every other trace in a combinatory pair-up process.

The use case has been implemented using both Dispel4py and GrPPI frameworks, both implementations have been tested using an increasingly large number of traces for cross-correlation. Due to the fact that GrPPI only works up to now for shared-memory architectures, both Frameworks have been compared using one single node with an increased number of cores. On the other hand, Dispel4py performance on a single node is being tested against several nodes but maintaining the same amount of global cores. This shows the drawback suffered when splitting working cores into several distributed nodes. Each testing node contains two 18-core Xeon "Broadwell" processors and have 256 GiB memory. The compute nodes are all linked using a low latency, high bandwidth FDR Infiniband network.

Results

Figure 1 shows the compared performance of Dispel4py and GrPPI implementations on a single node with an increasing number of cores. The results show that for short number of cores the C++/GRPPI implementation is performing way better than the Python/Dispel4Py implementation. However, as the number of cores increase, the GrPPI performance decrease until it matches or it is slightly surpassed by the Dispel4Py version (which performance is constantly Increasing). This is due to the different treatment of the data. While GRPPI use a single copy of each trace that is shared for all computing stages, Dispel4Py perform a copy of the trace data for each stage. This drags the Dyspel4Py performance down when working on the same NUMA node. But when the number of cores increases, GrPPI starts getting worse because of the need to works on the memory of a different NUMA node than the working core. Figure 2 shows that performance using the same number of cores doesn't vary when using up to 4 nodes. That means that the low data size transfer and the network speed make a case of computation bottleneck rather than the opposite.

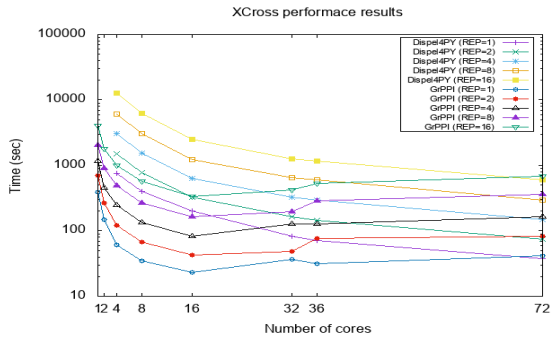

Figure 1 – Performance comparison (Dispel4Py/GrPPI).

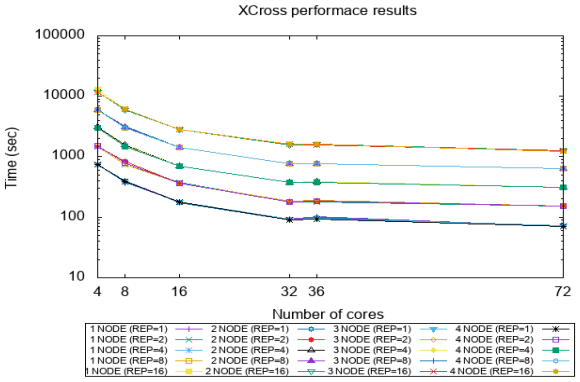

Figure 2 – Performance using Dispel4Py (MPI) up to 4 nodes.

Conclusions

The results shows that, in order to improve performance, data inside the NUMA node should be shared among the computing stages instead of copied. While among NUMA nodes (or actual nodes), data should be copied instead.

References

[1] Filguiera, Rosa, et al. Dispel4py: The International Journal of High Performance Computing App., 31(4):316–334, 2017. [2] del Rio Astorga, D, et al. Concurrency Computat: Pract Exper. 29(4): e4175, 2017.

Acknowledgements

The work has been performed under the Project HPC-EUROPA3 (INFRAIA-2016-1-730897), with the support of the EC Research Innovation Action under the H2020 Programme; in particular, the author gratefully acknowledges the support of Rosa Filgueira Vicente and the computer resources and technical support provided by EPCC.

HPC JAVA PROGRAMMING WITH THE PCJ JAVA LIBRARY

Ł. Górski

Interdisciplinary Centre for Mathematical and Computational Modelling, University of Warsaw, Poland

Introduction

PCJ library [1] is a software solution that enables parallel and distributed programming in the PGAS model on a JVM. Its capabilities and ease of use were already acknowledged in HPC community, as the library received an HPC Challenge Benchmark Class II Award for Code Elegance during SC14. PCJ implementations of selected standard HPC Benchmarks, including 1D FFT and RandomAccess, were the basis for the accolade.

The aim of the following study was to perform a deepened analysis of performance of selected PCJ codes to identify areas for further improvement (both in codes and the library itself). The tests were performed using, inter alia, FFT and RandomAccess benchmarks. Additionally, PCJ implementation of differential evolution algorithm was employed, which was previously implemented to support research in the area of biophysics (for the development nematode's C. Elegans connectome model [2]).

Methods

HLRS's HazelHen was used for benchmarking. It is a Cray XC40 supercomputer system consisting of 7712 compute nodes, each equipped with two Intel Xeon E5-2860 v3 processors, as well as 128 GB of RAM. Thanks to the Java's portability and the fact that the applications were pretested on University of Warsaw Okeanos system, rapid deployment of PCJ applications was possible.

Results

Due to space constraints only, selected results will be presented and briefly discussed. Figure 1 shows the performance achieved by the PCJ library for FFT. Good scaling was achieved up to ca. 4000 threads.

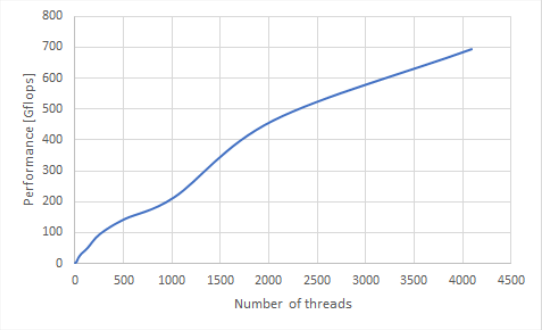

Figure 1 – Performance achieved by PCJ for the calculation of 1-D complex FFT of size 2^27 (strong scaling).

In case of evolutionary computation, a scaling close to linear was achieved (Figure 2).

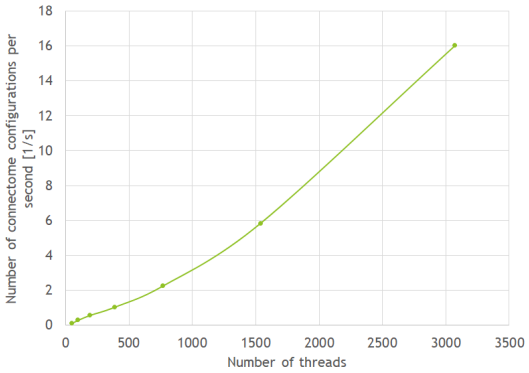

Figure 2 – Number of different configurations of nematode's connectome evaluated per second. The evaluations were performed in a weak scaling regime, with 20 iterations and 5 candidate solutions per thread.

Conclusions

We were able to achieve good scalability results and optimize resource usage on the HPC cluster. However, PCJ library is still lacking in terms of communication performance. The integration with lower-level communications libraries for better-performing communication should be studied for feasibility.

References

[1] M. Nowicki, Ł. Górski, P. Bała PCJ – Java Library for Highly Scalable HPC and Big Data Processing, 2018 International Conference on High Performance Computing & Simulation (HPCS), pp:12-20, 2018. [2] Ł. Górski, F. Rakowski, P. Bała, Parallel differentia evolution in the PGAS programming model implemented with PCJ Java library, International Conference on Parallel Processing and Applied Mathematics (PPAM), pp: 448 – 458, 2015.

Acknowledgements

The work has been performed under the Project HPC-EUROPA3 (INFRAIA-2016-1-730897), with the support of the EC Research Innovation Action under the H2020 Programme; in particular, the author gratefully acknowledges the support of dr. Alexey Chepstov, HLRS and the computer resources and technical support provided by HLRS.

INTEGRATING OMPSS WITH MAGNOLIA

M. Haveraaen[1], X. Martorell[2]

[1]University of Bergen (UiB), Norway; [2]Barcelona Supercomputing Centre (BSC), Spain

Introduction

Given the fast pace by which new and increasingly heterogeneous hardware architectures are introduced, portability of HPC software is becoming a pressing problem. Using standardised APIs to shield hardware-oriented code layers from problem centred code layers is one approach to achieve portability.

In the context of explicit finite difference solvers for PDEs, the discretisation layer can be reduced to a lean API consisting of two families of collective array functions [1]: one family represents the application of an elemental function to all elements of the array, the other represents data permutations. The latter family embodies communication between threads, cores and accelerators. This API can be an effective shield between the hardware architecture (e.g., sequential, multicore or GPU) and the user domain (PDE solvers).

Here we investigate how we can utilise such an API with efficient compilers and libraries for multicore and GPU computing. Specifically, we look at using OmpSs [2], developed at BSC, as backend for such abstractions. For the frontend we are using the Magnolia programming language, developed at UiB. Magnolia has powerful features for investigating and expressing domain abstractions [3], while its configurable compiler generates C++ and Cuda code.

Methods

For the project we have annotated implementations of these collective array functions with OmpSs and OpenMP directives, and used the annotated implementations as backends for the Magnolia compiler. We also developed several high-level implementations of solvers for Burgers' equation in Magnolia. Especially significant are the coordinate-free, the Opt5 and the Opt8 solver versions, which include different optimisations. This gives a combination of 3 solvers with 4 backends (sequential+2 multicore annotations, and Cuda), each with 2 data management schemes. These 24 configurations were tested on various data sizes.

Results

The runtime experiments yield a complex picture regarding efficiency of the different variants on sequential, multicore and GPU architectures. For instance, runtime increases linearly with data size on all CPU variants, while having a highly non-linear increase on the GPU. Figure 1 illustrates surprising behaviour of the memory management optimisation for one set of multicore annotations: the OmpSs annotation gains efficiency while OpenMP loses significantly. On the GPU this optimisation gives significant benefits. Analysis shows that multicore parallelism is achieved by all relevant backends for all solver variants, and that the degree of cache misses in general is low. The compiled code seems to give an unexpectedly low CPU utilisation.

Figure 1 – Profile of Opt5 running on 6 threads, with OmpSs (rows 1&2) and OpenMP (rows 3&4) annotations, using unmanaged (row 1&3) and explicitly managed (row 2&4) memory.

Conclusions

The project confirms that a carefully selected API can function as an effective shield between the user level code and the hardware architecture, thus significantly increasing portability of code.

The observed CPU underutilisation spawns the question: are there further opportunities for rearranging the code towards higher efficiency?

The solution may lie in using more integrated collective array operations, thus moving away from the lean API investigated in this project.

References

[1] Eva Burrows, Helmer André Friis, Magne Haveraaen: An array API for finite difference methods. ARRAY@PLDI 2018: 59-66. http://doi.acm.org/10.1145/3219753.3219761. [2] Alejandro Duran, Eduard Ayguadé, Rosa M. Badia, Jesús Labarta, Luis Martinell, Xavier Martorell, Judit Planas: Ompss: a Proposal for Programming Heterogeneous Multi-Core Architectures. Parallel Processing Letters 21(2): 173-193 (2011). https://doi.org/10.1142/S0129626411000151. [3] Magne Haveraaen: Domain Engineering the Magnolia Way. Er s h o v I n f o rma t i c s Co n f e r e n c e 2 0 1 7 : 1 9 6 - 2 1 0 . https://doi.org/10.1007/978-3-319-74313-4_15.

Acknowledgements

The work has been performed under the Project HPC-EUROPA3 (INFRAIA-2016-1-730897), with the support of the EC Research Innovation Action under the H2020 Programme; in particular, the first author gratefully acknowledges the support of Barcelona Supercomputing Centre and the computer resources and technical support provided by BSC.

WORKFLOW FOR SCIENTIFIC DATA VISUALIZATION USING HPC CLUSTER

M. Hrabánková

IT4Innovations, VŠB – Technical University of Ostrava, Czech Republic

Introduction

Visualization of scientific data can be a time demanding task and the graphical result should be of a high quality. One of the tools for 3D graphics creation and visualization is called Blender and the aim of this project was to design a workflow for parallel loading and processing of scientific data using modules in Blender Node editor. With this approach it is possible to achieve a high quality result and shorten the time needed for computation as much as possible.

Methods

Current modules for scientific data processing in Blender are using a COVISE application, which works with one aggregated dataset and process it sequentially. This is time and memory

demanding especially in case of large datasets. To accelerate the overall data processing up to visualization it is necessary to work with decomposed data.

The COVISE application was not designed to work with decomposed data, thus the solution was to use a successor of this application, which is called Vistle. The modules in Vistle can reuse a domain decomposition used during simulation. Each module is a parallel MPI program that uses OpenMP within nodes and whole workflow can be distributed across several computational nodes.

The solution of Vistle and Blender integration was designed in the way that both applications can run on an HPC cluster, thus the data processing and the consecutive rendering can be computed in parallel. Vistle runs as a separate application and Blender connects to it via TCP connection and the setting of modules parameters is done using python interface of Vistle. After the modules and pipeline is set, Vistle will read and parallely process the data. The last module will create a new TCP connection to Blender and send final data for further processing in Blender. Modified version of Blender Cycles renderer, which is called CyclesPhi and is a part of development at IT4Innovations, can be used for parallel rendering on a cluster.

Implementation for Blender will be written as a plugin and a user interface for setting the modules parameters will be done in Blender nodes editor as it was previously designed for Blender COVISE nodes.

Results

data in further processing was tested on data in OpenFoam format, which were divided into 6 domains. The data were at first read in Vistle and then the streamlines were computed. The result of computation is in Figure 1.

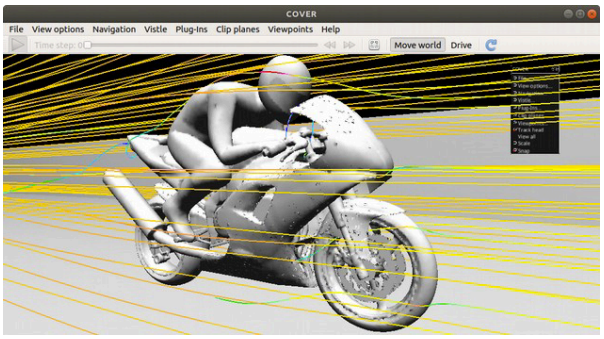

Figure 1 – Result of computation in Vistle.

The time measurement was performed on visualization cluster in HLRS with different number of computational nodes, from 1 to 6. The measured times are in the Table 1 and Figure 2.

Number of nodes	1	2	3	4	5	6
Time(s)	36.9	18.5	12.9	12.5	12.4	6.47

Table 1 – Result of time measurement.

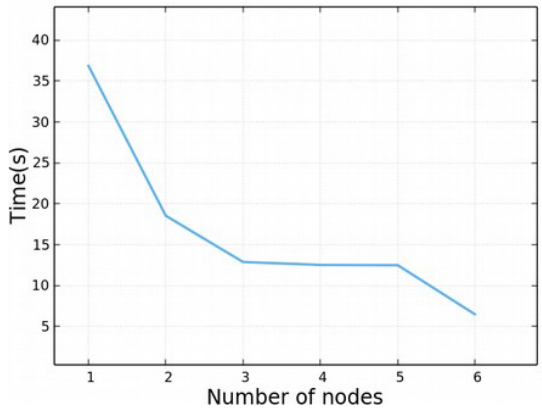

Figure 2 – Result of time measurement.

Conclusions

The designed solution of Vistle and Blender integration will allow to run the processing and then rendering of data in parallel on an HPC cluster, which was the goal of this project. The values measured during the testing in Vistle show that the processing time improves, when more computational nodes are used, and the time is dependent on the decomposition of input data.

References

[1] Vistle website, https://vistle.io/index.html. [2] Blender website, https://www.blender.org

Acknowledgements

The work has been performed under the Project HPC-EUROPA3 (INFRAIA-2016-1-730897), with the support of the EC Research Innovation Action under the H2020 Programme; in particular, the author gratefully acknowledges the support of Uwe Wössner and Martin Aumüller from the visualization department and the computer resources and technical support provided by HLRS.

GENERATING EFFICIENT FFT CODE FOR GPU FROM PATTERN-BASED ABSTRACTIONS

B. Köpcke[1], M. Steuwer[2]

[1]University of Münster, Germany; [2]University of Glasgow, United Kingdom

Introduction

The Fast Fourier Transform is a well-known algorithm used in many high-performance applications, ranging from signal and image processing to more recent usage in convolutional neural networks. Traditionally FFTs were implemented in high-performance libraries such as FFTW. As there are many possible implementations of FFTs, each with their own trade-offs and performance characteristics, it is challenging to provide an optimal implementation for each input size and target device, i.e. there is no performance portability. Additionally, some modern devices support specialized hardware for small matrix-multiplications which can be used to compute FFTs even faster. Targeting this hardware breaks portability in general. This is why we investigate the automatic generation of fast implementations of FFT on GPUs starting from a functional high-level pattern-based abstraction which only describes what to compute and not how to compute something.

Methods

Fast Fourier Transforms (FFTs) are fast implementations of the Discrete Fourier Transform (DFT). The DFT is computed as a complex-valued product of the square DFT matrix and a vector. The general idea of FFT is to decompose the DFT matrix into a product of multiple matrices. These matrices are sparse and the non-zero values appear in regular patterns. This allows for efficient multiplication implementations. Combining these efficient implementations leads to a significant reduction of computational complexity in comparison to the implementation of a general matrix-vector multiplication.

Manually-optimized FFT implementations for accelerators, such as GPUs, are usually written using low-level programming approaches like OpenCL or CUDA. In order to achieve high performance, expert knowledge of the hardware architecture and of the mathematical properties of FFTs is required to best exploit the hardware. Unfortunately, FFT implementations optimized for one hardware device often deliver poor performance when executed on other devices the code has not been tuned for. This is because hardware architectures vary significantly across accelerator types and even generations. This shows that low-level programming approaches are not performance portable.

To enable performance portable programming, the Lift compiler [1] has been developed to generate efficient code for different hardware architectures. A high-level program is composed of patterns with formally defined semantics. A program is rewritten in order to introduce hardware-specific optimizations such as the use of parallelism, by applying semantics preserving rewrite rules. In order to use Lift in the context of FFTs we are looking at how to express this class of algorithms using the existing patterns in Lift while maintaining a close connection between the Lift programs and mathematical notations that describe the matrix-vector operations that make up different FFT algorithms.

Results

During this research visit, we developed abstractions of operators that closely resemble the mathematical notations used by domain expert. We combined these abstractions to express full FFT algorithms and generate OpenCL code. Figure 1 shows our experimental results for two different FFT algorithms (i.e., Stockham and Cooley-Tukey) with different optimizations in comparison to two highly-tuned reference library implementations. The library cuFFT is CUDA-based and clFFT is OpenCL-based. We note that we achieve significantly lower runtimes than clFFT on the Nvidia GPU but that on the AMD GPU our fastest version is still slower than clFFT. We published our findings in detail in our paper “Generating Efficient FFT GPU Code with Lift” which will be presented at the International Workshop on Functional High-Performance and Numerical Computing in August of 2019. In addition, these results have been presented at the 12th International Symposium on High-Level Parallel Programming Applications.

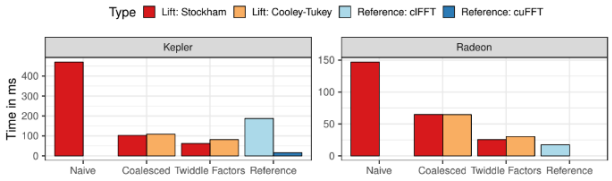

Figure 1 – Performance results comparing Lift generated FFT code with reference libraries.

Conclusions

Our experimental results show that it is possible to generate efficient FFT code from high-level abstractions that closely resemble mathematical notations. They also show that there is still room for performance improvements, e.g., through the use of specialized hardware. We will continue to focus on the application of Lift in HPC in the future. Our work represents the continuation of a long-lasting successful collaboration between the Universities of Glasgow and Edinburgh and the University of Münster under the Lift project. We, the visitor and the host of this HPC-Europa3 collaboration, are actively continuing our collaboration and will keep doing so in the future.

References

[1] Hagedorn B et al, High Performance Stencil Code Generation with Lift, Proceedings of the 2018 International Symposium on Code Generation and Optimization:100-112, 2018.

Acknowledgements

The work has been performed under the Project HPC-EUROPA3 (INFRAIA-2016-1-730897), with the support of the EC Research Innovation Action under the H2020 Programme; in particular, the author gratefully acknowledges the support of Michel Steuwer (University of Glasgow) and the computer resources and technical support provided by EPCC.

IMPROVING PERFORMANCE OF MUTATION TESTING IN LARGE HPC SYSTEMS

A. Núñez

Departamento Sistemas Informáticos y Computación Universidad Complutense de Madrid, Spain

Introduction

Mutation testing [1] is a valuable technique to analyse the suitability of a test suite. Basically, this technique focuses on introducing syntactic changes in the source code of a program by generating different versions of it, each containing a fault. These faulty programs are called mutants. The idea is that if a test suite is able to distinguish between a program and the generated mutants, it should be good at detecting "real" faulty implementations. Hence, mutation testing can be applied to determine the effectiveness of a test suite and helps during the testing stage.

One of the main challenges of mutation testing is the long execution time required to completely execute the testing process. First, testing non-trivial applications requires generating a vast number of mutants. Second, the required test suite to properly test these applications usually consists of a large number of test cases. It is important to remark that, although mutation testing is considered as a valuable testing technique, it has not been adopted by the industry due to the high computational cost necessary to test complex applications.

In order to mitigate these issues, we developed an approach focused on reducing the computational cost associated with mutation testing and hence, obtaining the results in a reasonable time period. The main goal is to use HPC techniques for parallelizing the mutation testing process and, therefore, exploiting the computing resources of the system to increase the overall performance. This contribution, called EMINENT, is a scalable, dynamic, and HPC-oriented algorithm based on embarrassingly parallel computation ideas. EMINENT has been implemented using C and MPI.

Proposal

This work focuses on alleviating the overhead generated in the inter-process communication during the execution of the mutation testing process using EMINENT [2]. In this process, high amounts of data are sent between processes through the communication network, like the source test cases and additional files containing information of the test (e.g. a matrix stored in disk). The main objectives of this work are following listed:

1.- Analysing the scalability and performance of EMINENT in large HPC systems focusing on the interprocess communications.

2.- Analysing the obtained metrics for locating existent bottlenecks in the communication system.

3.- Proposing strategies to alleviate the located drawbacks.

Results

The progress achieved during my research stay can be summarized in three points.

a) The scalability and performance of EMINENT has been studied in a large HPC system – called Cirrus - using 2 different applications: the bzip compressor and an image filtering application. The main objective is to measure the ratio between the obtained performance and the physical resources used in the experiment. In essence, we observe how the performance varies when the number of physical machines, where EMINET is executed, is increased. The maximum number of processes used in these experiments is 1024.

b) The obtained results in the previous experiments allowed us to discover two main bottlenecks. Since the general scheme of EMINET uses a single process to distribute the workload among the rest of the processes, it presents a serious bottleneck. Moreover, the compilation phase also causes an important drop in the EMINENT performance. In the current version of EMINET, the master process is in charge of compiling all the mutants and, therefore, it requires a high computational cost.

c) After a careful analysis of the discovered bottlenecks, 2 main alternatives have been designed. First, the schema of EMINET has been improved to alleviate the first bottleneck. In this case, different processes – called coordinators - will be in charge of distributing the workload among the rest of the processes and receiving the results. Additionally, we plan to parallelize the compilation phase by using all the processes to compile the mutants.

References

[[1] DeMillo, R.A, Lipton, R.J and Sayward, F.G. Hints on test data selection: help for the practicing programmer. IEEE Comput. 11 (4), 34–41, 1978. [2] Canñizares, P. C, Merayo, M. G and Núñez, A. "EMINENT: EMbarrassINgly parallEl mutatioN Testing," in International Conference on Computational Science, ICCS'16, pp. 63–73, 2016.

Acknowledgements

The work has been performed under the Project HPC-EUROPA3 (INFRAIA-2016-1-730897), with the support of the EC Research Innovation Action under the H2020 Programme; in particular, the author gratefully acknowledges the support of David Henty and the computer resources and technical support provided by EPCC, The University of Edinburgh.

PERMONSVM – THE SVM IMPLEMENTATION ON TOP OF PETSC

M. Pecha

VŠB-Technical University of Ostrava, Czech Republic

Introduction

Support Vector Machines (SVMs) belong to the conventional machine learning (ML) techniques, and they are practically used for both classifications and regressions. Despite the fact that deep learning (DL) is getting popular in recent years, SVMs are still applicable for particular tasks in various scientific areas including bioinformatics, geosciences, and image analysis. Unlike the DL underlying architecture, SVMs could be considered as the single perceptron problems that find the learning functions that maximise the geometric margins. Therefore, we can simply explain the qualities of a learning model and the underlying solver behaviour.

Researchers not only in ML community can meet with various SVM implementations designed for running on shared memory systems, accelerators, e.g. graphics cards or XeonPhis, that employ heuristic-based QP-SVM solvers. However, an efficient HPC solution does not exist. The PermonSVM package provides a scalable parallel solution of the linear C-penalized SVMs for the bias and no-bias classification types. It is written on the top of the PETSc framework and utilizes PermonQP package to solve the dual SVM formulation.

Methods

Unlike the commonly used heuristic-based QP-SVM solvers such as stochastic coordinates descent, sequential minimal optimisation in the SVM frameworks, PermonSVM solves the resulting QP problem employing MPRPGP (Modified Proportioning with Reduced Gradient Projection) implemented in PermonQP. Essentially, the MPRGP is an active-set method for solving the QP problems with bound or box constraints; such types of QP problems arising from no-bias SVM classifications. The basic version can be considered as a modification of the Polyak algorithm. The MPRGP combines the proportioning algorithm with the gradient projections. Alternatively, one can use suitable Tao solver for bound or box QP problems.

In the case of the bias-classifications, the optimality conditions are extended by the linear constraint. For taking care of this type of constraint, the SMALXE algorithm is exploited, and the inner box or bound constrained problem is solved by the MPRGP algorithm or convenient Tao solver.

Results

We benchmark PermonSVM on publicly available datasets downloaded from LIBSVM webpages. The largest problem successfully solved was dataset related to suspicious URL prediction with more than 2 million examples and over 3 million features.

Attained accuracy was 99.09% computed on 120 cores in 30 seconds. Graph demonstrated that strong scalability is illustrated in Figure 1.

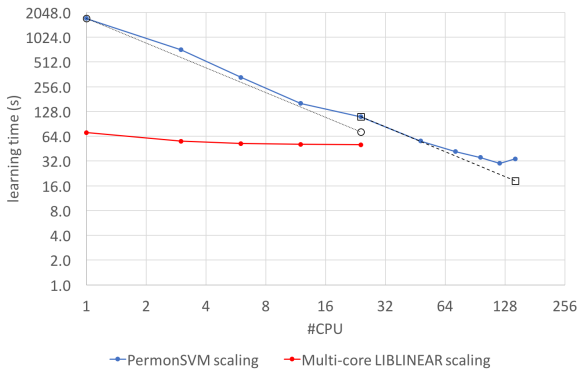

Figure 1 – URL dataset, strong scalability.

Conclusions

We have demonstrated the viability of the PermonSVM package and, moreover, our work was awarded as the best paper [1] at the AETA 2018 conference. Therefore, in the coming years, we would like to focus on developing and optimising underlying QP solvers for non-linear (kernelised) SVMs, and multiclass/multilabel approaches (One vs One, One Vs Rest, Crammer & Singer) for problems contain hundreds of classes or labels. Further objectives will be adding nu-SVM and p-SVM formulations, and general lp-SVM, developing robust hyperparameter optimisation techniques, namely random search, Bayesian optimisation, and model calibration techniques such as logistic or isotonic regression on top of the classification model.

References

[1] Pecha M. et al., Analysing l1-loss and l2-loss Support Vector Machines Implemented in PERMON Toolbox, Lecture Notes in Electrical Engineering. (In print). [2] Dostál Z. et al., Minimizing Quadratic Functions Subject to Bound Constraints with the Rate of Convergence and Finite Termination, Computational Optimization and Applications, 30:23-43, 2015.

Acknowledgements

The work has been performed under the Project HPC-EUROPA3 (INFRAIA-2016-1-730897), with the support of the EC Research Innovation Action under the H2020 Programme; in particular, the author gratefully acknowledges the support of School of Mathematics, University of Edinburgh, and the computer resources and technical support provided by EPCC.

ADVERSARIAL RISK ANALYSIS FOR OBFUSCATION ATTACKS

A. Redondo, J. Brynielsson

ICMAT-CSIC, FOI-KTH

Introduction

Obfuscation techniques are used by attackers to create malware hard to detect, these techniques have two main forms: metamorphism and polymorphism [1]. Polymorphism methods changes the binary code maintaining one of the parts intact in each new copy. Anti-malware tools used to find the unchanged part to detect it. Metamorphism methods used to be more advance obfuscating the code making substitutions, transportations, dead code insertion or register renaming. The method creates a different malware copy making it difficult for anti-malware tools to detect it, disinfect or quarantine due to the binary signature will be different in each iteration.

Methods

We propose a framework based on hybrid analysis which combine static and dynamic features extraction from the binaries perceiving their behaviour. The framework combines the extraction of static features such as operation codes, registers, API calls, entropy, files read, written, deleted, copied, moved, recreated, opened, length of file operations among others [2] and the extraction of dynamic features executing malware in a controlled environment Cuckoo Sandbox [3]. Once we have extracted the malware features, we use Naïve Bayes (NB), Random Forest (RF) and Gradient Boosting (XG) algorithms to classify the malware. We simulated large scale malware files provided by VirusTotal [4] collected from 2017 and 2018. We obfuscate around 16000 files from 2017 and 12000 from 2018 through metamorphic engine metame [5]. We extracted the most frequent features that change before and after the obfuscation process.

Results

We made 1000 experiments using 1075 features extracted from binaries, obtaining 51% mean accuracy from NB, RF and XG. Then, we simulated 1000 experiments using the 32 most frequent features which used to change during obfuscation process through metame, see Figure 1. We note that the accuracy increases 13% with NB, 36% RF and 46% XG.

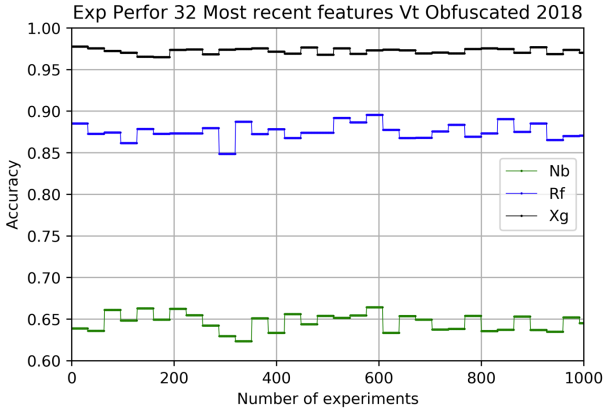

Figure 1 – Accuracy NB, RF and XG in 1000 experiments.

Conclusions

We simulated a large-scale malware obfuscated files extracting the features used to change when the malware is obfuscated through metame. We note that using these extracted features the ML algorithms Näive Bayes, Random Forest and Gradient Boosting perform much better increasing the accuracy in 13% with NB, 36% RF and 46% XG. We built a Bayesian Adversarial Risk Analysis model prototype to simulate the attacker behaviour. The model will contribute to progress in the field to test different obfuscation engines and detect malware with higher precision.

References

[1] You, I., & Yim, K. Malware obfuscation techniques: A brief survey. In Broadband, Wireless Computing, Communication and Applications (BWCCA), 297-300, 2010. [2] Baldangombo, U., Jambaljav, N., & Horng, S. J. A static malware detection system using data mining methods, 2010. [3] Cuckoo Sandbox, https://cuckoosandbox.org/, [4] VirusTotal, https://www.virustotal.com/. [5] Metame, https://github.com/aOrtega/metame/.

Acknowledgements

The work has been performed under the Project HPC-EUROPA3 (INFRAIA-2016-1-730897), with the support of the EC Research Innovation Action under the H2020 Programme; in particular, the author gratefully acknowledges the support of Joel Brynielsson from Department of Theoretical Computer Science, the computer resources and technical support provided by KTH-PDC and Virus Total to provide the corresponding malware files to the study.

EXPLOITING DEEP HYBRIDDATA CLOUD SERVICES USING DISPEL4PY

D. Rodríguez González

Instituto de Física de Cantabria (IFCA - CSIC), Santander, Spain

Introduction

Interest in deep learning has spread rapidly in the last few years due to the spectacular successes achieved in some applications. In consequence the availability of machine learning algorithms, frameworks and libraries is growing [1]. However, deep learning also requires considerable computing resources (often provided by GPUs) and expertise.

The H2020 project DEEP Hybrid DataCloud (DEEP from now on) aims to support intensive computing techniques that require specialized HPC hardware, like GPUs or low-latency interconnects, to explore very large datasets. A Hybrid Cloud approach enables the access to such resources that are not easily reachable by the researchers at the scale needed in the current EU e-infrastructure.

On the other hand, at the University of Edinburgh extensive work has been done on data intensive computing, and in particular in dispel4py [2], a parallel stream-based dataflow framework for formulating and executing data-intensive methods. It is based on a simple and abstract model of the logic required (DISPEL). Dispel4py is a Python implementation of the DISPEL language that not only constructs and describes abstract workflows, but encapsulates executables as Python objects. The model comprises nodes, called Processing Elements (PEs) connected through data streams.

One of interesting features of dispel4py is that it allows users to construct abstract workflows with no knowledge of the underlying execution infrastructure. This allows workflows to be portable across different computing platforms, and thus users can focus on their workflows design, i.e. describing actions, input and output stream and their connections.

The objective of the project was to integrate DEEP services in Dispel4py workflows.

Methods

We analysed the dispel4py framework, and worked on possible extensions in collaboration with Dr Rosa Filgueira and Dr Javier Fernández Muñoz.

We selected two of the existing DEEP services examples in order to test the integration possibilities, namely the speech recognition (https://marketplace.deep-hybrid-datacloud.eu/modules/speech-keywords-classifier.html) and the dog breed classifier (https://marketplace.deep-hybrid-datacloud.eu/modules/dogs-breed-detector.html).

Due to the restrictions in the environment, and the practicality of it, we only implemented the deep neural networks inference, and no the training in those workflows. The network models were generated at IFCA and then transferred to Cirrus for their use by the workflows.

Once deployed, DEEP services can be accessed through a REST interface, using which we integrated the inference service in the dispel4py workflows.

Finally, we developed a new deep neural network model to be deployed as a DEEP Service and executed using a dispel4py workflow. The model is used to segment brain tumours (gliomas) using the BRATS 2018 challenge dataset [3].

We implemented the training in Python using the Keras library, the architecture used was based on U-net [4]. For reading and manipulating the imaging data we used the NiBabel library. The development and testing was done in Cirrus at the EPCC.

Results

Integrated the two pre-existing DEEP services in dispel4py workflows.

A prototype extension of dispel4py that uses ZeorMQ as communications library.

A new example deep learning application that in the future could be implemented in DEEP using dispel4py for running the workflow was developed.

Conclusions

We showed the feasibility of integrating the DEEP services in a dispel4py workshop. In order to ease this it would be convenient to develop a library that would hide the DEEP services details (REST interface) from the potential user.

References

[1] Nguyen, G. et al., Artif Intell Rev, 52(1):77-124, 2019. [2] Filgueira R et al., Int. J. High Perform. Comput. Appl., 31(4):316-334, 2017. [3] Menze, B et al., IEEE Trans Med Imaging, 34(10):1993-2024, 2015. [4] Ronneberger, O. at al, MICCAI, LNCS, 9351, 234-241, 2015.

Acknowledgements

The work has been performed under the Project HPC-EUROPA3 (INFRAIA-2016-1-730897), with the support of the EC Research Innovation Action under the H2020 Programme; in particular, the author gratefully acknowledges the support of Dr Rosa Filgueira, EPCC, University of Edinburgh and the computer resources and technical support provided by EPCC.

HITCTRLBLAS: A PERFORMANCE-PORTABLE HETEROGENEOUS BLAS LIBRARY BASED ON THE CONTROLLERS FRAMEWORK

E. Rodriguez-Gutiez[1], A. Moreton-Fernandez[2], A. Gonzalez-Escribano[2], D.R. Llanos[1]

[1]University of Valladolid, Valladolid, Spain

Introduction

BLAS libraries contain a set of linear algebra routines designed for reusability and performance. They are essential in many scientific computing fields [1], a key client for HPC resources. For this reason, several vendors have designed their own BLAS versions. These versions take into account architecture-specific details of their products to better improve performance. Examples of specific libraries include cuBLAS (for CUDA-enabled Nvidia GPUS) and MKL (for Intel products such as Xeon or Xeon Phi devices). Other entities such as research groups have presented their own alternatives as well, like MAGMA.

However, there are several issues associated with many of the solutions introduced. First, the BLAS interface is standardized [2], but implementations show API differences in practice, particularly in heterogeneous environments. This affects code reusability and portability. Second, although several of these BLAS variants for heterogeneous devices offer interfaces that try to hide data transfers, their reusability on coprocessors is poor in most cases. Thus, obtaining good performance in highly heterogeneous systems still requires using several lower-level interfaces from multiple vendors in the same code, which requires higher development effort.

In order to solve the issues presented above, we design and implement a performance-portable BLAS library. It is based on the Controllers [3] parallel programming framework. This framework allows programmers to tag kernel functions with a set of characteristics, like their name, the target processor family (e.g. CUDA, Xeon Phi), architecture they are tuned for, etc. Several functions can be tagged with the same name but different target architectures, thus defining a set of kernels with the same functionality but each one written using different language flavors (CUDA, LEO for Xeon Phi, plain C) and tuned for specific coprocessors, or CPU cores. When a user asks the library to launch a kernel by using its name, the framework looks among those defined for the most appropriate one for the target. It is also possible to define generic kernels that can be executed on any platform.

Methods

We propose a solution to the problem of BLAS libraries portability across heterogeneous devices. Our proposal implies an extension of the controllers framework, by including new kernel type tags. This solution also features a new library of wrappers using the extended kernel types. We use an incremental prototype methodology to implement solutions to the technical problems into the framework. We use an experimental method based on case studies to validate the approach. The cases are selected to be representative of different problem classes and computation vs transfer time scenarios.

Some of the test cases implemented include *GEMVER (a BLAS 2.5 primitive), an iterative Matrix multiplication, and the Sobel operator. These examples were selected to test data reusability, overlapping between communication and computation, transfer times, and the ability to mix calls to low level kernels written by the user with calls to kernels from our new library.

Experiments are executed on Titan Black, Knights Landing and Knights Corner Xeon Phi platforms.

Results

The codes within our solution are fully portable across the selected devices. They show some overhead due to the abstractions introduced for kernel management. This overhead decreases with input size, ranging from 8% to 3.5% on GPUs, and from 25% to 4% on Xeon Phis.

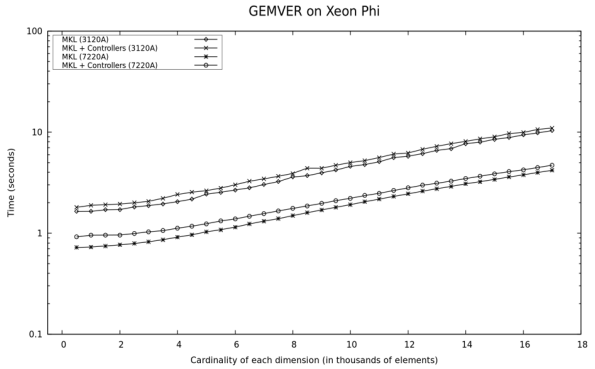

Figure 1 – Execution time comparison for Xeon Phi devices between a reference code and one using our solution.

Conclusions

We design and implement a portable BLAS library tool that provides a common interface for multiple lower level libraries targeting diverse heterogeneous platforms. Data transfers are transparently managed with low performance overhead. Results show that the new abstractions introduce low overhead, and provide performance portability.

References

[1] Blackford L. S. et al., ACM Transactions on Mathematical Software, 28(2):135-151, 2002. [2] Dongarra J et al., The International Journal of High Performance Computing Applications, 16(2):115, 2002. [3] Moreton–Fernandez A. et al., The International Journal of High Performance Computing Applications, p. 1094342017702962, 2017.

Acknowledgements

The work has been performed under the Project HPC-EUROPA3 (INFRAIA-2016-1-730897), with the support of the EC Research Innovation Action under the H2020 Programme; in particular, the author gratefully acknowledges the support of Dr. Christophe Dubach, the School of Informatics of the University of Edinburgh, and the computer resources and technical support provided by EPCC.

TIME SERIES COLLABORATIVE EXECUTION ON CPU+GPU CHIPS

J.C. Romero[1], Á. Navarro[1], A. Rodríguez [1], R. Asenjo[1], M. Cole[2]

[1]University of Málaga, Spain; [2]University of Edinburgh, United Kingdom

Introduction

Time series motif (similarities) and discords discovery is one of the most important and challenging problems nowadays for time series analytics. We used an algorithm called "scrimp" that excels in collecting the relevant information of time series. Starting from the sequential algorithm we developed different parallel alternatives: dynamic distribution using Intel TBB, static distribution using C++11 threads and a heterogeneous ParallelFor Template for CPU+GPU using Intel TBB for CPU and OpenCL for GPU.

Methods

We have used the scrimp [1] algorithm to find motifs and discords in time series. The input data (the time series values) is divided into subsequences that should be compared with all the remaining subsequences of the time series, following a sliding window approach. The subsequence to subsequence comparison is based on a z-normalized Euclidean distance (Equation 1). This distance represents the similarity between the two subsequences we are comparing. The output of the algorithm is another time series called "Matrix Profile" which, for each subsequence, stores the minimum distance to all the other subsequences and the index of the subsequence that resulted in this minimum distance.

$$d(\hat{x},\hat{y}) = \sqrt{2 \cdot m \cdot \left(1 - \frac{\sum_{i=1}^{m}(x_i \cdot y_i) - (m \cdot \mu_x \cdot \mu_y)}{m \cdot \sigma_x \cdot \sigma_y}\right)}$$

Equation 1 Distance between two subsequences

Because we compare each subsequence with all other ones, the computation space can be seen as an upper triangular matrix where the all-to-all distances are stored. A careful analysis of the computations implied by Equation 1 results in a parallel implementation that concurrently traverses the diagonals of the matrix. So, the parallelization of the algorithm is based on dispatching the diagonals to the available threads. The resulting workload is unbalanced because every diagonal has different size. Getting a balanced distribution of the diagonals is therefore a must. To that end, we have proposed three different distribution strategies for the scrimp algorithm: Dynamic, Static and Heterogeneous.

Dynamic: Based on the tbb::parallel_for algorithm from Intel TBB we let the work-stealing scheduler to dynamically assign the diagonals to the worker threads (one per core).

Static: Assuming each element of the matrix will be computed in the same amount of time for any core, we came up with an equation that yields N sets of diagonals. Each set will have approximately the same number of matrix elements. With this equation, and setting N equal to the number of cores, we compute a static distribution of the diagonals.

Heterogeneous: We also implemented a heterogeneous distribution of the workload using a scheduler previously developed in our group [2]. The scheduler dynamically dispatches the diagonals to the GPU and the CPU in order to exploit both devices at the same time.

Results

In our summer stay we used ARCHER (at EPCC) in order to assess the dynamic and static distributions. ARCHER only features CPU cores, so heterogeneous results are not provided here. Figure 1 shows the speedup of the Dynamic and Static distribution for different time series sizes.

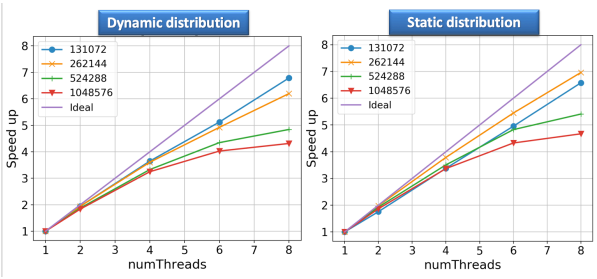

Figure 1 – Dynamic vs Static distribution.

The static distribution ends up scaling slightly better than the dynamic one. This is because the static scheduler exhibits less scheduling overhead and exploits the cache better due to larger blocks of diagonals.

Conclusions

We have implemented three different data distributions for the scrimp algorithm. The static distribution resulted in less overhead and better locality. Afterwards, the heterogeneous implementation was evaluated on a Broadwell heterogeneous chip (CPU+GPU) and this alternative outperformed the homogenous ones.

References

[1] Matrix Profile XI: SCRIMP++: Time Series Motif Discovery at Interactive Speed. Yan Zhu, Chin-Chia Michael Yeh, Zachary Zimmerman, Kaveh Kamgar and Eamonn Keogh, ICDM 2018. [2] Navarro, Angeles, Corbera, Francisco, Rodríguez, A, Vilches, Antonio and Asenjo, Rafael. (2018). Heterogeneous parallel_for Template for CPU–GPU Chips. International Journal of Parallel Programming. 10.1007/s10766-018-0555-0.

Acknowledgements

The work has been performed under the Project HPC-EUROPA3 (INFRAIA-2016-1-730897), with the support of the EC Research Innovation Action under the H2020 Programme; in particular, the author gratefully acknowledges the support of Dr. Murray Cole in the Informatics Forum and the computer resources and technical support provided by EPCC (Edinburgh Parallel Computing Centre, United Kingdom).

MACHINE LEARNING-BASED RESOURCE MANAGER FOR ACCELERATED NEUROSCIENTIFIC WORKLOADS

H. Sidiropoulos[1], *C. Strydis*[2]

[1]*MicroLab National Technical University of Athens, Greece;* [2]*Neuroscience department Erasmus Medical Center Rotterdam, The Netherlands*

Introduction

High-performance computing (HPC) in recent years is used in brain studies through computational models. Simulating neuronal networks on various platforms is an active field of research [1][2]; a major challenge is the sheer computational complexity that many of these neuron models entail. The variety of models commonly used and their complexity, results in a variety of computational workloads [1]. We developed a resource manager that predicts the performance of these workloads depending on the neuronal model and population, the neuroscientist wants to study. With the aid of machine learning algorithms, the resource manager is classifying the model and predicts the simulation time. We studied the performance of our simulator engine [2] on a multi-compartmental Hodgkin Huxley model of part the Inferior Olive, which also modelled Gap Junctions.

Methods

The main computational effort for a simulation run lies in the iterative progression of the model's state, through successive timesteps. In order to generate data for the machine learning training, performance was measured running 1000 simulation steps of the simulation. Tests showed that initialization had an insignificant impact on total run time.) In order to investigate neural structure processing performance, synthetic truncated models were generated for the given compartments/neuron and ion channel gates/compartment parameters. A simulation was run and timed for each combination of the CPU count, neuron population count, net density, compartments per neuron, ion channel gates per neuron parameters specified below:

- Neuron counts considered are: 1000, 2000, 4000, 8000, 16000 neurons.
- Neuron connectivity densities considered are: 0%, 25%, 50%, 100% of total possible synapses.
- Neuron compartment counts considered are: 1, 2, 4, 8, 16 compartments per neuron.
- Compartment gate counts considered are: 1, 2, 4, 8 gates per compartment.

The ML algorithm used were regression algorithms, broken into different zones.

Results

The results show clearly that run time increases quadratically with population size, as a previous analysis of the computational workload would suggest. For an unconnected population, run time was measured to be linear to population size. Analysis of the experimental results showed that the relative effect of additional intra-neuron complexity on run time is an additive factor that is linear on the number of state variables added per cell (compartments and gates per compartment). So, in order to get good prediction with high confidence we broke up our problem in zones where in each zone we created a parameter vector for the regression algorithm. Figure 1 shows the performance of the ML algorithm in such a zone, compared with the real performance of the simulator. The data points are new and not in the training dataset. We clearly see that the prediction is very close to the actual performance.

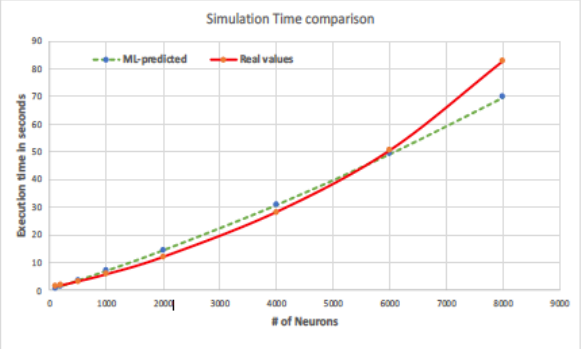

Figure 1 – Comparison between the ML algorithm predicted performance and the actual performance of some simulations.

Conclusions

In this work we studied the performance of our simulator engine on a multi-compartmental Hodgkin Huxley model of part the Inferior Olive, which also modelled Gap Junctions. We developed a machine learning resource manager that depending on the model characteristics predicts the simulation time of the model in different platforms. We broke the performance of the simulator into zones and train regression algorithms into these zones, thus increasing the confidence of the prediction of our resource manager.

References

[1] Georgios Smaragdos, Georgios Chatzikonstantis, Rahul Kukreja, Harry Sidiropoulos, et al. (2016). "BrainFrame: A nodelevel heterogeneous accelerator platform for neuron simulations." http://doi.org/10.1088/1741-2552/aa7fc5. [2] G. Chatzikonstantis, H. Sidiropoulos, et al. "Multinode implementation of an extended Hodgkin–Huxley simulator", Neurocomputing, Volume 329.

Acknowledgements

The work has been performed under the Project HPC-EUROPA3 (INFRAIA-2016-1-730897), with the support of the EC Research Innovation Action under the H2020 Programme; in particular, the author gratefully acknowledges the support of Strydis Christos an Erasmus Medical Center and the computer resources sand technical support provided by SURFsara.

OPTIMIZING THE ALLREDUCE ALGORITHM WHEN EXECUTED ON OVERSUBSCRIBED CPUS IN SHARED-MEMORY NODE CLUSTERS

G. Utrera[1], J.M. Bull[2]

[1]Computer Architecture Department, Universitat Politècnica de Catalunya, Barcelona, Spain; [2]EPCC, The University of Edinburgh, Edinburgh, UK

Introduction

Virtualization is the ability to run several workloads on a single host server, thereby maximizing the utilization of that host server. To accomplish this, physical resources on a host are oversubscribed. Virtualization enables data centres to focus on the needs of business applications, but it can make resource allocation more challenging.

Recently, CPU oversubscription was also used in a strategy to concentrate the idle cycles of unbalanced applications in such a way that one or more CPUs are freed from execution [1]. This strategy applies on MPI parallel applications, iterative and with frequent global synchronizations, which is a common case in HPC applications (i.e. simulations).

A profiling study [2], showed that many HPC applications spend more than 80% of their execution time performing collective operations, thus impacting directly in their scalability. As a result, MPI collectives are of particular interest.

The main objective of this work is to improve the performance of the reduction collective operation when CPUs are oversubscribed with processes from the same parallel application.

Methods

We redesigned the reduction algorithm (MPI_Allreduce) at intra-node level, by adding a new stage in the hierarchical reduction algorithm at each oversubscribed CPU.

In order to exploit the fact that processes attached to the same CPU share all cache levels, we define a memory region to be shared by all those processes. In this way, the reduction operation is first performed locally at each CPU (note that all operations suitable for reduction must be commutative and associative). In addition to this, the calculation is pipelined and processed in parallel by all those processes. After that, local results are combined following the reduction algorithm provided by the current MPI library in use.

The shared memory region was defined using two approaches: 1) using the mmap operating system call; and 2) using the shared memory MPI operations introduced in the MPI-3 standard (MPI_Win).

Results

Experimental results performed on Archer and Cirrus, using a synthetic benchmark (a sequence of MPI_Allreduc operation) are promising. In Figure 1, it can be seen improvements up to 3x over the standard implementation, when oversubscribing up to four processes per CPU, on one node and with message sizes between 8 KB and 1 MB.

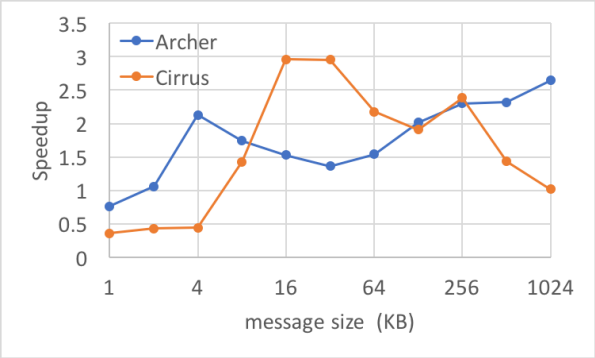

Figure 1 – Ratio of execution time between MPI_Allreduce operation from the native MPI library and the MPI_Allreduce operation from the optimized implementation with 4 MPI processes per CPU, varying the message size (bigger is better).

Conclusions

The performance in collective operations has a great impact in HPC applications. We believe our results may alleviate some drawbacks when CPUs are oversubscribed with processes from the same parallel application with frequent synchronizations.

Scaling the number of nodes would generate better results, as latencies in the inter-node communication give more opportunities for overlapping communication and calculation.

References

[1] Utrera G et al., Journal of Parallel and Distributed Computing, 134: 37-49, 2019.

[2] Chunduri S et al, Proceedings of the International Conference for High Performance Computing, Networking, Storage, and Analysis, SC'18, IEEE: Article 30, 2018.

Acknowledgements

The work has been performed under the Project HPC-EUROPA3 (INFRAIA-2016-1-730897), with the support of the EC Research Innovation Action under the H2020 Programme; in particular, the author gratefully acknowledges the support of Dr. J. Mark Bull and the EPCC and the computer resources and technical support provided by the EPCC.

QM/MM VALIDATION OF KINETIC MODEL FOR PERMEATION THROUGH BACTERIAL PORINS

S. Acosta Gutiérrez

Department of Physics, University of Cagliari, Cagliari, Italy

Introduction

Combining all-atom molecular dynamics simulations with single molecule electrophysiology experiments we reported the first detailed voltage effect on the transport kinetics of a small zwitterionic antibiotic (norfloxacin) through OmpF [1]. Based on these results, we proposed a two-step kinetic model for the transport of polar molecules through the OmpF model pore. The main objective of the visit was to characterize the pore/molecule interaction during the translocation through the narrow constriction region, ultimately representing the bottleneck for transport. By using ab-initio methods we focused on the importance of electrostatic interactions in the transport mechanism through nanopores, elucidating aspects that are treated with a mean-field approach with classical force field, such as the polarization effects and the role of water molecules through bridging pore and molecule via hydrogen bonds.

Methods

Car Parrinello molecular dynamics [2] aims to combine the advantages of two ab initio molecular dynamics methods: it uses the dynamic propagation of electrons of the Ehrenfest molecular dynamics, but at the same time uses a large enough time step from Born Oppenheimer molecular dynamics. This is achieved by using a fictitious mass for the electronic degrees of freedom. Electrons acquire a classical kinetic energy and their dynamics, together with the one of nuclei, can be propagated using the following equations of motion:

$$\mu_{elec}\frac{\partial^2\phi_i(t)}{\partial t^2} = -\frac{\partial}{\partial\phi_i^*}\left(<\psi|\hat{H}_{elec}|\psi> - \sum_{i,j}^{n}\Lambda_{ij}(<\phi_i|\phi_j> - \delta_{ij})\right) \quad (1)$$

$$M_I\frac{\partial^2}{\partial t^2}\vec{R}_I(t) = -\nabla_I\int\partial\vec{r}\psi^*(\{\vec{r}\}_n;t)\,\hat{H}_{elec}\psi(\{\vec{r}\}_n;t) \quad (2)$$

Results

The awarded computer time (25% of the total requested amount) was enough to perform the calculations only for one of the proposed systems and learn to use the software. The selected system was Norfloxacin + OmpF for which the classical study was already completed and published. For the two selected current-blocking states extracted from the fully converged free energy landscape of Norfloxacin translocation through OmpF at low and high-voltage we performed a 50ps QM MM simulation to verify the molecule orientation. In Figure 1 a,d the two selected states are depicted; for each state the ligand and the interacting residues are shown as licorice. The coordinates of norfloxacin and the interacting residues within 3Å from the QMMM calculation are superimposed in onto the MD initial state (Figure 1 b, e) for the two states. The configuration is rather well conserved, for state one (Figure 1b, MD-ES1) the average rmsd of the QMMM coordinates to the initial MD configuration is 0.99 Å ± 0.020 Å, while for MD-ES2 (Figure 1e) the r.m.s.d. is 1.18 Å ± 0.044 Å. In the case of state one (MD-ES1) when the interacting charged residues D113 and R167 are taken into account into the QM region (Figure 1c), the r.m.s.d. is 0.25 Å ± 0.33 Å. If one compares the last snapshot of the QMMM calculation with only norfloxacin in the QM region with the one obtained when the two charged interacting residues are taken as QM (Figure 1f) the r.m.s.d. difference is 1.41 Å.

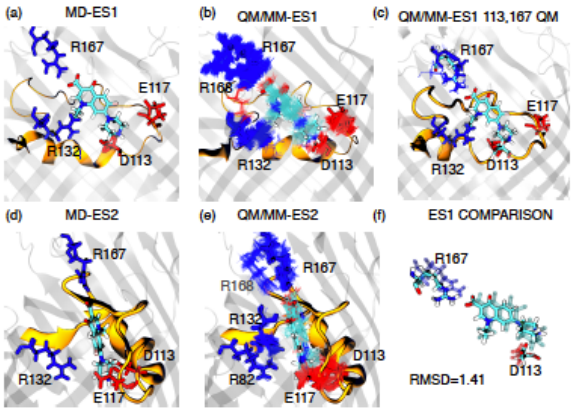

Figure 1 - Cartoon representation of the pore-ligand conformation studied: ES1 and ES2 (current blocking states (1)). Norfloxacin is showed as licorice as well as the charged interacting residues, coloured according to their charge.

Conclusions

Although, not all the proposed configurations were run, we can conclude that the classical force field used in the molecular dynamics simulations and enhanced sampling calculations is accurate enough to describe the system and the captured MD-states are correct. This implies the relative orientation of norfloxacin to the axis of diffusion of the porin is correct and hence the proposed kinetic model in [1]. The proposed model relies in the calculated intrinsic electric field of the porin and its tuning along the axis of diffusion. The confirmation of the molecular probe orientation, validates the calculated intrinsic electric field as well as the water polarization based method behind its calculation.

References

[1] H. Bajaj et al., ACS Nano 11(6), 5465−5473 (2017). [2] R. Car, M. Parrinello, Phys. Rev. Lett. 55, 2471(1985).

Acknowledgements

The work has been performed under the Project HPC-EUROPA3 (INFRAIA-2016-1-730897), with the support of the EC Research Innovation Action under the H2020 Programme; in particular, the author gratefully acknowledges the support of Prof. Carme Rovira from the Departament de Química Inorgànica i Orgànica and Institut de Química Teòrica I Computacional (IQTCUB), Universitat de Barcelona and the computer resources and technical support provided by BSC.

STUDYING GLUCOSE TRANSLOCATION THROUGH THE OMPF WIDE PORE CHANNEL USING MULTIPLE QUANTUM REGIONS WITH QM/MM-MD TECHNIQUES

J. Ainsley[1], J. Torras Costa[2]

[1]Department of Cancer Therapeutics, Institute of Cancer Research, London, United Kingdom; [2]Department of Engineering and Chemistry, Polytechnic University of Catalonia, Barcelona, Spain

Introduction

OmpF is a channel protein found in the membranes of Escherichia coli bacteria, it controls the passive diffusion of ions, metabolites and other small molecules through the bacterial cell membrane.[1] The interactions between the solute molecules and the amino acid residues of the channel wall create a selectivity towards certain ions and solutes based on a range of properties apart from molecular size; properties such as charge, valence, characteristic aqueous solvation and specific short-range interactions.[2] These short range interactions, known to play an important role, are difficult to simulate properly using classical force field approaches.[2] Understanding the basis for the selectivity mechanisms of wide channel proteins is a vital consideration in the development of antibiotic drugs which need to penetrate the membrane.

Methods

The OmpF crystal structure with membrane orientation data was downloaded from the OPM database (code:3pox), the structure was prepared using similar conditions to a previous similar publication. [3-5] A 225ns unbiased MD simulation was used to equilibrate the 284,171 atoms of protein and membrane structures and the 175,653 atoms of solvent and ions. From the MD trajectory, a frame representing the cluster structure was extracted to be used as the starting point for the Umbrella Sampling (US). US at the MM level was then performed, the coordinate for the pulling was defined based on the previous QM/MM-MD US study of OmpF. [3]

81 US windows were created, each underwent 120ps of equilibration and a 10ns production run, glucose was restrained by a 150 kcalmol-1 harmonic potential. The MM US trajectory was analysed using the Weighted Histogram Analysis Method (WHAM) to construct the Potential of Mean Force (PMF) plot. [6] The maz-QM/MM-MD US was performed using Pupil to interface Amber18 and NWChem, using the DFT m06-2x functional with a 6-31G basis for 400 steps of equilibration and 2000 steps of production with a 1fs timestep. [7-9] Glucose was treated as one QM region and the side chain atoms of the five important residues of the selectivity filter region as another separate QM region. The resulting trajectory was also analysed with WHAM to construct a PMF plot.

Results

The PMF profile (figure 1) of the QM/MM-MD simulation reveals a subtler energy landscape navigated by glucose during the translocation process. In the QM/MM-MD simulations we have observed two distinct minima directly before and after the selectivity filter region, whereas in the MM PMF profile no such minima are observed.

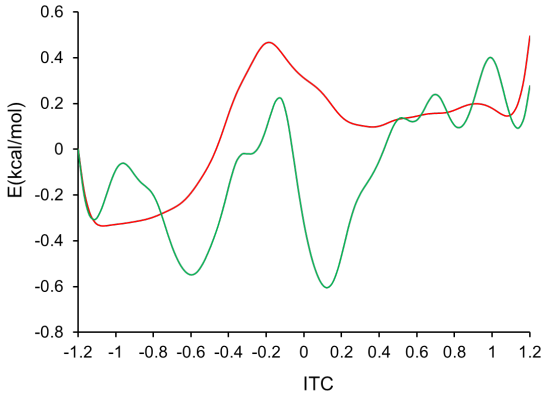

Figure 1 - The PMF profile of the QM/MM-MD umbrella sampling (green), MM umbrella sampling (red).

Conclusions

Both MM and QM/MM profiles predict the translocation process to be isoenergetic (<0.6kcal/mol at 300k), this in consistent with experimental studies of OmpF.[2] As expected, the most significant differences in the PMF plots are seen as glucose passes through the selectivity filter region (-0.6 to 0.2), at this point the two quantum regions glucose and the sidechains of residues R42, R82, R132, D113 and E117 are in the closest proximity This is likely due to the QM treatment of the glucose-protein interactions. An analysis relating to the individual windows structural interactions will follow in a publication.

References

[1] Aguilella, V.M., et al., Int. Biology, 3(3): p.159-172, 2011. [2] Alcaraz, A., et al., Biophys J., 96(1): p.56-66, 2009. [3] Lomize, M.A., et al., Nuc. Acids Res., 40: p.370-376, 2012. [4] Efremov, R.G., J.Struct.Biol. 178: p.311-318, 2012. [5] Ahumada J.C., et al., J. Phys. Chem. B, 123(1): p.86-94, 2018. [6] Grossfield, A., "WHAM: the weighted histogram analysis method, http://membrane.urmc.rochester.edu [7] Torras, J., et al., J. Chem. Comp.,29(10): p.1564-1573, 2008. [8] Case, D., et al., AMBER 18. 2018. [9] Valiev, M., et al., Comp. Phys. Comm., 181(9): p.1477-1489, 2010.

Acknowledgements

The work has been performed under the Project HPC-EUROPA3 (INFRAIA-2016-1-730897), with the support of the EC Research Innovation Action under the H2020 Programme; in particular, the author gratefully acknowledges the support Joan Torras-Costa, Department of Engineering and Chemistry, Polytechnic University of Catalonia, Barcelona, Spain and the computer resources and technical support provided by the BSC.

FREE ENERGY PERTURBATION GUIDED OPTIMIZATION OF ANTIVIRALS TOWARDS CHIKUNGUNYA VIRUS

L. Battini[1,2], D.E. Álvarez[2], M. Bollini[1] and Z. Cournia[3]

[1]Centro de Investigaciones en Bionanociencias, CONICET, Argentina; [2]Instituto de Investigaciones Biotecnológicas, CONICET, Argentina
[3]Biomedical Research Foundation, Academy of Athens, Greece

Introduction

Chikungunya virus is the causing agent of a neglected viral disease that has re-emerged in the last decade. E1 and E2 are the envelope proteins of the virus and are responsible of the virus adsorption and entry into the host cell. E1 and E2 form a heterodimer, three heterodimers form a spike and 80 spikes are arranged with icosahedral symmetry in the viral envelope (Figure 1). With the main objective of developing an inhibitor of chikungunya infection we have performed a virtual screening against the E1-E2 heterodimer and we were able to identified a small molecule that inhibits the early stages of the viral life cycle. Our next goal is to optimize the antiviral activity of the compound. In order to guide the synthesis and biological evaluation of novel derivatives, we propose to use the Free Energy Perturbation (FEP) method, which is a powerful tool in computer aided drug design [1].

Methods

Molecular dynamics (MD) simulations were done in Gromacs [2]. The protein was described using the Amber99SB ILDN forcefield and the organic compounds were parametrized using Antechamber with the GAFF2 force field. The obtained parameters and topologies were converted to Gromacs format using Acpype. The Lenard Jones and Coulomb cut-offs of the real space were set to 10 Å. The long-range electrostatics interactions were treated with PME. The system was solvated with tip3p water and neutralized with the required concentration of Na or Cl ions. The system was minimized with the steepest descent algorithm and thermalized to 310 K. Then, the system was equilibrated for 200 ps in the NVT ensemble and for 1 ns in the NPT ensemble. The production run was done in the NPT ensemble using the v-rescale thermostat with a time constant of 0.1 ps and the Parrinello-Rahman barostat with a 2 ps time constant. The integration step was of 2 fs and all bonds involving H atoms were constrained with the LINCS algorithm. The leap – frog integrator was used.

For the FEP simulations the topologies were prepared using FESetup [3]. For each FEP calculation we used 16 windows of 5 ns of production run. Previously the system was minimized and equilibrated as described above. For FEP calculations we used Langevin dynamics with a time constant of 2 ps and an integration time step of 1 fs. The results were analysed with the gmx bar program within Gromacs using the BAR method.

Results

We first aimed to construct a biologically representative model that considered the interaction between the different E1-E2 heterodimers in the viral spike and had an adequate size (Figure 1 B). We used the rigid body definitions given by Voss and co-workers in 2010 [4]. We selected all the domains or rigid bodies that had an aminoacid as much as 25 Å away of the binding pocket in the atomic model of the viral spike (PDB ID: 3j2w). We obtained a model that remained stable in MD simulations. We restrained the position of the backbone atoms near the artificial ends and in those residues interacting with domains not included in the final model.

We performed FEP calculations of a congeneric series of ligands with known activity. The obtained results are shown in Figure 1 D. The correlation between the experimental and calculated ΔΔG is not good. This may be due to different reasons, but mainly because the experimental ΔΔG difference is not too large. Given that the estimated error of the FEP method is near 1.5 Kcal/mol [1] this means that the difference in activity between the tested compounds is within the error of the method.

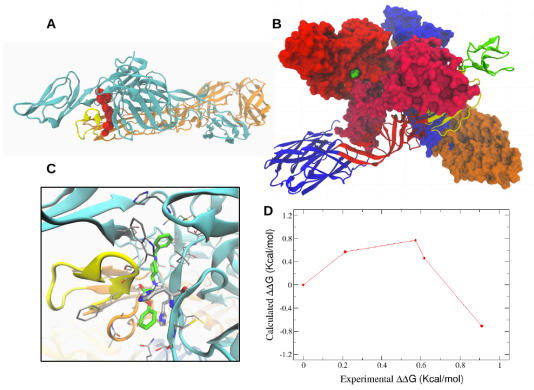

Figure 1 - (A) Representation of the E1-E2 heterodimer. E1 is coloured in orange E2 in cyan and the binding pocket in red. (B) Ectodomains of E1 and E2 in a viral spike. In the background one heterodimer is represented as surface and coloured as in A. In the foreground a heterodimer is coloured according to the rigid bodies defined by Voss and co-workers 4. The reduced model used for FEP calculations is represented as a red surface. (C) representation of the active compound in the MD simulation with the protein receptor. The compound is coloured in green. The modifications were done in the bottom aromatic ring. (D) Relationship between the calculated ΔΔG and the experimental value.

Conclusions

Although results were inconclusive, we could set up an initial system and acquired experience in the FEP method. This was the main goal of the visit, and will enable us to continue with the FEP guided optimization of the chikungunya inhibitors in future work.

References

[1] Cournia Z et al., Journal of chemical information and modeling, 57.12:2911-2937, 2017. [2] Abraham MJ et al., SoftwareX, 1:19-25, 2015. [3] Loeffler HH et al., Journal of chemical information and modeling, 2485-2490, 2015. [4] Voss JE et al., Nature, 468.7324:709, 2010.

Acknowledgements

The work has been performed under the Project HPC-EUROPA3 (INFRAIA-2016-1-730897), with the support of the EC Research Innovation Action under the H2020 Programme; in particular, the author gratefully acknowledges the support of Dr. Zoe Cournia of the Biomedical Research Foundation of the Academy of Athens and the computer resources and technical support provided by GRNET.

UNRAVELLING THE DIMERIZATION CONFORMATIONAL LANDSCAPE OF KRAS ON A MEMBRANE

Z. F. Brotzakis, Z. Cournia

Biomedical Research Foundation, Academy of Athens, Greece

Introduction

Every year, 3.2 million Europeans are diagnosed with cancer, the second most common cause of death in Europe. Among other RAS proteins, KRAS controls cellular proliferation which can be severely dysregulated upon KRAS mutations. It has been shown that KRAS dimerization on membranes participates in the activation of the MEPK pathway [1,2], and that point mutations such as G12D, increase dimer affinity and thus cell proliferation [3]. Yet, there is no available structural model and the respective populations for the dimer interface of KRAS on membranes, thus hampering in structure-based drug design efforts.

Moreover, existing dimer models in vacuum are qualitative and controversial and are usually based on docking protocols which undergo serious approximations [2,4]. In the present study we pushed the boundary of existing knowledge and pursued to unravel the KRAS dimer formation mechanism, find the population of different dimer states using coarse grained molecular dynamics simulations.

Methods

Molecular dynamics simulations were performed using the Martini coarse grained forcefield [5], due to its relevant parametrization in reproducing well lipid environments. Parameters for the HVR linker of KRAS were obtained from the literature [6]. The GTP coarse grained forcefield parameters were derived in this study (see Figure 1A.) by fitting the bonded angular and dihedral angle potential forms of a coarse grained beads from an all atom MD simulations of GTP in water using gromacs [7]. The system was first setup using insane script (see Fig 1B), thereafter energy minimized and then equilibrated for 5 ns in the NPT ensemble. The production run was 500 ns in the NPT ensemble at 310K and 1 bar. The resulting trajectory was analysed using the gromos clustering algorithm on the backbone atoms of Martini, using a cut-off of 0.25 nm.

Results

We first fit the all atom MD simulation of GTP in solution to a coarse grained forcefield. The corresponding parameters for the bonded, angular and dihedral angles can be provided upon request. We show a representative fit in Figure 1A. Clustering analysis of the 500 ns coarse grained MD simulation shows 5 dominant clusters (see Figure 1C). Among them, the third most populated cluster corresponds to the dimer complex suggested by Muratcioglou et al [1], where interfaces h3 and h4 interact. The most populated cluster #1 in this preliminary study, involves interactions of residues 35-45 with 155-168. Cluster #2 involves interactions of residues 35-45 with 85-100, cluster #4 involves interactions of residues 35-45 with 125-135, and cluster #5 involves interactions of residues 47-49 with 131-139.

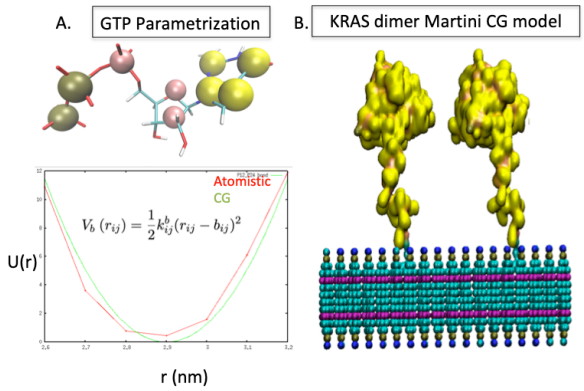

Figure 1 - A) Parametrization of GTP into coarse grained particles B) Martini starting model for a KRAS4B dimer membrane GTP water complex. C) 5 most occurring clusters from a 500 ns CG MD simulation.

Conclusions

In our study, we have introduced a tangible protocol for studying the KRAS dimerization on a membrane, followed by preliminary MD results on possible dimer complexes. Analysis of the MD trajectory shows agreement of one of our harvested dimer structures with literature findings, such as the h3-h4 complex found by Mutatcioglou et al. Our simulations need to be extended and/or coupled to enhanced sampling protocols such as Metadynamcs in order to have a quantitative picture of the complete binding landscape.

References

[1] Muratcioglu S et. al. Structure, 23(7):1325-35,2015. [2] Prakash P et al., Sci. Rep. 7:40109, 2017. [3] Nan X et al., PNAS, 112(26):7996-8001,2015. [4] Amborgio C et al.,Cell, 172(4):857-868,2018. [5] Marrink SJ et al. J. Phys. Chem. B, 111 (27):7812-7824, 2007. [6] Atsmon-Raz Y et al.,J. Phys. Chem. B,121(49):11132-11143, 2017. [7] Abraham et al., SoftwareX 1-2:195-125, 2015.

Acknowledgements

The work has been performed under the Project HPC-EUROPA3 (INFRAIA-2016-1-730897), with the support of the EC Research Innovation Action under the H2020 Programme; in particular, the author gratefully acknowledges the support of Zoe Cournia from the Biomedical Research Foundation Academy of Athens and the computer resources and technical support provided by ARIS HPC centre.

STRUCTURAL INVESTIGATION OF DE NOVO DNA METHYLATION

D. Dogan[1], I. Faustino[3], S.-J. Marrink[3], E. Karaca[1,2]

[1]Izmir International Biomedicine & Genome Institute, Turkey; [2]Izmir Biomedicine and Genome Center, Turkey; [3]University of Groningen, Germany

Introduction

DNA methylation at cytosines is integral to embryonic development and cellular differentiation in eukaryotes. De novo methyltransferases, DNMT3A/3B, assist establishing specific methylation patterns throughout the genome. DNMT3A/B enzymes modify CpG, as well as non-CpG sites, i.e. CpA, CpT and CpC sites [1]. For example, DNMT3A was observed to target the first cytosine at a CAC motif while DNMT3B prefers to methylate CAG motif in embryonic stem cells. Among different DNMT3s, DNMT3Bs was shown modify CpG sites with higher efficiency than DNMT3As [2-4].

To interpret the available genomics data at the structural level, we modelled the catalytic units of DNMT3A/3B enzymes bound to their experimentally probed DNA sequences (CGC, CAG, CAC) and traced their interaction profiles with molecular dynamics simulations.

Methods

Modelling DNA-bound DNMT3A/B complexes: We used DNMT3A's catalytic domain bound to its CpG sequence as a template (PDB ID: 6F57) to model the following complexes: DNMT3A-CAC, DNMT3A-CAG, DNMT3B-CGC, DNMT3B-CAC, DNMT3B-CAG. For DNMT3B modelling, Phyre2 server [5]; for DNA modelling, 3DNA; for complex refinement, HADDOCK2.2 server was used [6].

Molecular Dynamics: SAM parameters were taken from the literature [7]. Proteins' protonation states were predicted with PDB2PQR Server by setting pH to 7.0. The complexes were parallelly simulated under the effect of amber14sb-parmbsc1 force field with GROMACS 2018.1 package [8]. Before each simulation, the complex systems were solvated with TIP3P water molecules in a dodecahedron box. Neutralized complexes were minimized, heated over 100ps, relaxed slowly and equilibrated for 100 ps at 298K and 1 atm. Finally, for each complex, a total of 600 ns long simulation was generated.

Analysis: 3DNA and Gromacs tools were used to trace the equilibration time. As a result, the second half of each trajectory was chosen for further analysis. Interfacea and mdanalysis python packages were used to calculate the potential energy and hydrogen bond profiles, respectively [9, 10].

Results& discussion

According to the total energy profile comparison, DNMT3B binds to any DNA sequence with lower potential energy than DNMT3A (Fig. 1). In accordance with this, the number of hydrogen bonds across the DNMT3-DNA interface is higher in the case of DNMT3B complexes (data not shown). Among different DNA

sequences, both DNMT3s bind to CpG sites the strongest. These observations provide with the first structural insight supporting the proposed DNMT3 methylation patterns.

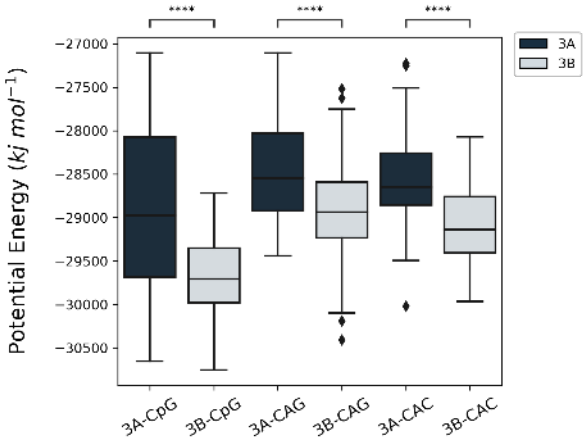

Figure 1 - Potential energy values of each complex calculated by using nonbonded forces with OpenMM. Independent t-test was used to calculate the p-values (**** indicates p value lower than 1.00e^{-4})

Outlook

As we could not depict any DNMT3-preferentiality towards CAC and CAG sites, we plan to calculate and dissect the individual residue-nucleotide interaction energetics over time.

References

[1] Zhang, Z.M., et al., Structural basis for DNMT3A-mediated de novo DNA methylation. Nature, 2018. 554(7692): p. 387-391.; [2] Handa, V. and A. Jeltsch, Profound flanking sequence preference of Dnmt3a and Dnmt3b mammalian DNA methyltransferases shape the human epigenome. J Mol Biol, 2005. 348(5): p. 1103-12.; [3] Gowher, H., et al., Mechanism of stimulation of catalytic activity of Dnmt3A and Dnmt3B DNA-(cytosine-C5)-methyltransferases by Dnmt3L. J Biol Chem, 2005. 280(14): p. 13341-8. ; [4] Lee, J.H., S.J. Park, and K. Nakai, Differential landscape of non-CpG methylation in embryonic stem cells and neurons caused by DNMT3s. Sci Rep, 2017. 7(1): p. 11295.; [5] Kelley, L.A., et al., The Phyre2 web portal for protein modeling, prediction and analysis. Nat Protoc, 2015. 10(6): p. 845-58; [6] van Zundert, G.C.P., et al., The HADDOCK2.2 Web Server: User-Friendly Integrative Modeling of Biomolecular Complexes. J Mol Biol, 2016. 428(4): p. 720-725; [7] Senn, H.M., D. O'Hagan, and W. Thiel, Insight into enzymatic C-F bond formation from QM and QM/MM calculations. J Am Chem Soc, 2005. 127(39): p. 13643-55; [8] Ivani, I., et al., Parmbsc1: a refined force field for DNA simulations. Nat Methods, 2016. 13(1): p. 55-8; [9] Michaud-Agrawal, N., et al., MDAnalysis: a toolkit for the analysis of molecular dynamics simulations. J Comput Chem, 2011. 32(10): p. 2319-27; [10] Rodrigues, J. Interfacea. 2018; Available from: https://github.com/JoaoRodrigues/interfacea.

Acknowledgements

The work has been performed under the Project HPC-EUROPA3 (INFRAIA-2016-1-730897), with the support of the EC Research Innovation Action under the H2020 Programme. The authors gratefully acknowledge the support of the Molecular Dynamics Group at University of Groningen, the computer resources and technical support provided by SURFSARA.

A VISUALIZATION PIPELINE FOR COMPUTATIONAL NEUROSCIENCE

K. Katsantonis[1], C. Strydis[2]

[1]Microprocessors and Digital system lab, School of ECE, National Technical University of Athens, Greece; [2]Erasmus Medical Center, The Netherlands

Introduction

Modeling bio-physically accurate neuronal models is a complex procedure that involves heavy parameter fitting and a lot of trial and error. Bio-physically accurate neuronal populations consist of neurons who have multiple compartments and even simulating a small network of them can produce large amount of data. Those data can be hard to evaluate in order to decide whether the computational model of the neuron is worth further studying or not. We propose a high performance visualization pipeline capable of providing a high level representation over this large amount of data giving neuroscientists a powerful tool able to assist them in the quick evaluation of models.

Methods

The visualization pipeline consists of three stages. The first stage is the neuronal population simulation by which the raw data is produced. We used for the simulation stage the accelerated simulator proposed by G. Chatzikonstantis et al. of the extended Hodgkin-Huxley model [1]. We did multiple production runs using a number of parameters and network sizes on the nodes offered by SURFsara's Cartesius supercomputer [2]. The second step of the pipeline is the post-process of the raw data. In this stage we convert the raw data to multiple structured files, in a format that can be parsed by Paraview [3], so that each file represents one timestep of the simulation. The tool which we developed for this stage of the pipeline can either convert the raw data to simple csv files or to vtk files. The csv files are easier to understand however they don't contain information regarding the connection of the neurons and thus the visualization ends up simpler but, in some cases, more useful, whereas the vtk files contain neuron connectivity and thus lead to more complete visualizations. The third step of the visualization includes the parsing of the processed output by Paraview and the graphical representation of the simulation as an animation on a GPU accelerated node. We represented the soma of each neuron with a sphere and the connections with tubes.

Results

Figure 1 is an example of the animated representation of the simulation which is the last step of the pipeline. The different colour nuances represent the different intensity of the variable of interest, which in the specific figure is the voltage of the soma. Note that this animated simulation uses the vtk file format on the second stage and thus the connections between neurons are visible. Performance-wise the bottleneck of the pipeline is the second stage as each simulation timestep is converted to separate file which uses-up the whole IO bandwidth available by cartesius, so even though stage two was created multithreaded there was not a specific benefit observed by using more than two threads.

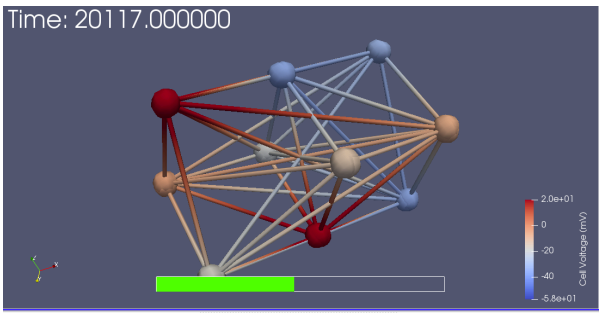

Figure 1 - 3D animation of ten neurons. Red spheres represent neurons spiking while the state of the rest can be easily inferred by colour.

Conclusions

We created a prototype three-stage visualization pipeline that can be used to study neuronal network models, capable of running on GPU accelerated nodes. The feedback from the neuroscientists was positive, and we will continue to develop our pipeline in terms of features and performance.

References

[1] G. Chatzikonstantis, H. Sidiropoulos, C. Strydis, M. Negrello, G. Smaragdos, C. D. Zeeuw, and D. Soudris, "Multinode implementation of an extended hodgkin–huxley simulator," Neurocomputing, vol. 329, pp. 370 – 383, 2019. [2] SURFsara, "Cartesius: the dutch supercomputer," 2019. [3] P. U. Guide, "Paraview list of readers," 2019.

Acknowledgements

The work has been performed under the Project HPC-EUROPA3 (INFRAIA-2016-1-730897), with the support of the EC Research Innovation Action under the H2020 Programme; in particular, the author gratefully acknowledges the support of Ass. Prof. Christos Strydis at the Erasmus Medical Center and the computer resources and the technical support provided by SURFsara.

MOLECULAR DYNAMICS STUDY ON THE CYTOCHROME P450 MEDIATED C-H HYDROXYLATION OF NON-AROMATIC N-HETEROCYCLES

N. Kress[1], B.S. Jones[1], M. Tavanti[1], M. Garcia-Borràs[2], S. Osuna[2], S.L. Flitsch[1]

[1]Manchester Institute of Biotechnology & School of Chemistry, University of Manchester, United Kingdom; [2]CompBioLab group, Institut de Química Computacional i Catàlisi (IQCC) & Departament de Química, Universitat de Girona, Spain

Introduction

The P450-mediated C-H hydroxylation has great potential in the late-stage synthesis of nitrogen containing pharmaceutical compounds [1]. However, strong nitrogen haem interactions can obstruct C-H hydroxylation [2]. Intriguingly, we found a starting activity for the conversion of (S)-2-methylpyrrolidine 1 to (S)-2-pyrrolidinemethanol 2 using CYP151A2 from Mycobacterium sp HE5 (MorA). Here, we use long-scale molecular dynamics (MD) simulations to study the dynamical behaviour of 1 in MorA in comparison to an in silico generated design and non-active CYP116B46 from Tepidiphilus thermophilus (TT) to obtain insights into this promising activity.

Methods

SWISS-Model was used to generate a homology model of MorA based on the crystal structure (PDB ID: 3p3l) of the P450 enzyme AurH from Streptomyces thioluteus (36.1 % sequence identity) [3]. Together with the TT crystal structure (PDB ID: 6gii) [4], these receptors were used for all simulations. TT N-terminus was modelled using the I-Tasser server [5]. Modelling was based on the haem ferryl states and protonated 1. For ligand parametrization and MD simulations, a previously described protocol based on the Gaussian09 and AMBER16 software was applied [6] Long-timescale MD simulations were performed on the CTE-POWER supercomputer of the BSC-CNS. The most populated structures of MorA and TT were derived by 3 x 1000 ns simulations. These were used for molecular docking of 1 using AutoDock VINA (implemented in YASARA) [7]. Subsequently, 3 x 500 ns simulations including the ligand 1 were performed. Rosetta.design was used to predict in total nine MorA designs stabilizing an identified near attack conformation [8]. The designs were subsequently assessed by MD simulations (3 x 500 ns).

Results

MD trajectory comparison of 1 in MorA and TT unravels greater mobility of 1 in MorA, because one dominating binding mode in the very apolar TT active site prevails. In this, the protonated nitrogen of 1 forms two hydrogen bonds, one to ferryl oxygen and another to the carboxy group of haem 13-propionate, moving out-of-plane. Close binding of N-H to Fe=O can obstruct C-H hydroxylation [2]. Plotting this amine-haem distance against the catalytic methyl-haem distance for each MD snapshot, these different populations of conformational 1 states in MorA and TT wild type (Wt) are visualized (Figure 1). In TT, close unproductive amine-haem binding dominates, while MorA shows more productive binding serving as an explanation for observed catalytic activity.

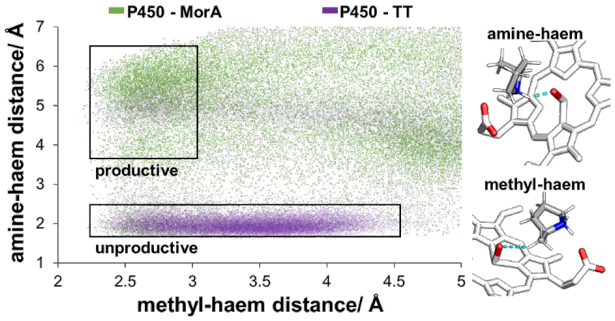

Figure 1 – Amine-haem distance plotted against methyl-haem-distance for 75000 MD snapshots of MorA (green) and TT (purple) indicating productive and unproductive ligand populations. Distances are measured from respective ligand hydrogens to ferryl oxygen as graphically indicated (cyan).

MorA simulations revealed some ligand nitrogen binding to out-of-plane propionate, but not to ferryl, that supports productive near attack conformations for methyl hydroxylation. A MorA quintuple variant (I85A/L86E/G240A/T291A/N386S) stabilising this conformation was calculated by Rosetta.design. Subsequent MD analysis for this design indeed resulted in a significantly increased propionate out of plain state. While **1** eventually left MorA Wt active site, increased active site binding is found in the design.

Conclusions

Increased mobility in a wider MorA active site together with alternate hydrogen bond acceptors prevents trapped binding of ligand nitrogen to ferryl consistently seen in TT. This serves as an explanation for observed catalytic activity in MorA. Surprisingly, out-of-plane haem propionate movement seem relevant for ligand binding. An estimated MorA design stabilises ligand binding in the active site, which might translate to increased activity. The findings provide valuable insight in productive and potentially inhibitory binding of such N-heterocycles in P450s.

References

[1] Urlacher et al., Trends Biotechnol, 37(8):882-897, 2019. [2] Zhang et al., Front Chem, 5(1):1-10, 2017. [3] Waterhouse et al., Nucleic Acids Res, 46(W1):296-303, 2018. [4] Tavanti et al., Biochem Biophys Res Commun, 501(4):846-850, 2018. [5] Roy et al., Nat Protoc, 5(4):725-738, 2010. [6] Narayan et al., Nat Chem, 7(8):653-660, 2015. [7] Krieger et al., Bioinformatics, 30(20):2981-2982, 2014. [8] Kuhlma et al., Science, 302(56490:1364-1368, 2003.

Acknowledgements

The work has been performed under the Project HPC-EUROPA3 (INFRAIA-2016-1-730897), with the support of the EC Research Innovation Action under the H2020 Programme; in particular, the author gratefully acknowledges the computer resources and technical support provided by BSC-CNS.

DEVELOPMENT OF PHARMACOLOGICAL TOOLS FOR DIRECT OR INDIRECT INHIBITION OF SBDS FUNCTION

T. Kronenberger[1], A. Poso[1,2]

[1]Department of Internal Medicine VIII, University Hospital Tuebingen, Germany; [2]School of Pharmacy, University of Eastern Finland, Finland

Overview

Cancer cells sensitivity to inhibitors of rRNA synthesis can be a result of mutations that up-regulate the ribosome biogenesis rate or regulation (1). Shwachman-Bodian-Diamond syndrome (SBDS) is one of the ribosomal components, bridging the interface between the big and small subunits and mainly involved in the ribosome maturation (2). Ribosomal interference is known to impair cell proliferation and to induce senescence, which can be used to stop cancer proliferation and even for treatment when combined with a second therapeutic option.

As outlined in the proposal SBDS is composed of three main domains (DI – III, Figure 1a), which present high flexibility among themselves. SBDS can range from a fully open conformation to a closed (Figure 1a and b) one where the interface between domain I and II is covered by the residues Ile196 and Lys197 from domain D-III. SBDS is active when in the open conformation, with residues such as Lys151 interacting with other ribosomal proteins (EFL1), while most of the other interface parts interact with ribosomal DNA (3). On the other hand, the inactive closed conformation seems to be structurally accessible, as observed by multiple NMR states reported in the literature (PDB IDs: 2KDO and 2I9N).

Additionally, we conducted apo-structure simulations, a total amount of 600 ns simulation time, to derive relevant conformations for the next rounds of virtual screening or analogue searches. Important point interactions were observed along the simulations, such as Glu94 (D-I) – Arg220(D-III), Asp119 (D-II) and both the Lys197 (D-III) and Arg42 (D-I), Leu196 (D-I) and Val97 (D-III), and transiently Arg128 (D-II) and Glu221 (D-III). It is worth note a hydrophobic pocket between domains II and III composed of Trp41, Leu49, methyl group from Thr91 and Tyr130, which contributed to a druggable pocket (Figure 1c).

As the next step, we aimed to pharmacologically address the transient pocket present in the closed conformation, stabilizing the inactive state of the protein. The addressed pocket was found to be a common NMR state, identified using SiteMap among the structural pool (Drug-Score > 0.8), but also similarly present among the structures generated from the simulations.

We initially screened around two million compounds, from the commercially available Enamine library, looking for potential SBDS inhibitors. After visual pose evaluation, twelve compounds were selected for molecular dynamics simulation. Compounds with stable interaction within the pocket were tested on a cellular level, for senescence induced phenotype characteristic from SBDS depletion (data not shown).

The four active compounds were used as the template for analogue search and for shape screening against the pre-prepared Molport compound library, available from Poso's group in Kuopio, from which a consensus list was further analysed using molecular dynamics. From all simulations, eleven compounds showed the ability to stabilize SBDS' closed conformation and a common interaction feature was the addressing of domain's I-II hydrophobic pocket by rings (example compounds are shown in Figure 1d and e). As the next step in this project those compounds are being tested in phenotypic assays, using knockdown models generated by our partners (AK Zender), and aim to follow up with complementary structural studies.

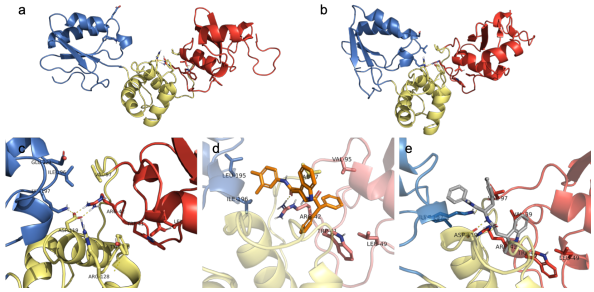

Figure 1 – Representative structures from SBDS apo-structure simulation and virtual screening results. Representation of the closed (a, inactive) and open (b) conformations of SBDS accessed post 600 ns MD simulation, where (c) illustrates the identified pocket for virtual screening from a representative frame. Domain I is represented in red, domain II in yellow and domain III in blue, all polar interactions are highlighted by dashed yellow lines. (d and e) a representative frame of different analogues selected from the Molport library after the virtual screening with docking followed by molecular dynamics simulation.

References

[1] Scala et al., Oncogene. Feb 25;35(8):977-89, 2016. [2] Orelio et al., PLOS ONE. Jun 13;6(6):e20727., 2011. [3] Finch et al., Genes Dev. May 1;25(9):917–29, 2011.

Acknowledgements

The work has been performed under the Project HPC-EUROPA3 (INFRAIA-2016-1-730897), with the support of the EC Research Innovation Action under the H2020 Programme; in particular, the author gratefully acknowledges the support of Antti Poso (Universtiy of Eastern Finland) and the computer resources and technical support provided by HPCE3-CSC.

INVESTIGATION OF HSP90 ALLOSTERIC REGULATION WITH BIOMOLECULAR SIMULATIONS

F. Marchetti[1,2], A. Pandini[3], G. Colombo[1,4]

[1]Dipartimento di Chimica, Università degli Studi di Pavia, Italy; [2]Dipartimento di Chimica, Università degli Studi di Milano, Italy; [3]Department of Computer Science—Synthetic Biology Theme, Brunel University London, United Kingdom; [4]Istitutodi Chimica del Riconoscimento Molecolare, Consiglio Nazionale delle Ricerche, Milan, Italy

Introduction

Hsp90 is a chaperone protein that is fundamental for cell development and maintenance that intervene in the folding process to activate a variety of substrate "client" proteins. Many clients are involved in oncogenesis, therefore Hsp90 is recognized as a facilitator of ''oncogene addiction'' [1]. The chaperone is an omodimer with each chain divided in three domains: a N terminal domain, a middle domain and a C terminal domain. X-ray, SAXS and kinetic data showed that ATP binding induce global conformational modulations on the whole protein and ATP hydrolysis are fundamental for the rearrangement of the client binding-site residues that drives the activation of the client [2]. Hsp90 functionalities is based on modulation of protein-protein interactions with client and cochaperone proteins forming multiprotein complexes. Therefore protein-protein interactions could be the target for the discovery and development of new drugs, in particular for new alternative to ATP-competitive compounds. In fact, those orthosteric inhibitors impact indiscriminately on the whole Hsp90 functional spectrum, blocking all the processes that depend on it. For this reason, the development of new allosteric compounds could improve the generation of client-specific inhibitors/modulators: allosteric ligands were indeed shown to destabilize the complexes necessary for client folding and cause cancer cell death via different mechanisms than classical ATP-competitive drugs.

In this context we carry out molecular simulation on Hsp90 in complex with experimentally characterized ligands to analyse how allosteric signal transmission is modulated with different molecules focusing on the differences between activators and inhibitors.

Methods

All-atom MD simulation in explicit water were carried out for the selected ligands using the Gromacs 2018 package and the Amber03 force field. The protein-ligand complex was solvated in a dodecahedric box with TIP3P water molecules, counterions were randomly added to ensure overall charge neutrality. After a 100ps equilibration the simulation was conducted in NPT ensamble at 300 K and 1 bar, using Berendsen thermostat and Parrinello-Rahman pressure coupling. The radius of non-bondedVan der Waals interaction was set to 0.925 nm and electrostatic interaction were treated with Particle Mesh Ewald method. Ligands were prepared with Antechamber software.

Distance Fluctuations are defined as the time dependent mean square of the of the distance between the C-alpha of two residues.

Results

We run MD simulations of Hsp90 in complex with three different ligands: one activator (cc26) and two inhibitors, novobiocin and NDH2.

The aim is to observe if the compounds induce different effects on the protein dynamics, in particular if there are allosteric modulation between the ligands binding site, located between the middle and the C terminal domain, and the ATP hydrolysis site in the N terminal domain.

The effect of the ligands on protein flexibility and coordination between domains can be quantified computing the distance fluctuations (DF), in fact if the distance among two residues have little variation is it reasonable to assume that the residues are coordinated in the dynamic.

In the figure 1 is reported the DF between the monomers computed for every domain. The DF for the N terminal domains is lower in the case of the activator ligands respect to the inhibitors, suggesting that inhibitors molecules tend to reduce coordination among N terminal domains.

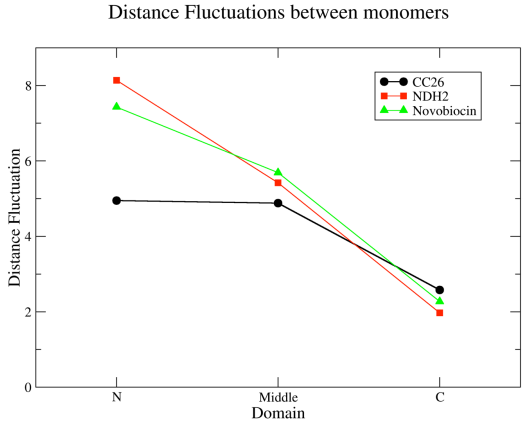

Figure 1 – Average DF compute between the same domain of different monomers, the results are reported for the three ligands studied.

Conclusions

With the MD simulations we observe the presence of allosteric signals and the difference in modulation between inhibitor and activator molecules. On this basis we can integrate the acquired information in the structure selection to build a framework for the prediction of the biological impacts of the ligands in terms of activation or inhibitions of the chaperone functions. The facilities made available were good performing allowing performance of 50 ns/day on our huge system.

References

[1] Neckers, L.; Workman, P., Hsp90 Molecular Chaperone Inhibitors: Are We There Yet? Clinical Cancer Research 2012, 18, (1), 64-76. [2] Ali, M. M. U.; Roe, S. M.; Vaughan, C. K.; Meyer, P.; Panaretou, B.; Piper, P. W.; Prodromou, C.; Pearl, L. H., Crystal structure of an Hsp90-nucleotide-p23/Sba1 closed chaperone complex. . Nature 2006, 440 (7087), 1013-1017.

Acknowledgements

The work has been performed under the Project HPC-EUROPA3 (INFRAIA-2016-1-730897), with the support of the EC Research Innovation Action under the H2020 Programme; in particular, the author gratefully acknowledges the support of Alessandro Pandini, Brunel University and the computer resources and technical support provided by EPCC.

MECHANICAL UNFOLDING OF TALIN PROTEIN USING METADYNAMICS

V.V. Mykuliak[1], G. Bussi[2], A. Laio[2], V.P. Hytönen[1]

[1]Faculty of Medicine and Health Technology, Tampere University, Tampere, Finland, and Fimlab Laboratories, Tampere, Finland; [2]Scuola Internazionale Superiore di Studi Avanzati (SISSA), Trieste, Italy

Introduction

Talin is a key mechanosensor protein at the focal adhesions, that couples the extracellular matrix with intracellular actin filaments via the transmembrane integrin receptor. Talin rod domain consists of 13 alpha-helical subdomains, which function is regulated by mechanical signals. The rod domain undergoes unfolding under mechanical load what changes affinity to different binding partners and leads to opening of buried binding sites. In this project, unfolding and refolding of the strongest talin rod subdomain R9 [1] was studied using metadynamics simulation.

Methods

Talin rod subdomain R9 was used in the metadynamics simulation. 2KBB PDB structure was used as a starting conformation. The simulation was performed using Gromacs 2018 [2] and PLUMED 2.5 [3] at Galileo (CINECA) and Sisu (CSC) supercomputers. The CHARMM27 force field [4] and explicit TIP3P water model in 0.15 M KCl solution were used and the total charge of the system was neutralized by K+ and Cl- ions. The size of the simulation box was 9 nm x 9 nm x 30 nm, and the systems consisted of the 237 515 atoms. The energy minimization of the system was performed in 10 000 steps using the steepest descent algorithm, followed by 1 ns equilibration of the system using harmonic position restraints put on all protein heavy atoms. The metadynamics simulation was performed using an NPT ensemble, where the Berendsen weak coupling algorithm was used to control both pressure and temperature at 1 atm and 310 K respectively.

To study unfolding and refolding of the talin rod subdomain R9 in the metadynamics, the following two collective variables (CVs) were selected: end to end distance and native contacts. For the end to end distance, the C-alpha atoms at N- and C-terminal residues were used. The native contacts were selected as a shorter that 0.7 nm distance between C-alpha atoms excluding neighbouring 4 residues. The total number of the selected native contacts in folded R9 was equal to 244. A Gaussian height of 2.5 kJ/mol was employed. The Gaussian width was set to 0.25 nm and 2.94 for the end to end distance and native contacts CVs respectively. The Gaussian biases were applied every 500 time steps (1 ps). The rotations of the protein were removed by restraining xy components of the distance between the C-alpha atoms of terminal residues. The two walls at 4 nm and 29 nm for the end to end distance CV were used since the length of the box was 30 nm and completely unfolded R9 can reach approx. 50 nm.

Results

The metadynamics simulation was initiated with completely folded R9 (Figure 1a), which consists of 5 alpha-helices. The end to end distance was extended together with decreasing the number of the native contacts (Figure 1d,e), and the protein was unfolded to 3-helix intermediate [5] at approx. 30 ns. The R9 structure was completely unfolded at approx. 213 ns (Figure 1b). Following the unfolding, the secondary structure was refolded, but complete refolding of the tertiary structure was not achieved during the simulation time of over 1.5 µs. Only partially refolded tertiary structure was observed (Figure 1c) at approx. 752 ns, where 150 native contacts were formed.

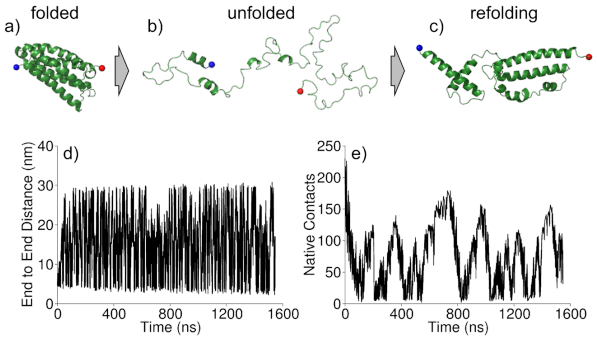

Figure 1 – Unfolding and refolding of the talin rod subdomain R9. Structure snapshots representing (a) folded, (b) unfolded and (c) refolding conformations captured at 0 ns, 213 ns and 752 ns respectively. (d) Protein end to end distance and (e) number of the native contacts as function of time during the metadynamics simulation.

Conclusions

Talin rod subdomain R9 is rather large protein for this setup. While unfolding is straightforward, the refolding requires significant optimization, which would take microseconds to achieve complete refolding, and thus is computationally expensive because of the large system size. Within 1.5 µs metadynamis, the R9 unfolded and partially refolded, but complete refolding was not achieved.

References

[1] Haining AWM et al., ACS Nano, 10:6648–6658, 2016. [2] Abraham MJ et al., SoftwareX, 1–2:19–25, 2015. [3] Tribello GA et al., Comput Phys Commun, 185:604–613, 2014. [4] MacKerell A et al., J Phys Chem B, 102:3586–3616, 1998. [5] Mykuliak VV et al., PLoS Comput Biol, 14:e1006126, 2018.

Acknowledgements

The work has been performed under the Project HPC-EUROPA3 (INFRAIA-2016-1-730897), with the support of the EC Research Innovation Action under the H2020 Programme; in particular, the first author gratefully acknowledges the support of Prof. Giovanni Bussi at the Molecular and Statistical Biophysics Group of SISSA, and the computer resources and technical support provided by CINECA.

GPU ACCELERATION ON A NOVEL BIOPHYSICALLY-ACCURATE NEURAL NETWORK SIMULATOR

S. Panagiotou

Microprocessors & Digital Systems Lab, National Technical University of Athens, Greece

Introduction

This visit concerned the topic of simulation of extended Hodgkin-Huxley neuronal networks, at large scale. The factors contributing to this effort were: an existing general-purpose neural simulator code from MicroLab NTUA; field and application knowledge, about in silico experimentation protocols and cutting edge models in research practice, from Neuroscience Department, Erasmus MC; GPU cluster resources, and technical support, provided by SurfSARA; and the insights on how to accelerate the simulator for practical use cases. through the requirements analysis, code development and performance benchmark runs, undertaken during the visit.

Methods

Our group is developing a high-performance simulator of extended Hodgkin-Huxley models, that supports runtime-configurable ion channel dynamics, to meet the needs of research proposing new models. The typical simulation use cases for multicompartmental Hodgkin-Huxley models were assessed. This field is still on an early stage of development, due to the difficulty of obtaining accurate biophysical models and data for dynamical biological processes, the high computational costs of simulating at this level, and the model complexity that prevented commonly-used packages from utilizing parallel computing resources effectively. Due the limitations of existing neural simulator packages, the network structures explored are still very simple; they typically consist of clusters of identical neurons, whose neurons are connected to each other accordingly to simple statistical models. To support these cases, Support for uniform-probability and Gaussian connectivity models was added, and the simulator was ported to the CUDA GPU platform for performance evaluation. The simulator was then benchmarked against a parameter space of neuronal networks to be simulated, with varying neuron population sizes, synaptic connectivity densities, connectivity models. Scalability on HPC hardware was also examined, with the compute and memory load being distributed the GPU cluster nodes, for simulation.

Results

The performance results gathered from the simulations run for the parameter grid described above, provide insights on how run time and system efficiency change for different simulation and runtime scenarios. In every case, run time depended linearly on amount of neurons, total amount of synapses and simulation iterations, as would be expected in a simple, hardware-agnostic analysis of the simulation algorithm. Under multi-node runtime conditions, strong scalability is eventually limited by communication latency between nodes. The statistical properties of the connection model between neurons proved to have an interesting effect on both run time and simulation scalability; when connections were more likely to exist between physically close neurons, the simulation ran much faster for the same amount of synapses, than when connections had the same chance of occurring between any pair of neurons. This speedup was evident both in intra-node computations, and inter-node communications. We assume this speedup happened because the spatial domain decomposition in both cases keeps most communicating neurons close to each other in side the hardware that simulates them, greatly reducing inter-communication traffic and delays in both the GPU network-on-chip and the InfiniBand network.

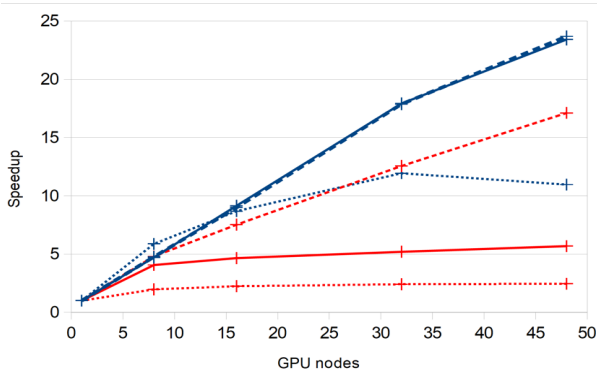

Figure 1 – Performance scalability, per GPU nodes used, network size and density, and connectivity distribution. Solid, dashed and dotted lines represent 4M neurons, 100 synapses/neuron 4M neurons, 10 syn/neuron, and 256K neurons, 100 syn/neuron respectively; Blue lines represent Gaussian connectivity model, and red lines represent uniform connectivity model.

Conclusions

This visit was successful in both the technical development parts, as well as the technical know-how development and international cooperation and networking aspects of its objectives. The presented work will undergo further development, following an iterative a development cycle; feedback about the new features will be gathered from neuroscientists, the suggestions made will be translated into new features for the simulator, and subsequent benchmarks will be run to assess and improve the simulator's performance. These improvements will in turn expand the range and complexity of models researchers can work with, allowing them to find out what new features should be developed further on.

Acknowledgements

The work has been performed under the Project HPC-EUROPA3 (INFRAIA-2016-1-730897), with the support of the EC Research Innovation Action under the H2020 Programme; in particular, the author gratefully acknowledges the support of Christos Strydis, Neuroscience Department, Erasmus Medical Center, and the computer resources and technical support provided by surfSARA.

WHOLE DAY MATTERS: CHANGES IN 24-H MOVEMENT BEHAVIOUR

A. Pulakka

Department of Public Health, University of Turku and Turku University Hospital, Turku, Finland

Introduction

In terms of movement, 24-h time period is distributed between sleep, sedentary behaviour (SB), light physical activity (LPA) and moderate-to-vigorous physical activity (MVPA). Time within a 24-h period is finite, thus a change in time spent in one behaviour necessarily effects time spent in other behaviours. This concept of "whole day matters", represents a paradigm shift in the field of physical activity and sleep research [1].

The overall aim of the study is to develop and test the methods for analysing 24-hour movement behaviour from wrist-worn accelerometers and to examine the changes in 24-hour movement patterns around retirement. Here we present changes in 24-hour movement behaviour between work days and days off.

Methods

Altogether 842 participants from the Finnish Retirement and Aging Study (FIREA, www.utu.fi/firea) wore triaxial ActiGraph accelerometers on their non-dominant wrist for 7 days and 6 nights. Daily time spent in the four behaviours at the second measurement point of the study was identified with R package GGIR developed by van Hees and colleagues [2,3]. We used cutpoints of 30 mg for LPA [4] and 100.6 mg for MVPA [5]. The GGIR was run as array jobs using ARCHER supercomputing service at EPCC and Taito cluster at CSC.

The data were analysed by compositional data analysis which takes into account the co-dependence of the variables [1,6]. To obtain the compositional means we transformed data into isometric log-ration (ilr) coordinates. In this case, both the exposure (proportion of time in different activity behaviours during work days) and the outcome (proportion of time in different activity behaviours during non-working days) were compositional data. Then, we compared the differences in the compositions between non-working and working days.

Results

Of the participants, 583 (69%) had working and non-working days at the second measurement point and had been using the accelerometer for minimum of 4 days in total. Mean age of the participants was 63 years (SD 1.1), 84% of them were women and 70% had no-manual occupation.

Figure 1 presents the duration of the day the participants spent in sleep, sedentary, LPA and MVPA movement behaviours in working days and non-working days. Preponderance of MVPA over the other behaviours was lower on non-working days and MVPA in relation to other behaviours was more during working than non-working days.

Furthermore, participants with high MVPA during working days tended to have slightly higher LPA in relation to other behaviours on non-working days. If participants were more active with LIPA during working days, they had more SB in relation to sleep during non-working days.

There was more sleep in relation to the other movement behaviours during non-working days than during days off. When excluding sleep and focusing on waking hours, there was more MVPA in relation to LPA and SB, and less LIPA in relation to SB during working days than during non-working days.

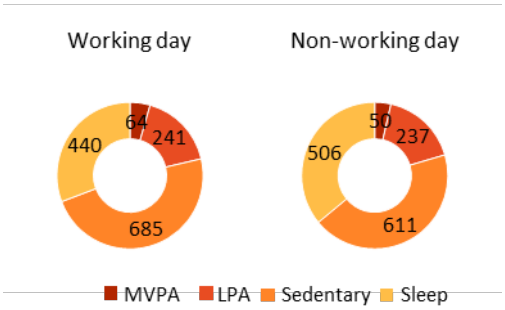

Figure 1 – Time spent in moderate-to-vigorous physical activity (MVPA), light physical activity (LPA), sedentary and sleep during work days and days off.

Conclusions

The GGIR algorithm is a feasible way for analysing physical activity data from wrist-worn accelerometers, and the analysis is greatly speeded up with high performance computing. We found differences in the 24-hour movement composition between working and non-working days, namely that participants had less sleep and more of MVPA, LPA and SB during working days.

References

[1] Chastin SFM et al., PloS One 10:e0139984, 2015. [2] van Hees VT et al., J Appl Physiol 117(7):738-744, 2014. [3] van Hees VT et al., PLoS One 10:e0142533, 2015. [4] Rowlands A et al. Med Sci Sports Exerc 50(2), 2018. [5] Hildebarnd M et al. Med Sci Sports Exerc 46(9), 2014. [6] Dumuid et al., Stat Methods Med Res 27(12), 2018.

Acknowledgements

The work has been performed under the Project HPC-EUROPA3 (INFRAIA-2016-1-730897), with the support of the EC Research Innovation Action under the H2020 Programme; in particular, the author gratefully acknowledges the support of professor Sebastien Chastin from Glasgow Caledonian University and the computer resources and technical support provided by EPCC.

STRUCTURE, DYNAMICS, AND APPARENT GLASS TRANSITION OF STEREOREGULAR POLY(METHYL METHACRYLATE)/GRAPHENE INTERFACES THROUGH ATOMISTIC SIMULATIONS

A.F. Behbahani[1,2], S. Mehdi Vaez Allaei[3,4], G.H. Motlagh[1], H. Eslami[5], and V.A. Harmandaris[2,6]

[1]Advanced Polymer Materials and Processing Lab, School of Chemical Engineering, College of Engineering, University of Tehran, Iran; [2]Institute of Applied and Computational Mathematics, Foundation for Research and Technology - Hellas, Heraklion, Greece; [3]Department of Physics, University of Tehran, Iran; [4]School of Physics, Institute for Research in Fundamental Sciences (IPM), Tehran, Iran; [5]Department of Chemistry, College of Sciences, Persian Gulf University, Boushehr 75168, Iran; [6]Department of Mathematics and Applied Mathematics, University of Crete, Heraklion, Greece

Introduction

Polymer/solid interfaces are encountered in several important and demanding applications like nanocomposites and thin films. Interfaces are particularly important in graphene-based nanocomposites because of graphene's enormous specific surface area. The goals of our work are threefold: (i) to investigate the effect of tacticity on the interfacial structure and dynamics of stereoregular PMMA chains confined between graphene layers, (ii) to study the effect of temperature on the properties of PMMA/graphene interface, and (iii) provide estimates of the local and overall Tgs of the hybrid model systems and insights into the relations between interfacial structure and Tg.

Methods

Atomistic MD simulations were performed for interfacial PMMA/graphene systems. Samples of i-, a-, and s-PMMA, confined between graphene layers were simulated. Confined model systems consist of 80 PMMA chains, containing 20 chemical repeat units. A single periodic and flexible graphene sheet was placed in the simulation box parallel to the xy-plane, and periodic boundary conditions were used in all three directions. The applied periodic boundary conditions render our model as a multilayered film of PMMA, confined between infinite graphene sheets with layer thickness of about 10 nm. All model systems were studied at different temperatures: 580 K, 550 K, 520 K, and 490 K.. Simulation times were from 0.25 μs to 1.1 μs at each temperature. A snapshot of the simulation box is illustrated in Figure 1.

Results

An interfacial region, with higher local apparent Tg (which has been called Tα for which τ(Tα) = 10 μs) relative to bulk, was observed in the vicinity of graphene, for all PMMA stereoisomers. The interphase thickness, as determined from the perturbation of density and local dynamics, remains almost constant (around 2 nm) in the temperature range studied here. Concerning the effect of tacticity, i-PMMA chains become elongated near graphene, show a better interfacial packing, and have the highest shift of Tα at the interface. While the shift of T α for interfacial adsorbed layers is substantial, the Tα of entire confined films (for which the weight fraction of graphene is about 7 wt %) is not dramatically affected by graphene (particularly for a- and sPMMA).

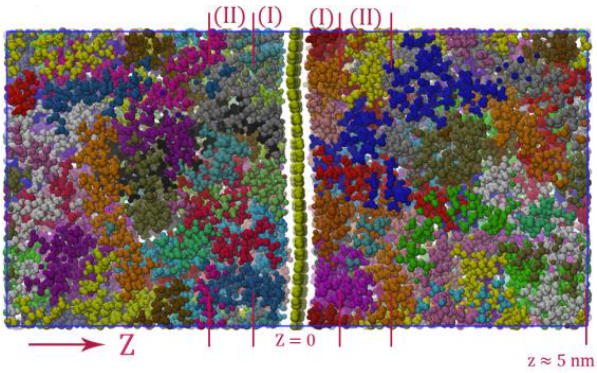

Figure 1 - A (top view) snapshot of the simulation cell. Multiple colours have been used for representing different chains. Interfacial regions around the graphene are also depicted (layers I and II).

Conclusions

(a) i-PMMA shows a better interfacial packing for relative to other stereoisomers. (b) Interfacial dynamics shows a stronger temperature dependence relative to bulk. (c) At very short distances from the surface, a considerable shift in apparent Tg was observed. The effect is more pronounced for i-PMMA.

Acknowledgements

The work has been partly performed under the Project HPC-EUROPA3 (INFRAIA-2016-1-730897), with the support of the EC Research Innovation Action under the H2020 Programme; in particular, the author gratefully acknowledges the support of Department of Mathematics and Applied mathematics, University of Crete, and IACM FORTH and the computer resources and technical support provided by Greek Research & Technology Network (GRNET) in the National HPC facility ARIS.

Note: Please read the published paper in Macromolecules, 2018, 51 (19), pp 7518–7532

MAKING GRAPHENE MORE REACTIVE: THE EFFECT OF CORRUGATION AND SUBSTITUTIONAL DOPING

A.S. Dobrota[1], I.A. Pašti[1], N.V. Skorodumova[2,3]

[1]University of Belgrade - Faculty of Physical Chemistry, Serbia; [2]Department of Materials Science and Engineering, School of Industrial Engineering and Management, KTH, Sweden; [3]Department of Physics and Astronomy, Uppsala University, Sweden

Introduction

In the light of the world's increasing population, pollution, and energy requirements, the need for novel green, renewable energy sources are in the centre of scientific interest of many research groups. Graphene-based materials are considered as good candidates for electrochemical energy conversion and storage applications, including fuel cells, batteries and supercapacitors. While pristine graphene is chemically inert (interacts weakly with species of interest in this field), introduction of defects in graphene alters its electronic structure and reactivity [1–4]. Corrugation of the basal plane was suggested as the main source of enhanced reactivity of O-functionalized graphene [2]. Graphene can often be found in corrugated form, e.g. when grown on a substrate. We focus on the corrugation of the graphene basal plane, the changes in reactivity that in induces, and explore the effects of doping the so corrugated graphene.

Methods

DFT calculations were carried out within the generalized gradient approximation and PBE exchange correlation functional [5] using ultrasoft pseudo-potentials as implemented in the PWscf code of Quantum ESPRESSO distribution [6,7]. The plane wave kinetic energy cutoff was 36 Ry, while the charge density cutoff was 576 Ry. Pristine graphene was modelled in (3√3×3√3)R30o cell with 54 C atoms. The 1. irreducible Brillouin zone was sampled using a Γ-centered 4×4×1 grid of k-points generated by the general Monkhorst-Pack scheme [8]. Convergence with respect to the vacuum layer thickness and the k-point mesh was confirmed. Doped graphene was modelled by substituting one C with dopant atom, resulting in dopant concentration of ~1.85 at%. N was chosen as a dopant of similar atomic size as C, which does not corrugate the plane itself, and P as a larger dopant whose presence induces a topology change. Corrugation was achieved by reduction of the supercell by 1, 3 and 5 % in xy plane, and relaxation of all atoms.

Results

The structures gained by reduction of the dimensions of the graphene layer differ in topology depending on the percentage of the reduction. While reduction of the supercell by 1% leads to very small changes in the structure, and the surface is still flat, reduction by 3 or 5 % results in significant corrugation of the layer and obvious patterned protrusions of carbon atoms from the basal plane (Figure 1). In case of doped graphene, the situation is similar, but the deformation energy is smaller, which means that it is easier to compress doped than pristine graphene. After successfully setting the models of corrugated pristine/doped graphene, we have investigated their reactivity towards adsorbates of electrochemical interest. We have found that while H adsorption on the corrugated all-carbon graphene surfaces leads to big topological changes of the surface (due to strong covalent bond formation), doped graphene surfaces keep their initial structure. Other investigated adsorbates do not disturb any of the surfaces significantly. For these, the reactivity of corrugated graphene does not differ significantly compared to the non-corrugated case. Slight improvements (stronger binding) have been observed in some cases. Sodium, which is of great interest for Na-ion batteries, interacts more strongly with corrugated (adsorption energy −0.81 eV) than flat non-doped graphene (−0.71 eV), while on doped surfaces corrugation does not improve the strength of this interaction.

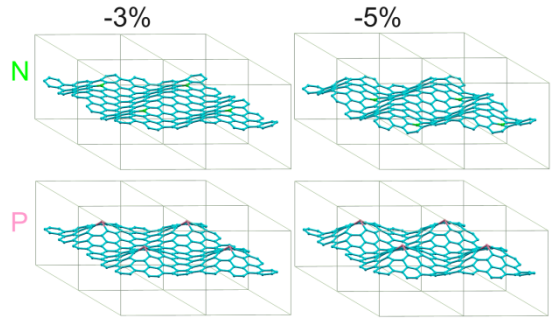

Figure 1 - Models of corrugated doped graphene (compression percentage indicated). Top row: N-doped, bottom: P-doped systems.

Conclusions

The topology of graphene is dependent on the presence of the dopant atoms and layer stress. Compressing the layer is easier in the presence of the dopant atoms. The reactivity of corrugated graphene surfaces depends on the type of dopant atoms present, the level of corrugation, and the type of adsorbate in question.

References

[1] Dobrota A. et al., Electrochim.Acta. 176:1092–1099, 2015. [2] Dobrota A. et al., Phys.Chem.Chem.Phys. 18:6580–6586, 2016. [3] Dobrota A. et al., Phys.Chem.Chem.Phys. 19:8530–8540, 2017. [4] Dobrota A.S. et al., Electrochim. Acta. 250:185–195, 2017. [5] Perdew J. et al., Phys. Rev. Lett. 77:3865–3868, 1996. [6] Giannozzi P. et al., J. Phys. Condens. Matter. 21:395502, 2009. [7] Giannozzi P. et al., J. Phys. Condens. Matter. 29:465901, 2017. [8] Monkhorst H. et al., Phys. Rev. B. 13:5188–5192, 1976.

Acknowledgements

The work has been performed under the Project HPC-EUROPA3 (INFRAIA-2016-1-730897), with the support of the EC Research Innovation Action under the H2020 Programme; in particular, A.S.D. gratefully acknowledges the support of Prof. N.V. Skorodumova and the computer resources and technical support provided by PDC-KTH.

SIMULATION OF STRUCTURES AND SORPTION PROPERTIES OF BORON-PHOSPHOROUS COVALENT ORGANIC FRAMEWORKS DOPED WITH TRANSITION METALS

K. Durka

Warsaw University of Technology, Faculty of Chemistry, Warsaw, Poland.

Introduction

One of the most important challenges in a contemporary material science is an efficient and safe storage of gases such as dihydrogen, methane or carbon dioxide. To this end, various types of novel porous materials have been developed. These include very promising systems termed Metal Organic Frameworks (MOFs) and Covalent Organic Frameworks (COFs).[1] The presence of imine or bipyridyl moieties favour the coordination of Pd (II). Such COFs were used as catalysts in Heck and Suzuki cross-coupling reactions. Until now only N-rich COFs were used as platforms for metal docking, while the phosphorous-based COFs are unknown. In this manuscript I present computational investigation on boron-phosphorous COF materials doped with the metal centres.

Methods

Adsorption equilibria was calculated using GCMC (Grand Canonical Monte Carlo) simulations. Whilst quantum systems occupy many energy eigenstates, GCMC simplifies this by fixing the chemical potential, volume, and temperature, whilst the number of particles fluctuates. All calculations were performed in MUSiC and RASPA software, from which a maximum BET surface area, maximum gas uptake, sorption isotherms were evaluated.

Results

In the first step sorption simulations were performed for referential compound: boron-triazine system that was studied in my previous work [2]. I have found that the sorption in most of the studied systems is by 30% overestimated as compared to the experimental results. The structural model was significantly improved by adding dislocations within the molecular layers, and modelling the surface sorption in single particle of 10 nm x 10 nm x 3 nm size (Figure 2). It seems that the size of the particle is very important in order to properly predict sorption properties of the system. The obtained results are close to the experimental ones.

The studied boron-phosphorous materials were subjected to quantum-chemical geometry optimization using periodic density-functional approach (B3LYP/TZVP level of theory) implemented in the CRYSTAL09 program package. The Palladium centres were docked to each phosphorous atom in agreement with the XPS analysis.

Both materials exhibit type-II sorption isotherms with relatively slow and almost constant increase of sorption in the pressure range of 0.05−0.8 P/P0. They have similar N2 sorption properties which suggests that the porosity is not significantly affected by introduction of Pd coordination centres. Based on the Raspa calculations both materials are also characterized by similar heat of nitrogen absorptions: 8 vs. 10 kJmol-1. In turn, in the case of H2 sorption MUSiC and RASPA calculations revealed the strong tendency for the framework-hydrogen interactions in the case of Palladium-doped structure, which confirm experimental results. The heat of hydrogen adsorption is two times higher in the latter case (5 kJmol-1vs. 10 kJmol-1) which owns mainly to Pd…H2 interaction.

Finally, I have performed similar hydrogen sorption calculations for structures doped with Ni ad Cu. The obtained results show that the Cu-based material is not very promising, while the Ni-doped COF is characterized by very similar parameters as Pd-COF.

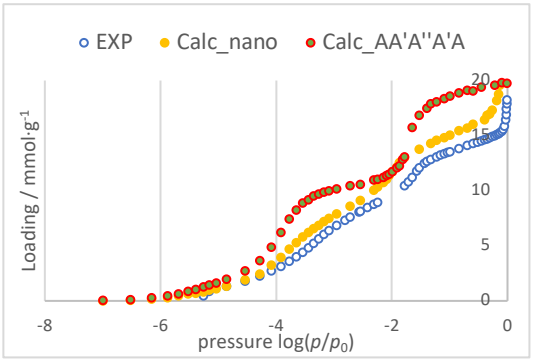

Figure 1 - Comparison of experimentally and theoretically predicted sorption isotherms for N2 at 77K.

Conclusions

In a summary, the project encompasses an interdisciplinary research aiming at the development of boron-phosphorous COFs and corresponding structures doped with transition metal atoms. From the studied systems the most promising are Ni-doped COFs, owing mainly to its good sorption parameters and low price. Therefore, these materials should be now the objects of further research.

References

[1] L. Chun-Yu, Z. Detao, Z. Zhenghang, X. Zhenhai, Adv. Mater. 2018, 30, 1703646. [2] K. Gontarczyk, W. Bury, J. Serwatowski, P. Wieciński, K. Woźniak, K. Durka, S. Luliński., ACS Appl. Mater. Interfaces, 2017, 9, 31129−31141.

Acknowledgements

The work has been performed under the Project HPC-EUROPA3 (INFRAIA-2016-1-730897), with the support of the EC Research Innovation Action under the H2020 Programme; in particular, the author gratefully acknowledges the support of Department of Chemical Engineering at the University of Bath and the computer resources and technical support provided by EPCC.

PREDICTING MAGNESIUM SILICATE NANOCLUSTERS USING MACHINE LEARNING

T. Lazauskas[1], S.M. Woodley[1], T. Macia[2], A. Cuko[2], S.T. Bromley[2,3]

[1]Kathleen Lonsdale Materials Chemistry, Department of Chemistry, University College London, United Kingdom; [2]Departament de Ciència de Materials i Química Física and Institut de Química Teòrica i Computacional (IQTCUB), Universitat de Barcelona, Spain; [3]Institució Catalana de Recerca i Estudis Avançats (ICREA), Barcelona, Spain

Introduction

Nanoclusters, or small nanoparticles, bridge the gap between bulk and the molecular scale and show a strong correlation between their size, morphology, and physical and chemical properties. These materials typically have dimensions below 2–5 nm and are in such size regime that current experimental techniques are insufficient for accurate and comprehensive structure characterisation. This is where computational approaches usefully complement and aid experimental studies to design future materials with desired or new optimal properties.

Nanoclusters of magnesium silicates are of tremendous importance. MgSiO is one of the most relevant families of compounds in both astronomy and geology, and is one of the main components of space dust and it is believed to be one of the major constituents of earth's mantle. Finding the most stable geometries and energies provide new details about the structures and that can be compared with the different bulk minerals, extending the phase diagram with a new variable, size. Even with the latest technological advances this proved to be challenging, thus new techniques, such as Machine Learning (ML) need to be explored.

Our study was split into two phases: in the first phase we have applied well-known methods and techniques to find and analyse MgSiO3 and Mg2SiO4 nanoclusters up to size of 10 structural units (s. u.); whereas, in the second phase we have reused the phase one results to predict the energies and properties of larger size nanoclusters (up to 27 s. u.) by applying ML techniques, namely, artificial neural networks (ANN).

Methodology and Results

During phase one, we have performed searches using global optimisation methods, such as Genetic Algorithm and Basin Hopping, on the interatomic potential (IP) energy surface.

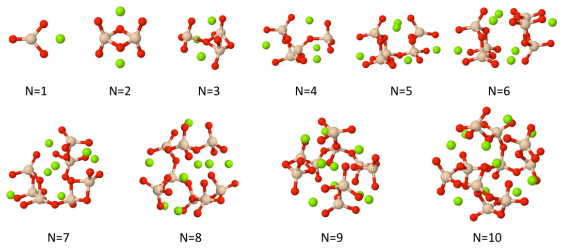

Figure 1 - Tentative global minimum configurations of MgSiO3 for sizes N = 1 – 10.

Then the lowest energy configurations were refined on the more accurate and orders of magnitude more computationally demanding Density Functional Theory (DFT) energy landscape. The resulting configurations (e.g. the most stable MgSiO3 configurations, Figure 1) then were analysed using in-house analysis tools in terms of structural and energetic properties, relative stabilities and mixing energies.

These results also laid the groundwork for the second phase of the project. We have reused the obtained configurations to train the ANN (Figure 2), which, in turn, was used to quickly assess DFT energy for larger size nanoclusters and act as a pre-screener for further DFT optimisation. This allowed us to significantly reduce computational costs by minimising the number of IP structures to be further geometrically optimised with DFT and efficiently investigate nanoclusters of sizes which were previously not accessible.

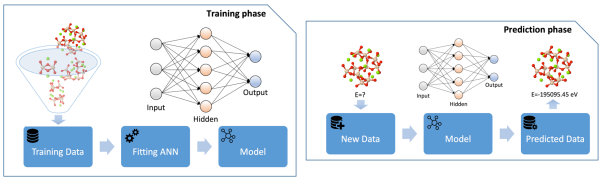

Figure 2 - Schematic representation of the training and prediction phases using ANN.

Conclusions

(The results obtained during this project paved the way for three scientific papers which are currently being finalised, where we discuss structural and energetic evolution of magnesium silicates with size, proposing a technique for machine learning enhanced structure prediction of nanoclusters, and more in-depth analysis of nanocluster configurations compared to experimental results.

This exploratory project also proved that ANN is a very efficient and surprisingly accurate method to be used as a pre-screener while performing searches using global optimisation methods. We recommended a more extensive use of ML techniques for future applications of structure prediction techniques

Acknowledgements

The work has been performed under the Project HPC-EUROPA3 (HPC17A4KQR), with the support of the EC Research Innovation Action under the H2020 Programme; in particular, the authors gratefully acknowledges the support of IQTCUB and the computer resources and technical support provided by BSC-CNS.

DYNAMICAL EFFECT IN THE WETTING OF SUPERHYDROPHOBIC SURFACES

S. Meloni[1], *A.M. Elena*[2]

[1]*Dept. of Chemical and Pharmaceutical Sciences, University of Ferrara, Italy;* [2]*Daresbury Laboratory, Sci-Tech Daresbury, United Kingdom*

Introduction

A textured hydrophobic surface can entrap gas/vapor in its surface corrugations that keeps a liquid deposited on it in a suspended state, also known as the Cassie-Baxter state. This suspended state is characterized by a reduced solid/liquid contact area which brings with it an enhanced hydrophobicity, usually denominated superhydrophobicity. Superhydrophobic surfaces are suitable for many technological applications. Upon the action of an external agent, e.g. pressure, surface textures can get wet and superhydrophobicity is lost.

Identify the mechanism of wetting and the opposite process, recovery, might bring to design more resistant and/or self-recovery surfaces. Wetting and recovery have been studied using only quasi-static methods, such as umbrella sampling, which neglect inertia, a key ingredient of fluid dynamics, including nanofluidics. Here we adapted, implemented and used the Forward Flux Sampling method, FFS, to go beyond the state of the art and identify inertia effects in the wetting and recovery mechanisms of a prototypical corrugation.

Methods

FFS is an algorithm that samples reactive trajectories. The progress of the transition is monitored by the value of an order parameter, here the number of liquid particles in the pore, N(r). A set of l consecutive, non-intersecting interfaces $N(r) = n_i$ is defined to partition the configuration space in regions.

The FFS algorithm consists of two steps. First one evolves one (or more) trajectory initialized in the reactant basin and crossing the first interface n_0. In the second step one evolves many trajectories starting from configurations at n_0 and reaching either n_1 or return back to n_0. The second step can be iterated for the other interfaces. The total transition path is obtained joining the pieces of trajectories between interfaces n_i and n_{i+1}.

Results

Our simulations show surprising results overlooked in the literature, that inertia significantly affects the mechanism of wetting and recovery to the level that the overall picture in presence and absence of inertia changes. In Figure 1 we compare the probability density to observe a difference ΔN of particles in the left and right half of the pore as a function of the overall wetting. One sees that the density is peaked at $\Delta N = 0$ when the pore is half empty and then splits in two branches, corresponding to the formation of a bubble in either the left or right corner of the grove, when more liquid enters into the grove. The splitting is of particular importance as this the configuration corresponds to the transition state, which has been the object of much attention to design textures with tailored properties.

Inertia completely changes the picture: the process starts, proceeds and completes with $\Delta N \sim 0$ all along it. In other words: no bubbles in the corners are formed during the wetting and the transition state corresponds to a configuration with a flat meniscus, that requires a different design of corrugations to prevent wetting.

These results have been recently accepted for publication on Nanoscale of the Royal Society of Chemistry.

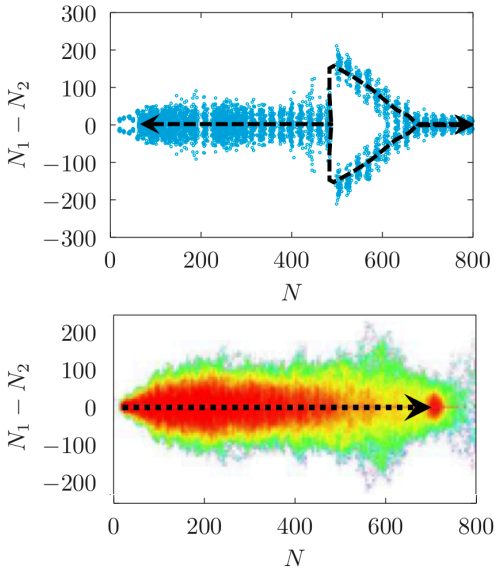

Figure 1 - Mechanism of wetting as obtained from quasi-static methods (top) and FFS (bottom).

Conclusions

We investigated the effect of inertia on the mechanism and kinetics of wetting and recovery of textured surfaces. We have shown that traditional, quasi-static simulation techniques are inadequate at investigating this process, for which one needs to include inertia. Our results open new perspectives for the in silico design of superhydrophobic surfaces and hydrophobic porous systems.

References

[1] Allen R. J. et al, Physical Review Letters, 94:018104, 2005.

Acknowledgements

The work has been performed under the Project HPC-EUROPA3 (INFRAIA-2016-1-730897), with the support of the EC Research Innovation Action under the H2020 Programme; in particular, the author gratefully acknowledges the support of the Daresbury Lab and the computer resources and technical support provided by the EPCC.

UNDERSTANDING THE STRUCTURAL PROPERTIES OF CHITOSAN AND HYALURONIC ACID USING MOLECULAR DYNAMICS SIMULATIONS

M. Kamly, L. Monticelli

Molecular Microbiology and Structual Biochemistry, UMR 5086 CNRS & University of Lyon, France

Introduction

Layer-by-Layer (LbL) deposition technique is a way for producing organic and hybrid organic-inorganic supramolecular assemblies without requiring extensive equipment. However, explaining the behaviour of the polymers in the LbL assembly remains a challenge due to major difficulties in structural characterization of the materials. We are particularly interested in the largescale behaviour of chitosan (CHT) and hyaluronic acid (HA), biocompatible co-polymers used in drug and gene delivery. One useful alternative is the prediction of system properties by MD simulations at large scales, which are at the moment only possible using coarse-grained (CG) models of the polymers. Building CG models for CHT and HA is the main goal of the present project.

Methods

In order to build coarse-grained models of our polysaccharides of interest, three steps are necessary: (a) mapping the all-atom structures to coarse-grained beads; (b) determining the type of beads we need to use, within the MARTINI framework; (c) determine the bonded interactions within each monosaccharide moiety, and then within each possible disaccharide. For the mapping, we will use the same mapping as for all other 6-membered ring sugars already existing in the MARTINI force field [1, 2]. The choice of the MARTINI bead type will be based on chemical similarity with the MARTINI building blocks, and eventually validated based on partitioning calculations (to be carried out in the future). Bonded interactions will need to be determined based on all-atom simulations of the appropriate building blocks. Nine possible dimers exist for chitosan, and four for hyaluronic acid. We built all 13 dimers with the do_glycans script, and simulated them in water using the GROMACS software [3] with standard simulation parameters for the GLYCAM06 force field [4]. In order to sample efficiently all possible relative orientations of the monosaccharides within the dimers, we used Metadynamics [5, 6] with the PLUMED plugin [7] for GROMACS.

Results

The first step in this project was to define the mapping of the disaccharide units, i.e. which atoms correspond to the CG beads. This was done using the general framework of the MARTINI v.3 CG model. Having established the mapping for the CG model, we calculated distribution of pseudo-bonds and pseudoangles from long time scale all-atom MD simulations.

For distributions of pseudo-dihedrals, instead, we used Metadynamics simulations. Some of the resulting distributions are shown in the Figure 1.

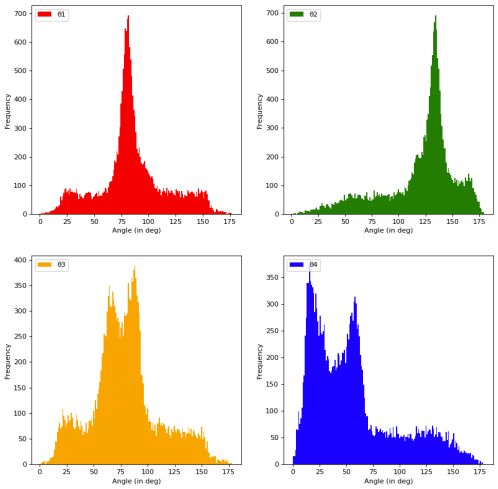

Figure 1 - Angle distribution for N-acetylglucosamine-deprotonated glucuronic acid (building block for HA).

Conclusions

During the HPCE3 project we built all-atom models for disaccharides corresponding to the fundamental units of two biological polymers, CHT and HA (9 and 4 different disaccharide building blocks respectively). We then performed MD and also Metadynamics simulations to sample the rotation around the glycosidic bond. From such simulations it is possible to extract all the information necessary to build a coarse-grained model for much longer polymer chains, which in turn will enable large scale simulations of polymeric materials and their self-assembly – that is the long-term goal of the present project.

References

[1] Marrink SJ, Risselada HJ, Yefimov S, Tieleman DP, & de Vries AH (2007) J Phys Chem B 111(27):7812-7824. [2] Monticelli L, et al. (2008) J Chem Theory Comput 4(5):819-834. [3] Abraham MJ, et al. (2015) SoftwareX 1-2:19-25. [4] Singh A, et al. (2016) Can J Chem 94(11):927-935. [5] Bussi G, Laio A, & Parrinello M (2006) Phys Rev Lett 96(9). [6] Barducci A, Bonomi M, & Parrinello M (2011) Wiley Interdisciplinary Reviews-Computational Molecular Science 1(5):826-843. [7] Bonomi M, et al. (2009) Comput Phys Commun 180(10):1961-1972.

Acknowledgements

The work has been performed under the Project HPC-EUROPA3 (INFRAIA-2016-1-730897), with the support of the EC Research Innovation Action under the H2020 Programme; in particular, the author gratefully acknowledges the support of M. Sammalkorpi (Department of Chemistry and Materials Science, Aalto University) and the computer resources and technical support provided by CSC.

IMPACT OF WC/CO/DIAMOND COMPOSITE WITH PERIDYNAMICS

E. Postek[1], Y. Schneider[2], S. Schmauder[2]

[1]Institute of Fundamental Technological Research, Polish Academy of Sciences, Poland; [3]Materials Testing Institute University of Stuttgart, Germany

Introduction

Metal Matrix Composites (MMCs) are widely used in several strategic industrial sectors, such as defence, aerospace, nuclear power plants, space exploration, being the primary source of technological progress in the others, for example, machining. In this communication, we use a meshless method that is peridynamics for simulation of the impact of a sample. Peridynamics is a nonlocal, meshless quite recently formulated method of stress analysis.

Nonlocal methods were developed for crystal analysis [1], [2]. The peridynamics was formulated for the first time by Silling [3, 4, 5].

Methods

The considered material WC/Co/diamond is a three phases composite. In our model, we assume ideally elastic properties of diamond, ideally elastic with damage criterion properties of WC and elastic-plastic properties of Co phase. The Co phase stands for a matrix in which the WC and diamond phases are introduced. The geometry of the sample is derived from CT-scans [6]. The CT-scan is visible in the top left corner in Fig 1 (a). The phases WC and diamond are shown in Figure 1 (a). The rest of the sample is the Co phase. The CT-scan was transformed into tetrahedrals with Simpleware program [7]. Then, the tetrahedral mesh was transformed into the peridynamics format. To perform the simulations, we use highly parallelized program PERIDIGM program from SANDIA Lab [7, 8].

Results

The discretization is done with 1663535 points. The material properties of the diamond are: Young's modulus 1210E+08 Pa, Poisson's ratio 0.22 and density 3440.0 kg/m3, the material is ideally elastic. The material properties of WC are Young's modulus 6.86E+11 Pa, Poisson's ratio 0.22, density 15880 kg/m3 and critical stretch 0.0005. The elastic-plastic Co material properties are Young's modulus 211.0E+09 Pa, Poisson's ratio 0.296, density 9130.0 kg/m3, yield stress 460.0E+06 Pa and hardening modulus 500.0E+07 Pa. The calculations needed 960 processes. An average run was about 900 sec. We did the scaling analysis of the problem up to 960 processes. It appeared very good.

In this example, the sample hits the rigid obstacle with the velocity of 150 m/s downwards. We could observe the stress and strain, equivalent plastic strain and damage parameter development in the course of the impact process. Exemplary results are shown in Figure 1(b). We observe the distribution of equivalent plastic strain in the Co phase at the end of the impact process. The equivalent plastic strain is higher close to the inclusions of WC and diamond.

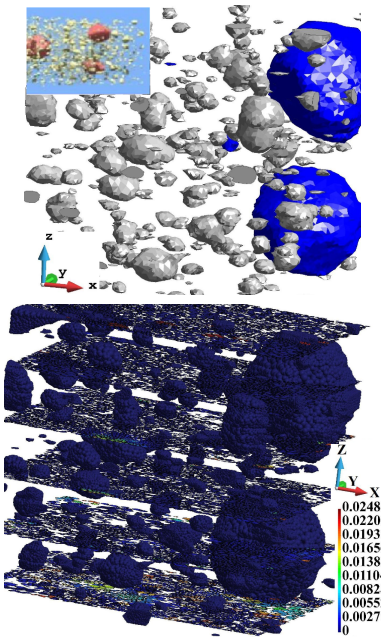

Figure 1 - CT-scan, WC and Diamond grains embedded in Co matrix (a); Equivalent plastic strains in horizontal cross-sections of the Co matrix (b).

Conclusions

We present a flow of calculations of a three-phase material WC/Co/diamond along with results of damage, plastic strains and Mises stresses. We found the PERIDIGM system very feasible to the analysis. Further research will focus on crack initiation in such kinds of composites.

References

[1] Rogula D., Nonlocal theory of material media, Springer, Wien, New-York, 1982. [2] Kunin A., Elastic media with microstructure, one dimensional models, Springer, Berlin, Heidelberg, New-York, 1982. [3] Silling SA., J. Mech. Phys. Solids, 48: 175-209, 2000. [4] Silling SA et al., Comput. Struct., 83:1526-1535, 2005. [5] Silling SA et al., J. Elasticity, 88:151-184, 2007. [6] Crostack H., In Proc. of SPIE, U. Bonse, Ed., 63181:63181A–1–63181A–12, 2006. [7] https://www.synopsys.com/simpleware.html [8] Mitchell JA., Sandia report, SAND2011-3166, 2011. [10] Parks ML et al., Peridigm Users'Guide, Tech. Report SAND2012-7800, Sandia National Laboratories, 2012.

Acknowledgements

The work has been performed under the Project HPC-EUROPA3 (INFRAIA-2016-1-730897), with the support of the EC Research Innovation Action under the H2020 Programme; in particular, the authors gratefully acknowledge the support of the Materials Testing Institute University of Stuttgart and the computer resources and technical support provided by HLRS.

ATOMISTIC SIMULATION OF CO2–POLYSTYRENE SYSTEMS

E. Ricci[1], N. Vergadou[2], G. Vogiatzis[3], M.G. De Angelis[1], D.N. Theodorou[4]

[1]Department of Civil, Chemical, Environmental and Materials Engineering, University of Bologna, Italy; [2]Institute of Nanoscience and Nanotechnology, NCSR Demokritos, Athens, Greece; [3]Department of Mechanical Engineering, Eindhoven University of Technology, Netherlands; [4]School of Chemical Engineering, National Technical University of Athens, Greece

Introduction

Molecular simulations are nowadays routinely employed to gain insight into the microscopic structure and dynamics of dense amorphous polymers, and to predict a wide range of properties of these materials. In this work, molecular simulation was applied to the study of CO2 solubility in atactic polystyrene. The effects of the molecular weight of the polymer as well as that of CO2 concentration at different temperatures were investigated.

Methods

The present study focused on atactic polystyrene (a PS) systems of different molecular weight (Mw), ranging between 2100 and 31200 g/mol. The systems were studied in a fully atomistic representation [1]. Initial configurations at low Mw were generated using the Rotational Isomeric State model, as modified by Theodorou and Suter [2], and were equilibrated using long Molecular Dynamics (MD) simulations. The higher Mw systems were generated and equilibrated at all length scales through a procedure consisting of coarse graining, equilibration via connectivity-altering Monte Carlo simulations at the coarse-grained level, and reverse mapping to the atomistic representation [3]. The bulk polymer structures were loaded with CO2 at various concentrations and MD simulations were performed to equilibrate the gas-polymer mixture systems.

The Henry law constants were calculated in the infinite dilution regime. Sorption isotherms of CO2 in each a-PS system were determined using an iterative scheme [4], consisting of series of MD simulations in the NPT ensemble and the Widom test particle insertion method [5], to ensure consistency between CO2 fugacity in the gas phase and in the gas-polymer mixture, at fixed gas concentration. The effects of temperature and CO2 concentration on the structure and segmental dynamics of the polymer were studied.

Results

In figure 1, the sorption isotherms of CO2 in the higher Mw system inspected are shown at three temperatures, ranging from 450 K to 550 K. In all the systems, the expected temperature and molecular weight dependencies were captured, and the results compared well with experimental data available at a similar temperature. In the presence of CO2 at high concentration, a significant acceleration of the segmental dynamics of the polymer occurred, which, at the macroscopic level, translates into the so-called “plasticization effect”. It was observed that this effect was significantly less pronounced in the high Mw system, whereas the more mobile low Mw system was more easily affected. Moreover, it was uncovered that the increased mobility is not limited to the chain ends, but the presence of the gas affects the whole chain to a similar extent.

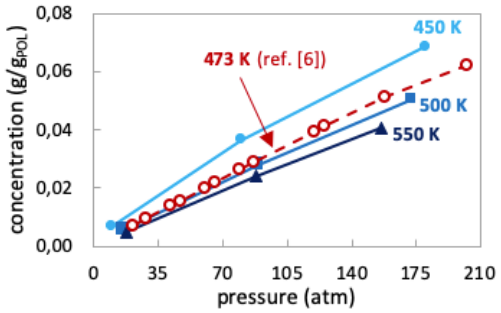

Figure 1 - Simulated sorption isotherms of CO2 in a-PS (Mw 31200 g/mol) at 450 K, 500 K and 550 K, compared with experimental data at 473 K from ref. [6]

Conclusions

A polymeric system containing a plasticizing agent was studied by means of molecular simulations. The effect of temperature and Mw on gas solubility were correctly represented and the results were in agreement with experimental data. Moreover, the effect of the gas concentration on the local dynamics of the polymer was studied. Plasticization and volume dilation effects were quantified, relating the microscopic mechanisms to the corresponding the macroscopic properties of the systems.

References

[1] Ndoro T. et al., Macromolecules, 44:2316-2327, 2011. [2] Theodorou D.N. et al., Macromolecules, 19:139-154, 1986. [3] Vogiatzis G.G. et al., Macromolecules, 47:387-404, 2014. [4] Spyriouni T. et al., Macromolecules, 44: 1759-1769, 2009. [5] Widom B. et al., J. of Chem. Phys., 39:2808-2812,1963. [6] Sato Y. et al., J. of Supercritical Fluids, 19:187-198, 2001.

Acknowledgements

The work has been performed under the Project HPC-EUROPA3 (INFRAIA-2016-1-730897), with the support of the EC Research Innovation Action under the H2020 Programme; in particular, Eleonora Ricci gratefully acknowledges the support of Niki Vergadou of the NCSR Demokritos and the computer resources and technical support provided by GRNET.

FORCE FIELD DEVELOPMENT FOR GA/SC-DOPED LLZO SOLID ELECTROLYTE

M. Rincon Bonilla[1], E. Akhmatskaya[1], H. Fruchtl[2], T. van Mourik[2]

[1]Basque Center for Applied Mathematics, Bilbao, Spain; [2]School of Chemistry, University of St Andrews, United Kingdom

Introduction

Li-ion batteries are today's gold standard for reversible energy storage. However, current designs rely on highly flammable organic liquid electrolytes, limiting their range of use in electric vehicles and stationary energy storage systems. In contrast, solid electrolytes do not suffer from such safety issues. Moreover, their excellent stability could enable metallic Li to replace graphite as the negative electrode, potentially providing high energy density and long cycle life. Currently, $Li_7La_3Zr_2O_{12}$ (LLZO) garnet constitutes the most promising solid electrolyte due to its outstanding conductivity and stability. So far, the highest reported conductivity is achieved when Ga and Sc are simultaneously doped in the Li^+ and Zr^{4+} sites of LLZO, respectively. Nonetheless, the optimal proportion of these ions is unknown, and experimental exploration is expensive and time consuming. In this project, we developed a database of ab initio-based configuration which allowed us to fit an accurate atomistic force-field of the system at hand. The force-field will be combined with advanced simulation techniques to estimate the concentrations of Ga and Sc that maximize ionic conduction.

Methods

Dual substitution with Ga^{3+} and Sc^{3+} in the Li^+ and Zr^{4+} sites of LLZO, respectively, was shown to yield a conductivity of 1.8 mS/cm [1]. Buannic et al. fixed the content of Ga^{3+} at 0.15 (the content leading to the experimental conductivity maximum for Ga-doped LLZO) and varied the content of Sc^{3+}. Likewise, we set the amount of Ga^{3+} to 0.15, and optimized the structure of Ga/Sc-doped LLZO (shown in Figure 1a) for the following set of concentrations: 0.0625, 0.125, 0.1875 and 0.25. The concentrations are such that all experimentally tested values are included. LLZO has partially occupied Li+ sites. Moreover, Sc^{3+} and Ga^{3+} can be doped in many combinations at any given stoichiometry. Hence, there is an enormous number of possible structures available at each concentration. To select a suitable structure, we randomly sampled 200.000 Li^+/vacancies/Sc^{3+}/Ga^{3+} combinations at each concentration and selected the 3 structures with the lowest electrostatic energy. The selected structures were optimized using the plane wave electronic calculations suite Quantum Espresso, and the resulting atom positions, energies, forces and stresses recorded. This task was performed at EPCC due to the high computational load involved (each system is 192 – 384 atoms in size, which is considered quite large for this kind of computation). The data generated was assembled as a reference database, in order to fit an analytical, atomistic force field of the composite system. To this effect, the force-matching algorithm coupled with an evolutionary optimization technique was employed, as implemented in the software potfit. Once the force field is extensively validated (future work), a battery of atomistic simulations will be performed for a wide range of Sc^{3+}/Ga^{3+} concentrations.

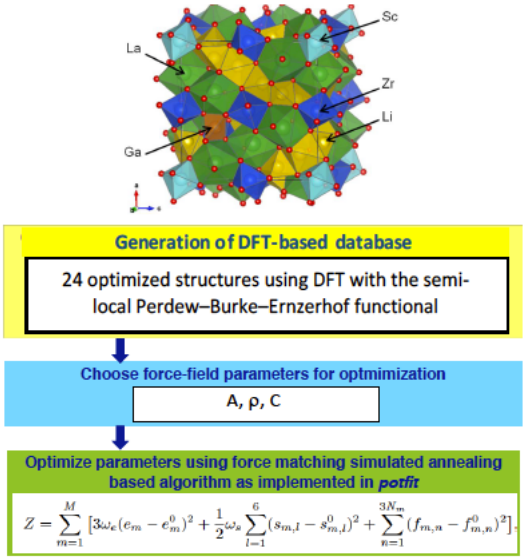

Figure 1 - (a) Structure of Ga/Sc-doped LLZO. (b) Methodology for generation of atomistic force-field.

Results and Conclusions

We have obtained a database of configurations for Ga/Sc-doped LLZO. The database was used to fit a forcefield of the form in eq. (1) according to the methodology described in Figure 1b:

$$V(r) = Aexp\left(-\frac{r}{\rho}\right) - \frac{C}{r^6} \qquad (1)$$

A, r and C are the fitting parameters (Figure 1b). We have found that the set of parameters reported in Table 1 match the energy, forces and stresses determined from the DFT simulations.

Pair	A(eV)	ρ(Å)	C(eV Å^6)
$Li^{0.56+}$-O $O^{1.2-}$	1123.86	0.22	0.000
$Ga^{1.7+}$-O $O^{1.2-}$	500.00	0.32	0.005
$Zr^{2.5+}$-O $O^{1.2-}$	500.00	0.37	0.141
$Sc^{2.0+}$-O $O^{1.2-}$	1210.84	0.30	0.036
$O^{1.2-}$-O $O^{1.2-}$	500.45	0.27	0.00
$La^{1.8+}$-$O^{1.2-}$	559.62	0.37	0.023

Table 1 - Force field parameters for the Ga/Sc-doped LLZO system.

References

[1] Buannic et al., Chem. Mater. 2017, 29, 1769-1778.

Acknowledgements

The work has been performed under the Project HPC-EUROPA3 (INFRAIA-2016-1-730897), with the support of the EC Research Innovation Action under the H2020 Programme; in particular, the author gratefully acknowledges the support of Tanja van Mourik at the University of St Andrews and the computer resources and technical support provided by EPCC.

INTRUSION AND EXTRUSION PROCESSES IN NANOPOROUS MATERIALS AS A NOVEL ENERGY STORAGE TECHNIQUE

M. Tortora[1], *S. Meloni*[2]

[1]*Dipartimento di Ingegneria Meccanica e Aerospaziale, Università di Roma La Sapienza, Italy;* [2]*Dipartimento di Scienze Chimiche e Farmaceutiche, (DipSCF), Università degli Studi di Ferrara (Unife), Italy*

Introduction

The general subject of this project is to investigate the storage of energy as interface energy through the intrusion/extrusion of a non-wetting liquid in a suitable porous material, e.g. water in a hydrophobic system: energy is stored during the charging process, when the non-wetting liquid is forced to intrude into the pores of the solid, and it is released upon spontaneous extrusion when the application of external pressure is ceased. The main objective is to determine empirical and more fundamental relations among the chemistry and morphology of the cavities of these materials, their intrusion pressure and their pressure hysteresis, i.e. a measure of the energy dissipated between the intrusion and extrusion processes. Our aim is to acquire a good working knowledge which would allow to design new smart materials with tailored properties, and, in turn, innovative devices based on them. During this first phase of the project, we studied via MD the intrusion/extrusion of water into/from a toy model of the Cu2L, a Metal-Organic Framework (MOF) which experimentally exhibits almost null hysteresis.

Methods

Our model of the Cu2L was built by carving it out a LJ solid, so it places in-between a fully atomistic model and a continuum one. As showed in Figure 1, the unit cell is characterized by two major cylindrical holes, with a circular and an elliptic section respectively, alternating on the xy-plane, as well as two smaller elliptic cylindrical holes on the sides. Restrained Molecular Dynamics (RMD) was employed to study the intrusion/extrusion of water into this system.

RMD allowed to calculate the Landau free energy Ω when a certain number of water molecules is forced into a pore of the Cu2L model. The Landau free energy quantifies the probability of a given configuration to happen; hence, comparing the probabilities, i.e. looking at the trend of the free energy, one is able to say if a given process is spontaneous, is hindered by an energy barrier, or can even take place. The free energy was computed for the circular pore and the major elliptic pore separately, and, in both cases, for the external pressure ranging from 0 MPa to 1 GPa.

Results

The free energy profiles are shown in Figure 2. They reveal that: since the free energy is monotonically increasing with respect to the number of water molecules forced inside, the circular pore is never wet at the considered pressures; on the other hand, the (major) elliptical one is intruded at some point when Pext is between 500 MPa and 1 GPa, when the free energy starts to exhibit a minimum. In other words, the major elliptical pores seem to play the only role in the intrusion/extrusion processes. Analyzing the MD trajectories, it turned out that the pores on the sides are never wet (at the analyzed pressures).

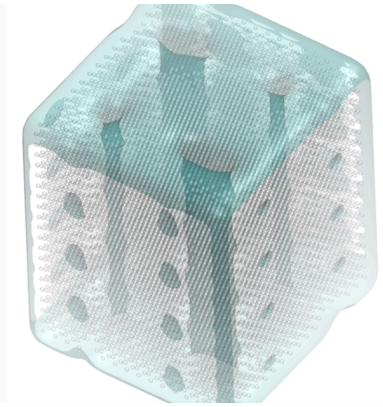

Figure 1 - Unit cell of our Cu2L model.

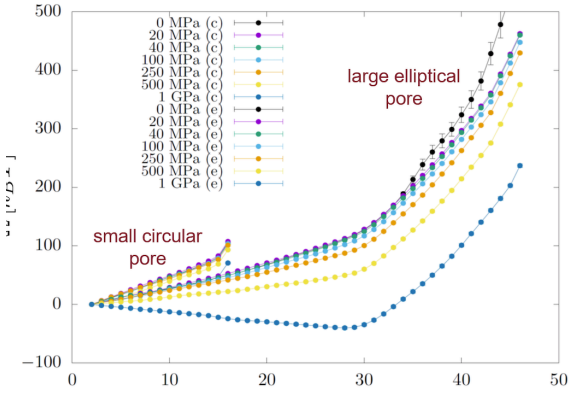

Figure 2 - Free energy profiles for the intrusion/extrusion process at different pressures.

Conclusions

Even though the obtained results are intriguing, we are at the beginning of our research and many paths still need to be explored. The next step will be to confront our predictions with the experimental data in order to better tune our model and, possibly, enrich it.

References

[1] Tinti A. et al., Intrusion and extrusion of water in hydrophobic nanopores, Proceedings of the National Academy of Sciences Journal, vol. 114, Nov. 2017.

Acknowledgements

The work has been performed under the Project HPC-EUROPA3 (INFRAIA-2016-1-730897), with the support of the EC Research Innovation Action under the H2020 Programme; in particular, the author gratefully acknowledges the support of the Science and Technology Facilities Council (STFC) and the computer resources and technical support provided by ARCHER.

LARGE-SCALE MOLECULAR DYNAMICS SIMULATIONS OF THE SELF-ORGANIZATION IN SOFT MATTER

F.D. Tsourtou[1], R. Apostolov[2] and V.G. Mavrantzas[1,3]

[1]Department of Chemical Engineering, University of Patras, Greece & FORTH-ICE/HT, GR 26504, Patras, Greece; [2]KTH Royal Institute of Technology, Stockholm, Sweden; [3]ETH Zürich, Department of Materials, Polymer Physics, Switzerland

Introduction

Polymer semiconductors based on thiophenes and polypeptides are soft materials whose macroscopic behaviour is dictated by chain self-organization at the nano-scale. High-molecular weight regioregular Poly(3-alkylthiophenes) (or rr-P3HTs) with more than 100 monomers per chain exhibit a semicrystalline structure, in which crystalline and amorphous phases coexist. Recently, experiments indicated that the chain packing of this embedded amorphous phase is of critical importance for the efficient charge transport properties [1]. On the other hand, the helix arrangement is considered as the typical secondary structure of polypeptides based on alanine (Ala) residues. An experimental study has currently revealed that melts of poly-L-alanine display helical and beta-sheets conformations [2].

The successful simulation of the morphology of these two systems sheds light into the deep understanding of the structure-property relationship on polypeptide folding mechanism as well as on the performance of optoelectonic devices, in which rr-P3HTs find applications. Hence, in the framework of the HPC-EUROPA3 project, we carry out atomistic Molecular Dynamic (MD) simulations of melts with large rr-P3HT and poly-L-Ala systems for the study of the dependence of thermodynamic and conformational properties (e.g., the density, the radius of gyration, the dihedral distributions, the pair correlation function, etc.) on molecular weight and temperature.

Methods

All MD simulations were carried out by using efficiently the case-specific tools of GROMACS package in the NPT statistical ensemble and for P = 1 atm. Large rr-P3HT systems containing 40, 90 and 150 monomers per chain (e.g., up to 810,432 atoms for 150-rr-P3HT) were simulated at T = 700 K (above the melting point) by applying a promising atomistic force field [3]. The carbon-hydrogen bonds distances were constrained with the LINCS algorithm and a timestep of 1.5 fs was used. A preliminary simulation of poly-L-Ala system consisting of 42 chains with 30 residues per chain at T = 600 K was executed by using Amber94 force field. In all cases, electrostatic interactions were calculated using the Particle-mesh Ewald method. All computational resources offered by the HPC-EUROPA3 program were used.

Results

Large-scale production MD simulations of the amorphous phase of rr-P3HT systems were carried out after a benchmarking evaluation on Beskow computing system of KTH-PDC center. The analysis of the trajectories included the dependence of the density (ρ), radius of gyration (<Rg2>) and persistence length (lp) on chain length (n) and is presented in Table 1. Apparently, only the mean-square radius of gyration is strongly dependent on the n as it increases with the elevation of the n. Our results are in a good agreement with the available literature data and are going to be published in future. As far as the simulation of poly-L-Ala melts is concerned, an optimal scheme of input data was selected and an emphasis was given on the efficient use of the post-processing modules of GROMACS package for the calculation of the hydrogen bonding degree and the Ramachandran plots.

n	ρ (g cm^{-3})	$\langle R_g^2 \rangle$ (Å^2)	l_p (Å)
40	0.777 ± 0.005	835 ± 19	20.6 ± 0.3
90	0.780 ± 0.003	2163 ± 31	21.1 ± 0.3
150	0.784 ± 0.001	3630 ± 30	20.7 ± 0.3

Table 1 - NPT MD simulation results for the density, the mean-square radius of gyration and the persistence length as a function of the rr-P3HT chain length at T = 700 K and P = 1 atm.

Conclusions

The computational resources offered by HPC-EUROPA3 program tremendously contributed to the successful completion of large-scale production simulations of long-length rr-P3HT chains. In addition, advice and recommendation by the host researcher were highly valuable and appreciated. The interactions opened opportunities for a forthcoming publication and the extension of our collaboration work with Dr. Rossen Apostolov.

References

[1] Noriega R. et al., Nat. Mater., 12(11):1038-44, 2013. [2] Floudas G. et al., Macromol. Rapid Commun., 30(4-5):278-298, 2009. [3] C. Poelking et al., Macromolecules, 46(22): 8941-56, 2013.

Acknowledgements

The work has been performed under the Project HPC-EUROPA3 (INFRAIA-2016-1-730897), with the support of the EC Research Innovation Action under the H2020 Programme; computer resources and technical support were provided by SNIC and PDC Centre for HPC at KTH Royal Institute of Technology; application experts support received by BioExcel Centre of Excellence. A special gratitude is given to Dr. Rossen Apostolov at KTH Royal Institute of Technology, Stockholm, Sweden for his constantly guidance and support.

A NEW PARALLEL MONTE CARLO METHOD FOR SOLVING FRACTIONAL PARTIAL DIFFERENTIAL EQUATIONS

J.A. Acebrón[1], R. Spigler[2]

[1]Department of Information Science and Technology, ISCTE - University Institute of Lisbon, Portugal; [2]Department of Mathematics and Physics, Roma Tre University, Italy

Introduction

Nowadays one of the most popular ways to exploit parallelism to solve numerically partial differential equations (PDE) is given by several kinds of numerical methods based on domain decomposition. However, implementing such a technique in HPC supercomputers gives rise to important problems concerning scalability and fault-tolerance of the associated parallel algorithms. In fact, it has been observed in many chances the lack of scalability and fault-tolerance when the number of cores involved are sufficiently large due mainly to the heavy inter-communication overhead. In the last few years, a new alternative was proposed based on novelty probabilistic methods. In short, the idea consists of generating only few interfacial values along a given possibly artificial interfaces inside the domain using a Monte Carlo method, obtaining approximate values interpolating on such interfaces, and then use such values as boundary data in order to split the original problem into fully decoupled subproblems. The method was called "probabilistic domain decomposition" method (PDD) [1], since it combines the two main ingredients, a probabilistic approach for the interfaces, and the classical domain decomposition.

The main aim of this three weeks research stay was to start a collaboration within the goal of developing algorithms for solving fractional differential equations (FPDEs) using probabilistic numerical methods conveniently generalized for dealing now with FPDEs as the core of a PDD algorithm.

Methods and Results

In the following, the most important results accomplished during the stay as well as the methods used so far are summarized:

Boundary value problems for FPDEs. While solving purely initial-value problems seems to be to some extent tractable, the case of boundary-value problems is quite different, and it was observed that the results depends strongly on the definition of the fractional derivative used so far. For this purpose, it was discussed and implemented two different numerical algorithms based on Monte Carlo, using the so called spectral fractional Laplacian. During this stay it was learnt that the spectral fractional Laplacian operator with Dirichlet boundary conditions is the generator of a suitable subordinate stopped Brownian motion. Therefore, it can be derived a generalized Feynman-Kac formula, where the corresponding Brownian motion is now replaced by a subordinate stopped Brownian. Since the solution is computed through an expected value of a given finite sample, whose elements are independent from each other, it becomes easily to parallelize. The parallelization was done mainly porting an existing sequential code to OpenMP, and some benchmarks was already run to test the scalability of the algorithm, showing in general a good scalability of the code.

New applications of FPDEs. Among the many applications already shown in the literature in the last few years, during this visit it was also analyzed the collective phenomenon of synchronization of a large population of nonlinear oscillators, driven by Levy fight processes [2]. The problem can be described mathematically by the so-called Kuramoto model [3], and essentially in the thermodynamic limit consists in a nonlinear fractional Fokker-Planck equation. More specifically, it was analyzed the properties of such model, in particular existence itself and stability of the incoherence solution, as well as bifurcation diagrams, and the existence of stationary synchronized solitons. This has been done numerically as well implementing a code, which has been conveniently parallelized following the ideas discussed previously.

Conclusions

For the specific case of the Kuramoto model subject to a Levy noise a remarkable finding observed, it was that unexpectedly the degree of synchronization of the population can be improved in presence of the Levy noise, attaining levels far beyond what it was observed when the classical random Gaussian noise was considered.

References

[1] J.A. Acebrón, M.P. Busico, P. Lanucara, and R. Spigler, “Domain Decomposition solution of elliptic problems via probabilistic methods”, SIAM J. Sci. Comput. 27 (2005) 440-457n. [2] V. Zaburdaev, Sn Denisov, and J. Klafer, “Lévy walks”, Rev. Mod. Phys. 87 (2015) 483-530. [3] J.A. Acebrón, L.L. Bonilla, C.J. Pérez-Vicente, F. Ritort, and R. Spigler, “The Kuramoto model: A simple paradigm for synchronization phenomena”, Rev. Mod. Phys. 77 (2005) 137-185.

Acknowledgements

The work has been performed under the Project HPC-EUROPA3 (INFRAIA-2016-1-730897), with the support of the EC Research Innovation Acton under the H2020 Programme; in particular, the author gratefully acknowledges the support of Prof. Renato Spigler, Department of Mathematics, Università “Roma Tre” and the computer resources and technical support provided by CINECA.

DEVELOPMENT OF DISTRIBUTED LINEAR SYSTEM SOLVERS IN THE TNL LIBRARY

J. Klinkovský

Department of Mathematics, FNSPE CTU in Prague, Czech Republic

Introduction

TNL (Template Numerical Library, see www.tnl-project.org) is a highly efficient general-purpose numerical library which can be used for scientific computations ranging from compositional flow in porous media to processing of medical data. The library supports computations on a single node which run either on the CPU or they are accelerated using GPU. Support for MPI computations in the library is being developed, TNL already provides distributed grids for basic computations on clusters. In this project we developed all necessary data structures for distributed linear algebra and implemented several distributed solvers for large linear systems based on preconditioned Krylov methods.

The main aim of this three weeks research stay was to start a collaboration within the goal of developing algorithms for solving fractional differential equations (FPDEs) using probabilistic numerical methods conveniently generalized for dealing now with FPDEs as the core of a PDD algorithm.

Methods

Krylov methods are iterative methods commonly used to solve large, sparse linear systems. They are based on the construction of an orthogonal basis of a Krylov subspace for given matrix A and vector v [1]. To implement a distributed solver based on a Krylov method, distributed variants of common data structures are needed. In the TNL library, we implemented data structures called DistributedArray, DistributedVector, and DistributedMatrix that can utilize any sparse matrix format implemented in the library. Furthermore, an efficient implementation of distributed operations such as scalar product or sparse matrix-vector multiplication is essential for Krylov methods.

The efficiency of sparse matrix-vector multiplication is strongly affected by the matrix sparsity pattern. Our implementation is based on reordering of the matrix using the reverse Cuthill-McKee method [2] and then solving the reordered system. This method leads to a banded sparsity pattern, so only neighbouring nodes need to communicate with each other and the communication can be fully overlapped with the computation on local rows of the matrix.

Results

The solvers developed were tested on linear systems arising from the MHFEM discretization of two-phase flow in porous media on unstructured tetrahedral meshes. The problem setup corresponds to the generalized McWhorter-Sunada problem in 3D with parameters described in [3]. For the largest problem available, the solver using the GMRES method and block ILU(0) preconditioner exhibits good scalability up to about 32 nodes and then the performance drops rapidly, see Table 1. Similar behaviour was observed also with other methods and preconditioners during the project duration. With the help of the CINECA User Support team, we were able to run a limited number of benchmarks after the project ended and they do not exhibit such behaviour, which indicates that the problem was caused by a temporary hardware or cluster configuration problem.

Nodes	Time [s]	Efficiency [-]	Iterations
1	371	1.00	440
2	163	1.14	389
4	79.1	1.17	400
8	40.2	1.15	407
16	20.1	1.15	413
24	13.8	1.12	422
32	9.96	1.16	405
40	22.6	0.41	450
48	21.8	0.35	555
56	15.1	0.44	421
64	13.9	0.42	456

Table 1 - Comparison of the computational time, parallel efficiency and iterations of the GMRES method on different number of nodes.

Conclusions

In the project we successfully implemented all planned data structures for distributed linear algebra in the TNL library and several distributed linear system solvers based on Krylov methods and Jacobi or block ILU(0) preconditioners. The benchmarks performed show good parallel scalability and the implementation based on the TNL library has potential to support even computations on GPU-accelerated clusters, although this was not tested as part of this project.

References

[1] Y. Saad, Iterative methods for sparse linear systems, SIAM, 2003. [2] E. Cuthill, J. McKee, Reducing the bandwidth of sparse symmetric matrices, Proceedings of the 1969 24th national conference, ACM, 1969, pp. 157-172. [3] R. Fučík, J. Klinkovský, J. Solovský, T. Oberhuber, J. Mikyška, Multidimensional mixed-hybrid finite element method for compositional two-phase flow in heterogeneous porous media and its parallel implementation on GPU, Computer Physics Communications, 2018.

Acknowledgements

The work has been performed under the Project HPC-EUROPA3 (INFRAIA-2016-1-730897), with the support of the EC Research Innovation Action under the H2020 Programme; in particular, the author gratefully acknowledges the support of the computer resources and technical support provided by CINECA.

MHFEM WITH BDDC FOR TWO-PHASE FLOW IN POROUS MEDIA IN 2D AND 3D

J. Solovský[1], R. Fučík[1], J. Šístek[2]

[1]Faculty of Nuclear Sciences and Physical Engineering, Czech Technical University in Prague, Prague, Czech Republic; [2]Institute of Mathematics, Czech Academy of Sciences, Prague, Czech Republic

Introduction

This paper focuses on the parallel implementation of a numerical method based on the mixed-hybrid finite element method (MHFEM). The parallel approach is based on the domain decomposition method with non-overlapping subdomains, which leads to the iterative solution of the Schur complement system. To improve the convergence of the iterative solver, the balancing domain decomposition based on constraints (BDDC) preconditioner [1, 2, 3] is employed in this work. We show the parallel implementation using MPI and highlight the critical parts of the algorithm. The parallel implementation in 2D and 3D is benchmarked and its speed–up and efficiency are computed.

Methods

The MHFEM-based numerical scheme with semi-implicit time discretization in detail described in [4] is used to discretize the underlying system of PDE describing the benchmark two-phase flow problem in porous media (the McWhorter and Sunada problem). As a result single large sparse linear system needs to be solved in each time step. The domain decomposition approach is employed to solve this system.

The whole computational domain is divided into N nonoverlapping subdomains. The local part of the original matrix can be assembled comprising the unknowns located in the given subdomain. Unknowns in each subdomain can be divided into two groups – those located at the interior and those located at the interface. We can reorder the equations and unknowns in each local matrix (first the interior unknowns, then the interface ones) to obtain a block partition of the matrix. The local part of the Schur complement is then obtained by eliminating the interior unknowns.

The Schur complement of the original matrix can be formally assembled from these local parts, but this is not done in the computation. Instead, the computation with the sub-assembled Schur complement is performed consisting of solving local problems and combining the results on the interface which can be efficiently done in parallel. The BDDC preconditioner is used to accelerate the convergence of the BiCGStab iterative method used to solve the system with the Schur complement matrix. The preconditioner consists of the local and global step. The local step can be easily parallelized, the global step requires the information from all the subdomains. In this work, the global problem is solved redundantly by each processor. This limits the number of subdomains that can be handled efficiently. The multilevel BDDC [2] can be used to overcome this limit, but this is beyond the scope of this work.

Results

Strong scalability test was performed both in 2D and 3D. All computations were run on the GALILEO cluster at CINECA with nodes equipped with two 18-core Intel Xeon E5-2697 v4 @ 2.30GHz processors and 128 GB RAM. Speed-up (S) and efficiency (Eff) are shown in the following table.

2D	Number of subdomains					
	16		64		256	
DOFs	S	Eff	S	Eff	S	Eff
178648	12.03	75.15%	40.70	63.60%	-	-
712226	11.81	73.80%	52.15	81.48%	171.09	66.83%
2841928	-	-	69.32	108.31%	185.57	72.49%
11358566	-	-	-	-	175.91	68.72%

3D	Number of subdomains					
	8		64		216	
DOFs	S	Eff	S	Eff	S	Eff
973750	6.80	85%	55.45	86.65%	34.72	16.01%
7807218	-	-	79.99	124.99%	161.97%	74.99%

Conclusions

The BDDC method customized for solving two-phase flow problems in porous media in 2D and 3D is presented. Th BDDC method is described together with its parallel implementation and its performance is demonstrated usin the benchmark problems of two-phase flow in porous media in 2D and 3D. The results of the strong scalability test presented in the paper show that for the 2D case, the parallel implementation preserves high efficiency for the increasing number of CPU cores. In the more complicated 3D case, with a fine mesh, the implementation preserves high efficiency for the increasing number of CPU cores used. For the coarse mesh in 3D, the efficiency decreases for the increasing number of processes. This can be attributed to subdomain problems getting too small for the strong scalability test. For certain setups both in 2D and 3D, the efficiency of the parallel implementation exceeds 100 %.

References

[[1] Dohrmann C. R., A Preconditioner for Substructuring Based on Constrained Energy Minimization, SIAM Journal of Scientific Computing 25 (2003) 246258. [2] Soused k B., Š stek J., Mandel J., Adaptive-ík B., Šístek J., Mandel J., Adaptive-Multilevel BDDC and its ík B., Šístek J., Mandel J., Adaptive-Multilevel BDDC and its Multilevel BDDC and its parallel implementation, Computing 95 (2013) 1087–1119. [3] Toselli A., Windlund O., Domain Decomposition Methods –Algorithms and Theory, Springer-Verlag, 2005. [4] FučíḰk B., Šístek J., Mandel J., Adaptive-Multilevel BDDC and its R., Mikyška J., Solovský J., Klinkovský J., Oberhuber T., Multidimensional Mixed-Hybrid Finite Element Method for Compositional TwoPhase Flow in Heterogeneous Porous Media and its Massively Parallel Implementation on GPU. Computer Physics Communications, 2018.

Acknowledgements

The work has been performed under the Project HPC-EUROPA3 (INFRAIA-2016-1-730897), with the support of the EC Research Innovation Action under the H2020 Programme; in particular, the first author gratefully acknowledges the support of prof. Fiorella Sgallari from Università degli Studi di Bologna and the computer resources and technical support provided by CINECA.

TRANSPORT PROPERTIES, EFFECTIVE MASS AND ELECTRONIC FITNESS FUNCTION OF NEW HEUSLER ALLOYS WITH HIGH FIGURE OF MERIT FOR POWER GENERATION

G. A. Adebayo[1] *and D. Ceresoli*[2]

[1]*Department of Physics, Federal University of Agriculture, Abeokuta, Nigeria;* [2]*CNR-ISTM, Department of Chemistry, University of Milan, Italy.*

Introduction

Due to developments of various techniques and simulation packages, Density Functional Theory (DFT) has become a very efficient and an important method to study and predict properties of new materials [1]. The advent of increased High Performance Computing power make possible a combination of machine learning and DFT to ascertain stabilities of several thousand compounds including the so called Heusler Alloys which find useful applications [2] as thermoelectric as well as photovoltaic devices. In this study, five half-Heusler compounds were identified with the aim of increasing their figure of merit through doping and predicting the thermoelectric properties, the effective masses and electronic fitness function. In the first part of the work, the above-mentioned properties were determined for the pristine compounds of HfCoAs, HfCoSb, HfIrAs, HfIrSb and ZrIrSb. In the second part of the work, we plan to dope the last three compounds with Ga, Sn and Sn respectively by constructing large supercells.

Methods

Generally, Half-Heusler alloys crystallize in C1b structure with space group F43m (#216) and compound combination of XYZ atoms at (0.25, 0.25, 0.25), (0.50, 0.50, 0.50) and (0.0, 0.0, 0.0). In the present work, the stable structures were determined and minimum energy in each configuration calculated. wavefunction cut-off between 40 and 50Ry were used. All structural calculations are done using the Quantum Espresso package. In the SCF calculations, we use up to 23x23x23 k-points in the primitive cell calculations. The thermoelectric transport properties, inverse effective mass and electronic fitness function were determined using the output from a Non-Self-Consistent Field (NSCF) calculations in accordance with the method employed by Zhang and Singh [3] as well as the BoltzTraP package [4]. However, to determine the effective masses in the conduction band, we first calculated the Power Factor (PF) of the materials in order to determine appropriately, the energies at which transport properties are to be calculated. Our approach is to locate the peak in the PF closest to the Fermi energy in the conduction bands and use the corresponding energy to determine other transport properties of the alloys. This allows to fine tune the energy close to the Fermi level where important physics are not missed.

Results

In recent time and due to applications in Photovoltaic and other devices, half-Heusler alloys have attracted multidisciplinary interests. Even though the advent of high throughput computational techniques made possible the prediction of the physical properties of thousands of structures, the rationalization of the calculated properties is still a matter of human investigation, based on the established knowledge of band-theory and acquired expertise.

Among the five alloys investigated, HfIrAs is the most attractive, and in the rest of the document, we will concentrate on it. As shown in Fig. 1, HfIrAs possesses a high Seebeck Coefficient at electron carrier concentration just above 1020/cm3 which increases with temperature. This is an unusual behaviour as semimetals generally have low Seebeck coefficients because of the absent of energy gap. The conductivity increases linearly with both electrons and holes carrier concentrations which is temperature dependent below 1020/cm3. The Power factor increases both with temperature and electron carrier concentration until above 1021/cm3 as seen in the bottom plots of Fig.1.

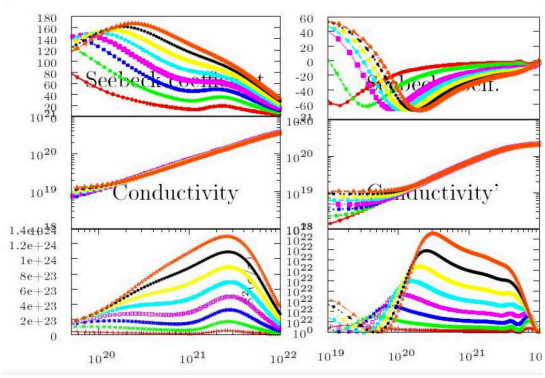

Figure 1 – HfIrAs semimetal: Thermoelectric transport properties of the undoped system.

Clearly, it is expected that doping will have a strong impact on the thermoelectric properties of HfIrAs. To this end, as part of the on-going collaboration between the authors, we are investigating the most favourable thermodynamic conditions for the formation of native and extrinsic defects in this material, and their effect on the electronic and transport properties.

Conclusions

In this work, first-principles calculations were used to determine the transport properties, effective masses and electronic fitness function of 5 half-Heusler alloys with a view to improve the figure of merit and other properties via doping (which will be done in the second part of the research work). In the semimetal HfIrAs, the major peak in the power factor is temperature sensitive and attains the highest value after electron carrier concentrations of 1021/cm3. The Seebeck coefficient in the semimetal decreases with electron carrier concentration after this value.

References

[1] P. Giannozzi et al., J.Phys.:Condens.Matter 21, 395502 (2009) http://dx.doi.org/10.1088/0953-8984/21/39/395502. [2] F. Heusler (1903). Über magnetische Manganlegierungen. Verhandlungen der Deutschen Physikalischen Gesellschaft (in German). 12: 219. [3] G. Xing, J. Sun, Y. Li, X. Fan, W. Zheng, D. J. Singh, Phys. Rev. Mater. 1, 065405 (2017); erratum ibid 1, 079901 (2017) [4] G. H. K. Madsen and D. J. Singh, Comput. Phys. Commun. 2006.

Acknowledgements

The work has been performed under the Project HPC-EUROPA3 (INFRAIA-2016-1-730897); in particular, GA gratefully acknowledges the support of CNRISTM, Department of Chemistry, University of Milan and the computer resources and technical support provided by CINECA.

Si NANOWIRES POLYTYPES FOR PHOTOVOLTAICS: UNDERSTANDING DOPING MECHANISM

M. Amato[1], S. Ossicini[2,3], E. Canadell[4] and R. Rurali[4]

[1]Laboratoire de Physique des Solides (LPS), CNRS, Université Paris-Sud, Université Paris-Saclay, Centre Scientifique d'Orsay, France; [2]Dipartimento di Scienze e Metodi dell'Ingegneria,Centro Interdipartimentale En&Tech, Universitá di Modena e Reggio Emilia, Italy; [3]Centro S3, CNR-Istituto di Nanoscienze, Modena, Italy; [4]Institut de Ciència de Materials de Barcelona (ICMAB–CSIC), Barcelona, Spain

Introduction

Novel Si nanowires polytypes can open the way to exciting applications as innovative group IV materials for next photovoltaic devices [1,2]. In particular, the higher absorption of hexagonal-diamond Si (2H-Si) NWs toward the visible region [3] together with the 3C/2H Si type II band alignment could suggest novel concepts in Si NWs photovoltaic devices. As is known, a reliable employment of a new material into photovoltaic devices requires a fundamental understanding of its doping process that can be decisive for its correct operation. The aim of this project is the theoretical characterization, through ab-initio methods, of the structural properties of boron (B) and phosphorus (P) single-doped Si NWs polytypes and their homojunctions [4]. Main objective of this proposal is to improve the comprehension of the relationship between the effect of a different electrostatic environment induced by a novel phase and the thermodynamical stability of the impurity.

Methods

All the calculations have been performed in the framework of DFT using the total energy code SIESTA and adopting the Local spin density approximation (LSDA). Core electrons were accounted by employing norm-conserving pseudopotentials of Troullier-Martins, while valence electrons were described through an optimized double-ζ polarized basis set. Ground state geometries were optimized with a conjugate gradient algorithm. B and P atoms were studied as common p- and n-type dopants in group IV bulk and NWs. It is worth noting that bulk 2H-Si is a reliable model for middle- and large-diameter NWs where quantum and surface effects are not present; these NWs, with diameters in the 20–100 nm range are those that are routinely fabricated and thus are more relevant for the applications [1,2].

Results

We performed an analysis of the thermodynamical stability of B and P dopants in 2H and 3C Si NWs using results of DFT formation energy calculations. Our main findings can be summarized as follows [4]: (i) for large diameters NWs (beyond the quantum confinement regime) a clear preference of B dopants for the 2H phase with respect to 3C is found as a consequence of the lower formation energy; (ii) in the same diameter range, P dopants do not show any preference of phase; (iii) in ultrathin nanowires, due to the lower symmetry with respect to bulk systems, both B and P dopants favour substitution at cubic lattice sites; (iii) a larger dopants concentration differences in different polytypes was shown, which can be relevant for 3C/2H homojunctions, as shown in Fig. 1; (iv) a clear surface segregation tendency for B dopants in both the phases is observed in ultrathin NWs.

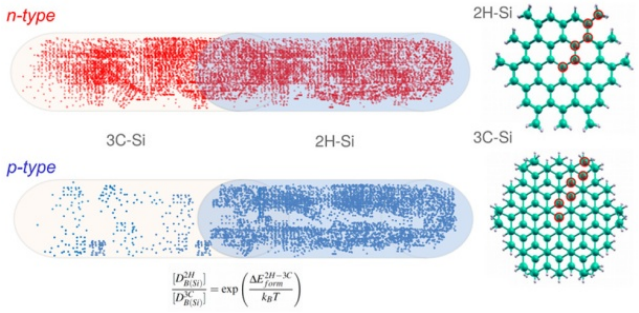

Figure 1 – Left panel: Qualitative distribution of B (bottom) and P (top) dopants in 3C/2H Si NW homojunctions at large diameters. Right panel: Cross section of 2H and 3C Si NWs. Reprinted from with permission from Ref. [4]. Copyright (2019) American Chemical Society.

Conclusions

We performed ab initio DFT calculations to elucidate the nature of B and P dopants stability in 2H- and 3C–Si NWs. We found that large diameter NWs have a clear preference for p-type dopants to be in the 2H phase as a consequence of the stronger tendency of these atoms to be in a trigonal environment. In the case of ultrathin NWs, there is only a moderate preference for both p- and n-dopants for the cubic structure. These findings shed light on the nature of doping process in 2H Si NWs and will certainly impact future experimental investigations.

References

[1] S. Assali, L. Gagliano, D. S. Oliveira, M. A. Verheijen, S. R. Plissard, L. F. Feiner, E. Bakkers, Nano Lett. 15, 8062-8069 (2015). [2] L. Vincent, G. Patriarche, G. Hallais, C. Renard, C. Gardès, D. Troadec, D. Bouchier, Nano Lett. 14, 4828-4836 (2014). [3] M. Amato, T. Kaewmaraya, A. Zobelli, M. Palummo, R. Rurali, Nano Lett. 16, 5694-5700 (2016). [4] M. Amato, S. Ossicini, E. Canadell, R. Rurali, Nano Lett. 19, 866-876 (2019).

Acknowledgements

The work has been performed under the Project HPC-EUROPA3 (INFRAIA-2016-1-730897), with the support of the EC Research Innovation Action under the H2020 Programme; in particular, the author gratefully acknowledges the support of ICMAB–CSIC and the computer resources and technical support provided by BSC.

STRONG COUPLING OF PLASMONIC NANOCAVITIES TO MOLECULAR EXCITONS

T.J. Antosiewicz[1], T.P. Rossi[2], T. Shegai[2] and P. Erhart[2]

[1]Faculty of Physics, University of Warsaw, Poland; [2]Department of Physics, Chalmers University of Technology, Gothenburg, Sweden

Introduction

Interaction between an optical mode and a quantum emitter is described in terms of the cavity quantum electrodynamics (cQED). In the regime of strong coupling, the emitter and the cavity form a unified light-matter polariton. In simple quantum optical models [1,2] matter is treated as a two-level system, leading to simplifications and inconsistencies in the description of material subpart. Here, we study polaritonic behaviour of a couple plasmon-exciton system by time-dependent density-functional theory (TDDFT), to overcome the abovementioned limitations.

Methods

To model light-matter interactions we use the real-time-propagation (RT) TDDFT approach [3] based on the localized basis sets [4] as implemented in the open-source GPAW package [5] with tools for analysing the electron-hole transition contributions to resonances and visualizing them as transition contribution maps (TCM) [6]. Calculations were carried out using the Perdew-Burke-Ernzerhof (PBE) [7] exchange-correlation functional in the adiabatic limit. The spectra are calculated using the δ-kick technique [3] in the linear-response regime and employing the dipole approximation for light-matter interaction. We use the default projector augmented-wave (PAW) [8] data sets and double-ζ polarized (dzp) basis sets in GPAW. The dzp basis set of Al includes diffuse 3p functions, which are important for describing plasmon resonances.

Results

Modelled systems consist of Al nanoparticles (regular truncated octahedra of 201, 586, and 1289 atoms with a resonance around 7.7 eV, whose collective nature is recognizable in the TCM in Fig. 1b,c in the lower-right corner) and benzene (transition at 7.1 eV with dipole moment μ_1 = 4.45 D). When coupled, the spectrum shows two polaritons (Fig. 1a) at 6.92 eV (lower) and at 7.68 eV (upper). Their symmetric and antisymmetric combination is visible in the induced densities and is archetypal for a strongly coupled system. All Al/benzene coupled spectra are fitted with a coupled harmonic oscillator model which has the form to obtain the coupling strength g as function of the Al nanoparticle size and number of benzene molecules. The fitted gs are plotted in Fig. 1g. For each of the Al-size the fitted values are linear with the square root of the number of molecules, as given by cQED $g = \sqrt{N}\mu_1 E_{vac}$, with one exception. For the smallest nanoparticle composed of 201 Al atoms the coupling strength g increases sub-linearly for $N \geq 4$.

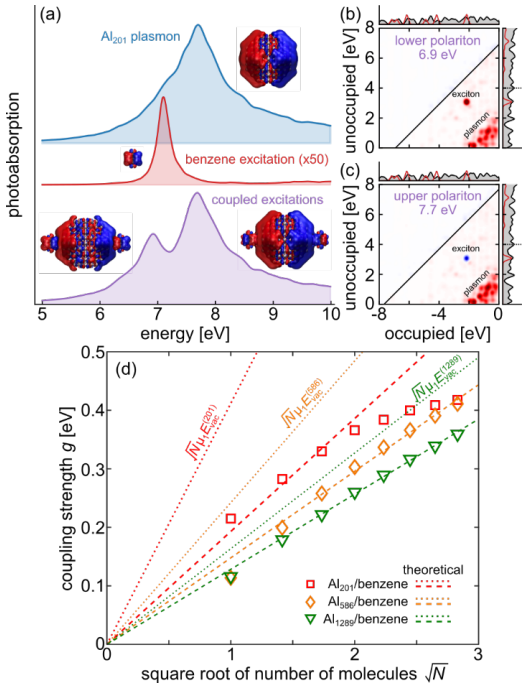

Figure 1 – (a) Strong Al-plasmon/benzene-exciton coupling gives lower and upper polariton states. (b,c) TCMs of the lower and upper polaritons are mixtures of the plasmon and exciton. (d) Coupling strength vs N. Dotted lines: $g = \sqrt{N}\mu_1 E_{vac}$, symbols fitted g values from TDDFT spectra, dashed lines mark the cQED dependence multiplied with the efficiency factor η.

Conclusions

First-principles TDDFT calculations are suitable for studying strong coupling between plasmons and molecular excitons and enable the capture of relevant interactions at the atomic level. This is very useful for studying coupling of molecules to picocavities slightly larger than the molecules themselves and ultrastrong coupling that leads to modification of the molecular ground state. The simple cQED description holds for atomic-scale systems, with only an efficiency factor needed to account for the electric field decay outside the nanoparticle. Based on the obtained coupling strengths, calculated mode volumes and field enhancements, reaching ultrastrong coupling with a single or a few molecules for single-particle cavities may prove challenging.

References

[1] Jaynes, ET et al., Proc. IEEE 51, 89 (1963). [2] Garraway, BM, Philos. Trans. Royal Soc. A 369, 1137 (2011). [3] Yabana, K, Bertsch, GF, Phys. Rev. B 54, 4484 (1996). [4] Kuisma, M et al., Phys. Rev. B 91, 115431 (2015). [5] Mortensen, JJ et al., Phys. Rev. B 71, 035109 (2005). [6] Rossi, TP et al., J. Chem. Theory Comput. 13, 4779 (2017). [7] Perdew, JP et al. PRL 77, 3865 (1996) & 78, 1396 (1997). [8] Blöchl, PE, Phys. Rev. B 50, 17953 (1994).

Acknowledgements

The work has been performed under the Project HPC-EUROPA3 (INFRAIA-2016-1-730897), with the support of the EC Research Innovation Action under the H2020 Programme; in particular, TJA gratefully acknowledges the support of Paul Erhart of the Department of Physics at Chalmers University of Technology and the computer resources and technical support provided by the Swedish National Infrastructure for Computing at PDC, Stockholm.

VORTICITY GENERATION FROM FIRST ORDER PHASE TRANSITIONS

P. Auclair[1] and M. Hindmarsh[2]

[1]AstroParticule & Cosmologie, Université Denis Diderot-Paris, France; [2]Department of Physics and Helsinki Institute of Physics, Finland

Introduction

Theories beyond the Standard Model can predict a thermal first order phase transition in the early universe during which bubbles of the broken phase nucleate, expand and transfer energy to the ambient relativistic fluid. While the expansion of the bubbles and the subsequent formation of sound waves in the fluid have been well studied in the past two decades, the formation of turbulence still needs to be better understood.

Previous simulations of the phase transition, starting from the nucleation of the bubbles up until the free propagation of sound waves did not last for sufficient time to see the formation of a turbulent and vortical velocity field.

The motivation for this project is to study an idealised version of the problem, starting with sound waves in a relativistic fluid and letting it evolve for several shock formation times to see if and how turbulence arises.

Methods

We modified the parallelized finite difference relativistic hydrodynamics code described in [1] and [2] in order to initialize sound waves with an arbitrary power spectrum. First, this allows us to put in initial conditions with arbitrarily large velocities, hence simulating strong phase transitions for which we lack long-lasting simulations. Second, since we do not need to resolve the short-lasting early stages of the phase transition, we let it evolve for several shock formation times.

We have tested the strong scaling of the code on Puhti, Sisu and Taito.

Results

Soon after initialization, we find a rapid formation of non-relativistic vorticity. We believe this to be due to the fact that the linearized equations we use to set the initial conditions break down as we enter the relativistic regime. The decomposition of the velocity field in terms of sound waves relaxes quickly to a quasi-static regime admitting a non-zero vortical component. This happens too rapidly to be a physical effect.

Running simulations for several shock formation times, we observe rare events during which kinetic energy is converted into thermal energy. These events happen at time-scales compatible with the formation of shocks. It remains to be understood whether these events can be interpreted as shocks or if they are an artefact of the finite size of the simulation.

At late times, we observe the decay of both the compressional and the rotational kinetic energy which are lost to the lattice. We have not been able to show any generation of vorticity due to non-linearities of the equations of motion.

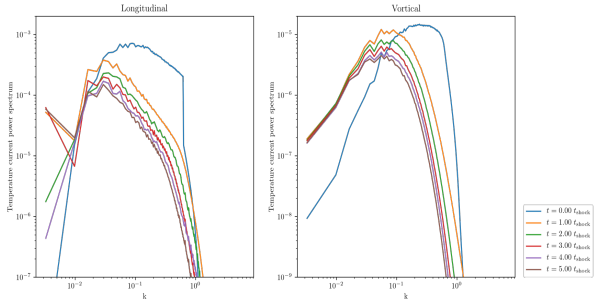

Figure 1 – Energy budget on a 980 cube grid, with root-mean-square velocity of 0.1

Conclusions

The next step for this project will be to investigate how to adapt the initial conditions of non-relativistic sound waves to the relativistic regime so that we can investigate the generation of vorticity from a purely compressional flow.
From our simulations so far, we have found that on long time-scales, the dominant mechanism for the decay of sound waves is dissipation due to numerical viscosity instead of the expected formation of shocks and generation of turbulence. This motivates the addition of a more realistic viscosity scheme in the numerical simulations.

References

[1] M. Hindmarsh, S. J. Huber, K. Rummukainen, and D. J. Weir, 'Numerical simulations of acoustically generated gravitational waves at a first order phase transition', Physical Review D - Particles, Fields, Gravitation and Cosmology, vol. 92, no. 12, 2015. [2] M. Hindmarsh, S. J. Huber, K. Rummukainen, and D. J. Weir, 'Shape of the acoustic gravitational wave power spectrum from a first order phase transition', Physical Review D, vol. 96, no. 10, 2017.

Acknowledgements

The work has been performed under the Project HPC-EUROPA3 (INFRAIA-2016-1-730897), with the support of the EC Research Innovation Action under the H2020 Programme; in particular, the author gratefully acknowledges the support of Mark Hindmarsh from the physics department in the University of Helsinki and the computer resources and technical support provided by CSC.

PARALLEL IMPLEMENTATION OF THE SPLIT-STEP FOURIER METHOD FOR THE HONG-OU-MANDEL EXPERIMENT WITH INTERACTING ELECTRONS

L. Bellentani[1], P. Bordone[1,3], X. Oriols[2] and A. Bertoni[3]

[1]Dipartimento di Scienze Fisiche, Informatiche e Matematiche, UNIMORE, Modena, Italy; [2]Departament d'Enginyeria Electrònica, Barcelona, Spain; [3]S3, Istituto Nanoscienze-CNR, Modena, Italy

Introduction

Electronic Hong-Ou-Mandel (HOM) interferometers can probe the inherent quantum correlations of charge carriers, thus exposing their fully quantum nature. Moreover, such device is being studied as a building block for the implementation of quantum computers [1]. Here, input/output channels are quantum Hall edge states (ESs) induced by a magnetic field applied perpendicular to a confined two-dimensional electron gas. A two-qubit operation can be obtained by exploiting electron-electron interaction [2]. The study of the exact interplay between two-electron correlations and the geometry of the device requires an efficient numerical modelling of the non-separable dynamics of the two-electron wave function (WF) in a 2D domain, thus leading to a four-degrees-of-freedom time-dependent problem, that we solve exactly with a parallel implementation of the Split-Step Fourier Method [3].

Methods

We firstly design the 2D external potential V(x,y) of a realistic sample (gold surface in Fig.1(a)), namely a quantum point contact, where electrons propagate. This structure acts as an electron beam splitter. By solving the single-particle Schrödinger equation in presence of the magnetic field B, we extract the exact ESs entailed by the geometry of the device in the initialization region (blue WFs in Fig.1(a)). Our electrons are then encoded in Gaussian wave packets (WPs) of ESs $\varphi\alpha(x,y)$ and $\varphi\beta(x,y)$, i.e. strongly-localized single-electron excitations with a finite distribution in energy. To afford the memory load for the allocation of the fermionic 4D WF $\psi(x1,y1,x2,y2)$, we adopt a data distribution with a Cartesian topology in the MPI paradigm. ψ is evolved by means of the Split-Step Fourier method, where the evolution operator for the two particles in our 2D geometry is iteratively applied [3]. The Cartesian data distribution entails 2D parallel Fourier transforms and anti transforms that we implemented in parallel from the FFTW3 library, with adequate per-row and per-column MPI communications. The properties of the two-particle system, as the bunching probability or the spatial entanglement, are finally computed as a function of the time evolution.

Results

With contrast to the traditional approaches used in literature, based on 1D effective and stationary models, our simulations include exactly the dynamical effect of the Coulomb interaction in 2D, which generally differs from the one in a 1D scheme [3]. By simulating the HOM experiment for different WP sizes (σ), we compare the bunching probability (P_{bun}) for two (i) non-interacting and (ii) interacting indistinguishable electrons. The linear trend of the stationary bunching probability in the first case (Fig.1(b)) - which fits the analytical P_{bun} provided by a simplified 1D model described in Ref. [3] - is clearly replaced by a saturation of the stationary $P_{bun}(\sigma)$ in presence of electron repulsion (Fig.1(c)). In Ref. [3], we further observe a similar trend in the *von Neumann entropy*, which measures the spatial entanglement for the antibunched configuration of the two-particle WF ψ.

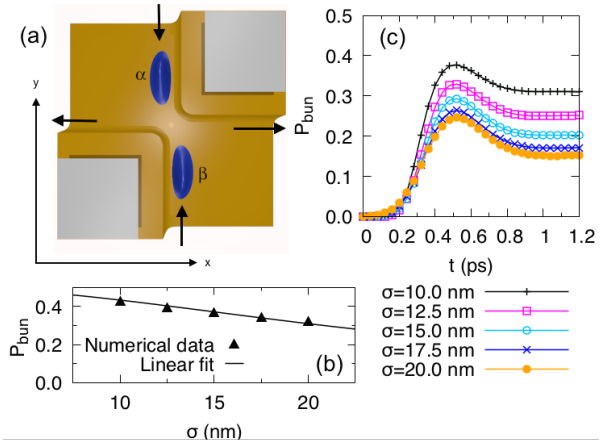

Figure 1 – (a) Geometry of the HOM interferometer and initial WPs. Pbun (b) for case (i) and (c) case (ii).

Conclusions

By simulating strongly localized single-electron excitations in 2D, sensitive to the energy selectivity of a full-scale quantum point contact, we characterize the exact interplay between the carrier Coulomb repulsion and their exchange symmetry in a HOM experiment. Our numerical results show that, in our operation regime, Coulomb repulsion dominates over the exchange interaction, so that we do not expect to recover the zero bunching probability in the plane-wave limit predicted by stationary models [1]. The inclusion of electron screening on Coulomb repulsion could provide additional information on the transition from a fully Coulomb-driven to a fully exchange-driven electron bunching and shed light on the validity of stationary non-interacting models.

References

[1] Dubois et al., Nature, 502:659–663, 2013. [2] D. Marian et al., J Phys: Condens. Matter, 27(245302), 2015. [3] L. Bellentani et al., arXiv:1903.02581[cond-mat.mes-hall],2019

Acknowledgements

The work has been performed under the Project HPC-EUROPA3 (INFRAIA-2016-1-730897), with the support of the EC Research Innovation Action under the H2020 Programme; in particular, LB gratefully acknowledges the support of Departament d'Enginyeria Electrònica of UAB, and the computer resources and technical support provided by BSC.

BUILDING A MINIMALIST MODEL FOR THE INTERACTION OF FUNCTIONALIZED METAL NANOPARTICLES WITH SUPERCHARGED GFP PROTEINS

G. Brancolini[1] and C. Holm[2]

[1]Institute Nanoscience – CNR-NANO, Center S3, Modena, Italy; [2]Institute for Computational Physics, University of Stuttgart, Germany

Introduction

Coarse-graining (CG) methodologies offer a trade-off between computational speed and accuracy.1 This project is framed in the broader perspective of obtaining atomistic potentials to be used in subsequent studies concerning high density coarse-grained colloidal NPs and protein-NPs with complementary charges, and their ability to form robust dyads of consistent size.

Methods

The potential of mean force (PMF) between 2 NP is obtained from a series of 93 umbrella sampling simulations. (Fig 1) A series of initial configurations is generated, each corresponding to a location wherein one NP is harmonically restrained at increasing centre of- mass (COM) distance from another NP via an umbrella biasing potential. The PMF is obtained by integration over the forces between the two NPs evaluated at different COM distances. The protein-NP binding is obtained with SDA7[2] rigid docking, adapted to the systems. The free energy of protein-NP binding is obtained by summing four types of interaction described as: (i) Coulombic electrostatic interaction (ElE) (ii) Electrostatic desolvation interaction (ElDesE) (iii) Non-polar desolvation (HyDesE) (Fig. 2).

Results

Jones potentials progressively more repulsive for low interparticle COM separations. (Fig.1). Two concentrations of ions are considered.

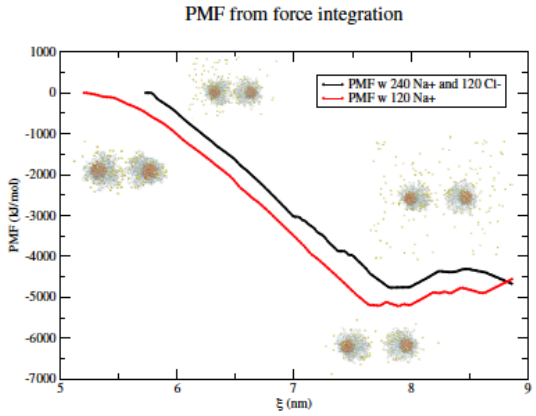

Figure 1 – PMF between a pair of NP-COO $(Au_{144}[L_{60}]^{-60}$ $[L=S(CH_2)_9(OC_2H_4)_4COO-])$ gold nanoparticles obtained from umbrella sampling atomistic simulations. In plot a comparison between PMF obtained with 120 Na+ neutralizing ions (red line) and with 240 Na+ and 120 Cl- (black line) is reported.

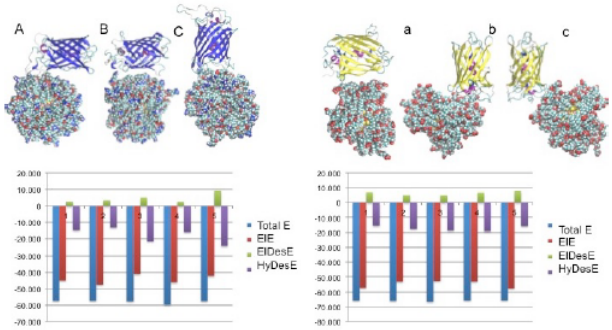

Figure 2 – Docking results between NP-ARG/-30GFP (left) and NP-COO/+36GFP (right). Where NP-ARG $(Au_{144}[L_{60}]^{+60}$ $[L=S(CH_2)_9(OC_2H_4)_4Arg^+])$ NP-COO $(Au_{144}[L_{60}]^{-60}$ $[L=S(CH_2)_9(OC_2H_4)_4COO^-])$.

The docking results predict different possible orientations for the binding between engineered GFPs (Green Fluorescent Protein) and the NPs, having comparable energies. Those poses will be investigated with umbrella sampling simulations to obtain PMF to be included in the CG model.

Conclusions

The present study represents an important step in the delivery of the CG strategy for studying NP-NP and protein-NP systems. Upon performing atomistic molecular dynamics simulations, it turns out that highly charged NP-COOs experience similar interactions with another NP-COO, regardless of the ion concentration. The results demonstrate the importance of simulations as a complementary tool to augment experimental studies that aim to co-engineer proteinnanoparticle interactions. The study represents a rational strategy for generating robust complexes in solutions at physiological ionic strengths, opening up new pathways for sensing, delivery, and imaging applications.

References

[1] Brancolini G et al., IJMS, 20(16):3866, 2019. [2] Gaboulline R et al., Biophys J, 72(5):1917, 1997. [3] Zhang X et al., Trends in Chemistry, 1(1):90, 2019.

Acknowledgements

The work has been performed under the Project HPC-EUROPA3 (INFRAIA-2016-1-730897), with the support of the EC Research Innovation Action under the H2020 Programme; in particular, the author gratefully acknowledges the support of Prof. Christian Holm at ICP Stuttgart and the computer resources and technical support provided by HLRS.

BUILDING A MINIMALIST MODEL FOR THE INTERACTION OF FUNCTIONALIZED METAL NANOPARTICLES WITH SUPERCHARGED GFP PROTEINS

N.C. Bristowe[1] *and M. Pruneda*[2]

[1]*School of Physical Sciences, University of Kent, UK;* [2]*ICN2-CSIC, Barcelona, Spain*

Introduction

Multiferroics are highly sought for their ability to exhibit multiple ferroic properties, ideally ferroelectricity and ferromagnetism. Their ability to combine charge and magnetic polarisation has tremendous potential for application in technological devices in which magnetic spin can be manipulated and controlled through applied electric fields, E, and charges through applied magnetic fields, H. One strategy for their design is to combine two ferroic materials together in a heterostructure, and make use of potential magnetoelectric coupling at the interface. A large number of experiments on perovskite interfaces have shown many exciting features, and a wide range of magnetoelectric coupling mechanisms have been proposed. The complexity of these systems, however, have made it difficult to probe these various mechanisms, both experimentally and theoretically. Recent advances in i) computational power and ii) code-development of first-principles methods based on Density-Functional Theory (DFT), have very recently allowed for the accurate large-scale simulations necessary to tackle these complex systems. Specifically, many of the proposed magnetoelectric mechanisms rely on a coupling of the spin axis and ordering with the lattice, with requires accurate large-scale spin-orbit DFT simulations. The objective of this project was to run such large-scale spin-orbit DFT simulations on a prototypical ferromagnetic perovskite oxide used in multiferroic heterointerfaces, (La,Sr)MnO_3. These calculations will enable a fundamental understanding of how interfaces effects, including strain and surface symmetry breaking, effect the lattice and any subsequent coupling to non-colinear spin ordering.

Methods

DFT simulations using the SIESTA code [1,2] were performed on epitaxially strained (La,Sr)MnO_3. To account for La/Sr disorder we utilised the virtual crystal approximation. Pseudopotential and basis information can be found in [3]. To mimic experimentally available substrates, the calculations fixed the in-plane lattice vectors to those of $LaAlO_3$, (La,Sr)(Al,Ti)O_3, $NdGaO_3$, $NdScO_3$ and $SmScO_3$ substrates. To investigate the possibility of strain induced structural phase transitions, we performed a random structure search method whereby initial structures were created from small random distortions to each atom in the 2x2x2 cubic perovskite supercell. Several initial structures were then relaxed at each strain state, out of which the ground state was determined. For each of these ground state structures at different strains, spin-orbit calculations [3] were performed to determine the magnetic easy axis, and the existence of any spin-canting.

Results

A sequence of different structural phases was found as a function of epitaxial strain. While compressive strain favoured anti-phase octahedral tilting around only the out-of-plane axis (a0a0c- in Glazer's notation), tensile strain favoured anti-phase octahedral tilting around one or two in-plane axes (a-a0c0 or a-a-c0 in Glazer's notation), depending on the degree of tensile strain. These results were later found to be sensitive to whether the constraint of the out-of-plane lattice vector direction was lifted, but nevertheless once lifted we found a similarly rich structural phase diagram of epitaxial (La,Sr)MnO_3. With these ground state structures, spin-orbit DFT simulations were performed to determine the easy axes of the ferromagnetic ordering. These calculations observed spontaneous canting of the FM spins for certain structures and certain easy axes where the point group symmetry would predict such Dzyaloshinskii–Moriya effects. Such a scenario is illustrated in Figure 1, which is akin to a weak-antiferromagnetic component on the predominant ferromagnetism. These results provide encouraging initial tests of the Siesta spin-orbit implementation [4].

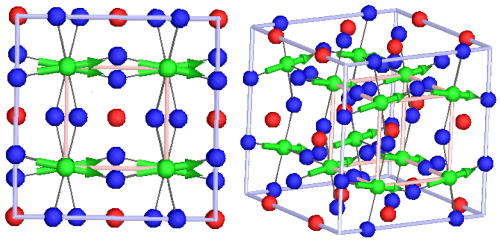

Figure 1 – Complex structural and magnetic orders in strained (La,Sr)MnO_3. Figure shows the structure of (La,Sr)MnO_3 (Blue spheres: Oxygen, Green spheres: Mn, Red spheres: La/Sr) under the epitaxial constraint imposed by $LaAlO_3$ which produces anti-phase octahedral tilting around an in-plane axis (a-a-c0 in Glazer's notation). Left: viewed along one of the in-plane axes, around which the octahedral rotate in an anti-phase fashion. Right: Same figure but rotated slightly for clarity. The predominant ferromagnetic axes points along an axis normal to the tilting axes, and a small antiferromagnetic canting can be observed. Images created using the isoviz software [5].

Conclusions

First principles calculations have been performed to examine epitaxial strain engineering of the prototypical ferromagnetic perovskite, (La,Sr)MnO_3. Epitaxial strain is found to tune both the ground state tilt pattern and magnetic easy axes. For some of these phases, spin-orbit calculations determine a spin-canting of the ferromagnetism. These results will eventually feed into surface and heterointerface simulations to investigate the many unusual properties experimentally observed in such complex magnetic systems.

References

[1] P. Ordejon et al Phys. Rev. B 53, R10441, 1996. [2] J. Soler et al J. Phys.: Condens. Matter 14, 274524, 2002. [3] V. Ferrari et al Phys. Status Solidi A 203, 1437 (2006). [4] R. Cuadrado et al. Phys. Materials 1 015010 2018. [5] B. J. Campbell et al J. Appl. Cryst. 39, 607-614 (2006).

Acknowledgements

The work has been performed under the Project HPC-EUROPA3 (INFRAIA-2016-1-730897), with the support of the EC Research Innovation Action under the H2020 Programme; in particular, the author gratefully acknowledges the support of ICN2-CSIC and the computer resources and technical support provided by BSC.

SIMULATING RARE EVENTS FROM ASTROPHYSICAL POPULATIONS

F.S. Broekgaarden

Anton Pannekoek Institute for Astronomy, University of Amsterdam, The Netherlands

Introduction

Gravitational-wave observations of double compact object (DCO) mergers are providing new insights into the physics of massive stars and the evolution of binary systems. Making the most of expected near-future observations for understanding stellar physics will rely on comparisons with binary population synthesis models. However, DCO mergers are a very rare outcome of such models. Studying DCOs and their progenitors requires calculating large synthetic populations, the vast majority of which never produce DCOs, which is highly computationally inefficient. We present a new sampling algorithm, STROOPWAFEL, that improves the computational efficiency of population studies of rare events, by automatically focusing the simulation around regions of the initial parameter space found to produce outputs of interest.

Methods

The algorithm first explores the initial parameter space until it finds a preliminary population of systems of interest. This exploring is done with sampling from the birth distributions which is a form of sampling commonly used in binary population synthesis. STROOPWAFEL then concentrates the later sampling towards regions in the initial parameter space that are in the vicinity of the initial parameters of the interesting binaries found during the exploration phase. This is an example of Adaptive Importance Sampling [1]
We implement the algorithm in the binary population synthesis code COMPAS [2,3,4], and compare the efficiency of our implementation to the standard method of Monte Carlo sampling from the birth probability distributions.

Results

We find that STROOPWAFEL can find $\sim 25 - 200$ times more DCO mergers than the traditional sampling method with the same size of simulation, and can speed up simulations by up to two orders of magnitude. Finding more DCO mergers automatically maps the parameter space with far higher resolution than when using the traditional sampling.

This increase in efficiency also leads to a decrease of a factor $\sim 3 - 10.5$ in statistical sampling uncertainty for the predictions from the simulations. This is particularly notably for the distribution functions of observable quantities, including in the tails of the distribution functions where predictions using standard sampling can be dominated by sampling noise. We also find that STROOPWAFEL handles well the bifurcations and stochasticity that naturally occur in binary population synthesis output surfaces and often pose a challenge for currently used sampling methods.

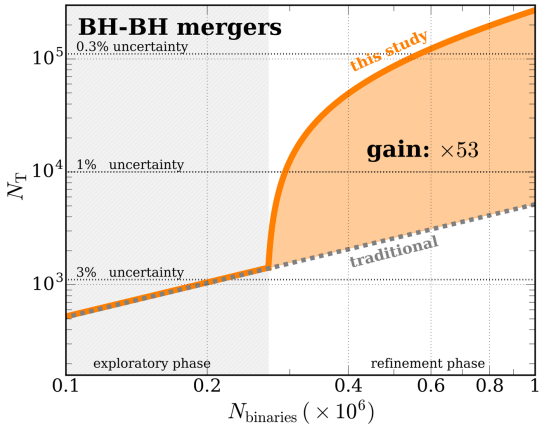

Figure 1 – Number of black hole binaries (BH-BH) found in the simulation N_T as a function of the number of binaries simulated $N_{binaries}$ for the traditional method (grey dashed line) and STROOPWAFEL (orange solid line). We find that our method obtains 53× more BH-BH mergers for the same computational cost.

Conclusions

Our STROOPWAFEL algorithm increases the efficiency of sampling rare events, making it possible for next generation binary population synthesis simulations to include more detailed stellar evolution models, explore more model variations to test the physical assumptions and explore in greater detail the tails of distribution functions.

References

[1] Cornuet J.-M. et al., Scandinavian Journal of Statistics, 39(798), 2012; [2] Stevenson S. et al., Nature Communications 8, 2017; [3] Barrett J.W et al., MNRAS, 477(4685), 2018; [4] Vigna-Gómez A. et al., MNRAS, 481(3), 2018.

Acknowledgements

The work has been performed under the Project HPC-EUROPA3 (INFRAIA-2016-1-730897), with the support of the EC Research Innovation Action under the H2020 Programme; in particular, the author gratefully acknowledges the support of the School of Mathematics, University of Edinburgh and Birmingham Institute for Gravitational Wave Astronomy, University of Birmingham and the computer resources and technical support provided by EPCC.

STABILIZING EFFECT OF MAGNETIC HELICITY ON MAGNETIC CAVITIES IN THE INTERGALACTIC MEDIUM

S. Candelaresi[1] *and F. Del Sordo*[2]

[1]*Division of Mathematics, University of Dundee, Dundee, United Kingdom,* [2]*Physics Department, University of Crete/FORTH, Greece*

Introduction

Observations of the intergalactic medium show the existence of radio bubbles of the size of 30 kpc [1]. They rise buoyantly from the galactic disk and remain stable for tens of millions of years. However, due to the Kelvin-Helmholtz instability they should be shredded in a much shorter time scale.

Helical magnetic fields, i.e. twisted, knotted and linked fields, are known to be highly stable [2, 3, 4]. Here we propose that the intergalactic bubbles can be stabilized by such a field.

Methods

As the intergalactic medium is a highly conducting gas we model it using the equations of magnetohydrodynamics. We solve these non-linear partial differential equations using the finite difference code PencilCode. The environment surrounding the bubble is simply modelled as a stably stratified atmosphere with decreasing density. We then insert the bubble close to the galactic disk with a lower density than the surrounding, but higher Temperature to balance the pressure forces. In order to test the effect of magnetic helicity on the stabilization we perform simulations with no magnetic field, with magnetic field and low helicity and one with a high value of helicity, but the same magnetic energy.
We then monitor the evolution of the bubble by observing the motion of the loci of high temperature. With this we can also calculate a proxy for the coherence of the bubble, which we define to be the average distance of the points inside the bubble to each other. A shredded bubble will have a high value of this distance.

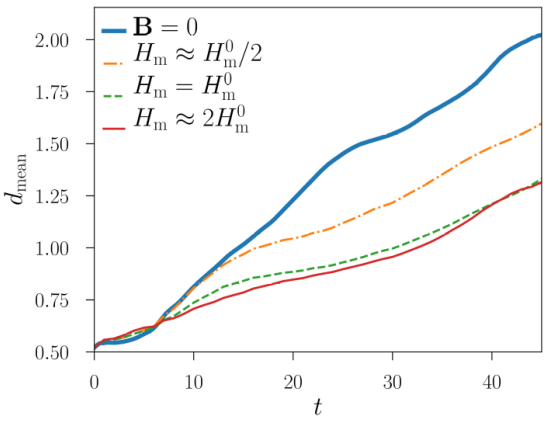

Figure 1 – Mean distance of the points within the bubble in time for the non-magnetic case and magnetic case with these different values of helicity.

Results

As hypothesized, we find that the presence of magnetic helicity has indeed a stabilizing effect on the bubbles (Fig. 1). We also show that the higher the magnetic helicity the more stable the bubble is. We observe this also in the slice plots taken in the centre of the domain (Fig 2).

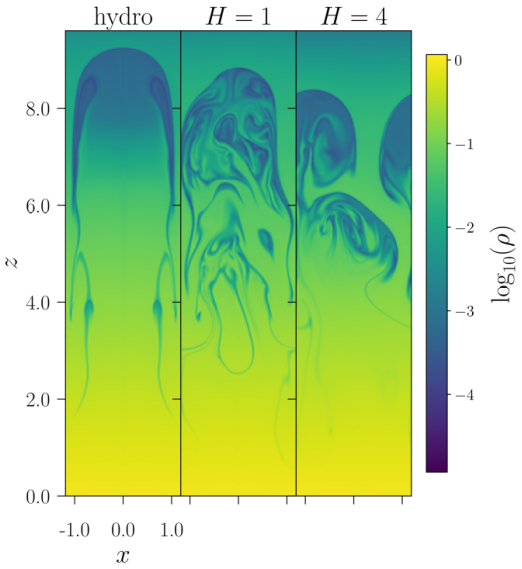

Figure 2 – Slices through the computational domain at final time showing the gas density for the non-magnetic case and low and high helicity case.

Conclusions

In this study we showed that a helical magnetic field inside the bubble can stabilize intergalactic bubbles. This effect is stronger the higher the magnetic helicity content, even with the same total magnetic energy. We propose that even weak, but highly helical, fields within the bubbles can explain their stability.

References

[1] Fabian A. C. et al., 2000, MNRAS, 318, 65; [2] Moffatt H. K., 1969, J. Fluid. Mech., 35, 117; [3] Del Sordo F. et al., 2010, PRE, 81, 36401; [4] Candelaresi S., Brandenburg A., 2011, PRE, 84, 16406.

Acknowledgements

The work has been performed under the Project HPC-EUROPA3 (INFRAIA-2016-1-730897), with the support of the EC Research Innovation Action under the H2020 Programme; in particular, the authors gratefully acknowledge the support of University of Crete and the computer resources and technical support provided by GRNET.

ELECTRONIC EXCITATIONS AND OPTICAL PROPERTIES OF SURFACES OF FLUORIDE CRYSTALS

G. Cappellini[1] and J. Furthmüller[2]

[1]Dipartimento di Fisica, UniCa, Cagliari, Italy, [2]IFTO, FSU-Jena, Germany

Introduction

For a long time fluorides and fluoride-type crystals have attracted much interest concerning their intrinsic optical properties and potential applications in optoelectronic devices in particular in the ultraviolet spectral region.

In the present project we will consider mainly the cubic compounds with cations belonging to main group II, in particular BaF_2 and CaF_2, with the purpose to calculate the electronic and optical properties using different levels of theory for their (111) surfaces.

Methods

We have used a computational code based on plane wave expansion of the electronic wave functions and ionic pseudopotentials within a repeated slab procedure.

The reliability of computational results in the description of surface electronic structure was improved by the use of large unit cell dimensions in the direction normal to the surface, with a sufficiently high number of atomic layers per slab and an equally large region of vacuum.

The theoretical schemes applied are density functional theory (DFT) and many-body perturbation theory using different approximations for exchange and correlation (XC): GGA (PBEsol), HSE06, G0W0, and GW0 or GW (with eigenvalue-self consistency in G or in G and W) [1].

Before and in parallel with the surface calculations we have determined also the ground-state and excited-state properties of the corresponding bulk systems. This either for methodological motivations but also to compare important observables as band gaps, ionization energies, or electron affinities between bulk and surface.

In more detail, for calcium fluoride various convergence tests at DFT-GGA level have been performed for the (111) surface, i.e., tests on plane-wave cut-off energy Ecut, k-point sampling, and dimension of the simulation cell. For excited-state properties different XC functionals have been used and comparison with existing experimental or theoretical results has been performed.

All data have been obtained using mainly the VASP computational code (VASP: http://www.vasp.at/) under the supervision of staff researchers at IFTO-FSU-Jena.

As a parallel task we determined also the electronic properties for the smallest clusters of the same fluorides, considered as nanometric fragments of their corresponding bulk systems. For these finite systems we were able also to calculate their absorption spectra, quasiparticle gaps and exciton binding energies [2].

Results

The atomic structure was obtained for bulk and surface systems within DFT-GGA. Structural relaxations were in general rather weak and as to be expected strongest close to the surface. The surface relaxation energy was small and also the surface formation energy was modest in good agreement with existing previous results.

With respect to excitations the surface fundamental gap was found to be slightly reduced with respect to the bulk value, in the case of CaF_2 by about 3% (about 0.35 eV) within the GW0 scheme. This gap shrinkage mainly results from a strong downwards (surface) shift of the conduction band minimum (more than 0.4 eV) while in contrast a much smaller downwards (surface) shift of the valence band maximum is observed (less than 0.1 eV).

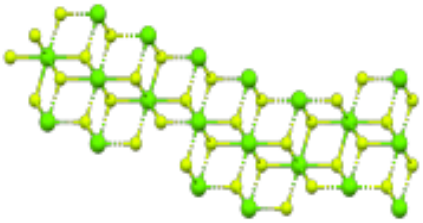

Figure 1 – Side view of the simulation slab for the CaF_2(111) surface.

For CaF_2 the ionization potential obtained in the GW0 scheme reproduced, within 5%, that calculated by using the cluster method, while the electron affinity obtained at HSE06 level was coincident with that after the cluster calculation. The comparison between bulk, surface, and cluster systems with respect to their optical properties demonstrated moreover that while for the formers these observables possess comparable values, on the other hand for the clusters much larger excitonic effects can be observed along with a red-shift of the onset energies.

Similar results were obtained for bulk BaF_2 and its (111) surface. The overall analysis of computed data either for ground-state of excited-state properties of both surfaces is still under way along with the discussion on the opportunity to forecast additional tests and calculations for electronic excitations and also optical properties [3,4].

Conclusions

In the present project we studied the non-polar (111) surface of two important fluoride compounds with respect to their electronic and optical properties. The use of different state of the art computational schemes permitted us to obtain new insight in those properties for materials which are of strategic importance for ultraviolet optical applications.

References

[1] Cappellini G et al., Phys. Rev. B, vol.87, 075203-1/9, 2013, doi:10.1103/PhysRevB.87.075203; [2] Mocci P, et al., Phys. Chem. Chem. Phys. vol.21, 16302/9, 2019, doi:10.1039/c9cp01038f; [3] Cadelano E et al., J. Phys. Cond. Matter, vol.26,125501-1/8, 2014, doi:10.1088/0953-8984/26/12/125501; [4] Matusalem F et al., J. Phys. Cond. Matter, vol.30,365501-1/8, 2018, doi:10.1088/1361-648X/aad65.4

Acknowledgements

This work has been performed under the Project HPC-EUROPA3 (INFRAIA-2016-1-730897), with the support of the EC Research Innovation Action under the H2020 Programme; in particular, the authors gratefully acknowledge the support of IFTO-FSU-Jena and the computer resources and technical support provided by HLRS-Stuttgart-De.

ROTATION AND PROPULSION IN 3D ACTIVE CHIRAL DROPLETS

L.N. Carenza[1], G. Gonnella[1], D. Marenduzzo[2] and G. Negro[1]

[1]Dipartimento di Fisica, Università degli Studi di Bari and INFN, Italy; [2]SUPA, School of Physics and Astronomy, University of Edinburgh, United Kingdom

Introduction

Chirality plays an important role in many biological systems. Biomolecules such as DNA, actin or microtubules form helical structures which, at sufficiently high density and in the absence of active forces, tend to self-assemble into twisted cholesteric phases. While much is known about the non-equilibrium dynamics of active systems [1], the behaviour of active chiral systems has not been widely investigated so far. Here, we study the effect of activity on a droplet of chiral matter, finding a surprisingly rich range of dynamical behaviours, ranging from spontaneous rotations to screw-like motion. The phenomena we uncover require both thermodynamic chirality and activity, and are linked to the non-trivial topology of the defects which form by necessity at the droplet surface. This work paves the way towards the control of motility modes – analogue to the ones found here – in chiral micro-organism occurring in nature, or in synthetic active matter.

Methods

In order to reproduce the chiral feature of active systems, we made use of the well-established active liquid crystal (LC) theory [2]. We considered a droplet of a cholesteric LC embedded in a passive fluid. The equilibrium properties are derived by a suitable Landau-De Gennes free energy functional [3] of which key parameters are the equilibrium cholesteric pitch p and the ratio between the droplet diameter and the pitch, $N \equiv 2R/p$, which also counts the number of windings of the director within the droplet. Activity is introduced through a coarse-grained description of force ζ and torque dipoles $\bar{\zeta}$. These result in a non-equilibrium stress that couple the hydrodynamics to the dynamics of the liquid crystal. The evolution equations have been solved by means of a hybrid Lattice Boltzmann (LB) approach where the hydrodynamics is treated through a predictor-corrector LB approach, while the equations describing the LC dynamics have been integrated with a standard finite-difference algorithm.

Results

In a standard nematic droplet (N=0) we identify three different regimes at varying the intensity of the active force ζ. For low activity the droplet is quiescent and two +1 antipodal point defect appear on its surface. As activity is increased over a certain threshold, the droplet sets into rotational motion about the axis defined by the two defects, with angular velocity proportional to ζ. Finally, at higher activity, energy injected is enough to enucleate pairs of oppositely charged defects that randomly move on the droplet surface in a chaotic fashion.

The behaviour is yet different when chirality is introduced. Under the effect of activity, the droplet still rotates at intermediate active dopings, but chirality is found to be fundamental for the relocation of the point defects. The surface defect pattern is now a pair of nearby +1 defects (see Fig.1) so that the rotational motion leads to the screw-like propulsion of the droplet. The results show that, for small activity, the droplet sets into a quiescent regime independently of the cholesteric power: this is characterized by weak bending deformation of the LC network on the droplet surface, which are not enough to power any self-sustained motion. As activity is increased different behaviours arise: for null or weak cholesteric power (N=1) stationary rotational motion sets up while screwlike propulsion needs the defects to relocate to one hemisphere creating a dipolar pattern. At higher cholesteric power (N>4), the droplet sets into the chaotic phase even at intermediate activity, a regime characterized by defect nucleation on the surface.

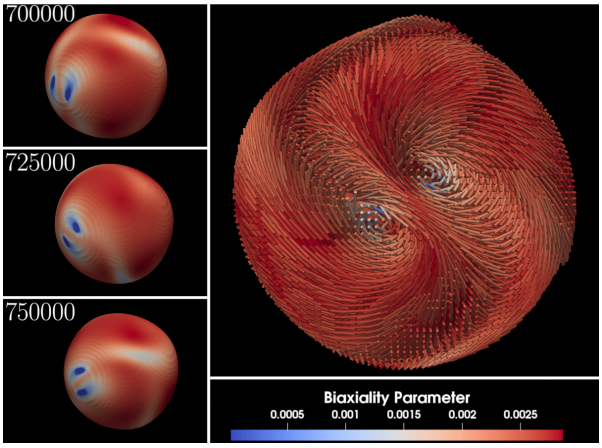

Figure 1 – Screw-like propulsion in a chiral droplet with active force dipoles. Left panels show snapshots at different times of chiral active droplet for the case at N = 2 and ζ = 10 −3. The contour-plot of the biaxiality parameter on the droplet surface serves to identify the position of the two +1 defects, whose configuration can be appreciated by looking at the right panel. The screw-like rotational motion generates a strong velocity field in proximity of the two defects that propels the droplet – as shown by the changing position of the droplet in left panels.

Conclusions

It is of interest to think of the generic models developed in this work with respect to the dynamics of self-motile and rotating living active gels, which are found in bacterial and eukaryotic cells. Our results show that there are multiple motility modes which chiral active microorganism may employ, and it would be of interest to look more closely for analogues of these in nature.

References

[1] S. Ramaswamy. J. Stat. Mech., 2017(5):054002, 2017; M.C. Marchetti, J.F. Joanny, S. Ramaswamy, T.B. Liverpool, J.J. Prost, M. Rao, and R.A. Simha. Mod. Phys., 85:1143, 2013. [2] K. Kruse, J.F. Joanny, F. Jülicher, J. Prost, and K. Sekimoto. Phys. Rev. Lett., 92:078101, 2004; L. Giomi, M.J. Bowick, X. Ma, and M.C. Marchetti. Phys. Rev. Lett., 110:228101, 2013; [3] P.G. de Gennes and J. Prost. The physics of liquid crystals. The International series of monographs on physics 83 Oxford science publications. Oxford University Press, 2nd ed edition, 1993.

Acknowledgements

The work has been performed under the Project HPC-EUROPA3 (INFRAIA-2016-1-730897), with the support of the EC Research Innovation Action under the H2020 Programme; in particular, the author gratefully acknowledges the support of School of Physics and Astronomy and the computer resources and technical support provided by Archer.

FIRST PRINCIPLES CALCULATIONS OF IMPURITIES IN ZNO

A. Chesnokov[1], N.V. Skorodumova[2,3]

[1]Department of Theoretical Physics and Computer Modelling, Institute of Solid State Physics, University of Latvia, Latvia; [2]Department of Physics and Astronomy, Uppsala University, Sweden; [3]Department of Materials Science and Engineering, KTH Royal Institute of Technology, Sweden.

Introduction

Transparent conducting oxides (TCOs) are electrically conductive materials characterized by low absorption of light. An important property of TCOs is a controllable type of conductivity achieved through doping. Doped zinc oxide (ZnO) is a material that is well-known for its n-type conductivity. It was demonstrated that the p-type conductivity occurs in amorphous ZnO-IrO_2 films [1]. In these films, the transition from the n-type to p-type conductivity occurs in response to the concentration of iridium. The aim of this work is to test the conditions for p-type conductivity in iridium-doped ZnO through the first-principles simulation of the material.

Methods

In the present work, the PBE0 hybrid exchange-correlation functional, as implemented in the massively parallel version of CRYSTAL17 was used. Atoms were described using a basis set (BS) of a linear combination of atomic orbitals adopted from literature. BSs for iridium and oxygen were adopted from [2], and BS for zinc was adopted from [3]. The Brillouin zone was sampled with a 3×3×3 Monkhorst-Pack mesh. The convergence limit for the self-consistent field procedure was set to 10^{-7} a.u. for both electronic and structural relaxation. Defective structures were modelled as either 3×3×2 or 2×2×1 supercells of wurtzite phase ZnO, with lattice constants a=3.25727 Å and c=5.19811 Å obtained from the primitive unit cell calculations (experimental values [4] are 3.2494 and 5.2054, respectively). All calculations of defective structures were spin-polarized; the use of symmetry operations was omitted, and the structural relaxation was performed for atomic coordinates only. Two distinct types of impurities were considered: Zn substitution with Ir either with or without an addition of interstitial oxygen atom(s).

Results

The two supercell sizes were chosen to represent low (2.8 at%, larger supercell) and high (12.5 at%, small supercell) concentration of iridium, matching those in the experiment [1]. Smaller supercell allows self-interactions between impurities due to periodic boundary conditions, however, values of defects' formation energies show trends like those in a larger supercell. Therefore, a smaller supercell is an acceptable (and computationally efficient) model. These trends indicate that interstitial oxygen atoms will tend to make Ir 6-coordinated, with higher concentrations tending to be more disordered, in good agreement with the experiment [1].

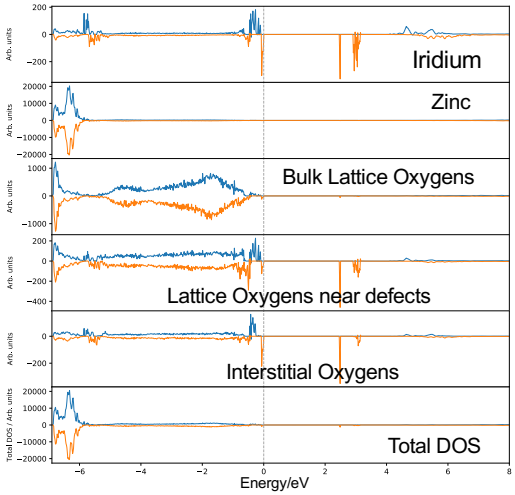

Figure 1 – Projected density of states (DOS, in arbitrary units) for a larger supercell with 1 Ir atom and 2 interstitial O atoms. Note the mixture of Ir and O states.

Conclusions

While this work shows a qualitative agreement with the experiment, it does not provide a definitive explanation for emergence of p-type conductivity in this system. Key findings from analysing charges and DOS plots (such as Fig. 1) of the investigated models are as follows. Interstitial oxygen atom(s) alone do not induce empty states above the Fermi level; at high concentration, Ir^{2+} ions can induce unfilled (virtual) states in the oxygen bands; even at low impurity concentration, ZnO/IrO_2 system has empty states in the oxygen bands. To unambiguously link these findings in a way that explains p-type conductivity, more careful work is needed, e.g. enumerating all possible oxidation states of Ir, exploration of other possible modes of electronic localization, energetics and possibility of O-O bond formation, inclusion of vibrational effects, etc.

References

[1] Zubkins et al., Thin Solid Films, 636:694, 2017. [2] Ping et al., J. Phys. Chem. C, 119(21):11570, 2015. [3] Gryaznov et al., J. Phys. Chem. C, 117(27):13776, 2013. [4] Sowa et al., J. Appl. Cryst., 39(2):169, 2006.

Acknowledgements

The work has been performed under the Project HPC-EUROPA3 (INFRAIA-2016-1-730897), with the support of the EC Research Innovation Action under the H2020 Programme; in particular, A. C. gratefully acknowledges the support of Natalia V. Skorodumova and the computer resources and technical support provided by KTH-PDC.

THE ROLE OF THE NON-ADIABATIC DYNAMICS IN THE EARLY UNIVERSE

D. De Fazio[1] and C. Petrongolo[2]

[1]Istituto di Struttura della Materia – CNR, Roma Italy; [2]Istituto per i Processi Chimico Fisici – CNR, Pisa, Italy

Introduction

The chemistry of the early Universe plays an important role in our understanding of the formation of the first cosmological objects. Molecular formation began in the recombination era, when the temperature was low enough for the newly formed atoms to survive and participate in further evolution. At the end of the era, atomic density was still too low for three body reactions to play any significant role: however, it was then that the first molecular species were postulated to be formed through radiative association. The formation of molecular species in the primordial Universe is extremely important, because roto-vibrational quantum states became available to participate in the cooling process, permitting the dissipation of the radiative energy and balancing the increase of the gravitational energy during the collapse of the first cosmological objects. Gas phase chemistry of formation and destruction of these molecules is therefore very important to get a good understanding of how galaxies and clusters came to be. Because H_2 and He are the dominant species in the early Universe scenario and can be ionized to H^+ and He^+ by cosmic rays, the first collisions of the He chemistry are $He + H_2^+$ and $He^+ + H_2$. The former collision is an adiabatic process on the HeH_2^+ ground electronic surface and was extensively investigated in the past [1]. On the contrary, the dissociative charge transfer process

$$He^+ + H_2 \rightarrow He + H^+ + H \qquad (R1)$$

proceeds via a conical intersection (CI) between the first two excited electronic states of HeH_2^+ and its dynamics is essentially unknown.

Methods

We here report the CI quantum dynamics of the reaction R1 for two vibro-rotational states *v,j* of H_2, in a range of collision energy from 0.01 up to 3 eV. We present coupled-channel initial-state-resolved reaction probabilities and integral cross sections (ICSs), computed via a two-coupled-state diabatic electronic representation, a time-dependent real wave-packet formalism, and a flux analysis. Dynamical calculations were performed by the code of Ref. [2], a very versatile methodology able to treat simultaneously several non-adiabatic effects [3]. The code has been extensively parallelized by an MPI parallelization on J (the total Angular Momentum) and on K (the projection of J on the body-fixed z axis) with excellent speed-up. The diabatic potential energy surfaces and the non-adiabatic coupling were obtained by analytical fits at high accurate quantum chemistry calculations made by the Aguado-Paniagua group of the Universidad Autonoma de Madrid.

Results

The Total ICSs of the reaction R1 for the ground roto-vibrational state of H_2 are shown in the Figure. The reaction shows a smooth fast increase with the collision energy. Below 0.5 eV, where the background reactivity is very low, strong resonance features appear. This behaviour is probably due to the appearing of the so called 'bound molecular states embedded in the Continuum', a particular Feshbach resonances state induced by the CI with lifetime of the order of the micro-second (see e.g. Ref. [4]). A fast convergence of the K projections (a critical parameter for the feasibility of the calculations) has been found. The calculation is very fast at high collision energy where a small number of time step is required. Otherwise, much slower has been found the convergence in the low energy region where the narrow resonances require a large number of time steps. Both reaction probabilities and ICSs at *v,j*=0,0 present three groups of resonances at <0.6 eV, due to a van der Waals minimum in the entrance channel and whose amplitude decreases with the energy. Preliminary calculations (not reported here) show that when H_2 is vibrationally excited to *v*=1, the reactivity increases by about two orders of magnitude.

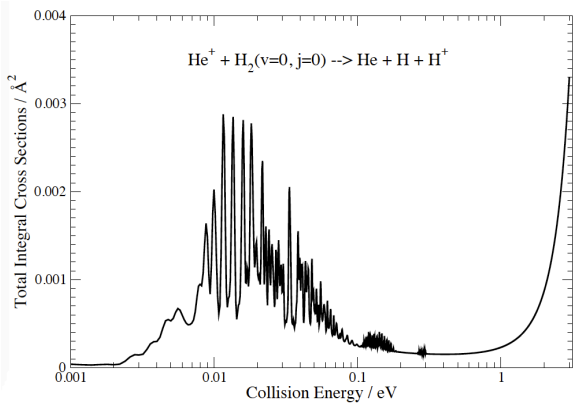

Figure 1 – Total ICSs as function of the collision energy for the reaction (R1). A logarithmic scale on the energy has been used to highlights the low energy resonance behaviour.

Conclusions

We have found that the yield of the reaction R1 is very small when H2 is in its ground roto-vibrational state. However, the strong resonance features at low energy and the enhancement of the reactivity for higher vibrational states, could make play an important role in the early Universe evolution at high redshift.

References

[1] De Fazio D PCCP 16:11662, 201. [2] Gamallo P et al., JCP 139:094303, 2013. [3] Gamallo P et al., PCCP 19:4454, 2017. [4] Cederbaum LS et al., PRL 90:013001,2003.

Acknowledgements

The work has been performed under the Project HPC-EUROPA3 (INFRAIA-2016-1-730897), with the support of the EC Research Innovation Action under the H2020 Programme; in particular, the author gratefully acknowledges the support of Dr. Tomas Gonzalez-Lezana of the CSIC of Madrid and the computer resources and technical support provided by BSC.

UNDERSTANDING THE SURFACE CHEMISTRY OF AMORPHOUS CARBON USING MACHINE LEARNING AND DFT

V.L. Deringer

Department of Engineering, University of Cambridge, Cambridge CB2 1PZ, United Kingdom

Introduction

Carbon is a chemical element with fascinating structural complexity, and this is especially true for its amorphous (non-crystalline) forms. Amorphous carbon materials are also highly interesting for applications: dense, "diamond-like" or "tetrahedral amorphous" (*ta*) forms have long been used for coatings due to their attractive mechanical properties, and more recently *ta*-C has been suggested as an electrode material for detecting bio-molecules. Still, open questions remain with regard to its atomic-scale structure. Accurate and predictive computer simulations are now needed to better understand the surface structure of *ta*-C as well as its chemical functionalisation (most prominently, with hydrogen and various oxygen-based functional groups), which in turn determines the (electro-) chemical behaviour of *ta*-C films.

Methods

We have recently introduced a machine-learning based interatomic potential for amorphous carbon [1] that makes use of the Gaussian approximation potential (GAP) framework [2]. GAP provides a method for accurately fitting the high-dimensional potential energy sur-face by "learning" quantum-mechanical (here, density-functional theory, DFT) reference data. Once developed and validated, a GAP can hence be used to carry out atomic-scale simulations at close-to-DFT quality but orders of magnitude faster. In an ongoing research collaboration with colleagues at Cambridge and Aalto Universities, we have been studying ta-C using atomistic GAP simulations. Most notably, we recently described the growth mechanism of *ta*-C films in large-scale, explicit simulations with hitherto inaccessible accuracy and in excellent agreement with experimental results [3].

However, the current version of the carbon GAP [1] has been "trained" for the pure element exclusively. The next challenge is therefore to extend the scope of simulations beyond that. We use a combination of different, complementary approaches: generating surface slab models in long GAP-driven molecular-dynamics (MD) simulations [4] and subsequently introducing functionalisation by density-functional methods. In the present case (Figure 1), we place oxygen atoms randomly on top of the slab models, and gradually heat the systems to observe preferred binding sites and reactivity.

Results

Our results are in line with chemical intuition and previous experimental knowledge (see the original work [4] for a detailed discussion): at low temperature, epoxy groups 1 are abundant at the surfaces but diminish gradually due to the ring strain; keto groups 3 play the most important role at higher simulation temperatures, and are expected to be abundant at ta-C surfaces.

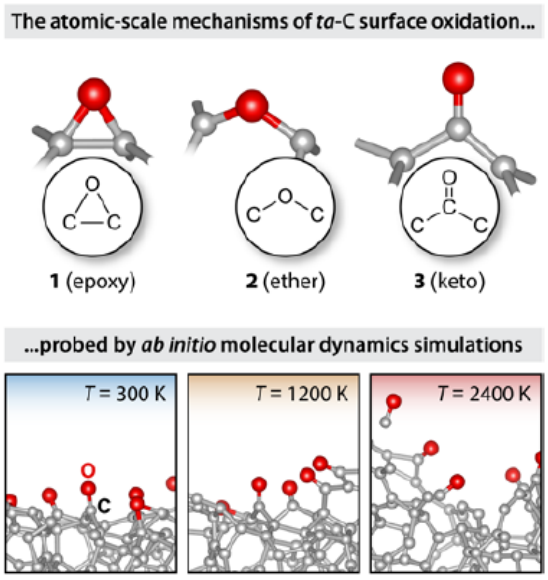

Figure 1 – Atomistic simulations of oxygen-based functional groups at the surface of a ta-C slab model. Top: Example fragments with chemical drawings; bottom: snapshots from ab initio MD simulations performed during the present visit. Adapted with permission from Ref. [4]. Copyright 2018 American Chemical Society.

Conclusions

Machine learning methods combined with DFT are opening up exciting new research directions for the accurate modelling and understanding of complex functional materials. The work performed during this visit [4] as well as our overarching and ongoing collaboration [3–5] attest to this for the technologically important case of amorphous carbon materials.

References

[1] Deringer V L & Csányi G, Phys. Rev. B, 95(09):094203, 2017. [2] Bartók A P et al., Phys. Rev. Lett. 104(13):136403, 2010. [3] Caro M A et al., Phys. Rev. Lett., 120(16):166101, 2018. [4] Deringer V L et al., Chem. Mater., in press; published online at DOI: 10.1021/acs.chemmater.8b02410. [5] Caro M A et al., Chem. Mater., in press; published online at DOI: 10.1021/acs.chemmater.8b03353.

Acknowledgements

The work has been performed under the Project HPC-EUROPA3 (INFRAIA-2016-1-730897), with the support of the EC Research Innovation Action under the H2020 Programme; in particular, the author gratefully acknowledges the support of Dr Miguel Caro and Prof. Tomi Laurila (Department of Electrical Engineering and Automation at Aalto University, Finland) and the computer resources and technical support provided by CSC – IT Center for Science, Finland.

PARALLEL SIMULATIONS OF BLOCK COPOLYMER NANOCOMPOSITES

J. Diaz[1] *and I. Pagonabarraga*[2]

[1]*Centre for Computational Physics University of Lincoln, UK;* [2]*Department of Fundamental Physics, Universitat de Barcelona, Spain*

Introduction

Simulations of Soft Matter systems (polymers, gels, colloids …) allow to gain insight over the formation of structures in the nanoscale. Simulating large systems is crucial in the study of intrinsically mesoscopic systems such as block copolymers (BCP): two or more chains of chemically distinct polymers joint together. BCP melts can serve as perfect templates to control the position of nanoparticles (NPs).

The ability to simulate large systems is crucial to study systems which can be compared with experimental results. To this end, parallel computing can be used.

Our aim is to improve the current state of simulations of block copolymer nanocomposite. To this end we use Fortran Coarrays to introduce a parallel implementation of the Cell Dynamic/Brownian Dynamic simulation scheme.

Methods

In this work, the crucial dynamic equations that determine the system at play are the Cahn Hilliard Equation

$$\frac{\partial \psi}{\partial t} = M \nabla^2 \frac{\delta F}{\delta \psi}$$

And the Langevin equation in the overdamped regime

$$v = \frac{1}{\gamma}(f + \sqrt{2k_B T \gamma}\xi)$$

Which results in a hybrid model that combines a continuous description of the BCP mixture and an individual description of the colloidal suspension [1]. This translates into an in-grid/out-of-grid which originates the difficulty of parallelisation.

Results

In order to introduce an efficient parallelisation scheme that requires a minimal modification of the original serial code, we chose the Coarray Fortran [2] approach over other methods such as COMPS or MPI as it naturally allows for domain decomposition.

In fact, we make use of a straight-forward domain decomposition method in which each processor assumes an even partition of the total system size. Inter-processor communications are required only for neighbouring domains. Furthermore, effort is made to minimise the memory requirements and each processor requires only the local version of the global variables.

In order to introduce a parallel Brownian Dynamics implementation, we need to have a way to spatially decompose the set of particles, so that NPs can be easily distributed among processors. We make use of a standard Cell List method in which NPs are distributed according to their position in the same spatial decomposition used for the CDS scheme. Each processor calculates the forces and contributions to the chemical potential of each particle within its subset, paying attention not to count NPs which are overlapping neighbouring processors. Conversely, an additional calculation is required so that each NP in neighbouring cells is checked on whether is overlapping the surrounding processors.

Finally, the scaling of the overall algorithm is checked for different number of processors. Finding a behaviour which is close to ideal (linear), as can be found in Figure 1. The scaling S=$T(1)$/ $T(n_p)$ relates the elapsed time for 1 processor and for n_p processors.

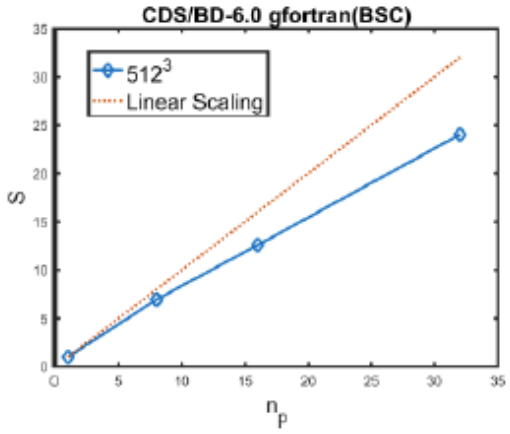

Figure 1 – Strong Scaling of the hybrid CDS/Brownian Dynamics code for 10^6 number of particles in a 512^3cube box.

Conclusions

Using the parallel implementation that has been presented we have been able to extend the previous CDS parallel model [3] into a hybrid CDS/Brownian Dynamics code that can reach considerable system sizes.

References

[1] Diaz J et al., Macro Theory and Simul (26): 1600050, 2017. [2] Fanfarillo A et al., Proc of the 8th Inter Conf on PGAS Prog Models, 2014. [3] Guo X et al. Macro Theory and Simul (16):779, 2006.

Acknowledgements

The work has been performed under the Project HPC-EUROPA3 (INFRAIA-2016-1-730897), with the support of the EC Research Innovation Action under the H2020 Programme; in particular, the author gratefully acknowledges the support of Ignacio Pagonabarraga from the Department of Fundamental Physics at the University of Barcelona and the computer resources and technical support provided by Barcelona Supercomputing Center (BSC).

HELIX FORMATION IN MITOTIC CYLINDERS

S. Franzini, D. Marenduzzo and C. Micheletti

SISSA, Trieste, Italy

Introduction

Chromatin, the complex fibre which constitutes chromosomes, is in a swollen state for most of the cell cycle. It displays a hierarchy of internal structures: at the smallest scale it forms loops and TADs (strongly interacting domains), while at larger scales it separates into compartments [1]. However, this hierarchy of structures, which are important for gene regulation, is completely lost when the cell starts its replication [2]. During mitosis chromatin undergoes a radical change which takes it from the swollen state to a cylindrical conformation. Here the action of a set of proteins called condensins shapes the polymer into an array of loop departing from a central backbone [2]. Until recently, the internal structure of these mitotic cylinders was unknown. However new experiments have found that the HiC contact maps of chromosomes in this phase display a secondary diagonal, meaning that the backbone must have a regular periodic structure [3]. Theoretical considerations have selected a helix shape as the most promising candidate for the backbone structure [3], however the physical mechanism leading to the formation of such a structure is still unknown.

Our objective is to find a simple physical mechanism able explain the formation of the secondary diagonal in experimental HiC data and to test whether the system prefers an inward helix (loops extruding from a central helical backbone) or outward helix (loops folded on the inside of a solenoidal structure). The idea that this structure is the outcome of some universal physical mechanism is rooted in two observations: the same pattern is observed in HiC maps of different cell lines and even different vertebrate organisms [3], which suggests a universal mechanism, rather than specific biological interactions, is responsible for the observed pattern.

Methods

The basic set up previously developed by the host group of Prof. Marenduzzo is a polymer brush in which two kinds of beads alternate in a 30nm fibre model. The loop beads interact through a soft potential which mimics the ability of the polymer to cross itself thanks to topoisomerases, while the backbone beads interact through the hard-core of a Lennard-Jones potential and are bound with a harmonic bond to the last bead of the following loop in the chain sequence. Different linear sizes of the loops were used, as well as a power law distribution of their sizes with different fixed averages. The model is completed by inserting bridging beads which interact with the polymer beads through a Lennard-Jones potential, and bind more strongly with the backbone beads. The bridging interaction leads to the formation of mitotic cylinders with a straight backbone. Starting with this set up we tested two models which could realistically lead to the formation of an helix in the backbone of the brush polymer. The first idea is to add a weak attraction between loop beads in order to model the effect of depletants. In fact, depletants induced attractions seem to promote the formation of helices in linear polymers [6]. A second idea is to add a twisting rigidity to the polymer and start from a rosette configuration [7] in which each loop has a fixed writhe +1, which is the experimentally measured writhe added by condensins proteins when they bind to chromatin forming a loop. The ratio behind this model is that the excess writhe of the loops can relax on the backbone by twisting it into a helix.

Results

We used different interaction strengths for the first model. Weak interactions only reduce the size of the cylinder, without other large-scale conformational changes, while strong interactions lead to the condensation of the loops into a “straight-jacket” around the backbone. However, for interactions whose strength falls in between these two extremes we can observe the collapse of the polymer into a globule where the backbone resembles an helix, albeit one with only one turn and a half. Regrettably this helical conformation does not possess the characteristics (radius, pitch) necessary to form a secondary diagonal in the contact maps. The second model also has some success in producing a helical conformation as it relaxes from the initial conformation. However, the helical conformation is rapidly lost as the polymer further relaxes and is completely disrupted by the action of the bridging beads.

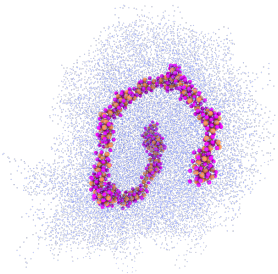

Figure 1 – Helix-like conformation obtained from the first model. The backbone (orange and purple) only forms one turn of the helix, while the loops (blue) surround it forming a blob.

Conclusions

Our results show that while it is possible to obtain helical conformations in a simple brush polymer model they are either short lived or do not possess the correct characteristics. Nevertheless, these results are also encouraging point a way forward. In fact, the helical conformations obtained through the first model resemble the configurations one would obtain by searching for the configuration that minimizes the volume occupied by short polymers [5]. In order to allow longer polymers to form a helix, one needs to apply a different criterion: the polymer needs to occupy the smallest possible volume on a local scale instead of globally. The same mechanism could be used to obtain a helix with a smaller pitch, compatible with experiments, also in our brush polymer model. Therefore, the next step of the work will focus on finding a model which reproduces this mechanism.

References

[1] B.R. Lajoie et al., Methods (2014). [2] A. Goloborodko et al., eLife (2016).[3] J.H.Gibcus et Al., Science 359, (2018). [5] A. Maritan et Al., Nature 406, (2000) [6] Y. Snir and R. D. Kamien 307, (2005) [7] C.A. Berkely et Al., JCP 140, (2014)

Acknowledgements

The work has been performed under the Project HPC-EUROPA3 (INFRAIA-2016-1-730897), with the support of the EC H2020 Programme; in particular, the author gratefully acknowledges the support of the Institute for Condensed Matter and Complex Systems of the University of Edinburgh and the computer resources and technical support provided by EPCC.

A DFT STUDY OF PD-PT-AU TERNARY NANOALLOYS

A.K. Garip[1], H. Arslan[1], D. Rapetti[2] and R. Ferrando[3]

[1]Department of Physics, Zonguldak Bulent Ecevit University, Turkey; [2]Department of Chemistry and Industrial Chemistry, University of Genoa, Italy; [3]Department of Physics, University of Genoa, Italy

Introduction

In recent years, binary and ternary metal nanoclusters take much attention due to the applications in fields such as catalysis, solid-state physics, chemical-physics, biomedicine and optics [1][2].

Methods

Gupta Level Calculations

The Gupta Potential energy function parameters are taken from reference 3, 4, 5 and 6 [3][4][5][6].

DFT Level Calculations

DFT calculations have been carried out using the Quantum ESPRESSO package, [7] employing a basis set of plane waves, ultrasoft pseudopotentials [8] and the Perdew-BurkeErnzerhof (PBE) exchange-correlation (xc-) functional [9]. The projector augmented wave method (PAW) type pseudopotentials which is generated with a Scalar-Relativistic Calculation were used for all relaxations. The energy cut-off for wavefunctions was 41.0 Ry and the cut-off energy for charge density was 448.0 Ry. Eigenvalues and eigenstates of the Kohn–Sham Hamiltonian have been calculated at the Γ point of a cubic cell of side of 17 Å, applying a Marzari-Vanderbilt smearing technique with a broadening of 0.02 Ry. A small enough mixing factor for the self-consistency was used to provide convergence. The positions of the atoms in the cluster were fully optimized until the forces were smaller than 0.02571 eV/Å per atom.

Results

The Gupta level calculations for the considered compositions of PdnPt13-nAu42 show that the icosahedral structures are energetically more favourable than decahedral structures as confirmed by DFT relaxations. The excess energy behaviours are given in Figure 1. For ternary PdnPt13-nAu42 icosahedron and decahedron structures, it is better to put a Pt atom at the central location. So the chemical orderings which the Pd atoms at subshell are energetically more favourable.

Conclusions

Both relaxed icosahedral and decahedral structures have surfaces completely occupied by Au atoms for all compositions. The chemical orderings which the Pd atoms at subshell are energetically more favourable for the icosahedral and decahedral structures. The Gupta level results have been compared with DFT level results. DFT results gave the same structure with some energetical differences.

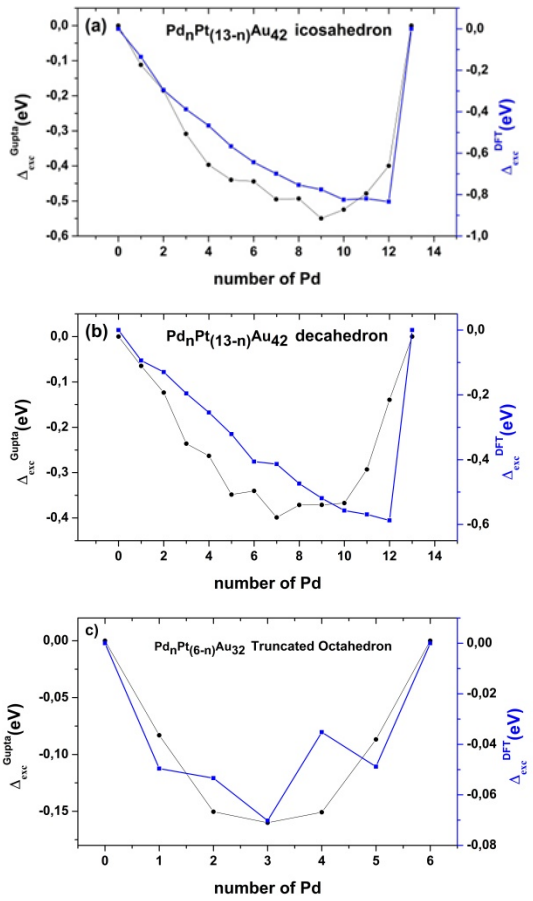

Figure 1 – The excess energy comparisons.

References

[1] Johnston RL., Atomic and Molecular Clusters. vol. 20024557. London; New York : Taylor & Francis, 2002. [2] Ferrando R et al., Chem Rev, 108:845–910, 2008. [3] Logsdail A et al., J Comput Theor Nanosci, 6:857–66, 2009. [4] Massen C et al., J Chem Soc Dalt Trans, 23:4375–88, 2002. [5] Paz-Borbón LO et al., J Chem Phys, 128:134517, 2008. [6] Rossi G et al., J Chem Phys, 122:194309, 2005. [7] Giannozzi P et al., J Phys Condens Matter, 21:395502, 2009. [8] Vanderbilt D. Phys Rev B, 41:7892–5., 1990. [9] Perdew JP et al. Phys Rev Lett, 77:3865–8, 1996.

MODELLING SUPERNOVA-DRIVEN DYNAMO WITH COSMIC RAYS

F. Gent[1] and G. Sarson[2]

[1]Aalto University, Finland; [2]Newcastle University, United Kingdom

Introduction

The majority of galaxies, similarly to our own Milky Way, are rotating about a super-massive central black hole. Most of the visible mass in each galaxy is condensed into stars with the remaining 10% or more comprising the interstellar medium (ISM) of ionized plasma, gas and dust, which fills the voids between the stars. The ISM is highly turbulent and plays a critical role in galactic evolution and structure, star formation and stellar feedback, accretion of material between the galaxies and the intergalactic medium (IGM). Away from the galactic centre, most of the visible material is compressed into a thin disk about the axis of rotation, where most stars form. As some of the larger, fast-burning stars approach the end of their life cycle they become supernova (SN), exploding huge amounts of energy and recycling some of their mass into the ambient ISM. This energy heats and stirs the ISM to drive turbulence, which redistributes some of the ISM into cold dense clouds form which the next generation of new stars are subsequently born.

As part of this process the magnetic field, which is ubiquitous throughout astrophysical bodies, is stirred and twisted by the turbulence and the large-scale differential rotation and stratification within the disk to form a dynamo, which grows the magnetic field on the smallest scales, but also orders the field on the scale of the disk. As it grows and evolves large scale structure the magnetic field provides a back reaction to the flow, effecting its kinetic properties. It is increasingly understood by astronomers and astrophysicists that this magnetic field is pivotal in explaining some of the poorly understood processes at work in the life cycles of galaxies, and our understanding of cosmic processes. Another key feature of SN-driven turbulence is the acceleration in the blast waves of plasma particles [1] to relativistic (light) speeds, which are understood to contribute as much energy to the ISM as each of the thermal and kinetic energy. The trajectories of these charged cosmic rays (CR) is strongly coupled to the magnetic field lines [2].

Methods

We have previously successfully employed the Pencil Code [3] to solve the equations of magnetohydrodynamics (MHD) to model a galactic dynamo in a highly compressible, thermally unstable ISM without CR. We use a vertically stratified sliding periodic box to model a differentially rotating segment of ISM under conditions typical of spiral galaxies and the solar neighbourhood in particular. Now we apply fluid approximation equations for CR energy and CR flux [2], to be able to examine the dynamo and subsequent ISM dynamics under much more realistic physical conditions. From this we aim to make predictions about the processes that give rise to star formation, galactic outflows and fountain, and derive sub-grid scale models of turbulence relevant to many unresolved astrophysical problems.

Results

The initial thermally stable hydrostatic ISM is perturbed be the random injection of SN, clustered mainly near the plane of the galactic disk. Until the resulting turbulence saturates the initial nano-Gauss field dissipates. Once the turbulence acquires a dominant Eigen-mode the dynamo starts to amplify the magnetic field (Figure 1).

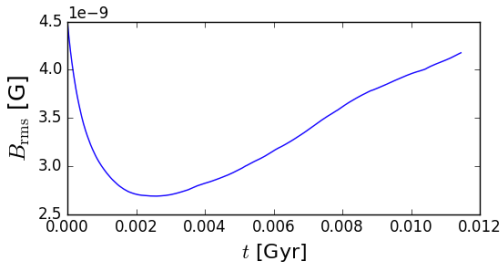

Figure 1 – Time evolution of the magnetic field.

At this stage the magnetic field is almost entirely random and CR diffusion is almost isotropic from the midplane, whence most of the SN occur. This is much more uniform than the thermal pressure distribution (Figure 2).

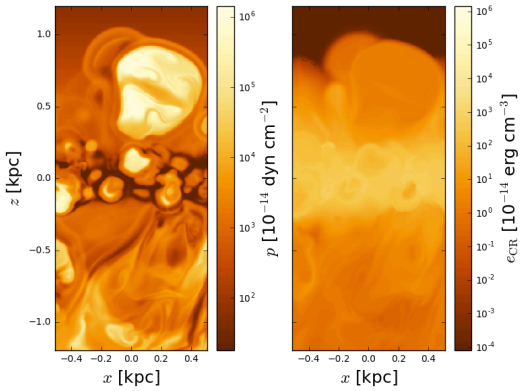

Figure 2 – 2D slices of thermal pressure and cosmic ray energy density form early kinematic dynamo stage.

Conclusions

We need to evolve the field over a Gyr to see the effect of a mean horizontal field on the CR distribution and its feedback on the global dynamics. Local SN simulations are required to explore which CR parameters will be most relevant.

References

[1] Kulsrud R. M., 2004, Plasma Physics for Astrophysics. Princeton Univ. Press, Princeton, NJ. [2] Snodin A. P., et al., 2016, MNRAS, 457, 3975. [3] Gent F. A., et al., 2013, MNRASL, 430, L40.

Acknowledgements

The work has been performed under the Project HPC-EUROPA3 (INFRAIA-2016-1-730897), with the support of the EC Research Innovation Action under the H2020 Programme; in particular, the author gratefully acknowledges the support of Newcastle University and the computer resources and technical support provided by EPCC.

STRUCTURAL CROSSOVER OF SMALL $(SIC)_N$ CLUSTERS

D. Gobrecht[1], S.T. Bromley[2,3] and J. Van Beeck[1]

[1]Institute of Astronomy, KU Leuven, Belgium; [2]IQTCUB, Barcelona, Spain; [3]ICREA, Barcelona, Spain

Introduction

In a previous study [1] we have shown that the lowest energy isomers of $(SiC)_n$, n = 1-16, can be binned in two structural cluster families: cages with purely alternating Si-C bonds (hereafter referred to as ALT) and structures exhibiting atomic segregations of Si and C (hereafter referred to as SEG). Whereas the lowest-energy configurations are dominated by the SEG family for small clusters (n < 12), clusters of the ALT family become more favourable for larger sizes (n > 12) and compete with the lowest-energy isomers of SEG family. In this investigation, we aim to rationalise the apparent energetic crossover between the two structural families SEG and ALT (structural transition) for sizes n > 12 that is observed at the M11/cc-pVTZ level of theory [2].

Methods

We extend our sample of $(SiC)_n$ clusters to a greater structural diversity and to larger sizes (n = 16-20). Moreover, we employ several techniques (bond counting, interatomic potentials, Generalised-Gradient-Approximation (GGA) and hybrid density functionals) to rationalise the total and relative potential energies of the clusters. As a representative for the GGA we choose the PBE functional [3], whereas the hybrid class of density functionals is represented by the B3LYP functional [4].

Results

None of the above methods can explain the observed energetic crossover at the M11/cc-pVTZ level of theory. Evidence for the reliability and accuracy of the M11 functional, compared to other applied methods, is based on a better agreement with experimental enthalpies at T = 0 K of the JANAF thermochemical tables and on the trends of the M11 HOMO-LUMO gap with cluster size n. Contrary to the other functionals, the M11 functional predicts the HOMO-LUMO gap of the ALT family realistically, approaching the band gap of 3C-SiC (E_{gap}(SiC) = 2.36 eV) with increasing cluster size. Moreover, the employed functionals PBE and B3LYP exhibit smaller average formal Mulliken charges for clusters of the ALT family, compared to the M11 functional.

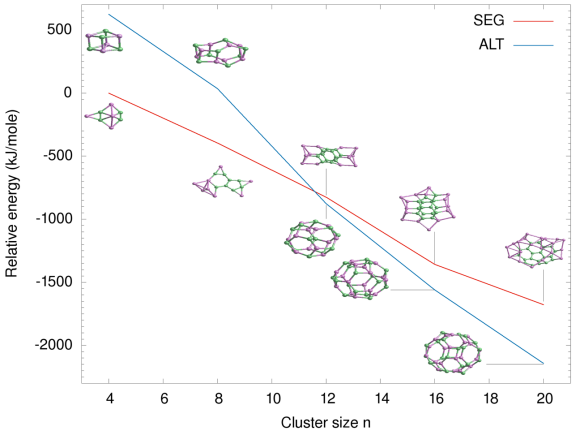

Figure 1 – Relative energies (in kJ/mole) of the lowest-energy clusters of both families (SEG (red) and ALT (blue)) versus cluster size n. Si atoms are in violet, C atoms are in green.

Conclusions

All these findings explain the high stability and low energy of the M11 optimised ALT clusters for n ≥ 12 and hint at electronic structure effects that are not captured by the PBE and B3LYP functionals. Furthermore, the observed structural transition cannot be explained by the number of bonds and its related bond strengths.

In summary, we find consistent results for members of the SEG family for all applied density functionals. For the isomers of the ALT family the situation is quite different. In terms of potential energy, HOMO-LUMO gap, and average Mulliken charge, the M11 optimised (SiC)n clusters show a clear offset with respect to the results obtained for other density functionals (PBE and B3LYP).

References

[1] Gobrecht D et al., ApJ, 840:117, 2017. [2] Peverati R and Truhlar D G, JPCL, 3:117, 2012. [3] Perdew J P et al., PRL, 77:3865, 1996.
[4] Becke A D, JCP, 98(2):1372, 1993.

Acknowledgements

The work has been performed under the Project HPC-EUROPA3 (INFRAIA-2016-1-730897), with the support of the EC Research Innovation Action under the H2020 Programme; in particular, the author gratefully acknowledges the support of Stefan T. Bromley and the Institute of Theoretical and Computational Chemistry of the Universitat de Barcelona (IQTCUB) and the computer resources and technical support provided by BSC.

ENERGY LEVEL MODIFICATION IN QUANTUM DOT – DYE HYBRIDS THROUGH LIGAND EXCHANGE

V. Golovanov[1] *and T.T. Rantala*[2]

[1]*South-Ukrainian National Pedagogical University, Odessa, Ukraine;* [2]*Department of Physics, Tampere University, Finland*

Introduction

The controlled charge transfer in quantum dot (QD) -organic dye hybrids is associated with photoinduced reactions in both directions, from dye to QD and vice versa [1]. In this context, theoretical modelling of the hybrid's functionalities will form a basis to construction of QD arrays manipulated and probed by photons or through quantum near-field interactions.

Methods

The QD with hexagonal wurtzite structure has been modelled using 6-layer slab and the most abundant (10$\bar{1}$0) surface. Due to the quantum confinement in the slab's perpendicular direction, our model is well reproducing the blueshift in energy, typical for the CdSe quantum dots [2]. The back surface of the slab was passivated with pseudohydrogens to ensure charge balance. Oxygen related species (O, OH) and typical ligands (Figure 1) commonly used for the passivation of QDs were adsorbed on the other side of the slab which was allowed to relax. The dye molecules (porphyrin and phthalocyanine) were anchored onto a surface via linkers of various lengths terminated by carboxylic groups.

Results

It was found that tilting of the dye relative to the QD's surface has a dual effect on the charge transfer. Shortening the distance between moieties enhances the tunneling probability for the electrons. By contrast, the electrostatic interaction between units may result in unfavourable relative position of the bands, which may hinder the electron transfer.

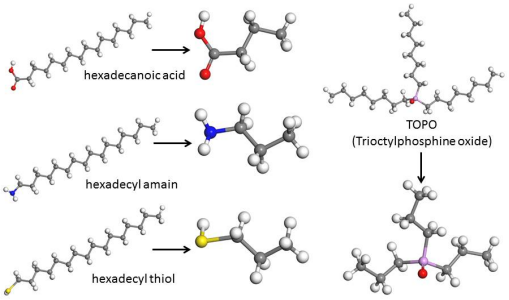

Figure 1 – Typical ligands used for the QD passivation.

Furthermore, linker may also have a twofold effect on the charge transfer by mediating the mutual conformation of the moieties and providing a suitable intermediate state for the charge transfer in QD-dye hybrids.

We have studied the effect of different species on the plane-averaged electrostatic potential of the CdSe slab. As it follows from the Figure 2, the potential undergoes big shifts, ±1eV, which may significantly affect the properties of the QD-based hybrids. Primitive adsorbates (O, OH) chemisorbed on the surface of QD have an opposite effect on the work function change, which opens an additional flexibility for the engineering of the charge transfer in the hybridized nanoparticles. The potential created by an adsorbate is screened by a dye molecule. The more dye is inclined, the more screened is the potential.

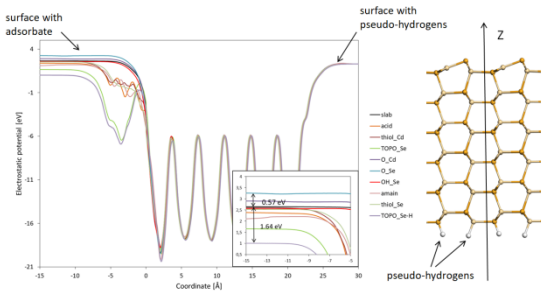

Figure 2 – Plane-averaged electrostatic potentials of CdSe slabs with different ligands.

Adsorbate	Electrostatic potential [eV]	Relative ES potential [eV]
No adsorbate	2,64	0
O_Se	3,24	+0,60
O_Cd	2,90	+0,26
OH_Se	2,56	-0,08
hexadecanoic acid	2,38	-0,26
hexadecyl amain	2,17	-0,47
hexadecyl thiol _ Se	2,53	-0,11
hexadecyl thiol _ Cd	2,60	-0,04
TOPO_Se	1,66	-0,98
TOPO_Se - H	1,01	-1,63

Table 1 - Parameters extracted from Figure 2.

Conclusions

The band energies of QDs can be modified by ligand exchange, resulting in energy level shifts of up to 1 eV. These energy level shifts provide a guide to the optimal ligand choice and device architecture for QD- hybrids photovoltaics.

References

[1] Golovanov V et al., Ukr. J. Phys., 64(1):63-71, 2019. [2] Arvani M et al., PCCP, 18, 27414, 2016.

Acknowledgements

The work has been performed under the Project HPC-EUROPA3 (INFRAIA-2016-1-730897), with the support of the EC Research Innovation Action under the H2020 Programme; in particular, the authors gratefully acknowledge the support of the computer resources and technical support provided by CSC–IT Center for Science, Espoo, Finland.

HIGH HARMONIC GENERATION IN MOLECULES

D. Gustin[1], M. Ruberti[2] and P. Decleva[1]

[1]Dipartimento di Scienze Chimiche, Universita' di Trieste, Italy; [2]Department of Physics, Imperial College London, United Kingdom

Introduction

High Harmonic generation (HGG) is a nonlinear optical process in which the frequency of laser light is converted into its integer multiples [1]. Ever since its discovery in the late 1980s, it has attracted a raising amount of attention that can be attributed to it being a promising tool for investigating and manipulating matter on the time scale of electron motion ($10^{-18}s$). This is achieved through two separate paths: on one hand HHG is being used to produce XUV and X-ray attosecond pulses [2] which can then be applied to study a wide variety of physical phenomena; on the other hand HHG can in itself be the carrier of information about chemical reactions, structural changes or even electron-hole dynamics with the necessary spatial and time resolutions. In order to extract such information, one needs to have an accurate understanding of the phenomena, which can be obtained via theoretical modelling and computation. Understanding the fine details of HHG in many-electron systems is extremely intricate and even with the huge advances in modern computing facilities, the amount of computational power and memory available are limited compared to what would be needed in order to move from atoms and small molecules to systems of higher chemical interest. Indeed, the ideal approach of solving the 3-D multi-electron time-dependent Schrödinger equation (TDSE) while accurately describing a dense-enough continuum, quickly becomes prohibitive with an increase in the number of electrons. In the present work, a density functional (DFT) scheme featuring the use of a multicentric (LCAO) B-spline basis for solving the three-dimensional TDSE is proposed as a reasonable compromise between accuracy and cost.

Methods

The numerical solution of the TDSE is obtained by expanding the wavefunction on a basis set and writing the TDSE as a system of ordinary differential equations (ODE). The solution is evaluated by discretizing the time interval into subintervals that are short enough to allow for the Hamiltonian to be considered constant within them. The time evolution of the wavefunction is then driven by the exponential of the Hamiltonian, which is computed approximately with good accuracy by employing reduced space generated by the Arnoldi-Lanczos algorithm [3].

The complexity of the calculation is strongly influenced by the level of approximation of the electronic structure. In the present method, this is done via a DFT scheme, which in the Kohn-Sham formulation [4] allows to reduce the solution of a N-particle problem to N-one particle problems in which the non-classical contributions to the Hamiltonian are modelled by a semi-empirical potential. By solving the Kohn-Sham equations one finds the initial bound states, which can be extended to describe the continuum by employing the multi-centre B-spline basis, which has already proven to be a good choice when dealing with similar phenomena that involve the photoionization process [5].
The HHG spectrum is then obtained from the expectation value of the electric dipole moment as the absolute square of the Fourier transform (FT).

Results

The method has first been tested on the simplest systems (H, H_2^+); then, its accuracy has been studied by comparing results to those obtained vie the algebraic diagrammatic construction (ADC) method (Ar, CO_2) [6][7]. Finally, the method has been applied to simulate HHG spectra for two molecular systems of higher chemical interest: benzene and pyrazine. The comparison between the two (figure 1) shows the effect that chemical modification (substitution of two C-H with N) can have on the harmonic emission.

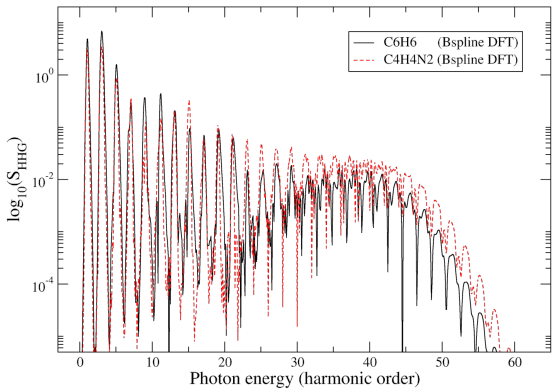

Figure 1 – HHG spectra of benzene (black) and pyrazine (red). The pulse has a peak intensity of $3.5 * 10^{14}\ \frac{W}{cm^2}$, the wavelength is $800nm$ and duration of 8 optical cycles.

Conclusions

The method has proven to be a valid approach for obtaining an accurate *ab initio* description of high harmonic generation. The computational effort in achieving such simulations is relatively contained, indeed, given access to high performance super-calculators, one can compute analogous results for other similar multi-electron systems within one day. Hence, in the upcoming future the method will be exploited to obtain results for more systems of high chemical interest, possibly opening the way to high harmonic spectroscopy as an active investigation tool of chemical systems.

References

[1] Eden J.G., Prog. Quant. Electron., 28(3-4), 197-246, 2004. [2] Jie Li et al., Nat. Commun., 8(1), 2017. [3] Saad Y., Numerical Methods for Large Eigevalue Problems, (1992). [4] Kohn W. et al., Phys. Rev., 140(4A):1133, 1965. [5] Bachau H. et al., Rep. Prog. Phys., 64 (12): 1815-1943, 2001. [6] Ruberti M. et al., J.Chem.Phys., J. Chem. Phys., 141, 164126, 2014. [7] Ruberti M. et al., Phys.Chem.Chem.Phys., 20, 8311, 2018.

Acknowledgements

The work has been performed under the Project HPC-EUROPA3 (INFRAIA-2016-1-730897), with the support of the EC Research Innovation Action under the H2020 Programme; in particular, the author gratefully acknowledges the support of Dr. Marco Ruberti from the Quantum Optics and Laser Science group (Imperial College London) and the computer resources and technical support provided by EPCC.

EFFICIENT PHASE SPACE SAMPLING OF A CACO3 COMPUTER MODEL: A NOVEL APPLICATION OF THE NESTED SAMPLING TECHNIQUE

G. Hantal[1], *L. Bartók-Pártay*[2]

[1]*Computational Physics Group, University of Vienna, Austria;* [2]*Department of Chemistry, University of Reading, United Kingdom*

Introduction

The enigmatic phenomenon of biomineralisation, the process by which living organisms incorporate minerals into their bodies, keeps intriguing researchers for decades. One of the really amazing aspects of this phenomenon is the precision by which organisms control the morphology as well as the polymorphism of the crystallites they incorporate into very complex structures. Despite the decades-long scientific efforts, our knowledge on the mechanism of this extremely precise morphology and polymorph control is still very limited. In this project, we focused on $CaCO_3$, the most abundant mineralising compound in invertebrate organisms, which has received continued attention over the last 30 years. In order to study biomineralisation computationally, one needs a reliable computer model that correctly reproduces the relative stability of the various polymorphs in a wide range of representative conditions. Therefore, we decided to determine the phase diagram of one of the latest, and probably the best, $CaCO_3$ computer model so far developed [1].

Methods

We used the nested sampling technique to explore the configurational space of the applied computer model [2]. Our ultimate goal was to thoroughly sample the basins corresponding to the particular polymorphs and to determine partition functions related to those basins. From these partition functions, for example (absolute) free energies can subsequently be derived. In this work, we used pymatnest, an open-source, highly parallel computer code to perform nested sampling calculations [3]. Nested sampling is a Bayesian sampling technique that can be used to efficiently sample very complex multidimensional functions (such as the potential energy surface defined in the configurational space) without any prior knowledge on the object to be sampled. The method operates with independent samplers, called 'walkers' that explore the function to be sampled concurrently but without any need for information from each other. Furthermore, since the NS procedure is independent of temperature, these quantities can be calculated at arbitrary temperatures in the post-processing phase. Another appealing feature of NS is that it samples the potential energy surface starting from the high-energy region, and thus no prior knowledge of the potentially stable structures is needed.

Results

The problem turned out to be more difficult than we originally expected. In fact, the number of walkers had to be increased to an unusually high number (in the order of 4000 – 5000, as compared to the more customary number of roughly 1000 walkers observed for simpler systems). This number was especially necessary at lower pressures. On the other hand, we noticed that considering 12 ion pairs resulted in noisy heat capacity curves, which made the determination of the phase boundaries inaccurate. Repetition of the calculations with 24 ion pairs (or even more) will be necessary to conclude the study and perform all the planned analyses.

Figure 1 shows the estimated phase diagram based on the position of the local maxima of the computed heat capacity curves obtained at different pressures. The model displays a melting transition at temperatures 1200 K higher than those experimentally measured. We also observed an order-disorder transition in the range of 1000-1500 K (confirmed by changes in the radial distribution functions). Further computations are needed to understand the nature of this transition.

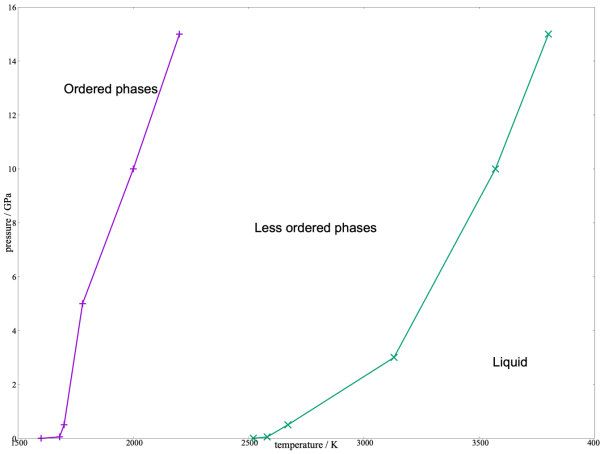

Figure 1 – Estimated phase boundaries determined from the location of maxima in the heat capacity curves. The points along the lines have an uncertainty of +/- 300 K.

Conclusions

We observed that larger system sizes and more walkers are needed to provide the necessary precision. Further computations will be needed to conclude the study that the applicant will try to cover from different sources.

References

[1] Raiteri P. et al., J. Phys. Chem. C 119:24447, 2015. [2] Pártay L.B. et al., J. Phys. Chem. B 114:10502, 2010. [3] https://github.com/libAtoms/pymatnest

Acknowledgements

The work has been performed under the Project HPC-EUROPA3 (INFRAIA-2016-1-730897), with the support of the EC Research Innovation Action under the H2020 Programme; in particular, the author gratefully acknowledges the support of Dr. Lívia Bartók-Pártay at the Department of Chemistry of the University of Reading and the computer resources and technical support provided by EPCC.

THE EFFECT OF DEFECTS AT LAO/STO INTERFACES

A.V. Kimmel

CIC nanoGUNE, Tolosa Hiribidea, San Sebastian, Spain

Introduction

Oxide heterostructures exhibits an exotic physical phenomenon emergent at the oxide interface such as high mobility two-dimensional electron gas (2DEG). However, the physical nature of 2D electron gases still remains elusive. In this work we study the properties of intrinsic defects that may occur at the interface between $LaAlO_3$ (LAO) and $SrTiO_3$ (STO). We study the most abundant defect in oxide material such as neutral oxygen vacancy, V_O.

Methods

We perform our calculations of LAO/STO interfaces with the Density Functional Theory (DFT) methods. We used a relatively large system to treat a system with defects: the lateral dimension of the system was chosen to be 4x4 unit cells. The LAO/STO (001) interface can be dually terminated, namely, either LaO/TiO_2 (LT) or SrO/AlO_2 (AS). Here, we calculate simultaneously the both interfaces, LT and AS, using a superlattice geometry.

Results

Our DFT calculations of ideal bulk LAO and STO compounds demonstrate that both systems are open gap insulators. Placing both materials together leads to electronic rearrangement and band bending (See Figure 1d). Here, the band bending leads to overlap of occupied states at AS interface leading to appearance of two-dimensional hole gas (2DHG). Another LT interface appeared at opposite side of the system and characterised by the appearance of two-dimensional electron gas (2DEG), which shown by blue spilled area in Figure 1c.

Partial Density of States calculated for each atomic layer in the heterostructure shows a characteristic bending of the bands due to uncompensated electric field in the system. The bands overlap at the LT and AS interfaces where occupied and unoccupied states overlap the Fermi energy forming 2DHG and 2DHG, respectively.

In the studied heterostructure the vacancy defect in STO part of the system placed at Sr- O layers, i.e. axial vacancy, is 0.3 eV more stable than the one in TiO2 layer (See Fig. 2a). The energy difference between axial (VO in SrO layers) and equatorial (VO in AlO2 layers) sites In LAO is only of 0.1 eV. Remarkably, we found that the relative stabilities of the vacancies in LAO/STO heterostructure vary with respect to the distance to the interface. Indeed, the vacancies at the adjacent layers of AS interface (TiO2 and LaO atomic layers) have the lowest energies among probed, while LT interface shows increased vacancy formation in LAO layer. This is because the formation of a neutral oxygen vacancy in ABO3 perovskite is related to localisation of two electrons at B-site cation. Since AS interface is the one accommodating hole gas, thus the appearance of two electrons would be electrostatically advantageous although damaging for the electron gas itself. In STO the stability of the vacancies is lower than in LAO, while there is a slope of energies - the closer to LT interface the higher the stability of the vacancy. We assume that at finite temperatures there is a natural drift of VO towards LT interface, where the vacancies appearing at LAO part will stabilise. However, vacancy diffusion to the highest stability sites at AS interface will be damaging for the 2DHG.

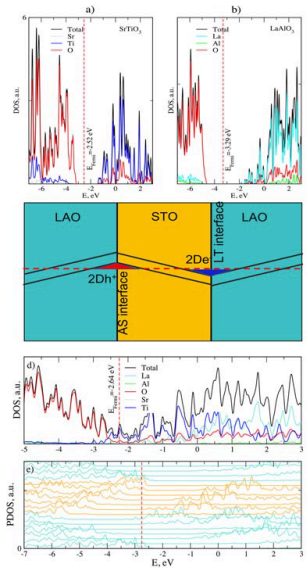

Figure 1 – Electronic properties of LAO/STO interfaces. Total density of states calculated for ideal bulk a) LAO and b) STO systems. c) Schematic representation of conduction and valence band profiles in LAO/STO system, where red and blue spilled areas correspond to 2DHG (2D h+) and 2DEH (2D e-), respectively. d) Total density of states calculated for LAO/STO heterostructure. e) Partial Density of States calculated for each atomic layer of heterostructure.

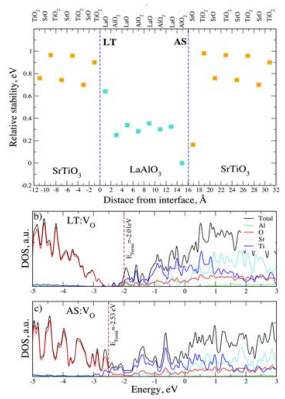

Figure 2 – Properties of neutral oxygen vacancies at interfaces of LAO/STO system: a) Stability of the VO defect as a function of the distance from; Density of States of LAO/STO system with VO at b) LT and c) AS interface.

Conclusions

In this work we found that oxygen vacancy defects would preferably accumulate at LT and AS interfaces, existence of a critical temperature above which vacancies will tend to migrate to AS interface making a damaging effect to 2DHG.

Acknowledgements

The work has been performed under the Project HPC-EUROPA3 (INFRAIA-2016-1-730897), with the support of the EC Research Innovation Action under the H2020 Programme; in particular, the author gratefully acknowledges the computer resources and technical support provided by ARCHER, EPCC.

DETECTING INTERMITTENT STRUCTURES IN TURBULENT COLLISIONLESS PLASMAS WITH MACHINE LEARNING

M. Kruuse[1] and J. Nättilä[2]

[1]Tartu Observatory, University of Tartu, Estonia; [2]Nordita, KTH Royal Institute of Technology and Stockholm University, Sweden

Introduction

Generation of turbulence is a ubiquitous phenomena in fluids and plasmas. Especially interesting is the formation of a turbulent cascade in a new, largely unexplored regime of relativistic turbulence in collisionless plasmas [1]. Extremely diluted, magnetically dominated uniform plasma that is stirred with large-scale motions quickly develops a turbulence cascade. In a presence of a strong ambient magnetic field the turbulent plasma forms magnetic tubes that are oriented along this external guide field. When these tubes collide and merge, a strong current sheet is formed in between to balance the suddenly flipping local magnetic field. Physically these intermittent sheet-like structures are thought to be responsible of the energy dissipation in the plasma. Understanding how they behave is essential for understanding the physics of the relativistic kinetic turbulence. A major problem is how to separate and analyse these localized structures. We use well-tested image processing and machine learning tools to identify these structures from direct numerical simulation data.

Methods

Main goal is to use state-of-the art deep learning algorithms to detect current sheets from spatiotemporal data. Before this step unsupervised machine learning algorithms will be trained to detect clusters from the data. This will provide us with insights to the data and rough labels for further supervised machine learning training.

We use an artificial neural network algorithm called self-organizing maps (SOM; [2]), to study the underlying structures of the high-dimensional data, obtain rough labels for training, and get insights to the physical processes.

The SOM provides us with clusters for each ndimensional input vector. The algorithm generates a 2-dimensional map of neurons, where each neuron has a vector of randomly sampled weights “living” in the n-dimensional space of the input data. Each input vector will be matched to its closest (calculated by the use of a distance metric) neuron on the map (Best Matching Unit or BMU). The BMU n-dimensional vector of weights and other neurons in neighbourhood (governed by the neighbourhood function in the algorithm) of the BMU will be updated using the used input vector data. The algorithm produces a map of neurons representing the input data in 2- dimensional space, with n-dimensional weight vectors. These neurons are then divided into clusters dependent on their similarity on the map. Each neuron connects to input vectors thus providing us with clusters of the input data.

Results

Figure 1 (left panels) depicts snapshots of the magnetically dominated turbulent collisionless plasma data in the view of one feature, the density of particles. By eye it is easy to see circular and elongated higher density regions (the yellow peaks in the figure). A SOM algorithm was trained to detect these structures from an 8- dimensional feature space. Right panels in Fig. 1 show the result of a SOM algorithm trained on the data. Different colours denote different clusters. We can see that the algorithm is able to grasp the underlying structures of the ndimensional space and separate particles visually to different clusters. As a next step, we are using these SOM results to train a deep neural network that automates this structure segmentation problem.

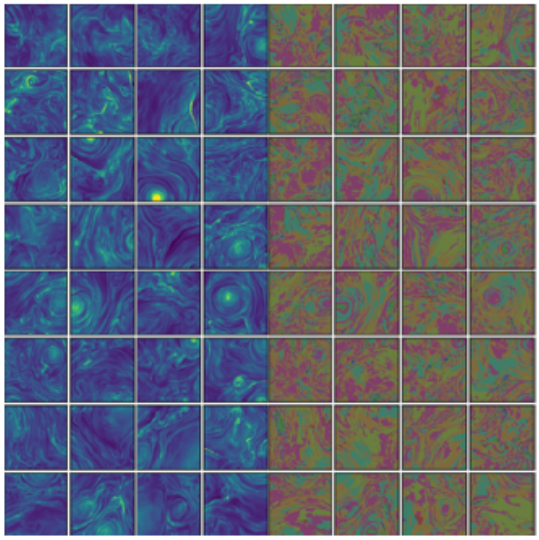

Figure 1 – 32 representative simulation snapshots used to train the image detection algorithm. Left panels show the plasma density (dark to light blue colours). Right panels show different data clusters as predicted by SOM algorithm (different colours denote different clusters).

References

[1] Nättilä J., arxiv:1906.06306, 2019. [2] Kohonen T., Self-Organizing Maps, Springer, 2001

Acknowledgements

The work has been performed under the Project HPC-EUROPA3 (INFRAIA-2016-1-730897), with the support of the EC Research Innovation Action under the H2020 Programme; in particular, the author gratefully acknowledges the support of Lilit Axner and the computer resources and technical support provided by PDC.

COUPLING MOLECULAR COOLING AND MULTI-PHASE STAR FORMATION

U. Maio

Leibniz Institute for Astrophysics, Potsdam, Germany

Introduction

Numerical simulations of primordial objects and determination of early molecule creation on first cosmic structures are fundamental issues that need to be investigated to increase our understanding on the formation, growth and evolution of primordial galaxies, also in light of current and future instruments (like ALMA, JWST, E-ELT, SKA, SPICA) that will be able to prove the very distant and young Universe. For this reason, it is necessary to develop detailed numerical models that can treat cosmic gas from its early phases down to its collapse and conversion into stars and galaxies. In this work, we couple a detailed treatment of non-equilibrium chemistry, with a state-of-the-art scheme accounting for multi-phase star formation and stellar feedback effects. These two modules are the basic "ingredients" in the modelling of early Universe.

Methods

We start from the chemistry module [1,2] based on a set of chemical reactions and corresponding partial differential equations integrated via a backward difference scheme, in a nonequilibrium approach. The simulation time-step is limited by the reaction rates for sake of convergence: this enables an accurate description of the chemical content of cosmic gas at different redshifts (z) and of its thermodynamical evolution, as well. The chemistry network is responsible for predicting the correct abundances of molecular gas at high over-densities and its density-dependent cooling rate. Following star formation is addressed by the recently developed three-phase scheme [3]. It consists of ordinary differential equations describing the flows of matter among three different phases of cosmic gas (a cold phase, a hot phase and a star formation phase), integrated with an adaptive Runge-Kutta integrator within the hydrodynamical time-step. The kinetic energy resulting from supernova explosions is re-distributed to neighbours, while thermal energy is given to the hot phase, whose long cooling times ensure that it is not immediately radiated away. In practice, star formation feedback injects entropy and shocks in the neighbouring particles, heats up the surrounding medium and pollutes the gas with heavy elements (the metallic species tracked are C, N, O, Ne, Na, Mg, Si, S, Ca, Fe). These two modules are coupled together to study early structure formation, chemistry evolution and galaxy assembly in different regimes.

Results

The implementation is tested and debugged by running numerical simulations of isolated galaxies shaped by a dark-matter potential, a stellar bulge and a gaseous disk (initial conditions are depicted in Figure #1 for face-on and edge-on views).

The assumed cosmological model is a standard model of an expanding Universe with cold dark matter, cosmological constant, expansion parameter in units of 100 km/s/Mpc, h=0.7, gaussian perturbations for the power spectrum having a slope of 1 and normalisation via mass variance within 8 Mpc/h radius of 0.8. We adopt two resolutions for the initial conditions of a galaxy with about 1e12 solar masses/h at redshift z=0. The high-resolution runs have dark matter and gas with initial particle mass of 1.3e7 and 4.8e6 solar masses/h for about 90000 particles per species. The low-resolution runs have darkmatter and gas particles with initial mass of 1.4e8 and 2.6e7 solar masses/h for about 14000 particles per species. Once run, the output snapshots are post-processed to assess the good behaviour of the developed model, by checking the thermal conditions in which molecular gas is found and if/when triggers star formation; by investigating the implications of stellar feedback mechanisms for the survival of molecular gas at different redshifts; and by studying the gaseous dynamical properties during stellar-mass assembly.

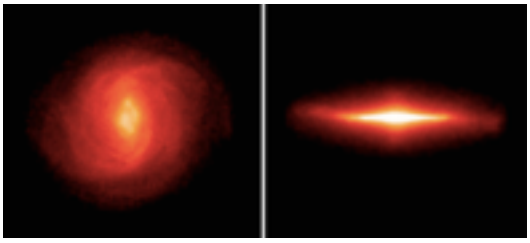

Figure 1 – Simulated galaxy seen face-on (left) and edge-on (right).

Conclusions

The analyses presented here are based on the implementation of an advanced theoretical model for primordial galaxy formation. A nonequilibrium molecular chemistry network [1,2] has been coupled with a multi-phase star formation scheme [3] and tested on a number of numerical simulations with different resolutions. This allowed us to develop a detailed model of molecular-driven star formation to study, in an advanced fashion, the interplay among molecular chemistry, star formation and feedback effects.

References

[1] Maio U.+, Mon. Not. R. Astron. Soc., 407:1003 (2010). [2] Maio U.+, Mon. Not. R. Astron. Soc., 460:3733 (2016). [3] Murante+, Mon. Not. R. Astron. Soc., 447:178 (2015).

Acknowledgements

The work has been performed under the Project HPC-EUROPA3 (INFRAIA-2016-1-730897), with the support of the EC Research Innovation Action under the H2020 Programme; in particular, the author gratefully acknowledges the support of the Italian National Institute for Astrophysics in Trieste (Italy), INAF-TS, and the computer resources and technical support provided by CINECA (Italy) under grant award HPC17ERW30.

A QUANTITATIVE UNDERSTANDING OF MICROSCOPY EXPERIMENTS OF POLYCYCLIC AROMATIC MOLECULES ON METAL SURFACES

M. Melle-Franco[1] *and D. Peña*[2]

[1]*Aveiro Institute of Materials, University of Aveiro, Portugal;* [2]*Centro Singular de Investigación en Química Biolóxica e Materiais Moleculares, Universidade de Santiago de Compostela, (Spain)*

Introduction

Cycloarenes constitute a fascinating class of polycyclic aromatic hydrocarbons (PAHs) that have attracted the scientific community for decades due to the singularity of their molecular and electronic structures. They serve as ideal platforms to investigate fundamental questions around the concept of aromaticity and, in particular, those related to the π-electron distribution in complex aromatic systems. We present a comprehensive computational study of Kekulene on gas-phase and on-surface as well as the simulation of non-contact AFM microscopy images.

Methods

We computed the kekulene molecule in vacuum and on the Cu(111) surface. The molecule on surface was computed with a QM/MM procedure where the copper surface is modelled by Molecular Mechanics (MM) and it is coupled to the molecule computed at the DFT level via a classical interaction derived empirically to reproduce experimental data. In addition, a third model where charge images in the metal were computed classically, QM/MM-CI was also tried. Two different DFT Hamiltonians were used PBE (for the QM/MM and QM/MM-CI models) and B3LYP for the vacuum model.

Results

Experimentally the CC bonds in kekulene show a large variation ranging from 1.35 to 1.47 Å. This is reproduced within 0.01 Å by B3LYP-def2-TZVP level calculations, Figure 1.

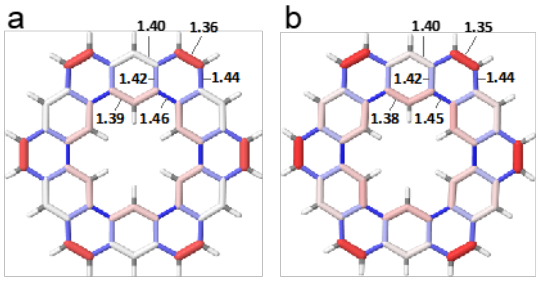

Figure 1 – (a) Molecular structure of kekulene (1) computed at the B3LYP-def2-TZVP level in vacuum. (b) Experimental structure from XRD, C2/c space group symmetry. The colours grade with distance from 1.33 Å (red) to 1.40 Å (white) and to 1.47 Å (blue). Bond lengths are in Å.

The bonding pattern of kekulene matches perfectly the predictions by π-sextet rule empirically derived by Erich Clar. This rule states that the most representative structure in benzenoid polyaromatic hydrocarbons corresponds to the average of the Kekulé resonance structures that possesses the largest possible number of disjoint aromatic π-sextets. An aromatic π-sextet is defined as six π-electrons localized in a single benzene-like ring separated from adjacent rings only by formal single bonds. For Kekulene there are 200 Kekulé possible valence structures, but it only has 1 Clar structure.

A similar structure and properties are obtained on-surface which indicates that, since kekulene carbon framework is flat, the gas-phase model can be a good approximation to model microscopy on-surface, Figure 2.

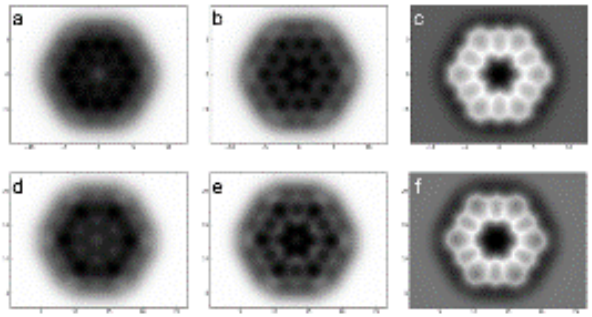

Figure 2 - PPM simulated AFM images with an amplitude of A = 1 Å computed with a B3LYP vacuum geometry without effective charges and with bending stiffness of k = 0.35 N/m at z = 3.7 Å in (a) 3.6 Å in (b) and 3.2 Å in (c) with respect to the molecular plane and with a PBE QM/MM geometry on Cu(1,1,1) and bending stiffness k = 0.35 N/m, with a d_z2 -like quadrupole tip (Qd_z2=-0.25 e^- Å^{-2}) at z= 3.4 Å in (d), 3.3 Å in (e) and 3 Å in (f) with respect to the molecular plane. All distances are in Å.

Conclusions

A comprehensive computational study of kekuelene, its structure and microscopy images was performed and compared very favourably with experiment [1]. The larges differences were found to be due to Hamiltonian, as B3LYP reproduces more accurately experimental (XRD) results than PBE, Figure 1. The bond alternation in gas-phase and with several on-surface models corresponds to Clar predicted structure.

References

[1] Pozo S.I. et al, Submitted, 2019.

Acknowledgements

The work has been performed under the Project HPC-EUROPA3 (INFRAIA-2016-1-730897), with the support of the EC Research Innovation Action under the H2020 Programme; in particular, the author gratefully acknowledges the support of Diego Peña, CIQUS Universidade de Santiago de Compostela and the computer resources and technical support provided by BSC.

PARTICLE-IN-CELL SIMULATIONS OF KINETIC INSTABILITIES AND KINETIC TURBULENCE IN SOLAR WIND CONDITIONS USING THE NEW ENERGY CONSERVING SEMI-IMPLICIT METHOD (ECSIM)

A. Micera[1,2]

[1]*Solar-Terrestrial Centre of Excellence, Royal Observatory of Belgium, Belgium;* [2]*Centre for Mathematical Plasma Astrophysics, KU Leuven, Belgium.*

Introduction

We present preliminary results from full PIC simulations of firehose instability and plasma turbulence, performed with ECSIM. Firehose instability is thought to be a crucial mechanism for constraining the observed electron and ion anisotropies in expanding astrophysical plasmas, such as the solar wind. Owing to the perfect stability and accuracy of the ECSIM code, the interplay between anisotropic protons and electrons in the firehose instability is extensively explored for the first time via 2D fully kinetic simulations. In addition, we explore a regime of plasma turbulence - low electron plasma beta - where recent studies suggest that the dynamics of physical processes that are believed to be responsible for the cascade at kinetic scales (nonlinear interaction of dispersive wave modes and magnetic reconnection), is expected to present features different from what typically observed in the solar wind.

Methods

A preliminary parameter scan was done to guarantee that the grid resolution and the size of the simulation box do not affect the simulation results. In particular, to investigate the interplay of proton and electron anisotropies in the firehose instability, and hence to find the appropriate parameters to make the simulations feasible, several 1D tests of the ECSIM code have been performed. Convergence analysis confirmed the exact energy conservation of the method and suggested that when it is applied to multi-scale problems it allows covering a wide range of resolutions without producing numerical instabilities. However, after this first parameter scan, we moved to larger two-dimensional simulations, which have been necessary to compare numerical results with observations.

Results

In our simulations of the full spectrum of firehose instability, electrons with a bi-Maxwellian initial distribution, isotropize earlier than ions. Electrons consume a part of the free energy produced by the temperature anisotropy more efficiently. Once they reach a condition of marginal stability (with the distribution function becoming close to an isotropic Maxwellian), protons start to be scattered by the interaction with the magnetic field fluctuations (produced also by electrons) until their total isotropization. One can also see that in the simulation in which both species are initially anisotropic, the isotropization of protons starts earlier than in the simulation of the proton firehose with isotropic electron distribution. As regards the simulations of turbulence, they exhibit a remarkable quantitative agreement with recent observations by MMS in the magnetosheath, allowing us to investigate simultaneously the spectral break around ion scales and the two spectral breaks at electron scales, the magnetic compressibility, and the nature of fluctuations at kinetic scales. Moreover, they allow us to provide predictions for observations by NASA's Parker Solar Probe mission in the solar corona. Our numerical simulations employing a low electron beta, typical of the solar corona, allow us to provide predictions for observations by NASA's Parker Solar Probe mission.

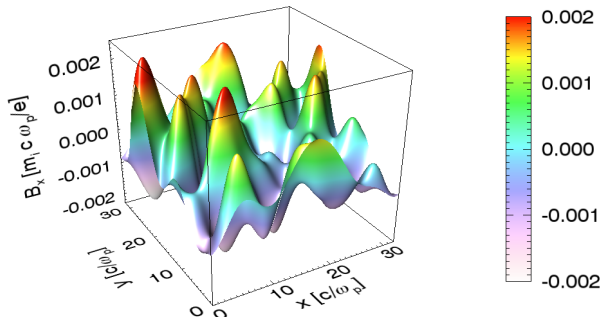

Figure 1 – Out of the plane magnetic field B_z into the turbulent cascade.

Conclusions

Our simulations of proton firehose instability in solar wind conditions obtained retaining a kinetic description for both protons and electrons, lead us to carry out work in an international refereed journal, which is currently under review [1].

Since the realistic simulation parameters are obtained thanks to in situ measurements of the solar wind, to improve the description of the unexplored inner heliosphere, the use of the oncoming Parker Solar Probe's data will be particularly important. Moreover, a work that aims to demonstrate the coexistence of kinetic instabilities with strong plasma turbulence in the expanding solar wind seems the most reasonable to continue the work started during the HPC-EUROPA3 project.

References

[1] A. Micera et al., 2019, arXiv: 1907.08502.

Acknowledgements

The work has been performed under the Project HPC-EUROPA3 (INFRAIA-2016-1-730897), with the support of the EC Research Innovation Action under the H2020 Programme; in particular, the author gratefully acknowledges the support of Elisabetta Boella and the computer resources and technical support provided by CINECA.

ANALYSIS OF NONDYNAMIC ELECTRON CORRELATION IN DFT

C. Naim

University of Pisa, Donostia International Physics Center, Italy

Introduction

The electron correlation energy is defined as the difference between the exact energy (E_{exact}) and the Hartree-Fock one (E_{HF}). This energy could be splitted into dynamic or nondynamic contributions:

$$E_{corr} = E_{exact} - E_{HF} = E_{ND} + E_{D} \quad .$$

Nondynamic correlation (NDC) is inadequately treated in most Kohn-Sham DFT (KS-DFT) approximations. An estimate of NDC in KS-DFT is therefore of paramount importance. Through the knowledge of the one-particle density matrix (1RDM) it has been shown [1] that it is possible to study the importance of correlation and its prevalent type for the system under investigation. However, the 1-RDM in the KS reference is idempotent, therefore it does not explicitly show correlation effects. In this work, starting from a KS electron density, recovered the correlated 1RDM following two different approaches.

Methods

If a method includes correlation, the occupancies of the natural orbitals (NOs) are fractional (different from 0 and 1). Our methods would be therefore focused in the construction of a set of occupancies and the corresponding NOs able to correctly describe correlation in the system. In the first route, we have fitted a correlated electronic density computed at the Variational Monte Carlo (VMC) level using an N-representable trial 1RDM. The correlated electronic density has been reconstructed on a grid by means of an appropriate gaussian smearing technique which was applied to a sufficiently large number of configurations from the VMC importance sampling. The fit was performed through a 1RDM computed from a wavefunction able to reproduce NDC effects, first with a General Valence Bond (GVB) wavefunction, and secondly the accuracy was increased employing a CASSCF one. The second route considered in this study involved Broken Symmetry DFT (BS-DFT) computations. In this way, we included NDC effects by breaking the spin symmetry and, subsequently projecting the 1RDM in a basis of NOs, we extracted the occupancies. Several DFAs have been considered to analyse how NDC is treated by unrestricted KS-DFT in the different rungs of the Jacob's ladder. The amount of correlation included in each method has been evaluated using global and local indicators of correlation [2]. The calculated occupancies would be then related to KS single particle energies through a Fermi-like distribution (FD), in order to reproduce indicators of correlation employing the diagonal elements of the single particle energy matrix projected on the NOs basis.

Results

As test cases, we have considered a set of 8 molecules in which NDC contribution is important. The size of these molecules and the computational cost of the VMC method have made it necessary the use of the supercomputers resources. These molecules are: BeH2(TS), O_3, cyclobutadiene(D2h), cyclobutadiene(D4h), m-, o-, p-benzyne and psb4. The methods investigated allowed the extraction of fractional occupancies and therefore the inclusion of NDC effects. In Fig 1 it is shown the comparison between the indicators of local NDC for the p-benzyne molecule. The two methods investigated correctly reproduce the prevalence of NDC effects in the regions in which the diradicals are located. Moreover, the same effects could be reproduced by the NOs obtained from the fit of the FD.

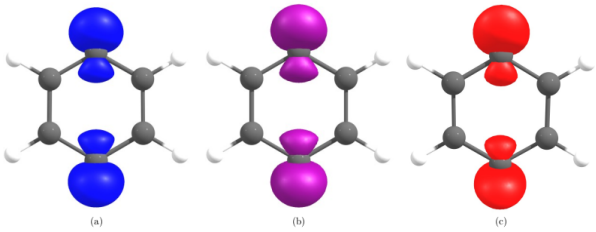

Figure 1 – Local indicators of NDC of para-benzyne for: (a) qmc-fit, (b) bs-b3lyp, (c) fit of FD for bs-b3lyp

Conclusions

The methods introduced in this work allow a qualitative reproduction of NDC effects for the tested systems starting from a KS-1RDM. By means of the FD it is possible to connect these results to single particle energies. These results could be employed in the development of new functionals based on local decomposition of NDC effects.

References

[1] Ramos-Cordoba, E.; Matito, E. Local Descriptors of dynamic and nondynamic correlation. J. Chem. Theory Comput. 2017, 13, 2705–2711. [2] Ramos-Cordoba, et al. Separation of dynamic and nondynamic correlation. Phys. Chem. Chem. Phys. 2016, 18, 24015– 24023.

Acknowledgements

The work has been performed under the Project HPC-EUROPA3 (INFRAIA-2016-1-730897), with the support of the EC Research Innovation Action under the H2020 Programme; in particular, the author gratefully acknowledges the support of Donostia International Physics Center and the computer resources and technical support provided by BSC-CNS.

RHEOLOGICAL CHARACTERISATION OF SUSPENSIONS OF SOFT DEFORMABLE DROPLETS IMMERSED IN NEMATIC LIQUID CRYSTALS

G. Negro[1] *and D. Marenduzzo*[2]

[1]*Dipartimento di Fisica, Università degli studi di Bari and INFN, Italy;* [2]*School of Physics and Astronomy, University of Edinburgh, United Kingdom*

Introduction

Concentrated suspensions of colloidal particles in a liquid solvent are ubiquitous in industry and nature. While hard sphere fluids have been studied extensively less is known about the flow response of suspensions of deformable particles. Here we characterize numerically the rheological properties of a suspension of soft deformable droplets. We perform both macro and micro-rheology numerical experiments.

Methods

The continuous dynamical variables are the nematic tensor, the concentration and the velocity field. The corresponding coupled dynamics equations are the advection-relaxation equation, the advection-diffusion equation and the Navier-Stokes equations. The latter is numerically solved using a Lattice-Boltzmann solver, coupled to finite difference method for the order parameters dynamics (concentration and nematic tensor) [1]. A different concentration field is associated to each droplet in the system, each evolving according to an advection-diffusion equation. Relevant time scales are reached thanks to the MPI implementation.

Results

We begin discussing the macro-rheology. The suspension of soft deformable droplets (red regions in Figure 1a) are immersed in a nematic liquid crystal (white rods in Figure 1a represent the director field). The whole system is enclosed between two walls (at y=0 and y=L=256). Periodic boundary conditions are applied in the x direction. A Pressure difference is also imposed between x=0 and x=L=256. We measured the apparent viscosity as a function of the pressure difference. Results are shown in Figure #1b. Two different transitions are visible. The first one is a yielding transition at very low values of ΔP. In fact, viscosity goes to infinity for very low values of ΔP, meaning that there exists a threshold under which droplets remain static. Above this threshold the system starts to flow as a whole, meaning that the entire system is drugged by the pressure difference. Enlarging the pressure difference a discontinuous shear thinning transition is observed. This marks the transition to a state in which the suspension behaves as a fluid. In the micro-rheology experiments a single droplet is chosen and drugged with a body force f (for example the black circled droplet in Figure 1a). We measured the mean droplet velocity in the steady state as a function of the body force f (Figure 1c and 1d), for different values of packing fraction. The micro-rheological characterization again confirms the existence of two transitions. A yield stress transition is signalled by the fact that there exists a threshold value of the body-force above which the dragged droplet starts to move. Above this threshold the droplet crosses the system, and in doing so, thanks to the elastic response of the nematic liquid crystal in which droplets are immersed, drags also the neighbouring droplets. The discontinuous shear thinning transition is signalled by a jump in the velocity over f plot. This means that, starting from that value of the force f, the system starts to behave as a fluid.

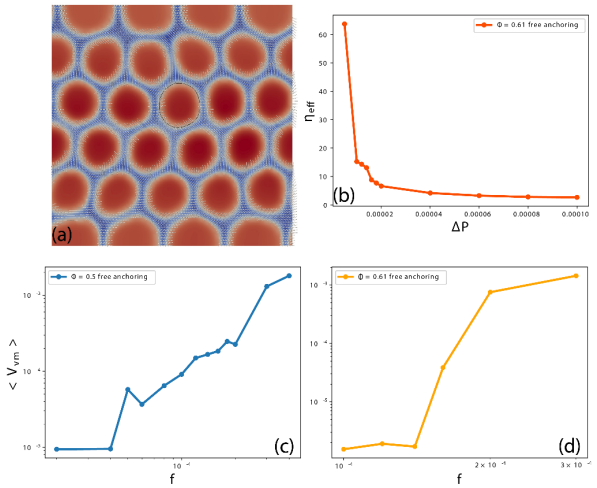

Figure 1 – (a)Snapshot of a simulation. Here the contour plot of the scalar order parameters is displayed, with superimposed director field. (b) Apparent viscosity vs pressure difference. (c)-(d) Steady state velocity vs body-force f.

Conclusions

Performing in silico macro and micro-rheological experiments we have shown the existence of two transitions in a suspension of soft deformable droplets immersed in a nematic liquid crystal: a yield stress transition and a discontinuous shear thinning transition.

References

[1] Eur. Phys. J. E (2019) 42:81.

Acknowledgements

The work has been performed under the Project HPC-EUROPA3 (INFRAIA-2016-1-730897), with the support of the EC Research Innovation Action under the H2020 Programme; in particular, the author gratefully acknowledges the support of Davide Marenduzzo of the University of Edinburgh and the computer resources and technical support provided by EPCC.

INTERACTION OF INTENSE FIELD WITH MATTER AND GAMMA RAY SOURCE

J F. Ong

Extreme Light Infrastructure - Nuclear Physics

The peak power of the laser is breaking a new record to 10 PW in 2019 at ELI-NP [1]. To perform the experiments with this laser in an efficient way, several aspects such as possible outcomes, optimised configuration, and the involved physical models have to be tested first through numerical simulations. However, the difficulty in laser-material interaction diagnosis lies in the need to detect physical reactions down to very small spatiotemporal scales, severely limiting the observation by existing measuring devices. In addition to the use of more advanced and expensive measuring probes, such as X-ray free-electron lasers, numerical simulation is the alternative option. The physical phenomena occurring inside the experimental sample can be confirmed by comparing the initial conditions of the simulation with the experimental data. Numerical simulation support for experimental data brings credibility and reliability to publications. Therefore, most of the large research facilities have established high-performance computing centres with unlimited access to thousands to hundreds of thousands of cores. Parametric space exploration through two-dimensional simulation, including quantum processes and radiation friction, can be used for preliminary research and scaling tests. Typically, a two-dimensional simulation requires the use of a few hundred cores and run for a few days or weeks. After that, three-dimensional simulations can be performed on significantly larger machines, with tens of thousands of cores to get the detail and more accurate results. The numerical simulations are indispensable for the implementation of the ELI-NP project.

The optimisations of the commissioning experiments by using equipment with characteristics beyond any existing machines are performed mostly by numerical simulations. Exploration of new experiment configurations and setups are the subject of the ongoing research topic. For that, we carried out a series of simulations on Laser Wakefield Acceleration (LWFA) and Target Normal Sheath Acceleration (TNSA). These simulations involve the usage of the developed numerical code in simulating the proposed experiment. In particular, this will include the use of Particle-In-Cell (PIC) code such as EPOCH and PIConGPU.

By using the laser parameters available in Institute of Plasma Physics & Laser (IPPL) and ELI-NP, we carried out a few simulations on ARIS. The simulations performed by using EPOCH code were run on THIN nodes.

For the simulations performed by using PIConGPU code, a few dependencies were installed on ARIS as a module and run on GPU nodes. Figure 1 shows the 2D slice of LWFA performed by using EPOCH3D code. The electron charges up to 15 nC was observed at T = 2940 fs. The electron bunch charge up to 30 nC is also observed after a longer simulation. The same simulation was repeated by using PIConGPU and a similar order of electron bunch charge was obtained. The execution on CPUs (EPOCH3D) takes up to 38400 core-hours (800 cores in 48 hours) while the execution on GPU (PIConGPU) take up to 1280 core-hours (16 GPUs, 160 cores in 8 hours) for 50000 timesteps. An extensive study for the execution time, domain decomposition in 2D and 3D was carried out for both codes. The paramedic study of PIC simulation on CPU and GPU on ARIS would provide an insight for the code user in choosing the optimised computational configuration in the future.

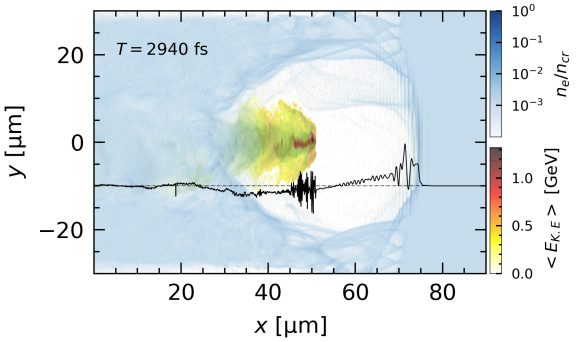

Figure 1 – Simulation result of LWFA by using 10 PW laser pulse in an underdense plasma with density ne = 0:0087ncr. The simulation was carried out by using 3-dimensional PICon- GPU and EPOCH code. 2D slice of electron density (white to blue colour map) and average kinetic energy (yellow to black) at z = 0. The lineout corresponds to the longitudinal electric field along x = 0.

Acknowledgements

We acknowledge the support of PIConGPU developers for the guidance during the installation processes. We also thank the developer of EPOCH and PIConGPU for helpful guidance in resolving issues in the simulation.

PLASMONIC SATELLITES IN HOMOGENEOUS ELECTRON GAS

Y. Pavlyukh

Department of Physics and Research Center OPTIMAS, Technische Universität Kaiserslautern, Germany

Introduction

In angular resolved photoemission spectroscopy (ARPES), an ultraviolet photon impinging onto a sample leads to the emission of an electron. Due to the interaction with other electrons, the particle undergoes multiple scatterings, which cause it to come with a reduced energy to the detector. In this project, we investigate the homogeneous electron gas (HEG) as a paradigmatic correlated electron system. This report is specifically focused on the electron-plasmon interactions and on the novel processes revealed by self-consistent calculations.

Methods

Here, we use our recently established approach—the positive definite diagrammatic approximations [1,2]—to perform extensive calculation in the nonequilibrium Green's function formalism. Because the respective Feynman diagrams are written in the Fermi Golden rule form, the spectral densities are manifestly positive as required by the probability interpretation.

Results

In Figure 1, the electron scattering rates (they are related to the lesser and greater components of the self-energy operator) are computed to the 2nd order in the screened Coulomb interaction, i.e., a subset of vertex diagrams is included. Already the one-shot calculations [3] are nontrivial, revealing the generation of two plasmons—this physical mechanism is hard to capture within the formalism of many-body perturbation theory (MBPT). Until recently, it was only possible to describe using the cumulant expansion, which has a number of conceptual limitations on its own, such as inability to describe states close to the Fermi level.

Higher-order self-consistent MBPT calculations, which are conserving [4] and do not suffer from these deficiencies, are rare and require additional approximations. For instance, in the self-consistent calculation for a model electron-plasmon system [5], the plasmons are kept "frozen", i.e., there is no feedback of the electron density on the plasmonic dispersion. Here, the feedback is incorporated for the first time into the calculations with a vertex function. In order to appreciate the difference, the input electron spectral function is taken in the form of two sharp satellites that accompany the quasiparticle peak. In reality, they are broadened due to dispersion of plasmons. Thanks to this 3 quasi-particle peaks (3qp) approximation, the screened interaction can be analytically computed (additionally showing a number of inter-band plasmons, Ωpl), and subsequently used in the electron self-energy allowing to resolve the origin of its spectral features.

For instance, the simultaneous creation of two intra-band plasmons (2ωpl) is now accompanied by a wealth of other mechanisms such as the generation of inter-band plasmons or the promotion of an electron to a satellite state (marked with different colours).

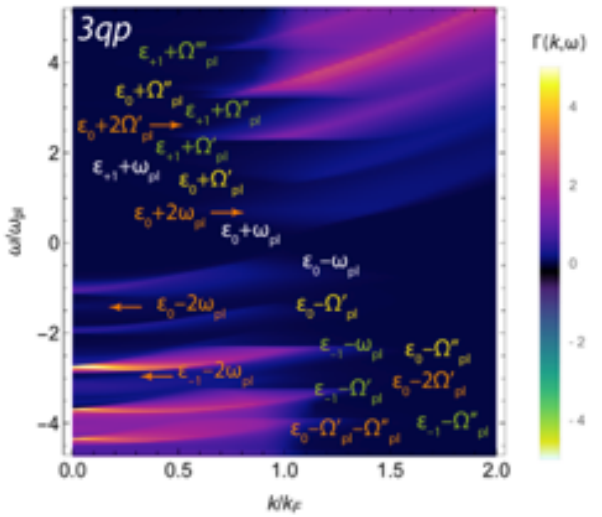

Figure 1 – The momentum- and energy-resolved scattering rates due to generation of the intra- (white) and inter-band (green) plasmons, and 2nd order processes (orange) in HEG with consistent and fully screened interactions.

Conclusions

For correlated electrons at metallic densities, the most efficient process is the one in which the additional energy is absorbed by collective excitations—plasmons. Electron-plasmon interaction is manifested in the electron spectral function in the form of satellites [6]. It is shown that they result from the quantum-mechanical superposition of different scattering channels. More detailed reports can be found in the forthcoming publications.

References

[1] Stefanucci et al., Phys. Rev. B 90, 115134 (2014). [2] Uimonen et al., Phys. Rev. B 91, 115104 (2015). [3] Pavlyukh et al., Phys. Rev. Lett. 117, 206402 (2016). [4] Holm and von Barth, Phys. Rev. B 57, 2108 (1998). [5] Pavlyukh, Scientific Reports 7, 504 (2017). [6] Riley et al., Nature Communications 9, 2305 (2018).

Acknowledgements

The work has been performed under the Project HPC-EUROPA3 (INFRAIA-2016-1-730897), with the support of the EC Research Innovation Action under the H2020 Programme; in particular, the author gratefully acknowledges the support of Prof. Robert van Leeuwen, Department of Physics, Nanoscience Center, University of Jyväskylä and the computer resources and technical support provided by the CSC-IT Center for Science (Espoo, Finland).

ON THE CONNECTION BETWEEN CLUSTER COOL-CORENESS AND COSMOLOGICAL SHOCK WAVES

S. Planelles

Department of Astronomy and Astrophysics, University of Valencia, Spain

Introduction

X-ray observations of galaxy clusters show that, within their virial radius, clusters are nearly self-similar. However, when more central cluster regions are observed, they can be classified in cool-core (CC) and non-cool-core (NCC) systems. Cluster properties result from a complex interplay between astrophysical (e.g. gas cooling, star formation, metal enrichment, SN and AGN feedback, …) and gravitational processes (e.g. mergers, gas accretion, shock waves, turbulence, …) [2]. Among other challenges, in order to reproduce the cluster CC/NCC dichotomy, different astrophysical processes have been included in simulations. Additional gravitational phenomena, such as shock waves, may also affect the energetic balance of the ICM. Within this context, it is very difficult to understand and simulate, in a consistent way, the interaction between gravitational and astrophysical processes at play in the formation and evolution of cosmic structures. Previous numerical studies have suggested a relation between the global dynamical state of clusters (relaxed or unrelaxed) and the strength of their associated shock waves [1,5]. However, so far, there is not such a study with a proper population of simulated CC/NCC clusters. Therefore, in this project we pretend to investigate the connection between the cluster cool-coreness and the strength of the shock waves developed in the gas within and around the cluster virial radius.

Methods

We analyse a set of re-simulations of 29 Lagrangian regions around massive clusters, performed with an improved version of the SPH GADGET-3 code [4]. These simulations, including gas radiative cooling, star formation, metal enrichment, SN and AGN feedback, have shown an excellent agreement with different cluster observations and have also reproduced the

CC/NCC dichotomy in terms of thermal and chemical cluster core properties [3].

In order to obtain the distribution of shock waves in these simulations, we apply a grid-based shock-finding algorithm [1]. This code needs to be applied on a computational grid where the main gas quantities are stored in cells of any given resolution. Therefore, we have prepared a post-processing code that proceeds as follows. For each selected simulated cluster, with virial radius Rvir, we build a cubical box, centred in the cluster position, with a side length of 4xRvir. The box is then discretised with a given number of cubical cells (128^3, 256^3, 512^3 and 1024^3 cells). Then, we select all the gas particles within a distance of $2xR_{vir}$ from the halo centre and, by means of a triangular shaped cloud method, we smooth their main properties onto the grid. After this, we apply the shock finder in order to compute the shock Mach number for several radial apertures from the cluster centre (R_{core}=0.05xR_{180}, R_{2500}, R_{500}, R_{vir}). Once this procedure is applied to the main 29 clusters, we are ready to analyse the distribution of shock Mach numbers as a function of z, cluster mass, cluster coolcoreness, cluster dynamical state and radial aperture.

Results

As an example of the preliminary results we have obtained, we show in Fig. 1 a zoom projection (with depth ~$0.1R_{vir}$) of the distribution of shock Mach numbers at z=0 as obtained around two clusters of our sample: D4 and D21. In terms of their global dynamical state and core properties, D4 and D21 have been classified, respectively, as unrelaxed/NCC and relaxed/CC clusters [3]. Although a visual inspection of these distributions dos not provide direct conclusions, we are now in place to address all sort of connections between the distribution of shock waves and the main virial and core cluster properties.

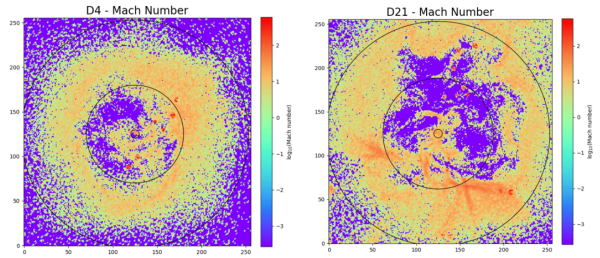

Figure 1 – Distribution of shock waves at z=0 (represented by the Mach number) for clusters D4 and D21. Each projection has a side length (thickness) of $2xR_{vir}$ ($0.1xR_{vir}$). The circles show R_{core}, R_{500} and R_{vir}.

Conclusions

We expect the final analysis of these results to shed some light on the interplay that may exist between astrophysical and gravitational processes in shaping virial and core cluster properties. Moreover, we expect the outcomes of this project to be very relevant in view of the possible future detection of cosmic shock waves by forthcoming radio facilities.

References

[1] Planelles S. et al., MNRAS, 428: 1643-1655, 2013. [2] Planelles S. et al., SSR, 188: 93.139, 2014. [3] Rasia E. et al., ApJL, 813: L17, 2015. [4] Springel V. et al., MNRAS, 364: 1105, 2005. [5] Vazza F. et al., MNRAS, 395: 1333-1354, 2009.

Acknowledgements

The work has been performed under the Project HPC-EUROPA3 (INFRAIA-2016-1-730897), with the support of the EC Research Innovation Action under the H2020 Programme; in particular, the author gratefully acknowledges the support of Prof. Stefano Borgani (Astronomical Observatory of Trieste, University of Trieste) and the computer resources and technical support provided by CINECA.

REMNANTS OF PRECESSING BINARY BLACK HOLES

L. Reali

Dipartimento di Fisica, Università degli Studi di Milano, Italy

Introduction

Binary black holes are prominent sources of gravitational waves. Systems where both holes are spinning represent the most general and complex scenario. The three angular momenta of the binary are all coupled to each other and precess, changing their orientations in space. Meanwhile, energy and angular momentum are slowly radiated away in the form of gravitational waves, causing the orbital separation to shrink and ultimately driving the black holes to merger.

The final mass, spin and recoil velocity of a black hole remnant are significantly affected by the precessional properties of its progenitor. The aim of this project was hence to explore the correlations between the dynamics of precessing binary black holes and the parameters of their merger remnants.

Methods

We developed a new evolutionary procedure for binary black holes by putting together the multi-timescale approach of [2,3] with the recent surrogate model of [1]. This allowed us to connect the asymptotic parameter space of precessing binaries to the properties (i.e. the final mass, spin and recoil velocity) of the merger remnant, thus mapping the general relativistic two-body problem from t=-∞ to t=+∞ (where t is time). We argue how, for a given astrophysical configuration, the predictions of the remnant properties necessarily suffer from theoretical uncertainties due to the high number of orbits and precessional cycles before merger. The final mass, spin and recoil velocity of the remnant are then set by the extraction of two random parameters: the precessional and orbital phases.

In order to characterize the precessional dynamics during the late inspiral, we also make full use of the concept of spin morphology [2,3].

Results

First of all, we focused on studying the impact of the uncertainty on the precessional and orbital phases on the estimates of the remnant parameters. We picked a certain binary configuration at $t = -\infty$, and we extracted thousands of different values of the precessional and orbital phases. For each couple of values, we predicted the corresponding mass, spin and recoil velocity of the merger remnant, thus providing an estimate of the range of the error produced by this random sampling. Then, we fixed the precessional phase and repeated the process extracting the orbital phase only, distinguishing the two different contributions to the uncertainty.

Finally, we explored how the remnant parameters are affected by the spin morphology at small separations. We considered populations of thousands of binary black holes with isotropically distributed spins at $t = -\infty$ and we exploited our procedure to provide an estimate of their merger remnant parameters. We computed the spin morphology at separations of $\sim 10r_g$(where r_g is the gravitational radius of the binary), showing that, as expected, details on how the various regions of the remnant parameter space are populated strongly depend on the features of spin precession at small separation.

Conclusions

In this work, we extensively studied the theoretical, unavoidable uncertainties on the estimates of the parameters of a binary black hole's merger remnant. We found that, as expected, the overall errors on the recoil velocity are huge (more than ∼50%), dominated mostly by the randomization of the orbital phase. On the other hand, the errors over the final mass are basically negligible to all practical purposes (being of order ∼0.1-0.5%), while the uncertainties over the remnant spin (that can reach values of∼3-5%) may play an important role when confronting theoretical predictions with measurements as the gravitational wave detectors keep on being improved.

Moreover, we confirmed that the properties of a merger remnants carry robust information on the spin dynamics of their precessing progenitors. Binary black holes with different spin morphologies at small separations tend to form remnant that cluster into different regions of the parameter space.

Our projects opens up many promising lines of research to interpret LIGO/Virgo data, and delivers new predictions to be tested in the upcoming age of high-precision gravitational wave astronomy.

References

[1] Varma V. et al., PRL, 122:011101, 2019. [2] Gerosa D. et al.,PRD, 92:064016, 2015. [3] Kesden M. et al.,PRL, 114:081103, 2015.

Acknowledgements

The work has been performed under the Project HPC-EUROPA3 (INFRAIA-2016-1-730897), with the support of the EC Research Innovation Action under the H2020 Programme; in particular, the author gratefully acknowledges the support of Dr. Davide Gerosa and the Institute for Gravitational Wave Astronomy at the University of Birmingham and the computer resources and technical support provided by the EPCC Centre.

GRAPHENE ADHESION ON DIFFERENT SUBSTRATES: AN AB INITIO ANALYSIS

P. Restuccia[1,2] *and M.C. Righi*[2]

[1]*Department of Chemistry, Imperial College London, United Kingdom;* [2]*Dipartimento di Scienze Fisiche, Informatiche e Matematiche, Università di Modena e Reggio Emilia, Italy*

Introduction

The search for novel lubricant materials and coatings has gained paramount importance in recent years to face the high economic and environmental costs related to friction and wear. Furthermore, the development of micro- and nano-electromechanical systems quests for new solutions for tribological problems that seriously compromise their functionality. For these reasons, solid lubricants earned great importance in technological applications concerning friction reduction [1]. Graphene emerges as a new lubricant with great potentialities due to its high strength, chemical stability and easy shear capability [2]. It is difficult to properly understand the atomistic origin of graphene lubricating effect over different substrates by experiments in real-time, thus first principles simulations represent a very powerful tool in this context. In particular, the passivating effect of graphene over different substrates can be analysed.

Methods

We perform density functional theory (DFT) calculations within the plane-waves/pseudopotential scheme [3], considering the local density approximation (LDA) for the exchange-correlation functional. We study graphene adsorption on iron, copper and copper dioxide (Cu_2O). In the case of iron, we considered the (110) surface as the most stable surface, whereas for copper and Cu_2O we considered the (111) surface. Graphene adsorption on the different substrates is studied using periodic supercells containing a slab and a vacuum region of 15 Å thickness. The in-plane size of the supercells is varied according to the lattice mismatch between the graphene layer and the surface: the (3x5√2) is used for the Fe(111) substrate, the (1x1) cell for Cu(111), and a (2x2) cell for the Cu_2O(111) surface. For all the considered systems, the residual lattice mismatch between graphene and the substrates is around 3%. We calculate the graphene binding energy over the different substrates as $E_{adh} = (E_{sub} + E_{graph} - E_{tot})/A$, where A is the in-plane area of the considered supercell, $E_{sub}(E_{graph})$ is the total energy of supercell containing the isolated substrate (graphene) and E_{tot} is the total energy of the same supercell containing the adsorbed graphene on the considered substrate.

Results

The optimized structures of graphene adsorbed on the three considered substrates are shown in Figure 1, along with the calculated binding energy, E_{adh}, and distance, d. We obtain the highest graphene binding energy for the Fe(110) substrate (0.75 J/m²), whereas the adhesion on Cu_2O(111) and Cu(111) is lower (0.54 J/m² and 0.21 J/m², respectively).

The results for bare copper are in agreement with previous theoretical calculations [4]. The difference in the binding energy can be explained by considering the reactivity of the atoms in the different substrates: the copper atoms of the bare substrate have fully occupied d orbitals and are less reactive when exposed on the surface than the Cu atoms belonging to the oxidized substrate, where the interaction with oxygen atoms results in several undercoordinated sites that are more reactive [5]. Moreover, graphene binds more strongly on Fe(110) than on the Cu(111)/Cu2O(111) substrates because the d states of iron, which are partially occupied, undergo rehybridization with π orbitals of graphene, promoting chemisorption instead of physisorption [6]. These differences in the binding energy can have a direct impact on the tribological behaviour of graphene on the different substrates, due to its chemical passivation effect.

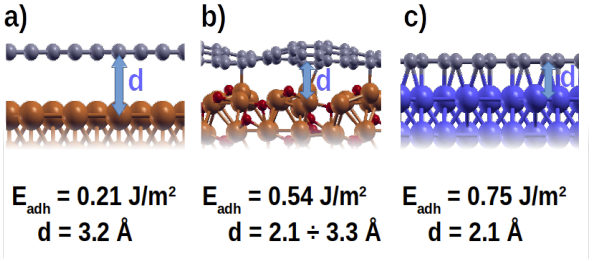

Figure 1 – Lateral views, adsoprtion energies and optimized distances of graphene on a) Cu(111), b) Cu_2O(111) and c) Fe(110) substrates. Gray, red, brown and blue balls indicate carbon, oxygen, copper and iron atoms, respectively.

Conclusions

We analyse the adsorption of graphene over different substrates and we find the highest binding energy when the bare iron surface is considered. This difference in the graphene adhesion is due to the different electronic structure of the substrates: iron has partially occupied d orbitals, which can hybridize with the graphene π orbitals, whereas copper d valence states are fully occupied, thus leading to graphene physisorption. Copper oxide has an intermediate behaviour since certain surface atoms are undercoordinated, thus leading to a selective strong interaction with graphene orbitals. This result confirms that graphene can be used effectively to passivate reactive surfaces, thus leading to a lubricant effect of chemical nature that can be exploited in many technological applications.

References

[1] Scharf TW et al., J. Mater. Sci., 48(2):511, 2013. [2] Berman D et al. Mater. Today 17(1):31, 2014. [3] Giannozzi P et al., J. Phys.: Condens.Matter 21(39):395502, 2009. [4] Khomyakov PA et al., Phys. Rev. B 79:195425, 2009. [5] Soon A et al., Phys. Rev. B 75:125420, 2007. [6] Vinogradov NA et al., Phys. Rev. Lett. 109:026101 (2012).

Acknowledgements

The work has been performed under the Project HPC-EUROPA3 (INFRAIA-2016-1-730897), with the support of the EC Research Innovation Action under the H2020 Programme; in particular, the author gratefully acknowledges the support of Imperial College London and the computer resources and technical support provided by EPCC.

TORSIONAL WAVE INTERACTIONS IN COMPLEX NETWORKS OF MULTIPLE FLUX TUBES

B. Snow, F. Gent, V. Fedun, S. Grant, D. Jess, G. Verth

Introduction

Observations of the solar photosphere reveal the complex nature of the solar surface and the plethora of small-scale motions present in our dynamic Sun. These features are of paramount importance in understanding the fundamental dynamics of the solar atmosphere because they increase the available magnetic energy, drive dynamics in the upper atmosphere, and contribute towards coronal heating. Many studies have been performed to analyse the propagation of torsional waves in a single flux tube and found that a number of wave modes can be excited. However, the solar atmosphere feature far more complex networks of multiple expanding and merging flux tubes and can introduce new mechanisms for heating the solar atmosphere. In particular, we have found that torsional Alfven waves can interact in merging flux tubes to create a shock that heats the ambient plasma by more than an order of magnitude [1]. A recent observation revealed a shock-like structure occurring in a complex network of closely-packed magnetic pores. This project uses the observed photospheric magnetic field to construct a 3D numerical equilibrium that is used as the initial conditions for MHD simulations. This allows us to provide a better understanding the physical processes in creating this shock structure in interpret the results using complimentary observational and numerical evidence.

Outcomes

The main outcome of this project involved extending the work of [2] to allow construction of networks of magnetic flux tubes from an HMI magnetogram of the solar surface. Synthesising realistic atmosphere is computationally expensive because the forcing terms between flux tubes need to be calculated, and many flux tubes need to be fitted, hence the requirement for HPC in generating the 3D atmosphere.

We wrote a series of new routines for the Pysac code that automatically locate the flux tubes and their magnetic field strengths, and construct the three-dimensional magnetic atmosphere. The photospheric magnetic field is obtained using SDO/AIA magnetograms and can easily be extended to other observations with other instruments.

The software we developed is able to generate 3D stable, non-force-free, magnetic atmospheres of the sun. An example atmosphere is included in the attached Figure, which shows the magnetic field lines above an observed photospheric magnetogram. The new code is parallelised and can run using HPC facilities.

The construction methodology and example atmospheres are published as [3].

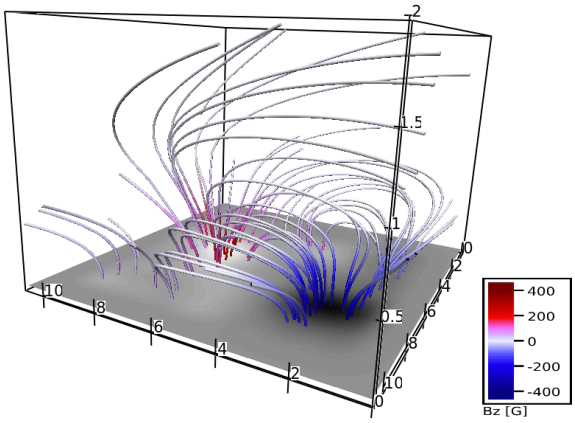

Figure 1 – Observed photospheric magnetic (lower colour map) and constructed magnetic field lines (coloured by vertical magnetic field strength).

Future work

Work is ongoing to perform numerical simulations using the constructed networks to analyse shock formation. In particular, we aim to construct an atmosphere from the observed magnetogram that appears to be showing the shock formation phenomena present in the numerical simulations of [1]. The numerical simulation will then allow us to fully analyse the formation of such shocks.

References

[1] B. Snow, V. Fedun, F. A. Gent, G. Verth, and R. Erdelyi APJ, vol. 857, p. 125, Apr 2018. [2] F. A. Gent, V. Fedun, and R. Erdelyi ApJ, vol. 789, p. 42, Jul 2014. [3] F. A. Gent, B. Snow, V. Fedun, and R. Erdelyi MNRAS, vol. 489, pp. 28{35, Oct 2019.

Acknowledgements

The work has been performed under the Project HPC-EUROPA3 (INFRAIA-2016-1-730897), with the support of the EC Research Innovation Action under the H2020 Programme; in particular, the author gratefully acknowledges the support of Fred Gent (Aalto University) and the computer resources and technical support provided by CSC.

DISSECTING THE ACTIVE GALACTIC NUCLEUS IN CIRCINUS – II. PARSEC-SCALE DUST EMISSION EXPLAINED BY A THIN DISK AND A POLAR OUTFLOW

M. Stalevski[1], K. Tristram[2] and D. Asmus[3]

[1]Astronomical Observatory, Belgrade, Serbia; [2]European Souther Observatory, Santiago, Chile; [3]Department of Physics & Astronomy, University of Southampton, United Kingdom

Introduction

Recent observations that resolved the mid-infrared (MIR) emission of active galactic nuclei (AGN) for the first time, surprisingly revealed that the thermal dust emission appears extended in the polar direction, at odds with the expectations from the canonical dusty torus. This polar dust, tentatively associated with dusty winds driven by radiation pressure, is found to have a major contribution to the MIR flux from scales of a few to hundreds of parsecs. One such source with a clear detection of the polar dust is a nearby, well-known AGN in Circinus galaxy. In the first paper [1], we successfully explained the observed peculiar MIR morphology of Circinus on large, tens of parsec scales with a model consisting of a compact dusty disk and an extended hollow dusty cone. In this work, we further refine this model on the small, parsecs scales to test whether it can explain the MIR interferometric data as well.

Methods

To calculate how the above described model would appear in the IR, we employed SKIRT (http://www.skirt.ugent.be), a state–of–the–art 3D radiative transfer code based on the Monte Carlo technique [2]. The primary source of the photons is an accretion disk approximated by a point-like source with anisotropic emission pattern, while its SED is described by a standard composition of power-laws. The dust is distributed on an adaptive grid with a large number of cells whose size is set by an algorithm ensuring the proper sampling of the dust density and optimal usage of the computational memory at the same time. The photons are propagated through the simulation box following the standard Monte Carlo radiation transfer prescriptions that take into account all the relevant physical processes: anisotropic scattering, absorption, and thermal re-emission.

At the end of the simulation, images and SEDs of the model can be reconstructed for the comparison with the observations in the entire wavelength range of interest.

Results and conclusions

We produced the images of our model consisting of a dusty disk seen almost edge-on and a dusty polar outflow in the form of a hyperboloid shell. Using these images, we simulated interferometric observations of the model to compare it to the MIDI data. From our investigation, we conclude that the disk + hyperboloid model is able to reproduce well the interferometric observations, i.e. the shape of the correlated flux as a function of the position angle, at all wavelengths, and at both shorthand long baselines.

Our results reinforce calls for caution when using the standard dusty torus models to interpret the IR data of AGN.

Further study of polar dust emission in larger samples is necessary to constrain its properties and assess its ubiquity in the whole AGN population. To meet this goal, new models of AGN dust emission are needed. We propose the here presented model of the AGN in the Circinus galaxy to serve as a prototype for the population of AGN with detected polar dust emission.

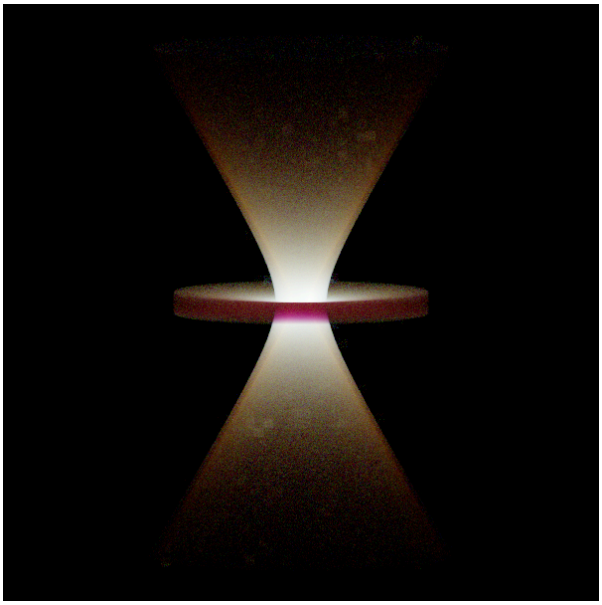

Figure 1 – A composite colour image of AGN in Circinus model obtained with radiative transfer simulations.

References

[1] Stalevski M., Asmus D., Tristram K. R. W., 2017, MNRAS, 472, 3854.
[2] Camps P., Baes M., 2015, Astronomy and Computing, 9, 20.

Acknowledgements

The work has been performed under the Project HPC-EUROPA3 (INFRAIA-2016-1-730897), with the support of the EC Research Innovation Action under the H2020 Programme; in particular, the author gratefully acknowledges the support of Vassilis Charmandaris from the Department of Physics, University of Heraklion, Crete and the computer resources and technical support provided by GRNET.

MACHINE LEARNING DETECTION TECHNIQUES FOR SPATIAL MODE RECOGNITION AFTER BEING PROPAGATED THROUGH ATMOSPHERIC TURBULENCE

A. Vallés[1], N. Bornman[2], A. Forbres[2], J.P. Torres[1], J. Leach[3]

[1]ICFO-Institut de Ciencies Fotoniques, Barcelona Institute of Science and Technology, Spain; [2]School of Physics, University of the Witwatersrand, South Africa; [3]IPaQS, SUPA, Heriot-Watt University, Edinburgh, United Kingdom

Introduction

Most free-space communication channels studies employ the polarisation of light and the spectral multiplexing technology. However, the amount of information that a photon can carry increases with the dimension of the Hilbert space. Therefore, it is reasonable to consider the spatial modes of light, which would allow one to go on step forward [1]. Photons can be described in terms of their spatial modes – the "patterns" of light. As there are an infinite number of spatial modes, entanglement in this degree of freedom offers the opportunity to realize high-dimensional quantum states [2].

In general, these modes are solutions of the free-space wave equation, so that they may be propagated over some extended distance in space and maintain their modal properties. Unfortunately, while photons are weakly interacting, they nevertheless experience disturbance due to the atmosphere in the form of optical turbulence. An obvious solution to this problem may be to use fibre systems, but the spatial modes that are often used in communication experiments are not properly propagated within optical fibres. That is why we study a new system to detect different spatial modes using a CCD camera after traversing a turbulence channel, and training a machine learning algorithm to properly distinguish between different outcomes.

Methods

We take advantage in this project from the numerous previous works proving how the functionalities of entangled states in quantum communications can be simulated by using the nonseparability properties of the well-known vector modes [3,4]. Considering in our particular case a superposition of Laguerre-Gaussian modes, also known as 'petal' modes, with different azimuthal and radial components ranging from l=[0..3] and p=[0,1], respectively. We encode the turbulence screens to interact with the spatial modes using Matlab, in order to simulate a real free-space communications link. Thus, being able to use these simulations to train two machine learning models: simple linear softmax regression model (y = Mx + b), and neural network model with two convolutional layers, a flattering layer, a fully connected layer and a 50% dropout layer. The training set consists of 4725 images from the simulated data, and the validation and test set of 1575 images. The neural network model training time to obtain a probability recognition accuracy of over 99% is one order of magnitude higher than the simpler model of linear softmax regression.

Results and conclusions

A particular example of the modal recognition results is shown in Figure 1, after having trained the machine learning algorithm with the simulated data. Obtaining over 90% probability of success in the detection of the proper spatial mode in most of the cases, even when the mode is highly distorted by the atmospheric turbulence as can be seen in the first two examples. There are few isolated cases where the probability drops below 50%, like in the third example, due to the petal-like intensity profile being chopped off. The missing 'petals' is clearly affecting the mode detection, but it is expected to be improved when considering a larger range of azimuthal and radial components, i.e., larger set of spatial modes. Further study needs to be carried out, broadening the parameters that we can detect using intensity profiles.

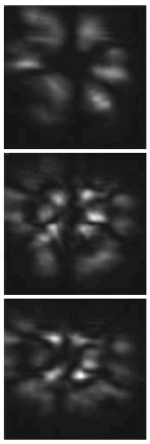

```
In [16]: categorise(test_addrs[92],True)
   ...:
Most likely mode: l,p = (3, 0) | Probability: 94
```



```
In [25]: categorise(test_addrs[50],True)
   ...:
Most likely mode: l,p = (3, 1) | Probability: 99.67
```



```
In [7]: categorise(test_addrs[32],True)
   ...:
Most likely mode: l,p = (3, 1) | Probability: 43.24
```

Figure 1 – Screenshots captured with a CCD camera on the left, showing the Laguerre-Gaussian 'petal' modes after traversing a real free-space communications link. A part of the code giving the results of the modal recognition outcome is shown in the right.

References

[1] Gibson G. et al., Opt. Express 12(22); 5448, 2004. [2] Agnew M. et al., Phys. Rev. A 84(6); 062101, 2011. [3] Milione G. et al., Opt. Lett. 40(21); 4887, 2015. [4] Ndagano B. et al., Nat. Phys. 13(4); 397, 2017.

Acknowledgements

The work has been performed under the Project HPC-EUROPA3 (INFRAIA-2016-1-730897), with the support of the EC Research Innovation Action under the H2020 Programme; in particular, the author gratefully acknowledges the support of Prof. Jonathan Leach and IPaQS from the Heriot-Watt University, and the computer resources and technical support provided by EPCC from the University of Edinburgh.

USING THE TEST-FIELD METHOD TO UNDERSTAND STELLAR DYNAMOS

M. Viviani[1], M.J. Käpylä[1,2], M. Rheinhardt[2], F. Gent[2]

[1]Max Planck Institute for Solar System Research, Göttingen, Germany; [2]ReSoLVE Centre of Excellence, Department of Computer Science, Aalto University, Finland

Introduction

Solar and stellar dynamos are still poorly understood. They are generating virtually all the magnetic phenomena on stars, hence influencing also space weather and climate, in our Solar System but also in exoplanetary ones. The main ingredients of dynamo action are differential rotation and turbulent convection. When talking about differential rotation (DR) we define two regimes, using the Sun as a reference point. If the equator rotates faster than the poles, we talk about solar-like DR, if the poles are accelerated with respect to the equator, we speak about anti-solar DR.

Our aim is to reproduce stellar dynamos and understand how they work by means of numerical simulations, solving the fully compressible equations of magnetohydrodynamics (MHD) in (semi-)spherical shells. This kind of models are called direct numerical simulations (DNS), and they require huge numerical resources. Recently [1], it has been shown that the current DNS models of the Sun can be explained as a Parker Dynamo Wave (PDW), which means that dynamo action is a result of differential rotation generating toroidal magnetic field from poloidal field (Ω-effect), and turbulent motions building up poloidal magnetic field from the toroidal one (α-effect) [2]. If the DR rotation is solar-like and the α-effect is negative (positive) in the northern (southern) hemisphere, this leads to an equatorward dynamo wave. In similar studies, with a lower rotation rate, the DR profile swaps to anti-solar like. If these models are run over a full azimuthal extent, cyclic solutions can be found [3]. During our HPC-Europa3 project we wanted to study if these exotic dynamo waves can also be understood with a similar theoretical framework as the solar-like solutions.

Methods

Given the complexity of DNS, to verify this hypothesis, dedicated data analysis tool needs to be employed. The method, already developed in the host group, is the so-called *Test-field method* [4], that utilizes mean-field theory to study the evolution of the mean magnetic field, that in the Sun and other slow rotating stars is axisymmetric. Under this approximation, the induction equation for the magnetic field takes the form:

$$\frac{\partial \overline{\boldsymbol{B}}}{\partial t} = \boldsymbol{\nabla} \times \left(\overline{\boldsymbol{U}} \times \overline{\boldsymbol{B}} + \overline{\boldsymbol{u} \times \boldsymbol{b}} \right) - \boldsymbol{\nabla} \times \eta \boldsymbol{\nabla} \times \overline{\boldsymbol{B}}$$

Here, $\overline{\boldsymbol{B}}$ and $\overline{\boldsymbol{U}}$ indicate the mean magnetic and velocity fields, resulting from the azimuthal average, while $\boldsymbol{u}$ and $\boldsymbol{b}$ are the fluctuating fields, that is the difference between the original field and the averaged field (i.e., $\boldsymbol{b} = \boldsymbol{B} - \overline{\boldsymbol{B}}$). The term $\overline{\boldsymbol{u} \times \boldsymbol{b}}$ couples the mean field with the fluctuations, acting as a generative term for the mean magnetic field, and it is called *electromotive force*, $\boldsymbol{\mathcal{E}}$. The electromotive force can be expanded in terms of the mean magnetic field and its derivatives, multiplied by some tensors, containing the information on the turbulent flow:

$$\boldsymbol{\mathcal{E}} = \boldsymbol{\alpha} \cdot \overline{\boldsymbol{B}} + \boldsymbol{\gamma} \times \overline{\boldsymbol{B}} - \boldsymbol{\beta} \cdot (\boldsymbol{\nabla} \times \overline{\boldsymbol{B}}) - \boldsymbol{\delta} \times (\boldsymbol{\nabla} \times \overline{\boldsymbol{B}}) + \cdots$$

Each of these coefficients, the *turbulent transport coefficients*, can be associated with a physical effect: for example, $\boldsymbol{\alpha}$ is related to the α-effect; $\boldsymbol{\beta}$ is the turbulent diffusion, an additional diffusivity that destroys the magnetic field.

Results

After obtaining the turbulent transport coefficients, we can use them for calculating the direction of a PDW, given by the Parker-Yoshimura rule [5]:

$$\boldsymbol{\xi}(\theta, \varphi) = -\alpha_{\varphi\varphi} \hat{\boldsymbol{e}}_{\varphi} \times \boldsymbol{\nabla} \Omega$$

The $\alpha_{\varphi\varphi}$ component of the α-tensor combined with the anti-solar DR of our DNS could explain the poleward migration of the magnetic field at the surface if the predicted direction is also poleward where the magnetic field is stronger, at the bottom of the convection zone. Figure 1 panel a) shows the direction of a PDW: where the field is stronger (in red), the Parker-Yoshimura rule predicts a poleward direction. We show in panel b) the direction of meridional circulation, that also can advect the magnetic field. But, when we also perform period analysis on our DNS and compare with period prediction for PDW and meridional circulation advection, we find that none of the two can explain the oscillation period of the magnetic field.

Conclusions

We checked our DNS against the predictions of the two most simple scenarios: the Parker-Yoshimura dynamo wave and advection by meridional circulation. Both of them failed to give a clear explanation. Further analysis, employing the full tensorial representation of the turbulent transport coefficients in a numerical mean-field model, is required.

References

[1] Käpylä, M. J., et al., A&A, 589, A56, 2016. [2] Parker, E. N., ApJ, 121, 491, 1955. [3] Viviani, M. et al., A&A, 616, A160, 2018. [4] Schrinner, M., et al., Astron. Nachr., 326, 245, 2005. [5] Yoshimura, H., ApJ, 201, 740, 1975.

Acknowledgements

The work has been performed under the Project HPC-EUROPA3 (INFRAIA-2016-1-730897), with the support of the EC Research Innovation Action under the H2020 Programme; in particular, the main author gratefully acknowledges the support of ReSoLVE Centre of Excellence, Department of Computer Science in Aalto, Finland, and the computer resources and technical support provided by CSC.

BOUNDARY ARTIFACT ANALYSIS IN MODELLING WITH STOCHASTIC DIFFERENTIAL EQUATIONS

M. Yip

Norwegian university of Science and technology, Department of physics, Trondheim, Norway

Introduction

Particle tracking in fluids has been of interest in many different academic areas. Marine transport modelling is mainly divided into two different numerical approaches, that is the Eulerian model and Lagrangian model. Eulerian model does not exhibit the individual path of each single particle. but in a Lagrangian model, a common scheme (PRS) used to implement reflecting boundary conditions can lead to an artefact, where one or more rapid oscillations occur in the concentration field close to the boundary. This is hereafter referred to as the boundary artefact. Because of this boundary artefact, Lagrangian models may fail to satisfy the well-mixed condition [1]. The project is to find out the cause of the boundary artefact, analyse it and give some suggestions to eliminate or reduce boundary artefact in Lagrangian models.

Methods

Two objectives to complete: 1. Compare PDE vs SDE in the mirrored diffusivity, find out what is wrong with the common reflecting scheme in SDE. 2. Use what we have learn from objective 1 to minimize the boundary artefact.

Results

Figure 1 shows the objective 1. We can see that the boundary artefact occur in the right middle region even though there is not a boundary. This mean that something is fundamentally wrong when we are applying the common reflecting scheme. It turns out the assumption, called Lipschitz condition has been violated when the derivative of diffusivity is not smooth. This is the condition for SDE behaves equivalently to PDE. The PRS is effectively mirroring the diffusivity domain. Therefore, The PRS is best apply at boundary which has derivative of diffusivity equal to zero. If our idea is correct, make the diffusivity has derivative equal to zero can avoid the boundary artefact. Figure 2 confirms our hypothesis.

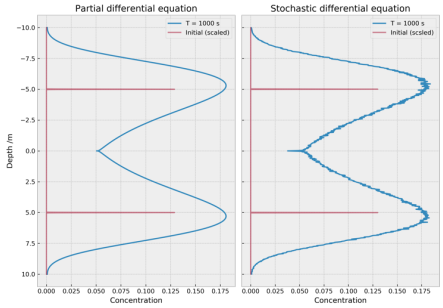

Figure 1 – Left figure simulated by PDE and right figure simulated by SDE.

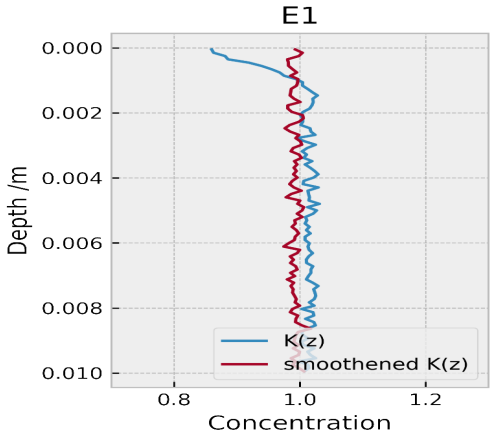

Figure 2 – Left figure simulated by PDE and right figure simulated by SDE.

Conclusions

PRS violates the Lipschitz condition in a very subtle way. Changing the diffusivity to have derivative zero, will eliminate boundary artefact. The reader may think this will change the physical reality. The answer is not quite. Wilson, J. D., & Flesch, T. K. [2] motion that we simply cannot know the statistical detail near the boundaries, and this is called “unresolved basal layer”. This gives us some free freedom to adjust the diffusivity near the boundaries.

For more detail, please contact me, and I may send you my master thesis and code.

References

[1] Thomson, D. et al., Journal of Fluid Mechanics, 180 180 ():529-556, 1987. [2] Wilson, J.D. et al., Journal of Applied Meteorology, 32(11):1695-1707, 1993.

Acknowledgements

The work has been performed under the Project HPC-EUROPA3 (INFRAIA-2016-1-730897), with the support of the EC Research Innovation Action under the H2020 Programme; in particular, the author gratefully acknowledges the support of Faculty of Natural Sciences, Department of Mathematics (Dr. Collin Cotter, Imperial College London, UK) and the computer resources and technical support provided by EPCC at Edinburgh UK. The author also wants to thank the supervisor (Dr. Tor Nordam, NTNU, Norway) for the constantly help.

LATTICE BOLTZMANN SIMULATIONS OF THIN FILM DYNAMICS ON ACCELERATOR DEVICES

S. Zitz, A. Scagliarini, J. Harting

Helmholtz Institute Erlangen-Nürnberg for Renewable Energy (Germany), Istituto per le Applicazioni del Calcolo"Mauro Picone" (Italy)

Introduction

Thin liquid films play an important role in many processes ranging from biology to geophysical phenomena, such as lava flows [1]. Therefore, their theoretical understanding and the ability to simulate these systems is of utmost importance to many processes. Most prominent ones are coating processes and inkjet printing.

This knowledge naturally extends into the field of renewable energies, as more and more solutions appear to build fast and cheap photovoltaics with printing methods such as slot die coating.

The aim of our project is therefore to create a model which is on the one hand capable of dealing with thin liquid film dynamics, but also be scalable to scan through a phase space of many independent variables.

A however much overlooked effect is the influence of thermal fluctuations. As the fluid film dries and therefore becomes thinner we expect that the dynamics due to fluctuations can no longer be neglected.

Ultimately this effect will shape properties of a given photovoltaic cell.

Methods

The fluid solver we use is based on the lattice Boltzmann method [2] and is written in C++. The name for our code is Swalbe, which is an acronym for: Shallow WAter Lattice Boltzmann solvEr. The main difference to other lattice Boltzmann methods is the choice of suitable equilibrium distribution functions. This means instead of approximating the Navier-Stokes equations our approach approximates the so-called thin film equation [3]. Yielding a two-dimensional computation domain for simulations of a three-dimensional problem. The method is parallelized with a directive-based approach, namely OpenACC [4]. This way computing regions are translated into CUDA (Compute Unified Device Architecture) kernels. Therefore, compiled code can be executed on accelerator devices, such as graphic processing units (GPUs).

To resolve the three-phase contact line dynamics we uses a wetting potential similar to the one used in [5]. This ensures that contact line phenomena are physically correct, e.g. droplet spreading. Capturing the stochastic features of thermal fluctuations, the model has been extended to simulate the stochastic thin-film equation. A similar approach but in a different framework has been applied in [5]. In our model we intertwined CUDAs pseudo random number library CURAND with OpenACC. As such we are able to generate random numbers in high quality on the device during run time.

Results

We have performed a series of thin-film simulations with our fluid solver. The dynamics of the three-phase contact line are correct represented and in agreement with analytical solutions. Both the Cox-Voinov law as well as Tanners's law have been measured and validated [3].

On the other hand, the model has been extended to be capable of simulating the stochastic thin-film equation, which is shown in Figure 1. In the lower left panel, the simulation is performed without thermal fluctuations while in the upper right we include the effect of thermal fluctuations. A structural difference can easily be spotted.

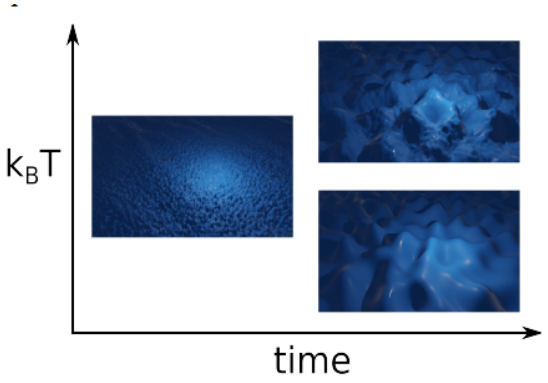

Figure 1 – Rendered snapshots of simulation data. The left panel depicts the initial condition, which is similar to white noise. The right panels present a late stage in the simulation. The lower panel shows the deterministic evolution while the top panel shows the stochastic one.

Conclusions

A new method to simulate thin-film dynamics has been thoroughly tested and benchmarked. An extension has been implemented to probe the effect of thermal fluctuations. Thus, it is possible for the first time to gather insights about 2D morphologies and patterns during dewetting processes. Due to the structure of the solver the method is perfectly suited for accelerator devices. Performance wise due to GPUs we see a speedup of about 20 times as compared to a CPU.

References

[1] Craster, R. V., Matar, O. K, Rev. Mod. Phys., 81(3):1131, 2009. [2] Krüger T. et al., The Lattice Boltzmann Methode, Springer, 2017. [3] Zitz S. et al., Phys. Rev. E, 100(3):033313, 2019. [4] Chandrasekaran S., Juckeland G., OpenACC for Programmers, Addision-Wesley Professional, 2017. [5] Nesic S. et al., Phys. Rev. E, 92(6):061002, 2015. [6] Grün G. et al., J. Stat. Phys, 122(6):1261, 2006

Acknowledgements

The work has been performed under the Project HPC-EUROPA3 (INFRAIA-2016-1-730897), with the support of the EC Research Innovation Action under the H2020 Programme; in particular, the author gratefully acknowledges the support of Andrea Scagliarini from the Istituto per le applicazioni del calcolo "Mauro Picone" and the computer resources and technical support provided by CINECA.

CONNECTIONS WITH DECISION MAKERS: THE CASE OF JOURNAL EDITORS IN ECONOMICS

L. Ductor, B. Visser

Middlesex University London, Erasmus University of Rotterdam

Introduction

Are connections with decision makers valuable? Do connections lead to better or worse decisions? And if they do, why is that?

We focus on an area of decision making where important connections with decision makers have a long history of being observable and where a much-used measure of the quality of a decision exists. We study connections with the editorial board members of more than 100 economics and finance journals over the period 1990-2011. The identity of the board members is readily obtained from the front matters of the journals, as are the periods in which they are active. Important types of connections, including co-authorship and a shared affiliation, between a scholar and a board member are easily obtained from bibliographical databases and CVs. To establish whether a connection with a board member is valuable, we look at publication records, while we turn o citation scores to infer the quality of the decision taken. Finally, most board members join a journal's board for a number of years and then step down. This rotation is the basis of our identification strategy to estimate the causal impact of connections, as in Brogaard, Engelberg and Parsons (2014) and Colussi (2017).

Methods

The value of a connection can be established at the department level and the individual level. To explain our identification strategy, consider the department level. Identification of the value comes from the 266 departments that in some years during our sample period have a faculty member on the editorial board of a specific journal while in other years they haven't. For such departments, we compare the number of publications in that journal across those two types of years. As our observation is a department-journal-year triple, we use a full set of pairwise fixed effects, department-year, journal-year and department-journal, to soak up unobserved heterogeneity. The same approach can be used to study the effect of connections with a board member at the individual level. At this level, we distinguish the effects on an editorial board member's co-author, colleague and mentee. At the individual level, we include author-journal-editor and journal-year fixed effects and account for individual time-varying characteristics, of both the connected author and the editor.

Results

We find large and significant effects of connections on the number of publications. At the department level, the annual number of publications in a journal more than doubles when a faculty member is on the editorial board of the journal. A substantial part of this increase stems from the fact that board members come from particularly productive departments. When we control for our set of pairwise fixed effects, the (marginal) increase in publications is still large, 31%, and highly significant. The increase is particularly large, 72%, for members who have been on the board for five years or more, see Figure 1. Effects on the number of publications at the individual level – co-authors (+6.6%), colleagues (+6.4%) and mentees (+12.6%) – are highly significant.

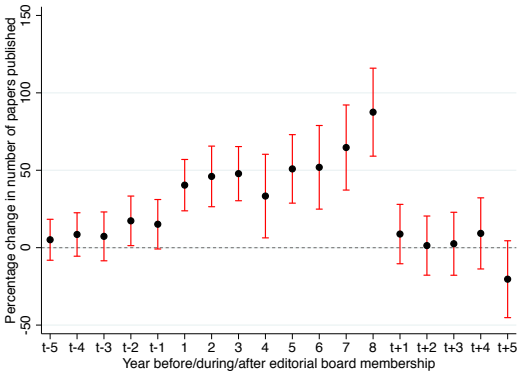

Figure 1 - Frequency of publication across a board member's tenure

Notes: The plots show the coefficients and 95% confidence intervals of dummies for each year before, during and after the appointment of the scholar as an editor. Year 8 includes the change in number of papers published when the scholar has been a board member at the journal for 8 years or more. Year t + 5 refers to the fifth year and beyond after board membership has ended. The baseline, 0.35, is the average annual number of publications prior to t-5.

Conclusions

We study the value of connections with editorial board members of more than 100 economics journals over the period 1990-2011. We identify a causal link between a connection with a journal's board and publication success by exploiting board membership rotation. A department increases its number of publications in a journal when one of its members is on hat journal's board. An analysis of citation patterns of faculties and colleagues show that papers published in the historical top 5 when a colleague is on the editorial board are more cited than papers published when no link is present. This suggests that, on average, the effect of any editorial favouritism is less strong than those of improved information about papers.

References

[1] Brogaard, Jonathan, Joseph Engelberg, and Christopher A Parsons (2014) 'Networks and productivity: Causal evidence from editor rotations.' Journal of Financial Economics 111(1), 251–270. [2] Colussi, Tommaso (2017) 'Social ties in academia: A friend is a treasure.' Review of Economics and Statistics.

Acknowledgements

The work has been performed under the Project HPC-EUROPA3 (INFRAIA-2016-1-730897), with the support of the EC Research Innovation Action under the H2020 Programme; in particular, the author gratefully acknowledges the support of the Erasmus School of Economics and the computer resources and technical support provided by SURFSara.